Final Report

UXO Corrosion – Potential Contamination Source

SERDP Project ER-1226

April 2004

Bonnie Packer
U.S. Army Environmental Command

Michael Chendorain
Lloyd Stewart
Praxis Environmental Technologies, Inc.

SERDP
DOD ▪ EPA ▪ DOE

REPORT DOCUMENTATION PAGE

Form Approved
OMB No. 0704-0188

PLEASE DO NOT RETURN YOUR FORM TO THE ABOVE ORGANIZATION.

1. REPORT DATE *(DD-MM-YYYY)*	2. REPORT TYPE	3. DATES COVERED *(From - To)*
April 2004	Final Technical	October 2001-April 2004

4. TITLE AND SUBTITLE
Corrosion of Unexploded Ordnance in Soil Environments

5a. CONTRACT NUMBER
GS05T02BMM1403; GS05T02BMM1448

5b. GRANT NUMBER

5c. PROGRAM ELEMENT NUMBER

6. AUTHOR(S)
Chendorian, Michael and Lloyd D. Stewart

5d. PROJECT NUMBER
ER-1226

5e. TASK NUMBER

5f. WORK UNIT NUMBER

7. PERFORMING ORGANIZATION NAME(S) AND ADDRESS(ES)
PRAXIS Environmental Technologies, Inc.
1440 Rollins Road Burlingame, CA 94010

8. PERFORMING ORGANIZATION REPORT NUMBER

9. SPONSORING/MONITORING AGENCY NAME(S) AND ADDRESS(ES)
USAEC
ATTN: SFIM-AEC-PCT
Aberdeen Proving Ground, MD 20101-5401

10. SPONSOR/MONITOR'S ACRONYM(S)
USAEC, SERDP

11. SPONSOR/MONITOR'S REPORT NUMBER(S)
SFIM-AEC-PC-CR-2004007

12. DISTRIBUTION/AVAILABILITY STATEMENT
This document is intended for public release with unlimited distribution.

13. SUPPLEMENTARY NOTES

14. ABSTRACT

This report covers the results of a field and modeling evaluation of UXO corrosion, including: 1) a simple protocol for sampling UXO for corrosion and presence of energetic in soils; 2) a database in excess of 160 individual ordnance samples; 3) a UXO Corrosion Model (called UXO-Corr-Mod II) which provides estimates of time to failure of a given UXO thickness based on soil and environmental factors; and 4) a UXO energetic release and transport model developed to predict groundwater loading of explosives released from buried sources.

15. SUBJECT TERMS
Corrosion Sampling, UXO, Unexploded Ordnance, Munition, Fate, Transport, Explosives

16. SECURITY CLASSIFICATION OF:			17. LIMITATION OF ABSTRACT	18. NUMBER OF PAGES	19a. NAME OF RESPONSIBLE PERSON
a. REPORT	b. ABSTRACT	c. THIS PAGE			Lloyd D. Stewart
U	U	U	U	189	19b. TELEPHONE NUMBER *(Include area code)* 650-548-9288

Reset

Standard Form 298 (Rev. 8/98)
Prescribed by ANSI Std. Z39.18

Table of Contents

List of Figures

List of Tables

2003 SERDP Final Technical Report - UXO Corrosion in Soil

U.S. Army Environmental Center, 5179 Hoadley Road, Aberdeen Proving Ground, MD 21010

1 Project background.

The 1998 Defense Science Board report estimated that 1,400 different sites, encompassing 10 million acres of land contain Department of Defense (DoD) unexploded ordnance (UXO) (Defense Science Board, 2003). Contained within the soil, these intact munitions corrode at vastly varying, site-specific rates. Depending on site conditions and UXO characteristics, the time to perforation (i.e., corrosion breakthrough of the metallic casing) can vary from roughly 10 years to several thousand years. Understanding the relative rate of corrosion greatly improves the assessment of risk to humans and the environment posed by the toxic energetic and constituent materials encased in UXO. The UXO are comprised of high explosives (e.g., RDX, TNT, HMX, and Tetryl), the metallic container, and lesser quantities of fuse materials. While the metallic container is not hazardous to human health, the explosive fill components each have their own characteristic toxicity, water solubility, and propensity for sorption; and thus, differing potentials to impact surface water and groundwater quality. To assess the environmental impact of these compounds appropriately, two fundamental questions must be answered first: how fast do UXO containers corrode and what factors determine the corrosion rate? The work of this project represents a first of its kind tool to answer these questions. The effort included sampling of UXO and soils under various environmental conditions across the United States and the simultaneous development of a technically sound corrosion model for evaluating site-specific times to perforation of UXO. The field data were used to calibrate the corrosion model and support realistic assessments of UXO as sources of environmental risk at U.S. military installations. The DoD must understand the rate and mode of UXO corrosion to form a basis for predicting when and where chemical constituents may be released to the environment. This information will provide prioritization capabilities and enable cost effective management with the limited resources available. Understanding the corrosion rate is the first element to "…maintain the long term viability of active ranges" and to "developing a risk-based priority system…(Defense Science Board, 1998)."

2 Objectives.

The three primary objectives of this project were to:

1. Collect and analyze soil and UXO scrap metal samples from several ranges across the country,
2. Evaluate the data to yield a physically based correlation (e.g. a simple PC model) for perforation rate of UXO under a variety of soil and climatic conditions, and
3. Collect and analyze soil samples around the UXO for explosives. This third objective was outside the scope of SERDP funding and was funded by the U.S. Army Environmental Center's Training and Support Division because of its importance in understanding risk.

The analyses of samples for the corrosion assessment focused on traditional chemical corrosion mechanisms; however, a subset of the samples included analyses for microbial corrosion. Corrosion induced by microbes is expected to contribute to UXO corrosion but no previous efforts attempted to quantify the impact. The correlation for corrosion rates in UXO developed from the data will be integrated into public domain software to facilitate its use by environmental risk assessors. Chemical analyses for explosives in numerous soil samples collected from soils at various distances from the UXO were performed on a small subset of the sampling events during this project. The objective of the limited explosives sampling effort was to provide more information on the potential for local transport of explosives from and adjacent to UXO if perforations have occurred.

3 Technical approach.

Collect and Analyze Soil and UXO Scrap Metal Samples for Corrosion Analyses. Soil and scrap metal samples were collected from firing ranges across the country. Soil samples were analyzed to quantify various physical, chemical, and biological properties. Metal samples were analyzed for various corrosion parameters (e.g., pit depths and pit density). Only sites with ordnance of known age are under evaluation so that corrosion rates can be established. In addition, only carbon steel based UXO were included in the results. Range sites chosen for the study exemplify a broad host of environmental characteristics. For example, one range is located in an arid environment with low soil organic matter content, low moisture content, high aeration, and clay rich (oxidizing) soil horizons. Another site had high rainfall and subsequently high soil moisture contents, low oxygen content, and greater affinity for anaerobic microbial metabolic processes. Testing sites with a wide range of characteristics yielded a more robust data set. Sample analyses provided the quantitative data to determine the UXO perforation rate (i.e. corrosion rate) at each site. A subset of the samples also included analyses for microbial corrosion to quantify the contribution of microbes to corrosion of UXO. UXO samples were collected during clearance activities. As such, only those found at a given site were sampled.

Build a Database of Results. A database of the site characteristics, sampling results, and pictures of UXO items was developed in Microsoft Access 2000 format. The database includes all results from this study and incorporates data from other studies. The purpose of the database is to provide information to future users and for model development (predictive models, risk assessments, etc.).

Develop a Predictive Tool for UXO Perforation Rate Validated with Field Data. A site-specific, physical-chemical corrosion model was developed based on the transport phenomena dominating UXO corrosion in soil. Determining which site parameters drive corrosion provides a scientifically-based method for determining sites posing a near-term threat of energetics release. The model for corrosion rates in UXO developed from the data has been integrated into soon-to-be-released DoD software to facilitate its use by DoD environmental risk assessors. The output of the corrosion model forecasts the time to UXO perforation based upon site soil and climatic conditions. The corrosion model was validated by the large and extensive data set acquired in this study. Additionally, soils and metal data from other military sites collected in previous UXO corrosion studies were incorporated into the database and used in the model validation.

Collect and Analyze Soil Samples for Explosives Transport. Chemical analyses for explosives in numerous soil samples were performed as a secondary objective to this project. These soil samples were collected from soils at various distances from the UXO. The objective of the explosive sampling effort was to provide more data sets to this and other DoD projects evaluating the transport of explosives through soils on current and former firing ranges. The UXO corrosion project is focused on evaluating UXO as a potential release point of underground contamination while the other projects are studying the transport of surface-based energetics (e.g. high and low order detonations) through soils. Sampling for explosives transport was conducted for as many ordnance as possible at each site.

4 Project accomplishments.

As a result of the UXO Corrosion Study, a variety of accomplishments have been achieved:

- A simple, efficient protocol has been developed for environmental sampling of UXO (for corrosion and energetic presence in soil).
- A database in excess of 150 individual ordnance samples,
- A UXO Corrosion Model (called UXO-Corr-Mod III) has been developed which provides estimates of time to failure for a given UXO thickness and corrosion rate profiles based on soil and climatic parameters
- A UXO release and transport model has been developed which predicts groundwater loading of energetics released from buried sources (such as UXO and underground low order detonations).

A sampling protocol was developed which enabled UXO field technicians and military EOD personnel to perform environmental sampling of UXO in the field. Due to the hazardous nature of the work, this protocol was written by explosive ordnance disposal (EOD) experts and environmental scientists. The sampling included soil sampling for chemical and physical parameters to estimate extent of corrosion, soil sampling to quantify energetic presence in soil, and metal sampling to quantify extent of corrosion. The finalized sampling protocol is provided in Appendix B1.

A database was developed in Microsoft Access 2000 and includes the results of sampling at fourteen sites. Seven sites were accessed through the Army Corps of Engineers via SERDP funding while funding to access and sample the remaining seven sites were provided by the

USAEC. The database contains 161 corrosion data points, 186 soil characterization samples (with analysis of 29 different soil chemical and physical parameters), 106 soil samples for analyses of TNT, RDX, and associated compounds. Tables are provided in the database which can be easily integrated into spreadsheets such as Excel. The database generates reports which provide summaries of the type of UXO found, the measured extent of corrosion, the modeled extent of corrosion and time to perforation, environmental parameters (soil and climatic), and provides pictures of the items as encountered in the field. Appendix B2 provides outputs of the reports found within the database.

A UXO Corrosion model has been developed which estimates perforation times for UXO and produces corrosion profiles for a given set of soil and climatic conditions. This third phase of the model named UXO-Corr-Mod III has improved upon previous versions by integrating generalized corrosion and diffusion through scales into a pitting corrosion model. Empirical relationships developed in early versions have been replaced with more physically based relationships in an attempt to provide more physically based estimates of corrosion rates. Also, the solution accuracy of the model has been improved by adding a numerical estimation of the corrosion rate. Previous solutions of the model have merely estimated corrosion rates and time to perforation as an average corrosion over the length of the exposure period. Phase III of the model estimates a nonlinear corrosion rate and estimates perforation times by integrating under the corrosion rate profile curve.

A Fortran based transport model which estimates groundwater loading of energetics buried in soil has been developed. The model requires inputs which characterize:

- the range characteristics (number, type and distribution of high explosive UXO over the area of concern),
- the soil physical properties (moisture content, porosity, etc.),
- the hydraulic characteristics (infiltration rate, groundwater velocity and aquifer thickness), and
- how the energetics are buried in soil (bare, partially exposed, etc.)

The results of the model provide detailed groundwater concentration profiles, maximum groundwater concentration, and average groundwater concentration exiting the range.

5 Unpublished Results.

The following three sections describe studies performed during this project which have not as of yet been published in other mediums. The first section (5.1) describes soil sampling and analyses for microbially induced corrosion. The following section (5.2) describes soil sampling for high explosives. Section 5.3 describes the results from comparing of the UXO Corrosion Model to the field data. Section 5.4 presents a summary of Appendix A4 which describes the energetic transport model.

5.1 UXO Corrosion and Microbial Activity

*Introduction***.** Soil samples were collected and analyzed for microbial parameters. The purpose of this study was to ascertain whether microbially induced corrosion (MIC) was quantifiable for a range of soil types and climatic conditions.

Methods. Up to three areas on the UXO exterior (depending on the UXO size) were swabbed and swab samples were shipped for microbiological analyses. Two to three soil samples were then collected for microbiological analyses where one sample was collected from soil adjacent to the UXO and remaining samples were collected at distances of nine and eighteen inches away from the UXO.

Soil Samples**.** 1 g of each soil sample was diluted in 9 ml of phosphate buffered saline (PBS; Sambrook and Russell, 2001) and vortexed for 30 s. Samples were then serially diluted in PBS and spread onto solidified agar plates to enumerate populations of microorganisms. Solid media included: (i) nutrient agar (NA; pH 6.8 ± 0.2; Difco Laboratories, Detroit, MI) and (ii) potato dextrose agar (PDA; pH 5.6 ± 0.2; Difco Laboratories)[see Appendix A]. One set of samples spread on nutrient agar was incubated aerobically for 7 days on the bench top to enumerate the heterotrophic aerobic microbial population. A second set of nutrient agar plates was incubated anaerobically for 21 days in glass canisters with an anaerobic gas generating system (GasPak Plus™, Becton Dickinson, Sparks, MD) to enumerate anaerobic heterotrophs. A third set was spread on PDA and incubated aerobically for 7 days to enumerate fungi/molds and acid-tolerant bacteria. Estimates of microbial populations were calculated by selecting the dilution plate which had between 30 and 300 colony forming units (CFU), counting the number of CFU and multiplying by the number of dilutions. A subset of aerobic bacterial CFU were randomly chosen for Gram staining to ascertain the general makeup of the bacterial community.

Swab Samples from UXO**.** Microbial populations colonizing UXO were evaluated with swab samples using liquid media (Dixie Testing and Products, Inc; Houston, TX) [see Appendix B]. Briefly, swab samples, taken from a 1-cm^2 area of the UXO, were suspended in a buffer solution before being transferred to growth media. One ml of the suspension was sequentially diluted 10-fold by a series of transfers with sterile syringes. The first 32 samples were diluted by 10-fold transfers up to 10,000 (10^{-5}); the remaining samples were diluted to a concentration of 10^{-10} of the initial suspension.

Environmental Scanning Electron Microscopy (ESEM) and Energy Dispersive X-ray Spectroscopy (EDS). Samples taken from each culture were centrifuged at 5,000 rpm for 10 min, the supernatant decanted, the cell pellet rinsed and resuspended in distilled water. The process was repeated three times to remove media and salts. The rinsed cell pellet was resuspended in 20 ml of 4% cacodylate buffered gluteraldehyde (25%; ACS grade, Fisher Scientific) overnight to preserve the cells. Just prior to imaging, the cells were centrifuged and rinsed (3X) to remove fixative and resuspended in distilled water. A 10 µl aliquot of fixed cells was placed on a Peltier™ cooling stage and maintained at 4°C to keep the samples hydrated. Cells were imaged using an environmental scanning electron microscope (ESEM; Model E3, ElectroScan/FEI Company, Hillsboro, OR) at a voltage of 20 kV and a water vapor pressure between 4.0 - 4.7 torr. The ESEM was coupled with an energy dispersive x-ray spectrometer

(EDS; Vantage™ DI+ X-Ray Microanalysis System, ThermoNoran, Middleton, WI). After ESEM imaging, the sample was transferred to a carbon stub to minimize background interference for EDS analysis. Chamber pressure was reduced to 2.0 - 1.5 torr to decrease beam scattering and facilitate EDS examination. Digital images and EDS spectra were analyzed using EasyMICRO software (ThermoNoran) according to the manufacturer's instructions. EDS spectra were collected in three areas for each sample.

Results and Discussion. Swab and soil samples were collected to assess the microbiological communities on and around the UXO items. Results of the microbiological analyses on the swab samples from the UXO surface are summarized in Figure 1. The bar graph depicts the average distribution of the different communities studied at each site sampled. Acidophiles, anaerobes, and general aerobes were all present in abundance on the ordnance items. Figure 1 illustrates that sulfate-reducing bacteria were found in very small quantities relative to the other three populations studied. Of the communities studied, sulfate-reducing bacteria have the most influence on corrosion. Figure 2 presents average community results from the soil samples. Soil samples were collected directly adjacent to UXO (location 1), six to nine inches from the UXO (location 2), and 30 to 45 cm from the UXO (location 3). All three soil samples for each item were collected at the same approximate depth into the soil. Figure 2 illustrates the average aerobic mesophilic populations in contrast to the acidophilic populations. The soil samples suggest that acidophilic populations are not influenced by the presence or absence of a UXO. Hence, acidophilic organisms are shown to be ubiquitous in soil at the sites studied.

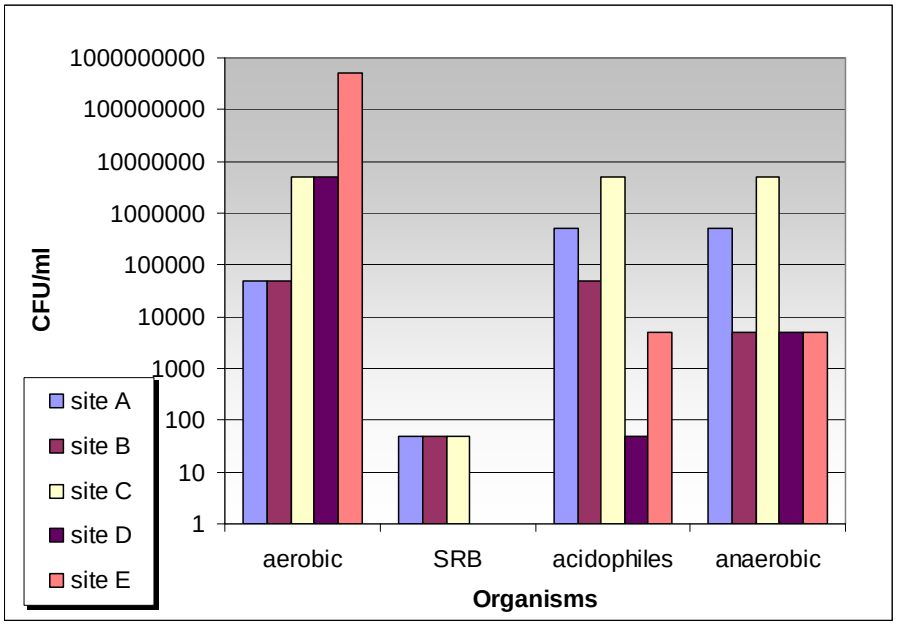

Figure 1. Results from swab sampling directly on ordnance items.

Scanning Electron micrograph images of UXO metal fragments were also collected during the microbiology study and did not definitively reveal the presence of microorganisms, although tunneling, described below is suggestive of microbiologically enhanced corrosion. All examined

fragments were iron. White deposits on the side exposed to soil contained silicon, aluminum, sulfur, potassium, copper and manganese. Distribution and concentration of elements varied among samples and within locations on a single sample.

Microbiological analyses described in this report all share a similar limitation. All analyses were performed using synthetic media that may not be representative of the community dynamics present in situ. Cultures grown in a laboratory environment on synthetic media can only detect, at best, 1 % of the true soil microbial population. In addition, laboratory environments tend to select for fastidious organisms. In a nutrient deprived environment such as soil, slower growing organisms are likely to be large contributors to the overall metabolic activity. Acid-producing organisms are known to accelerate corrosion processes. Since acid-producing organisms are difficult to culture, acidophilic selective media was used for analysis (potato dextrose media). Although acid-producing organisms are inherently acidophilic, not all acidophiles are acid producers. Hence, presence of acidophiles in soil is not conclusive evidence that acid-producers are present and active in the soil environment.

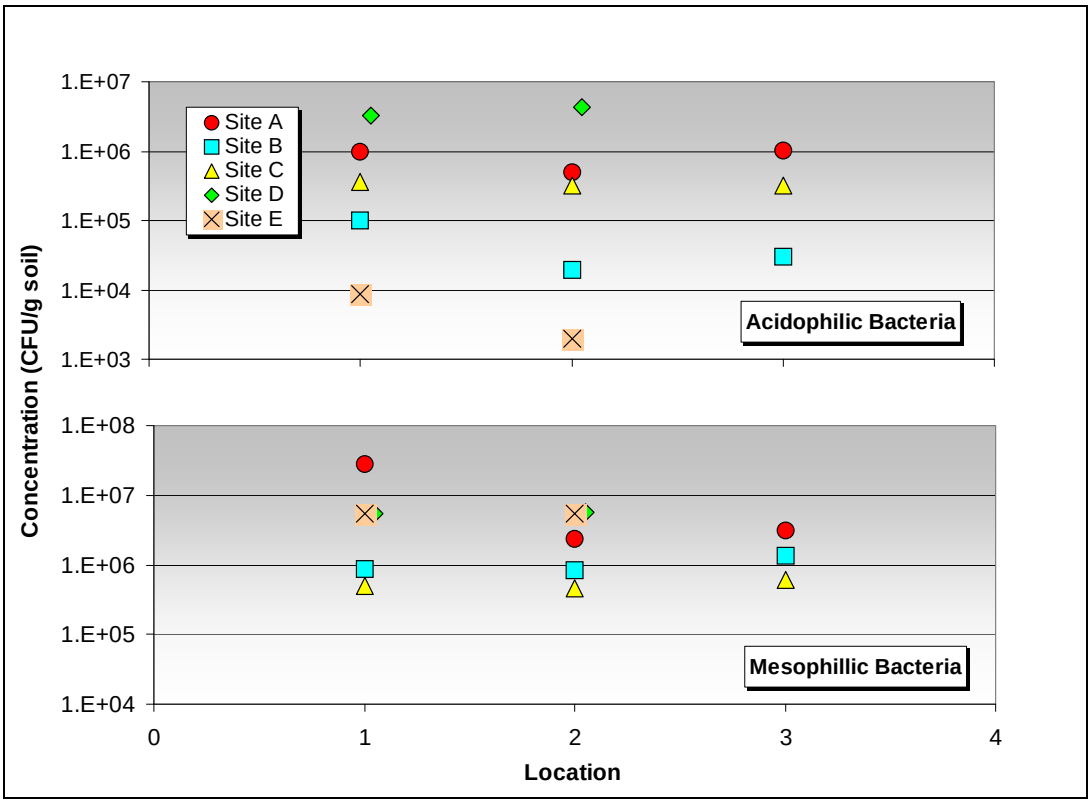

Figure 2. Acidophilic bacteria versus mesophilic bacteria populations.

As part of the microbiological study, fragments of the metal casing were documented photographically at 2X. Fractures and stresses resulting from the explosion during disposal were evident. Fragments were typically 4 to 9 mm thick. Pit depths ranged from 80 to 375 μm. Most pitting occurred within pits. Tunneling was also observed (see comment above). Two items examined had through wall penetration as shown in Figure 3. In Figure 3, sample B-01-MP1

was taken from a M1 anti-tank mine with a metal thickness of 0.159 cm and sample C-05-MP1 was taken from a M22 rifle smoke grenade with a metal thickness of 0.11 cm.

Figure 3. Through wall penetration from two separate UXO samples.

Analyses performed thus far have provided interesting insight into the nature of microbial community dynamics on and around an UXO. No microorganisms were observed on UXO fragments by the ESEM. However, this was most likely due to the nature in which the fragments were treated, i.e., exploded, retrieved and dried prior to microscopic analysis. A viable microbial community was shown to exist in and around the buried UXO. Aerobic microorganisms were found in high numbers both in the soil adjacent to the UXO and on UXO metals. Aerobes were greater than 10^4 cells cm^{-2} or CFU g^{-1} for both. Overall, there were more bacteria present than

fungi; however, fungi were relatively abundant at the sites visited. In addition, high numbers of acid producing bacteria were present on the metal and acid-tolerant bacteria and fungi were readily isolated from the soil. From these data it appears that naturally occurring acid producing microorganisms are the most likely group of organisms to drive corrosion inducing metabolic processes at the sites visited. Sulfate reducing bacteria, another important group of corroders were not found in significant numbers.

Microorganisms require water, nutrients and energy sources. In most subsurface environments, microbial growth is limited by water. The likelihood that microbiologically influenced corrosion will take place is directly related to water availability. Liquid water is needed for all forms of life and influences the distribution and growth of microorganisms. Water availability can be expressed as water activity (aw) with values ranging from 0 to 1.0. Microbial growth has been documented over a range of water activities from 0.60 to 0.998. Fungi are the most desiccant-resistant microorganisms and can remain active down to aw = 0.60, whereas few bacteria remain active at aw values below 0.9. Many soil bacteria may become inactive or form endospores (non-vegetative cells), which are resistant to the effects of desiccation and other harmful environmental conditions, during periods of dehydration or extreme nutrient deficiency. Endospores may remain dormant for long periods. When conditions are favorable, i.e., water is abundant or nutrients plentiful, endospores germinate into actively growing vegetative cells. Therefore, it is possible that some microorganisms cultivated in this study, although present, were not active *in situ* and their growth was stimulated by addition of nutrient rich media in the laboratory.

Microorganisms concentrate at interfaces, including soil/surface interfaces. Competition from other microbial communities, such as the high number of aerobic bacteria, may limit available nutrients in and around the UXO. Changes in pH due to the presence of acid producing bacteria on the metal may also be inhibitory to a variety of soil microorganisms. Most acid producing bacteria are facultative, that is, capable of switching from aerobic to anaerobic respiration. Acid producing bacteria produce organic acids from carbohydrates by a modified, reverse tricarboxylic acid cycle (TCA) during fermentative (anaerobic) growth. In addition, some acid producing bacteria carry out mixed acid fermentation, a complex process in which a carbohydrate is metabolized into several end products (organic acids, alcohol and gas). The type of organic acid produced and the proportion of each, depends upon the species of microorganism as well as the particular carbohydrate being utilized.

The microbial populations measured on the UXO are sufficient to cause localized corrosion. The most likely mechanism is acid production. Microbially induced corrosion of carbon steel is independent of pH over pH values 4.5 to 9.5. In this range, the corrosion products maintain a pH of 9.5 next to the steel surface, regardless of the pH of the solution. At a pH of 4 or below, hydrogen evolution begins and corrosion increases rapidly. Fungi and acid producing bacteria can reduce the pH locally to values below 4.0. The localized corrosion mechanism of the steel fragments was in many cases pitting, with pits inside pits, indicating multiple initiation sites. In other cases tunneling (holes characteristic of microbiological corrosion) was observed. Both types of localized corrosion are consistent with microbiological acid induced corrosion.

Results from this microbiological study were not able to produce any quantitative relationship between the specific microbial methods used and UXO corrosion. However, the results do suggest that microorganisms able to influence corrosion are ubiquitous in the different environments visited. Consequently, the model relies on soil physical and chemical properties, and climate characteristics to estimate corrosion. This assumes that ultimately these soil and climate properties are sufficient to include effects of microbially induced corrosion.

5.2 Presence of Energetics in Soil containing UXO

Introduction. Soil samples were collected when field technicians determined that exposed UXO were potentially high explosive filled. The purpose of this survey was to determine the extent of contamination by UXO and low order detonated ordnance found in soil.

Methods. Samples were collected and analyzed for TNT, RDX as well as degradation products, by-products, and impurities. The specific compounds are listed in Table 1. Compounds listed in Table 1 were analyzed using method 8095, Explosives by Gas Chromatography from SW-846, "Methods for Evaluating Solid Wastes" (USEPA, 2000).

Table 1. Energetic Compounds Tested.

Compound Name	Abbreviation
2-Amino-4,6-dinitrotoluene	2-ADNT
4-Amino-2,6-dinitrotoluene	4-ADNT
1,3-Dinitrobenzene	1,3-DNB
2,4-Dinitrotoluene	2,4-DNT
2,6-Dinitrotoluene	2,6-DNT
1,3,5-Hexahydro-1,3-dinitroso-5-nitrotriazine	DNX
1,3,5-Hexahydro-1-nitroso-3,5-dinitrotoluene	MNX
1,3,5-Hexahydro-1,3,5-trinitrosotriazine	TNX
Hexahydro-1,3,5-trinitro-1,3,5-triazine	RDX
Nitrobenzene	NB
Nitroglycerine	NG
2-Nitrotoluene	2-NT
4-Nitrotoluene	4-NT
Octahydro-1,3,5,7-tetranitro-1,3,5,7-tetrazocine	HMX
Penetaerythritol tetranitrate	PETN
2 n-methyl-n,2,4,6-Tetranitroaniline	Tetryl
1,3,5-Trinitrobenzene	TNB
2,4,6-Trinitrotoluene	TNT

At site E, the only energetic of concern was Ammonium Picrate. Hence samples from Site E were only analyzed for Ammonium Picrate using a modification of USEPA SW-846 method 8330 for both the extraction and analysis (USEPA, 2000).

Results and Discussion. Of the 161 UXO items excavated during this study, 59 were believed to contain high explosive material based upon on-site, expert Explosives Ordnance Disposal (EOD) opinion. Laboratory analyses on samples collected proximate to these items detected energetic material near four UXO items. The detected soil concentrations are provided in Table 2. Soil samples from the other 55 items analyzed contained no detectable level of energetic material. In Table 2, items with the –SC7 suffix refer to samples collected at least 18 inches from the UXO item. Table 2 indicates that energetics were detected in the control samples (-SC7) for items A-01, A-02, and A-03, but not in A-16-SC7. All four of these items were found at Site A and all were 60-mm rounds (approximately 0.46 cm thick). The detection of energetics away from the round suggests the energetic material may have entered the soil from a low-order detonation. In particular, A02 did not detonate loudly with its donor charge when disposed of by the EOD technicians, indicating that it may have been previously torn open. Alternatively, the detections in the –SC7 samples could be a result of cross-contamination from initial excavation of the item prior to collecting soil samples. Subsequent sampling activities in the project stressed the need for care during excavation to eliminate the possibility of cross-contamination. Visual inspection in the field of the rounds with detections did not conclusively find that the rounds had partially detonated. A-02 had the greatest energetic concentrations in soil. The other three items had orders of magnitude less energetic concentrations.

Table 2. Energetic Concentrations in Collected Soil Samples.

ID	RDX	TNT	4A-DNT	2A-DNT	2,6-DNT	2,4-DNT	2-NT
	(ug/kg)	(ug/kg)	(ug/kg)	(ug/kg)	(ug/kg)	(ug/kg)	(ug/kg)
A-01-SC1	8.24 J		11.3 J				
A-01-SC3	8.31 J						
A-01-SC7			8.84 J				
A-02-SC1		672	1104	8200		77	
A-02-SC3		1614	4742	34000	69	250	
A-02-SC7		26.4	293	870			
A-03-SC3							110 J
A-03-SC7							200
A-16-SC3	10.6 J		14.8 J				

J – Values were detected below calibration limits and are reported as estimates.

At site E, where ammonium picrate was used as the fill, no energetics were found in the soil. Six 76-mm rounds were found virtually intact. Two were found to have fuses loose and partially unscrewed; yet no soil contamination was detected.

Four out of fifty-nine potentially high explosive filled ordnance indicated energetic presence in nearby soil. However, given that 60 mm rounds have a casing thickness range of 0.25 to 0.76 cm, potential perforation times could be as early as 64 years based on the maximum corrosion rate found at site A and a non-decaying corrosion rate. This is a very conservative estimate since modeling results indicate that the corrosion rate decreases over time. In any case, it is not inconceivable that some of the energetic presence found at site A was a result of corroded rounds. Other possible sources for the energetics in the soils include low-order detonations and cross-contamination from nearby detonation events. Given the limited nature of the data, it is difficult to conclude the exact nature of the energetic source.

5.3 Results of UXO Corrosion Modeling of Field Data

Introduction. A mathematically based model of UXO corrosion in soil was developed. The following section reports the results from comparison of the field data collected during this study along with a brief overview of the theoretical basis for the model. A comprehensive discussion of the model and its components is presented in Appendix A2.

Model Theory and Development. Phase III of the UXO Corrosion Model (UXO-Corr-Mod III) is based on a variety of initial assumptions and has been developed for aerobic non-calcareous soils. The dominant mechanisms of corrosion of buried UXO are pitting and generalized corrosion. The model estimates rates of corrosion based upon these two fundamental mechanisms. Other corrosion mechanisms are not considered. Pit corrosion is described as a one-dimensional, linear, quasi-steady state transport process. Pitting corrosion rates are determined by successively increasing the pit depth and estimating the time required to reach each depth. The estimation of generalized corrosion is based on pitting factors which are determined within the model.

The fundamental chemical reactions which drive UXO corrosion are assumed to be the oxidation of elemental iron (anodic reaction) and the reduction of gaseous oxygen (cathodic reaction). Thus, anaerobic soils are not currently considered in this model. The anodic reaction is written as:

$$2Fe \rightarrow 2Fe^{2+} + 4e^{-} \quad (1)$$

while the complimentary cathodic reaction is:

$$O_2 + H_2O + 4e^{-} \rightarrow 4OH^{-} \quad (2)$$

Initiation of pitting corrosion occurs when oxygen at the UXO surface creates an electrochemical demand for electrons to drive equation 2. The pit forms as elemental iron is oxidized locally creating an anode (equation 1). This process is illustrated in Figure 4.

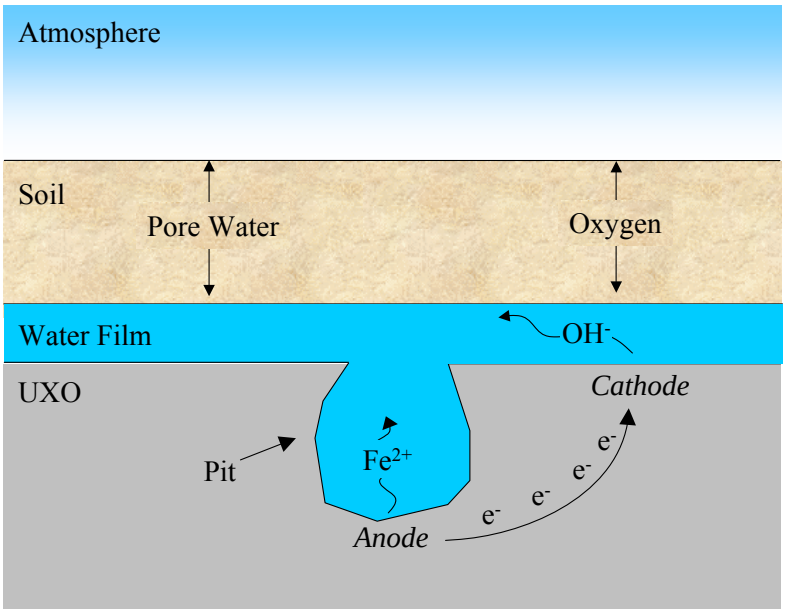

Figure 4. Schematic of newly formed pit with electrochemical anode and cathode.

As the pits grow, hydroxides and ferrous iron accumulate within the pit creating the potential for iron hydroxide precipitates to form. Further, the presence of carbonates and calcium in the soil create the potential for the precipitation of iron carbonate and calcium carbonate. These precipitates eventually form scales at the mouth of the pit which drastically reduce the rates of diffusion of ions (such as ferrous iron and oxygen) in and out of the pit. Schematically this is shown in Figure 5.

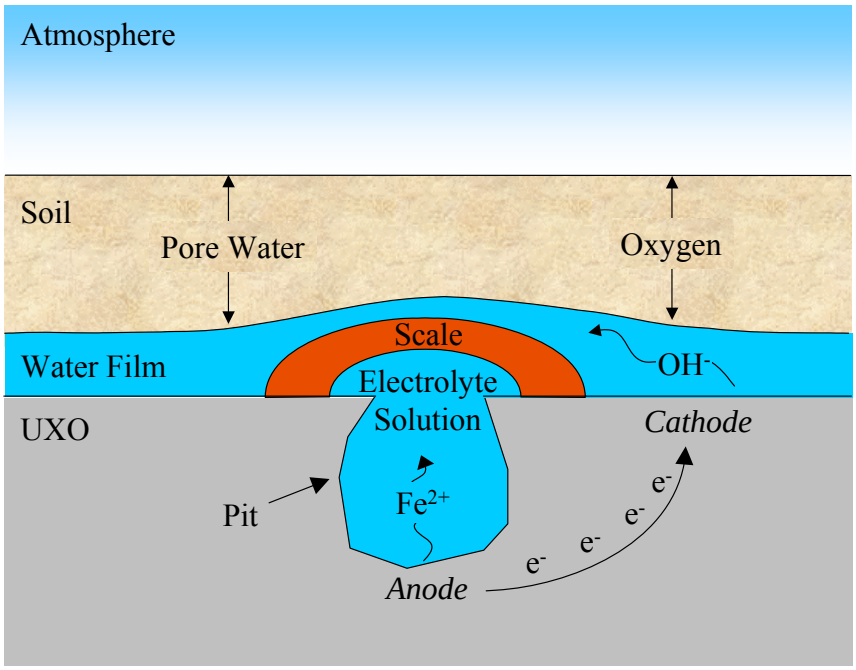

Figure 5. Scale formation over a pit.

Although pitting corrosion dominates the total corrosion rate at the beginning of the corrosion process, generalized corrosion occurs simultaneously. As scales form and reduce the pitting corrosion rate, generalized corrosion begins to impact the total corrosion rate more. Subsequently, at later times, the total corrosion rate is driven largely by generalized corrosion.

UXO-Corr-Mod III is written in Fortran and Visual Basic. The steps involved in the model are presented schematically in Figure 6. The majority of computation are performed in the pitting model. This section of the model calculates fluxes and iron, hydroxide, and common soil chemical components into and out of a growing pit. The pitting model is comprised of an anodic component and a cathodic component. Within the anodic component, ferrous iron flux rates are calculated based on soil chemical properties and equilibrium of common soil chemical constituents (such as carbonates, calcium, iron, organic acids, partial pressure of carbon dioxide, pH, etc.). Similarly, the cathodic components calculates hydroxide flux rates. Soil chemical equilibrium calculations are performed using the Solmineq 88 code (USGS, 1989). The pitting model assumes that the resulting pH values within the pit (from the anodic component) and at the wall of the UXO surface (from the cathodic component) should be in equilibrium. The pH of the two components is iteratively changed until an equilibrium is found between the two

components. Once stable values have been computed within the pitting model, a pitting corrosion rate is determined for a specific pit depth.

Additional factors are applied to this pitting corrosion rate to account for the formation of iron carbonate scales (siderite) and iron hydroxide scales. A pitting factor is calculated in order to determine the generalized corrosion rate. Finally these factors are compiled to produce a total corrosion rate. This total corrosion rate is calculated for successive pit depths in order to determine a corrosion rate profile. These calculations are also used to determine the perforation time for a given UXO thickness.

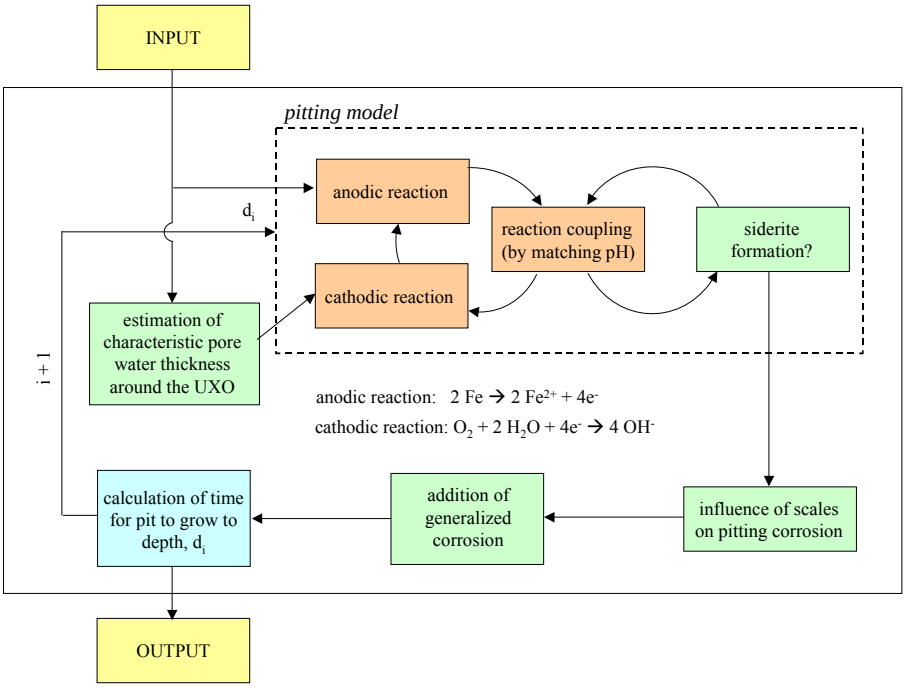

Figure 6. Flow chart of major components in UXO-Corr-Mod III.

Results and Discussion. Results from the field study were used to compare with UXO-Corr-Mod III. 148 data points were tested in UXO-Corr-Mod III. Of the fourteen sites where data was collected, two sites had calcareous soils which UXO-Corr-Mod III is currently not valid for. The next iteration of the UXO Corrosion Model is expected to include calcareous soil conditions.

For each site, samples were inputted into the corrosion model to predict a time to failure for a ¼ inch thick metal casing. The results were averaged for each site to compare with field data (Table 3). For sites where UXO-Corr-Mod is valid, the perforation times vary from 8 years (Site I) to 550 years (Site C). From the field data, time to perforation can not be accurately predicted and estimates of corrosion rates only yield a snapshot of corrosion at one time interval. Since corrosion rate is nonlinear, the maximum pit depth measured at a site was used to compare with model results. The maximum pit depth illustrates the greatest amount of corrosion observed for a given site and thus yields a conservative benchmark to compare the model to. Another factor to be considered in comparing pit depths to perforation times is the exposure time for measured

pit depth. Table 4 and Figure 7 present exposure times for the maximum measured pit depths for each site. With the exception of Sites D, J, Y, and Z, most of the metal had been exposed to corrosion between 40 to 80 years. Figure 8 presents a comparison between maximum pit depth versus predicted perforation time for a ¼ in. (0.64 cm) metal casing.

Table 3. Average predicted time to failure for ¼ in. (0.64 cm) thick metal casing using UXO-Corr-Mod.

Site	Average Time to Failure[1]	Number of data points	Site	Average Time to Failure[1]	Number of data points
	(years)			(years)	
A	170 ± 90	17	H	200 ± 97	8
B	540 ± 340	7	I	8 ± 7	6
C	550 ± 180	9	J	30 ± 26	21
D	calcareous soils	n/a	K	calcareous soils	n/a
E	400 ± 250	3	L	10 ± 5	31
F	760 ± 340	5	Y	540 ± 200	10
G	80 ± 80	10	Z	60 ± 21	21

[1] Confidence intervals based on 95 % confidence.

Table 4. Maximum measured pit depths.

Site	Maximum Measured Pit Depth		Exposure Period	Site	Maximum Measured Pit Depth		Exposure Period
	(mils[1])	(μm)	(years)		(mils[1])	(μm)	(years)
A	83	2.1	57 - 76	H	83	2.1	57 - 63
B	52	1.3	55 - 60	I	88	2.2	54 - 73
C	49	1.2	52 - 61	J	95	2.4	131 - 143
D	20	0.51	34 - 42	K	52	1.3	58 - 64
E	59	1.5	45 - 54	L	70	1.8	56 - 59
F	33	0.84	40 - 49	Y	69	1.7	85
G	43	1.1	56 - 61	Z	94	2.4	10 - 17

[1] mils = 1/1000 inches

The model compares well with maximum measured pit depths for eight of the twelve sites tested with an r^2 of 0.90. For four of the sites, UXO-Corr-Mod III appears to over predict corrosion rates and there underpredict perforation times. These four sites all had average pH values less than 5 suggesting that the model can be sensitive to low pH environments (Table 5). Additional site data is presented in Appendix A1. One other low pH site (Site Z with an average pH of 4.88) had the maximum measured pit from all the study sites and matched the pit trend exhibited by the higher pH sites (Figure 8).

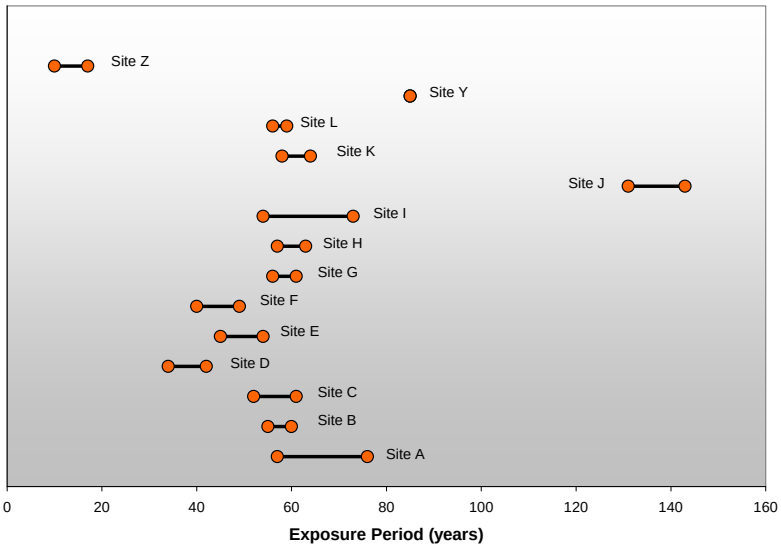

Figure 7. Exposure times for maximum pit depths.

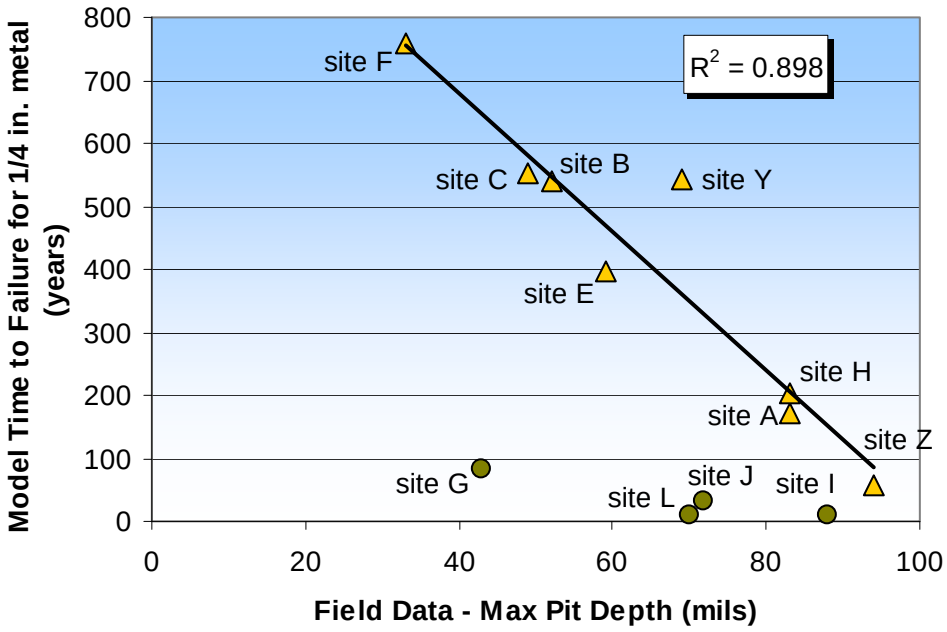

Figure 8. Comparison of UXO Corrosion Model results to field results.

Table 5. Average pH values.

Site	pH[1]	Site	pH[1]	Site	pH[1]	Site	pH[1]
A	5.30 ± 0.48	E	5.92 ± 0.49	I	3.17 ± 2.10	L	3.82 ± 0.19
B	6.08 ± 0.36	F	6.38 ± 0.40	J	4.65 ± 0.17	Y	6.69 ± 0.12
C	5.87 ± 0.31	G	4.72 ± 0.25	K	7.97 ± 0.06	Z	4.88 ± 0.14
D[2]	7.80	H	5.24 ± 0.25				

[1] Confidence intervals based on 95 % confidence.
[2] Only one sample collected at site D.

Additionally, the model can be used to calculate pit depths at a specific time interval. These results were used to compare with measured field data. Table 6 illustrates site averages and ranges for comparison between measured pit depths and modeled pit depths. Table 5 indicates generally poor fits between measured pit depths and estimated pit depths from UXO-Corr-Mod. UXO-Corr-Mod III was developed using data from Romanoff, 1957 and then calibrated with data from Site Z. With the exception of two datapoints, all samples were buried 21 years in soil or less. Figure 9 contrasts a younger UXO sample from site Z with an older UXO sample from site A. This suggests that UXO-Corr-Mod overestimates corrosion rates at time scales greater than 20 years. This attribute of the model is the primary focus of the next version of UXO-Corr-Mod and is presently under development.

Table 6. Comparison of UXO-Corr-Mod with measured pit depths.

Site	Average (% difference)	Range of model fits (percent difference)	Site	Average (% difference)	Range of model fits (percent difference)
A	120 ± 40	55 - 190	H	190 ± 200	56 - 460
B	210 ± 90	150 - 330	I	80 ± 20	50 - 120
C	270 ± 170	160 - 440	J	160 ± 16	140 - 190
D	calcareous soils		K	calcareous soils	
E	190 ± 13	180 - 200	L	370 ± 260	85 - 840
F	570 ± 230	320 - 870	Y	180 ± 45	140 - 240
G	430 ± 410	190 - 1100	Z	70 ± 60	5 - 160

Table 3 also illustrates the high degree of variability in model results for most of the sites. Coefficients of variation (CV, standard deviation divided by average) are compared between the model predictions, corrosion measurements, and other soil parameters (Table 7). Soil physical parameters such as porosity and moisture content are relatively stable in soil with low CVs ranging from 8 to 75 % (porosity) and 23 to 96 % (soil moisture content). Model results appear to have CVs similar to soil chemical parameters. CVs for model data range from 51 to 206 % for the various sites. Soil chemical parameters such as calcium, total carbonates, and sodium also exhibit high degrees of variation (Table 7).

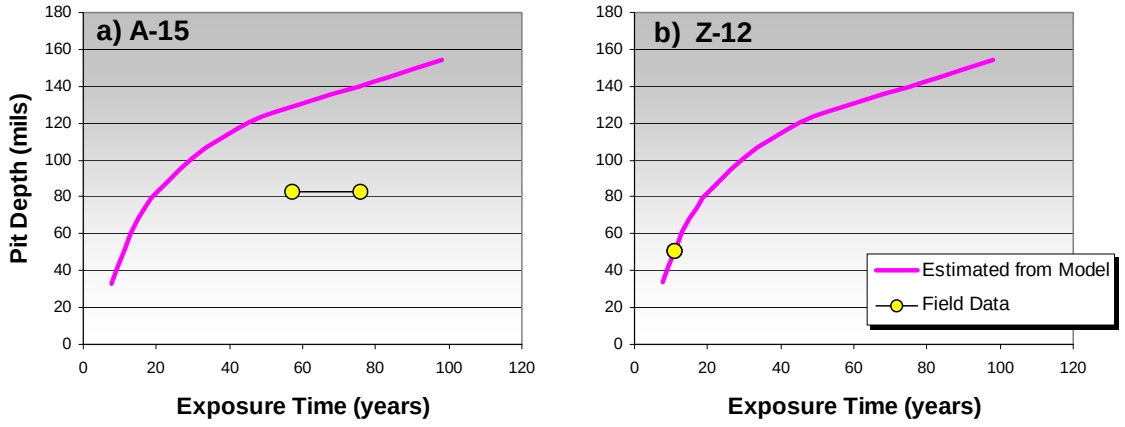

Figure 9 Model estimations of pit depth compared to measured pit depth. a) Sample A-15, b) Sample Z-12.

Table 7. Coefficients of Variation for selected parameters.

site	model[1]	max. pit depth[2]	calcium	carbonates[3]	moisture content	organic acids	pH	porosity	sodium
A	113	55	195	112	35	61	19	16	30
B	85	50	156	58	96	37	8	14	100
C	51	44	154	83	64	111	8	25	10
D[4]	n/a	n/a	n/a	n/a	n/a	n/a	n/a	n/a	n/a
E	56	96	27	60	27	22	7	13	15
F	52	50	38	55	54	35	7	11	3
G	154	61	55	n.d.[5]	46	0	8	17	9
H	69	44	40	157	30	36	7	22	100
I	113	26	217	275	76	109	83	75	125
J	206	35	149	253	27	14	9	10	42
K	n/a[6]	46	20	32	42	22	2	8	28
L	150	68	80	n.d.	42	79	14	19	27
Y	59	29	27	60	36	32	3	8	190
Z	82	40	67	110	23	113	7	19	6

[1] Model column refers to CV for time to failure predictions for a ¼ in. metal casing.
[2] Maximum pit depth of measured field data
[3] Carbonates includes the sum of bicarbonate and carbonate ions.
[4] Site D had only one data point.
[5] n.d. is not detected
[4] Site K has no model results since soils were calcareous.

The results of this testing illustrate that the model reasonably predicts corrosion rates and perforation times for periods less than 20 years. At longer time intervals, the model over estimates corrosion rates and under estimates perforation times. The model is currently valid for aerobic, non-calcareous soils. For pH values less than 5, UXO-Corr-Mod III greatly over estimates corrosion rates and subsequently produces unrealistically short perforation times. Additionally, a high degree of site variability was observed due to spatial heterogeneity of soil chemical properties which can yield a high variability in the model results. Subsequently, several soil samples should be collected in order to adequately assess the corrosive nature of a site.

The current version of UXO-Corr-Mod is deterministic in calculating a single specific perforation time and corrosion rate profile for a given data set. However, this calculated time is assumed to be the earliest time at which a round perforates. After the initial pinhole perforation, rounds will continue to corrode increasing the number of perforations. Therefore a significant release of energetics will not occur until an additional period of time passes after the initial perforation time. As such, the results of UXO-Corr-Mod III are considered conservative and results from this version should be used to assess qualitative risks from UXO.

5.4 Results of Transport modeling

Introduction. Once a UXO has become perforated in some way (via corrosion, cracking on surface, or low order detonation) it is important to understand how energetics move into groundwater. An energetics transport model has been developed which estimates groundwater loading of energetics buried in soil. The results of the model provide detailed groundwater concentration profiles, maximum groundwater concentration, and average groundwater concentration exiting the range. A detailed presentation of the model is found in Appendix A4.

Model Theory and Development. The purpose of the model is to provide an order-of-magnitude estimate for the maximum energetic groundwater concentration resulting from a UXO release. The model has four components. The first component describes the mass transfer of energetics out of a single corroded UXO and into the surrounding soil. The second component extends the single item solution to multiple items over the area of a range. The third component is a model for the energetics transport through the vadose zone down to groundwater. The final component is a groundwater transport model describing the migration of energetics through an aquifer. A depiction of the system is shown in Figures 10 and 11.

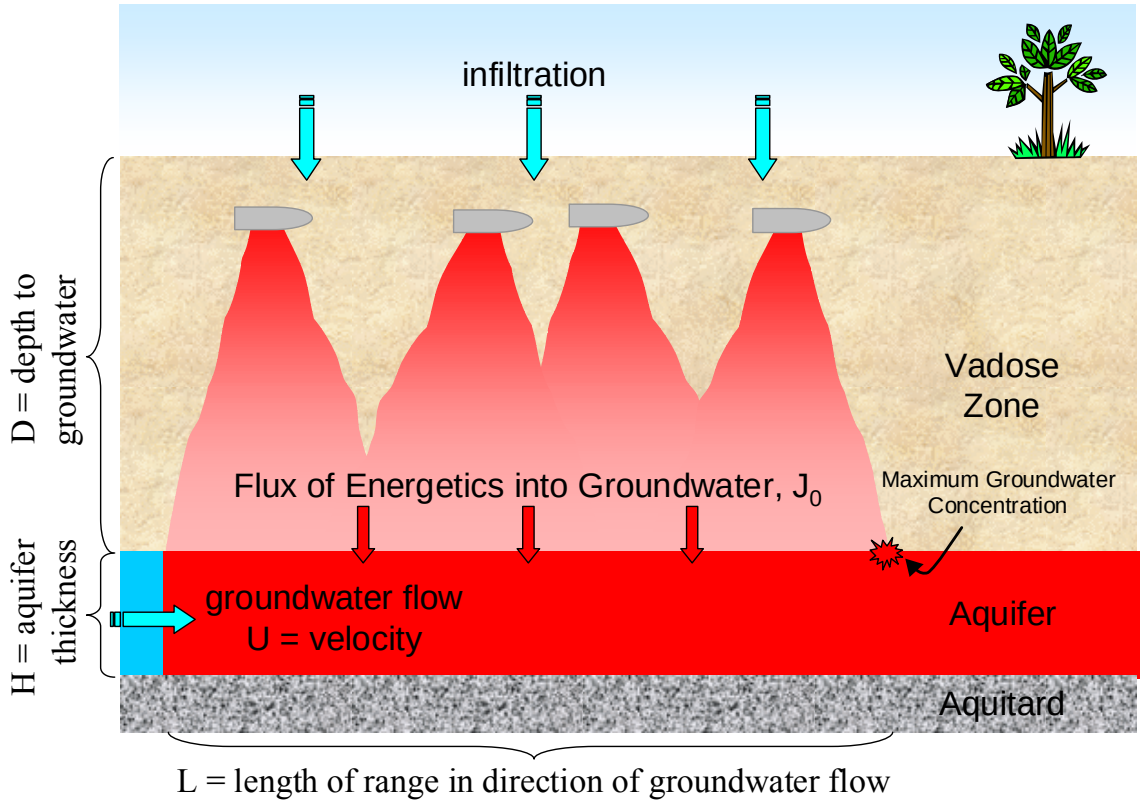

Figure 10. Description of Energetics Transport from UXO into Groundwater

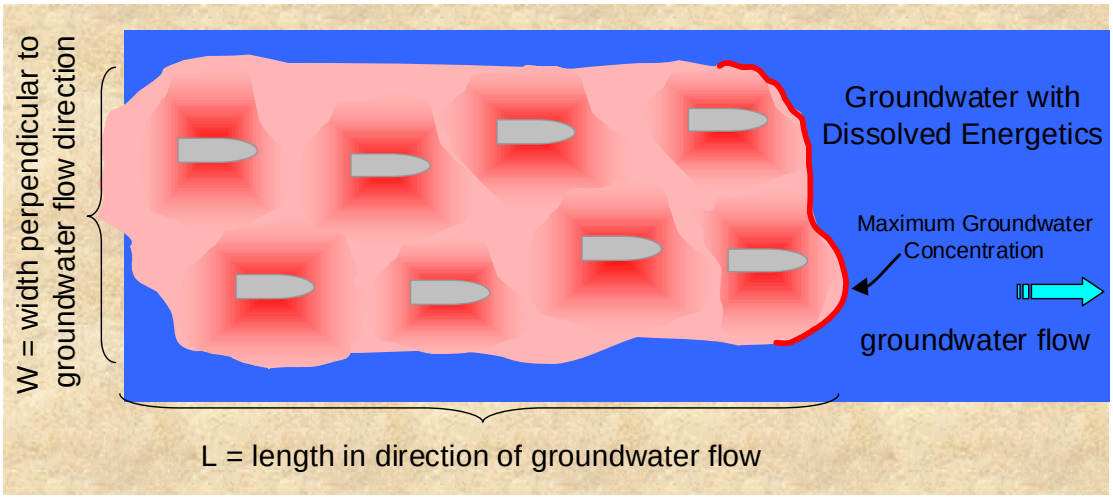

Figure 101. Plan View of Energetics Transport from UXO into Groundwater

The model requires inputs which characterize:

- the range characteristics (number, type and distribution of high explosive UXO over the area of concern),
- the soil physical properties (moisture content, porosity, etc.),
- the hydraulic characteristics (infiltration rate, groundwater velocity and aquifer thickness), and how the energetics are buried in soil (bare, partially exposed, etc.).

The model is summarized in Figure 12.

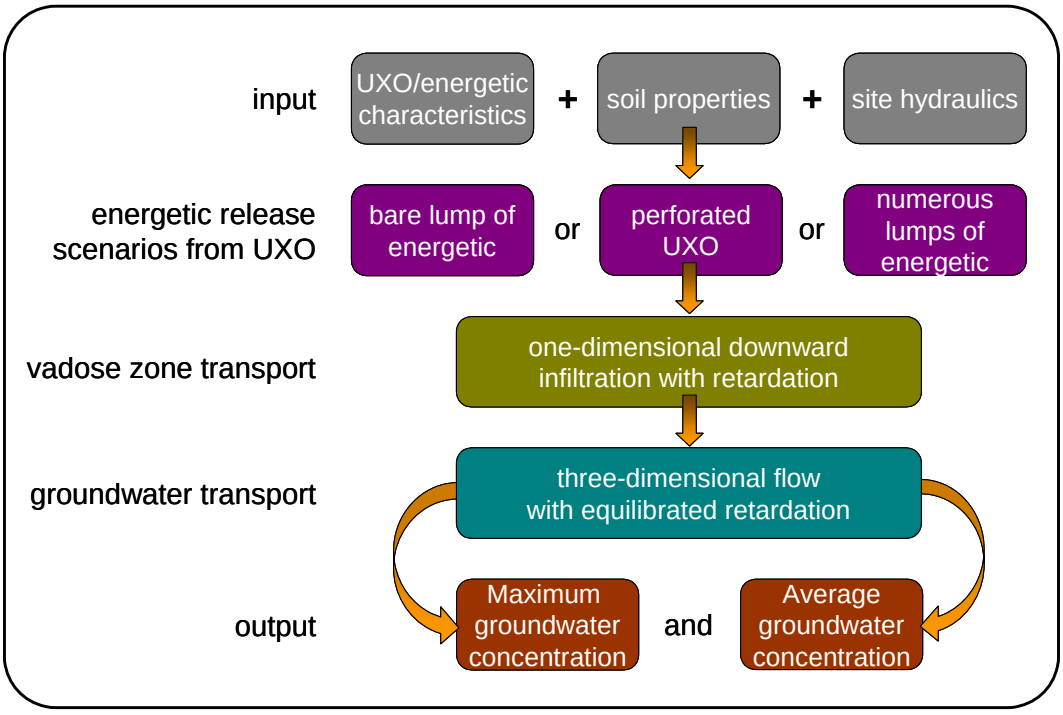

Figure 112. Flowchart for the UXO Energetics Transport Model

Results and Discussion. The model was used to estimate release of energetics into the soil and eventual potential groundwater concentrations. Three scenarios were used to estimate release of energetics into soil. The first scenario conservatively assumes a sphere with a diameter of 3.8 cm (1.5 inches) of Composition B (60% TNT, 40% RDX) is present in soil. Figure 13 shows the release rate for a soil with 21.8 % volumetric water content as a function of infiltration rate. During long periods where no precipitation occurs, the infiltration rate drops to zero and diffusion dominated mass transfer occurs where the mass release rate of RDX reduces to 0.15 grams/year and TNT reduces to 0.83 grams/year.

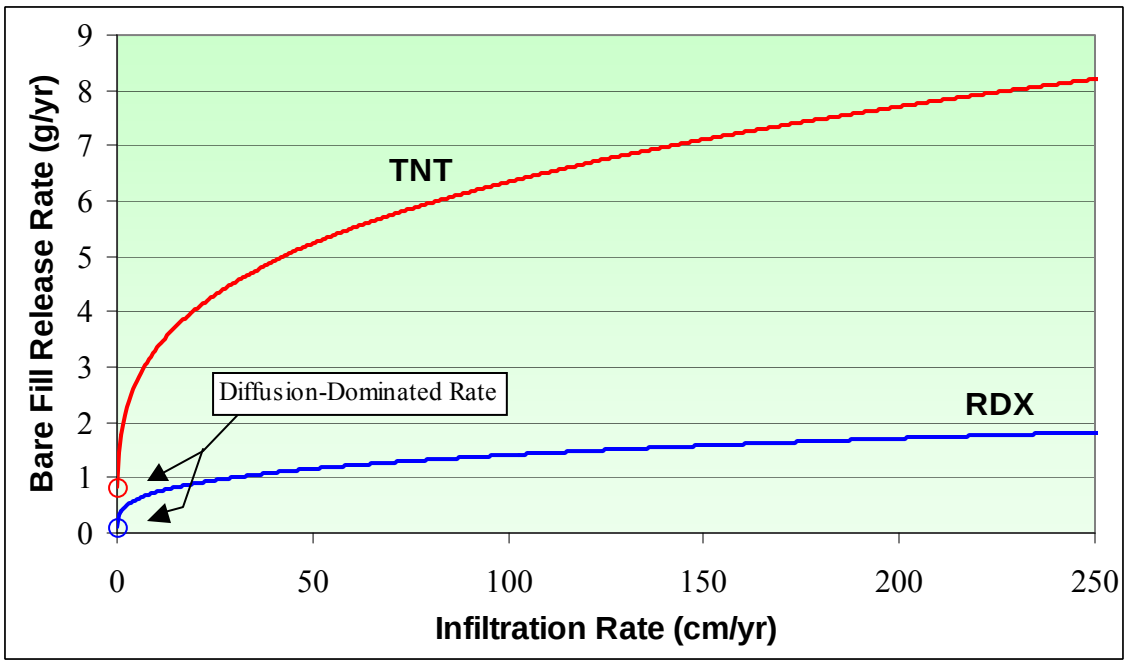

Figure 12. Mass Release Rate as a Function of Infiltration Rate for Bare Fill

A more realistic scenario of pitted UXO was also modeled assuming a uniform distribution of perforated holes on a UXO surface. After the eventual failure via corrosion of the UXO shell, water is imbibed by capillary suction into the very thin gap between the explosive fill and the metal shell casing. Molecular diffusion of the energetic material from the fill to the outer surface of the shell through water adds a mass transfer constraint. The mass transfer correlations presented for a bare object remain applicable; however, the surface solute concentration of energetic is no longer at the solubility limit. From the UXO corrosion study, the average pit density for all the items measured was 7.3 pits per square centimeter of shell surface. A typical radius for the pit is assumed to be 0.05 cm (0.02 inches) yielding a cumulative area for the pits of about 6% of the total shell area. Mass release rates for diffusion through these pits as a function of infiltration rate are illustrated in Figure 14 assuming a shell thickness of 0.46 cm (e.g., 60-mm mortar). Even at relatively low infiltration rates (less than 50 cm/yr), the mass release rate is dominated by energetic diffusion through the perforating pits. For infiltration rates over 50 cm/yr (20 in./yr), the mass release rates of RDX and TNT approach 0.14 and 1.2 grams per year, respectively. The RDX value is significantly less than the TNT value because the RDX diffusion

coefficient in water is about one third of the TNT diffusion coefficient. For infiltration rates approaching zero such that mass transfer from the shell to soil is dominated by diffusion, the mass release rates of RDX and TNT are about 0.07 and 0.5 grams per year, respectively. Under most scenarios, the mass release rate from corroded UXO with perforating pits will be dominated by diffusion through the pits and is strongly dependent on the number of perforating pits, the diameter of the pits, and the thickness of the shell.

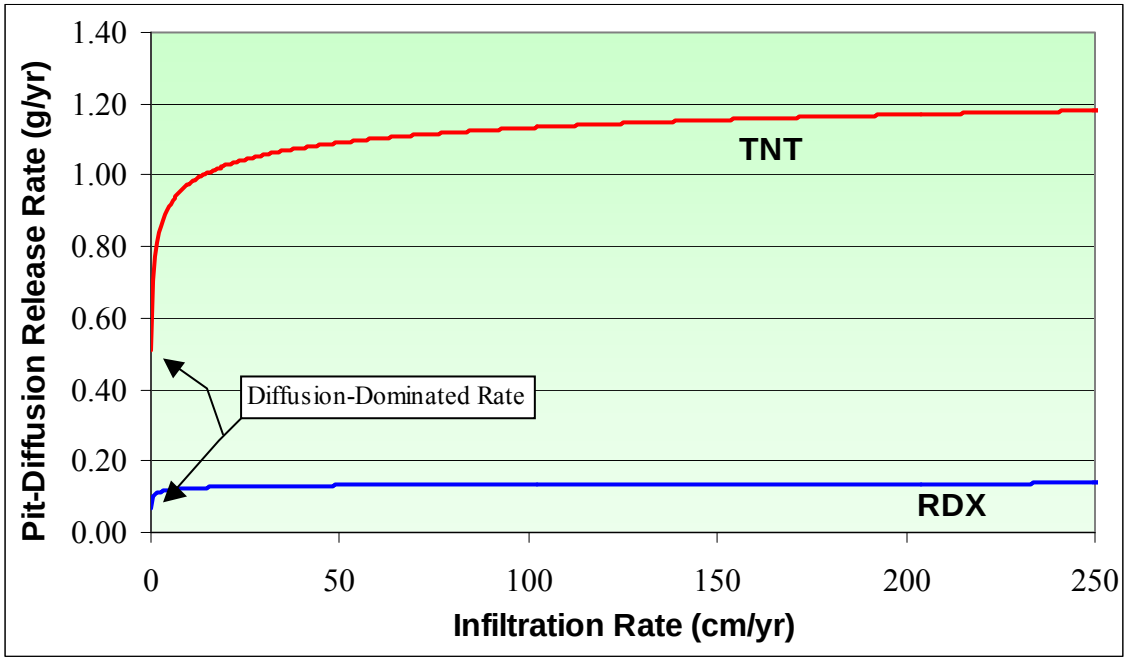

Figure 13. Mass Release Rate as a Function of Infiltration Rate for Corroded UXO Shell

A more speculative worst case for energetics leaching than a single bare volume of fill considers mass transfer by advection and diffusion from a completely corroded UXO with the fill disarticulated into many small, spherical lumps. The mass release rate of TNT is higher than RDX and can yield the disarticulation of the fill as the TNT holding the fill together is preferentially dissolved away. This action can leave many small lumps of RDX. Figure 15 illustrates the release rate from 600 grams of RDX in porous soil at various RDX particle sizes. The nominal construction of some CompB calls for mixing 0.04-cm (0.016-inch) RDX grains into molten TNT, so lump sizes at the far left of the figure may not be unrealistic after thorough corrosion of the shell and thorough erosion of TNT from the CompB. However, for a nominal initial mass of 600 grams, this grain size corresponds to over 500,000 tiny “lumps” and this number will not act independent of one another. The radius of 3.8 cm corresponds to roughly a single lump and the mass releases shown for various infiltration rates are consistent with the results presented in Figure 13 for bare fill.

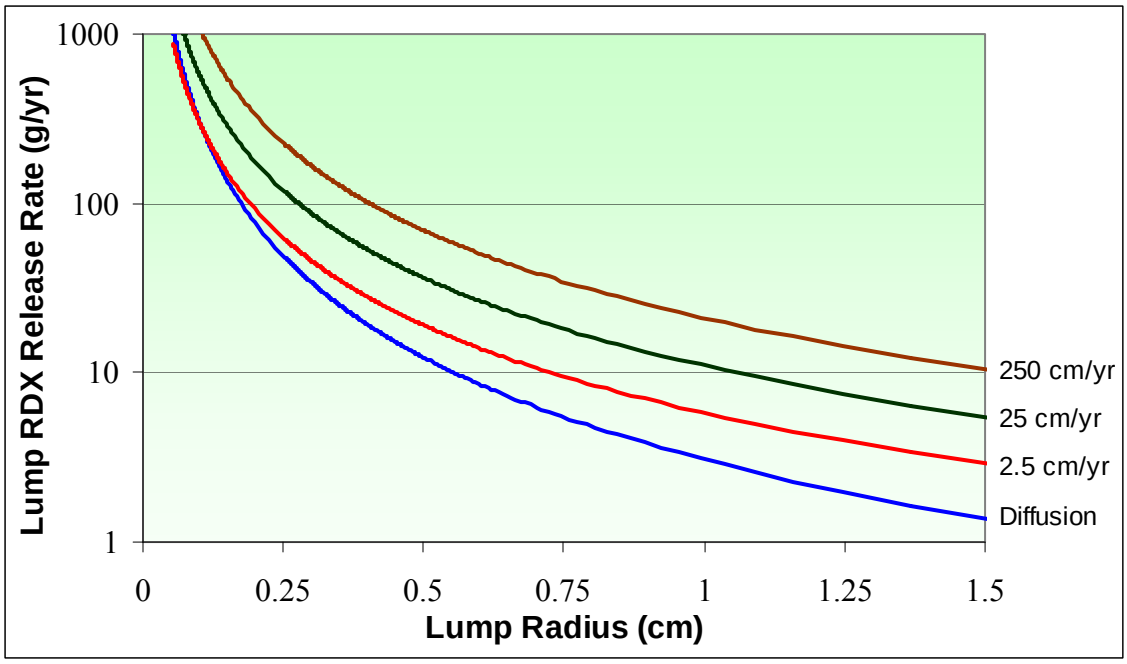

Figure 14. RDX Release Rate as a Function of Lump Size and Infiltration Rate for Bare, Disarticulated Fill

In most correlations for mass transfer, the flow rate over the buried object is assumed to be steady. However, rainfall is generally very episodic, i.e., it occurs infrequently for short durations. Below the soil surface, the soil tends to smooth out the infiltration rate such that the infiltration rate can be relatively steady at depths greater than 3 meters (10 feet). However, UXO are generally found from the soil surface down to a depth of about 30 cm (one foot) and rarely below 90 cm (three feet). Hence, the infiltration of water past most UXO items is highly transient. In addition, the correlation for the advectively-dominated mass transfer coefficient depends non-linearly on the water infiltration rate in the soil. Subsequent use of an average annual infiltration rate is highly conservative in comparison to using a transient, episodic infiltration rate. This is illustrated in Figure 16 where the conditions for Figure 13 are repeated except an annual infiltration rate of 93 cm/yr (36.5 in./yr) is assumed. Figure 16 shows the decreasing mass release rate with decreasing frequency of precipitation events. As the frequency of precipitation events decreases, then the intensity of each event increases so that the total annual infiltration (93 cm/yr) is conserved. The “Transient / Steady Mass Release” axis is a ratio of mass release rates between transient and steady infiltration conditions. The left hand side of the plot represents all precipitation occurring in a one-day-a-year event and the mass transfer is less than 20% of the total mass release rate if the infiltration was averaged over the entire year. If infiltration occurs only one-third of the days during the year, then averaging the infiltration over the entire year yields a mass release rate double the actual value. Hence, UXO energetic mass release rate calculations should use infiltration rates at the highest available precipitation sampling frequency.

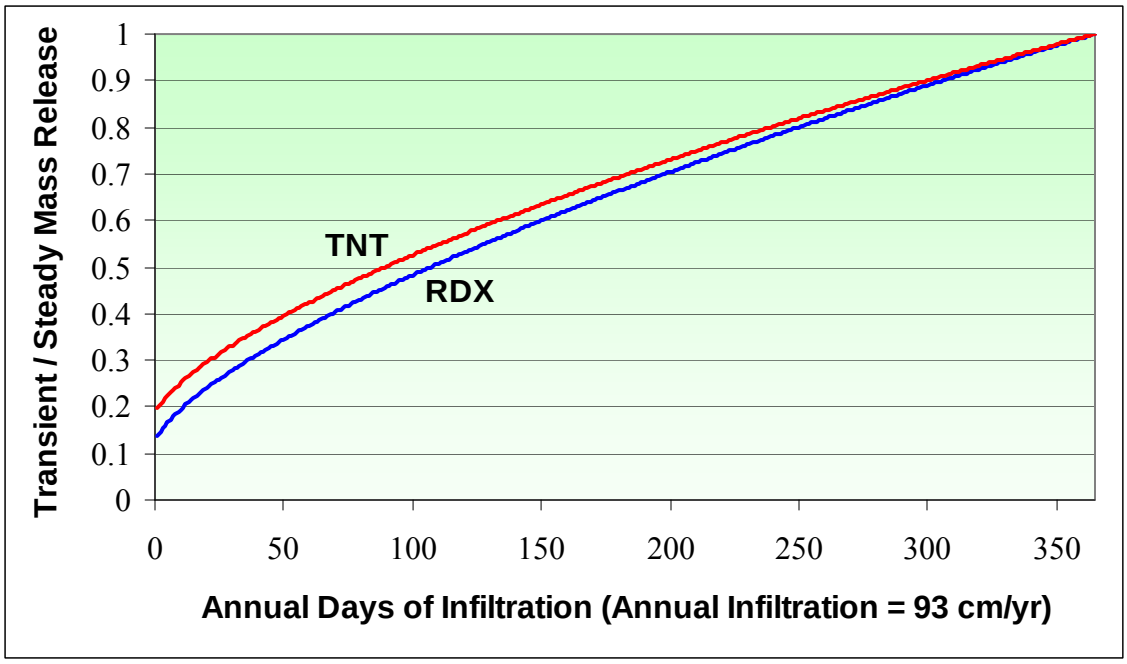

Figure 15. Comparison of Mass Release Rates Using an Annual Average Infiltration Rate (Steady) versus Transient Infiltration Data

These results of mass release rates are utilized as source terms for a vadose zone transport model where the energetics transport model is extended through the vadose zone to the interface with underlying groundwater. The vadose zone model assumes infiltration rates are steady which is generally valid for depths greater than 3 meters below the soil surface. In addition, the vadose zone is assumed to consist of soil with uniform physical and chemical properties. Currently, only one item is included in the model. Multiple items can easily be incorporated into the solution.

Assuming typical retardation coefficients for RDX and TNT as 1.3 and 4, respectively, an infiltration rate of 50 cm/yr (20 in./yr) and a depth to groundwater of 6 meters (20 feet), the time to reach groundwater for RDX would be about 16 years. Under similar conditions, TNT would require almost 50 years. TNT is known to degrade in soil. RDX degrades more slowly than TNT. Hence, if the travel time to groundwater is long, then a significant proportion of the energetic may degrade in the vadose zone and the impact to groundwater will be reduced. The estimated half-life of TNT in soils ranges from 1 to 6 months. This estimate was made on the basis of the estimated unacclimated aqueous aerobic biodegradation half-life (Howard et al. 1991). In laboratory tests by the EPA with sandy loam and sandy silt loam soils, the aerobic degradation half-life of TNT was determined to be only 5.7-7.7 days (EPA, 1989). Hence, values vary from site to site and range from 1 week to six months. Therefore, the degradation constants vary from 0.0038 day^{-1} to 0.1 day^{-1}. For a typical retardation coefficient of 4 and an infiltration rate of 50 cm/yr, the slow degradation constant suggests very little TNT will reach groundwater. However, degradation is highly site-specific. In a recent study, half-lives for RDX were calculated from first-order rate constants for three soils measured in the laboratory and varied from 94 days to 154 days (Jenkins et al., 2003). The site-specific half-life of RDX was

estimated in a lagoon 50 cm deep to range from over 2,000 days in winter to 456 days in summer (Army 1983). For a typical RDX retardation coefficient of 1.3 and an infiltration rate of 50 cm/yr, the slow degradation constant [i.e., ln(2)/2,000 days = 0.00035 day^{-1}] suggests little RDX will reach groundwater if the depth to groundwater exceeds three meters. As stated above, degradation is highly site-specific and laboratory measurements may not be directly applicable to field conditions.

Once the model determines energetic loading into groundwater at the top of the water table, calculations are made which determine the potential impact of UXO energetic release on underlying groundwater. As indicated, the degradation of energetics in the vadose zone can profoundly reduce the impact on underlying groundwater; however, for the present estimates the degradation is neglected. Degradation rates are highly site-specific and difficult to measure and neglecting degradation yields conservative estimates for the impact on groundwater. The resulting groundwater concentration varies linearly with the groundwater velocity, thickness of the aquifer, length of the range, and density of UXO items covering the range. These parameters are often difficult to estimate without a significant and varied field investigation. The mass release rate is a function of the infiltration rate, soil moisture content, energetic diffusion coefficient in water, energetic solubility in water, explosive fill geometry, and degree of perforating corrosion pits. All of these parameters can be estimated such that reasonable estimates for the energetic release rate from a corroded UXO can be obtained.

Example results for the corrosion study sites are presented in Tables 8 and 9 for 1-kg of CompB in the shape of a cylinder with a radius of 3.8 cm. For these results, the density of UXO items on the range is assumed to be 100 high explosive UXO items per square kilometer with a range length of one kilometer. The groundwater velocity and aquifer thickness are assumed to be 30 meters per year and 5 meters, respectively. These values are applied to all sites since no site-specific information was available. In this hypothetical UXO scenario, four of the ten sites had the potential to exceed groundwater standards for TNT (i.e., 0.002 mg/L) after thorough corrosion leaves bare explosive fill and none of the sites exceeded the standards for RDX. None of the scenarios exceeded groundwater standards when diffusion through perforating pits was included. The release rate of RDX is generally an order-of-magnitude less than TNT because of its lower solubility and lower diffusivity in water than TNT.

For TNT to exceed the groundwater standards under the pitting release scenario, the density of UXO items would generally have to approach 400 items per square kilometer and for RDX to approach the standards the density would need to be about 4,000 items per square kilometer. To illustrate this point, the results for Site B are plotted as a function of item density in Figures 17 and 18 for RDX and TNT, respectively. The plots include results assuming steady infiltration, periodic infiltration, and pit diffusion.

Table 8. Potential RDX Concentrations in Groundwater at Corrosion Study Sites.

Site[1]	Annual Infiltration Rate, I	Moisture Content, θ	Annual Days of Precip.	Individual Mass Release Rate		Average Groundwater Concentration	
				Bare Fill	Pitted	Bare Fill	Pitted
	(cm/yr)	(%Vol)	(Days)	(g/yr)	(g/yr)	(mg/L)	(mg/L)
A	16	19.3	149	0.60	0.081	0.0004	0.00005
B	3.3	7.5	133	0.87	0.075	0.00058	0.00005
C	13	7.8	157	1.50	0.094	0.0010	0.00006
D	1.8	21.8	196	0.37	0.091	0.00025	0.00006
E	1.0	11.8	175	0.51	0.088	0.00034	0.00006
F	1.0	2.4	151	1.97	0.080	0.0013	0.00005
G	15	23.6	160	0.52	0.084	0.00035	0.00006
H	22	15.8	155	0.78	0.082	0.00052	0.00006
I	2.5	19	149	0.40	0.083	0.00027	0.00006
Z	26	22.5	189	0.67	0.091	0.00044	0.00007

[1] Results for Sites J, K, L, and Y were not obtained.

Table 9. Potential TNT Concentrations in Groundwater at Corrosion Study Sites.

Site[1]	Annual Infiltration Rate, I	Moisture Content, θ	Annual Days of Precip.	Individual Mass Release Rate		Average Groundwater Concentration	
				Bare Fill	Pitted	Bare Fill	Pitted
	(cm/yr)	(%Vol)	(Days)	(g/yr)	(g/yr)	(mg/L)	(mg/L)
A	16	19.3	149	2.9	0.71	0.0019	0.00047
B	3.3	7.5	133	4.2	0.68	**0.0028**	0.00045
C	13	7.8	157	6.9	0.84	**0.0046**	0.00056
D	1.8	21.8	196	1.8	0.74	0.0012	0.00049
E	1.0	11.8	175	2.5	0.75	0.0017	0.00050
F	1.0	2.4	151	9.1	0.73	**0.0061**	0.00048
G	15	23.6	160	2.6	0.73	0.0017	0.00048
H	22	15.8	155	3.7	0.73	**0.0025**	0.00048
I	2.5	19	149	2.0	0.70	0.0014	0.00047
Z	26	22.5	189	3.2	0.78	0.0021	0.00052

[1] Results for Sites J, K, L, and Y were not obtained.

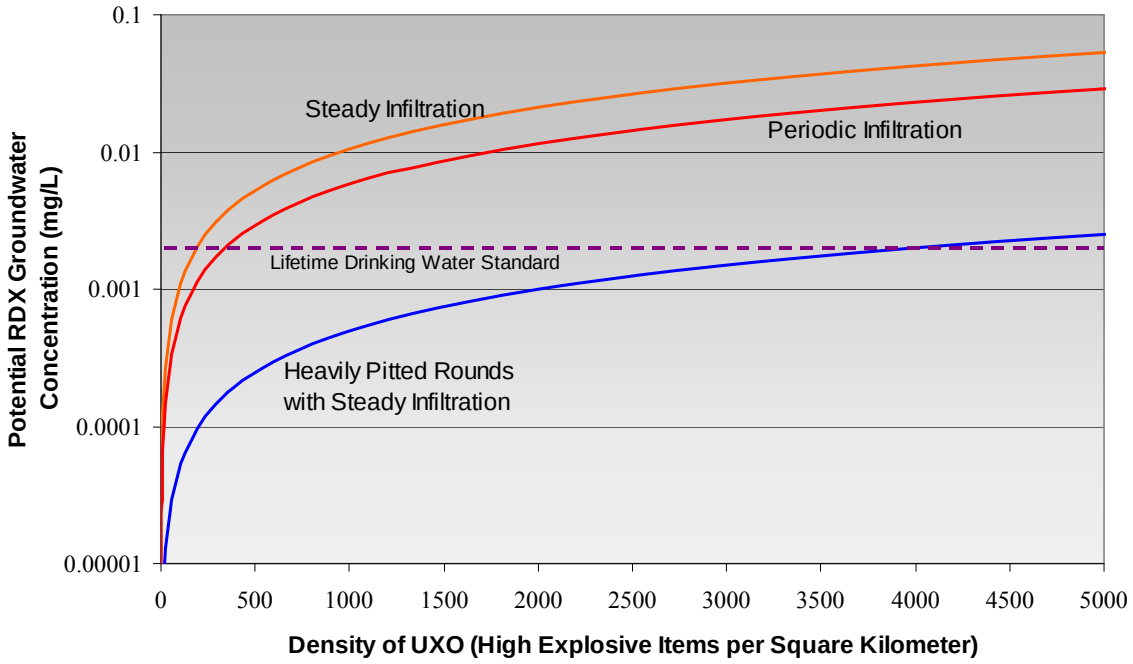

Figure 16. Potential RDX Groundwater Concentrations as a Function of UXO Density for Site B

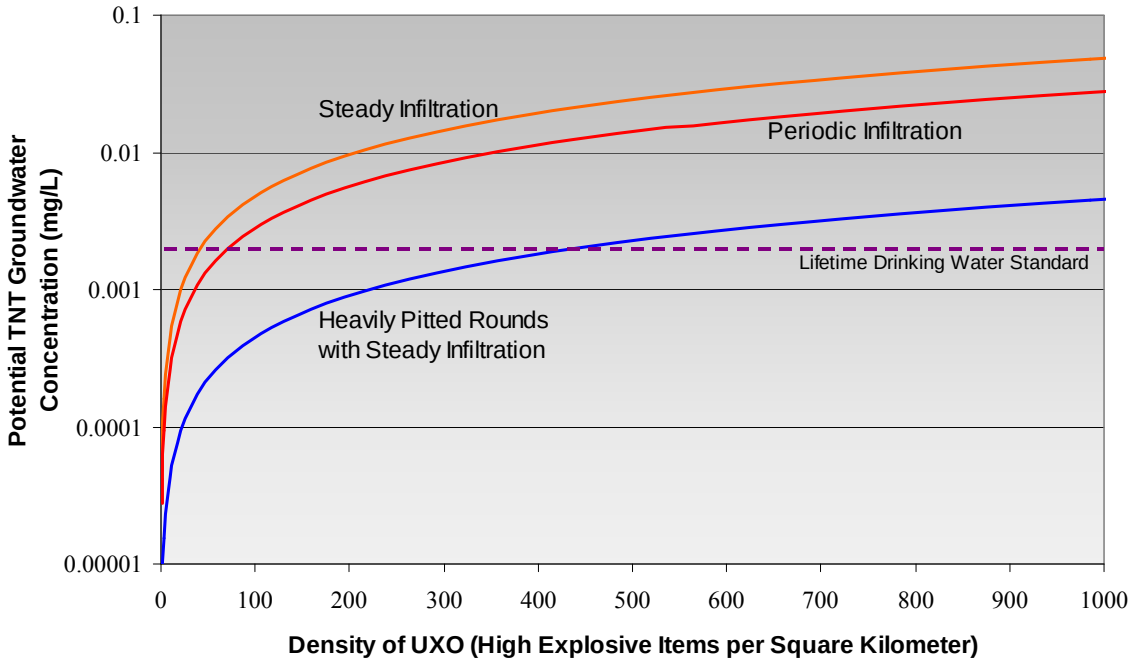

Figure 17. Potential TNT Groundwater Concentrations as a Function of UXO Density for Site B

6 Conclusions.

This study of UXO Corrosion in Soil has produced several useful tools, a sampling protocol, a database of soil, climatic, and corrosion measurements, a UXO corrosion model, and an energetic release to groundwater transport model. The sampling protocol is simple and efficient and enables the collection of samples for corrosion analyses as well as energetic soil contamination. This protocol could easily be integrated into current range maintenance practices to quantify potential environmental risks.

Fourteen different sites were visited resulting in sampling of 161 items which were analyzed for soil characteristics and extent of corrosion. Items collected had been buried over a large interval of time from Civil War era rounds to rounds deposited during the 1990's. Corrosion of metal samples was quantified in terms of pitting corrosion and generalized corrosion. Although more than thirty different soil and climate parameters were measured for each individual item sampled, only rainfall and variables associated with rainfall and arid environments (such as temperature, volumetric water content, alkalinity, texture, etc.) showed any correlation to pit depth. The average maximum pit depth for samples found in areas with annual rainfall less than 50 cm/yr was 560 ± 120 μm (22 ± 5 mils with 95 % confidence). Samples from sites with annual rainfall rates greater than 50 cm/yr had a slightly higher average maximum pit depth of 970 ± 90 μm (38 ± 4 mils with 95 % confidence). The distribution of maximum pit depths was much greater for samples collected from non-arid sites than from arid sites. These results indicate that areas with low rainfall generally produce less corrosive conditions.

The thickness of the UXO sampled ranged from 0.076 to 6.4 cm (30 to 2500 mils). No sample had a measured maximum pit depth greater than 0.25 cm (100 mils). This suggests that within 150 years, corrosion processes will penetrate less than 0.25 cm. Although several rounds showed indications of perforations during analysis, all perforated rounds sampled were less than 0.25 cm thick. However when UXO items were blown in place, the remaining fragments accounted for a small fraction of the original UXO. In these cases, it is possible that perforated regions were completely destroyed due to their fragile condition.

Of the 161 items sampled, only three samples appeared to be cracked or partially detonated. The remaining 158 items were either intact unexploded ordnance or metal fragments from fully detonated rounds. During the course of field sampling expert explosive ordnance disposal teams searched and excavated soil in order to make field distinctions on the types of rounds encountered and what kind of safety hazards were present. This led field technicians to differentiate between UXO and low order detonations. Low order detonated rounds expose energetic material to the soil without the time lag which occurs as UXO corrode. Subsequently these low order rounds present environmental risks much earlier than UXO which must first wait for metal containers to corrode before leaking explosives into the environment.

Another important observation made during field activities is the extent of corrosion which occurred on the upward facing portion of a UXO (topside) versus the downward facing portion of a UXO (bottom). Results indicated that buried items corrode more rapidly on their bottom. This effect is likely the result of differences in matric forces between the soil and UXO combined with evapotranspiration. Since the capillary suction of water is less on the UXO

surface than overlying soil, water would tend not to accumulate on the upper side of the UXO surface except under conditions of high hydraulic head such as high rainfall environments. On the underside of the UXO, however, water would be expected to accumulate at the interface between the UXO and underlying soil due to the air entry potential of the soil.

The current version of the UXO Corrosion Model is a useful tool to qualitatively assess the corrosive nature of a site. Perforation times are calculated by the model to assess the environmental risks posed by specific rounds at specific sites. As described in section 5.3, the model's results are highly variable for a given site. Therefore, it is strongly recommended that a significant number of soil samples be collected which represent all areas of a specific range before assessing the corrosion rate. These samples should be analyzed for the variety of parameters required for the model's input. The model is currently valid for aerobic, non-calcareous soils. For pH values less than 5, UXO-Corr-Mod III over estimates corrosion rates and subsequently produces highly conservative perforation times. UXO-Corr-Mod produces a single specific perforation time and corrosion rate profile for a given data set. However, this calculated time is assumed to be the earliest time at which a round perforates. After the initial pinhole perforation, rounds will continue to corrode increasing the number of perforations. Therefore a significant release of energetics will not occur until an additional period of time passes after the initial perforation time. As such, the results of UXO-Corr-Mod III are considered conservative and results from this version should be used to assess qualitative risks from UXO.

Range managers evaluating risks associated with environmental contamination by UXO must consider the impacts of fractured and low order detonated UXO as well as corroding UXO. The ground surface may be rocky and tend to crack open rounds upon impact. Additionally, specific rounds with higher potentials to partially detonate may be in use or have historically been used at a site.

An energetic transport model has been developed which determines release rates of TNT and RDX from Composition B into soil. The model uses the calculated release rates as source terms in the vadose zone and calculates transport through the vadose to the groundwater table. Once the model determines energetic loading into groundwater at the top of the water table, calculations are made which determine the potential impact of UXO energetic release on underlying groundwater. As indicated, the degradation of energetics in the vadose zone can profoundly reduce the impact on underlying groundwater; however, for the present estimates the degradation is neglected. Degradation rates are highly site-specific and difficult to measure and neglecting degradation yields conservative estimates for the impact on groundwater. The resulting groundwater concentration varies linearly with the groundwater velocity, thickness of the aquifer, length of the range, and density of UXO items covering the range. These parameters are often difficult to estimate without a significant and varied field investigation. The mass release rate is a function of the infiltration rate, soil moisture content, energetic diffusion coefficient in water, energetic solubility in water, explosive fill geometry, and degree of perforating corrosion pits. All of these parameters can be reasonably estimated such that reasonable estimates for the energetic release rate from a corroded UXO can be obtained.

Results for the corrosion study sites are used in examples calculations for 1-kg of CompB in the shape of a cylinder with a radius of 3.8 cm (1.5 inches). For these results, the density of UXO items on the range is assumed to be 100 high explosive UXO items per square kilometer with a range length of one kilometer. The groundwater velocity and aquifer thickness are assumed to be 30 meters per year and 5 meters, respectively. These values are applied to all sites since no site-specific information was available. In this hypothetical UXO scenario, four of the ten sites had the potential to exceed groundwater standards for TNT (i.e., 0.002 mg/L) after thorough corrosion leaves bare explosive fill and none of the sites exceeded the standards for RDX. None of the scenarios exceeded groundwater standards when diffusion through perforating pits was included. The release rate of RDX is generally an order-of-magnitude less than TNT because of its lower solubility and lower diffusivity in water than TNT. For TNT to exceed the groundwater standards under the pitting release scenario, the density of UXO items would generally have to approach 400 items per square kilometer and for RDX to approach the standards the density would need to be about 4,000 items per square kilometer.

7 Transition Plan.

A transition plan has been developed which will facilitate use of the data and results obtained in this study as well as distribution of the tools developed during this project. In order to make results and data available to interested researchers and site managers, this report along with peer-reviewed journal articles will be made available to the general public. Once approved by the USAEC, the UXO Corrosion model (UXO-Corr-Mod III) will be made available to the DoD community.

Also UXO-Corr-Mod III will be updated to include anaerobic corrosion, and calcareous soils and then integrated into the Army Risks Assessment Modeling System (ARAMS) in FY 2004. This will facilitate its use by the DoD Risk Assessment Community.

8 Recommendations.

At the completion of this project several improvements are still possible to further strengthen the utility of the corrosion model and transport model. This report documents the third phase of the development UXO-Corr-Mod. Several aspects of the model may still be improved. Several empirical relationships exist within the model. Future versions of the model should replace these empirical relationships with physically based equations. These include further improvement of the equation for the water film thickness. One possibility is to use infiltration models to determine the amount and height of water at the UXO surface. Also, diffusion through scales on the UXO surface is currently described by an empirical relationship derived from Romanoff's data (Romanoff, 1957). Equations should be developed which incorporate a porosity and diffusivity for the scale as well as a mass balance to calculate the scale thickness for modeling the transport of ions through the scale into and out of the underlying pit.

The transport model which describes energetic release into groundwater currently has no user interface and would require extensive knowledge of Fortran for individual use. As such it is

recommended that user friendly graphical interface be developed which would give a much wider audience access to the model.

9 References.

Defense Science Board. 1998. Report of the Defense Science Board Task Force on Unexploded Ordnance (UXO) Clearance, Active Range UXO Clearance, and Explosive Ordnance Disposal (EOD) Programs. Office of the Under Secretary of Defense for Acquisition and Technology. Washington DC.

Defense Science Board. 2003. Report of the Defense Science Board Task Force on Unexploded Ordnance. Office of the Under Secretary of Defense for Acquisition and Technology. Washington DC.

Howard PH, Boethling RS, Jarvis WF, et al. 1991. Handbook of environmental degradation rates. Chelsea, MI: Lewis Publishers, 454-455.

Jenkins, T.F., C. Bartolini,and T.A.Ranney, 2003, "Stability of CL-20, TNAZ, HMX, RDX, NG, and PETN in Moist,Unsaturated Soil," U.S. Army, ERDC/CRREL TR-03-7, April 2003.

Romanoff, M. 1957. Underground Corrosion. National Association of Corrosion Engineers, Houston, TX.

United States Department of the Army (Army), 1984, Technical Manual TM 9-1300-214, Military Explosives. Washington, DC.

United States Environmental Protection Agency (USEPA). 1989. Treatability potential for EPA listed hazardous wastes in soil. Report no. EPA/600/S2-89/011. Ada, OK: U.S. Environmental Protection Agency, Robert S. Kerr Environmental Research Laboratory. Document no. PB89-166581.

United States Environmental Protection Agency (USEPA). 2000. Test Methods for Evaluating Solid Wastes: Physical/Chemical Methods (SW-846). USEPA, Washington, D.C.

United States Geological Survey (USGS). 1989. SOLMINEQ.88, a computer program for geochemical modeling of water-rock interactions. US Dept. of Interior, USGS, Menlo Park, CA.

Appendix A1

Corrosion of Unexploded Ordnance in Soil
Field Results

(submitted to Environmental Science and Technology)

PRAXIS
ENVIRONMENTAL TECHNOLOGIES, INC.
1440 Rollins Road, Burlingame, California 94010
(650) 548-9288

Corrosion of Unexploded Ordnance in Soil - Field Results

Michael D. Chendorain*, chendo@praxis-enviro.com, 650-548-9288, 650-548-9287 (fax), Praxis Environmental Technologies, Inc., 1440 Rollins Rd., Burlingame, CA 94010
Lloyd D. Stewart, PhD, Praxis Environmental Technologies, Inc., 1440 Rollins Rd., Burlingame, CA 94010
Bonnie Packer, PhD, U.S. Army Environmental Center, 5179 Hoadley Rd., Aberdeen Proving Grounds, MD 21010

Abstract. Unexploded ordnance (UXO) are found on 400,000 Ha of land across 1,400 different sites in the United States. In many cases, the UXO contain high explosives (e.g., RDX, TNT, HMX, and Tetryl) posing a risk to groundwater quality. This paper provides the results from a field survey of 161 UXO found on inactive Army ranges distributed throughout the mainland United States. Soil from near UXO and metal samples from UXO were collected from fourteen sites. Soil samples were analyzed for a variety of chemical and physical properties. Metal samples were analyzed for pitting corrosion. Climate data was also obtained. Samples had been buried from Civil War era through the 1990s. Photographs taken in the field illustrate that pitting and generalized corrosion occurs more rapidly on the underside of an UXO. Field observations also revealed that low order detonations and UXO are difficult to distinguish in the field. Pit depth measurements suggest that no UXO corroded more than 0.25 cm (under the environmental conditions and exposure times encountered). Low rainfall environments had shallower pits (560 ± 120 μm) than moderate and high rainfall environments which produced deeper (960 ± 90 μm).

Introduction. A 2003 Defense Science Board report estimated that 1,400 different sites, encompassing 400,000 Ha (10 million acres) of land contain Department of Defense unexploded

ordnance (UXO) (Defense Science Board, 2003). Contained within the soil, these intact munitions corrode at varying, site-specific rates. Depending on soil and climatic conditions and UXO characteristics, the time to perforation (i.e., corrosion breakthrough of the metallic casing) can vary from roughly 10 years to several thousand years. Understanding the relative rate of corrosion significantly improves the assessment of risk to humans and the environment posed by the toxic energetic and constituent materials encased in UXO. Many UXO are comprised of high explosives (e.g., RDX, TNT, HMX, and Tetryl), the metallic container, and lesser quantities of fuse materials. While the metallic container is not hazardous to human health, the explosive fill components each have a unique toxicity, water solubility, propensity for sorption, and persistence in the environment. Thus, differing potentials to impact surface water and groundwater quality. To assess the environmental impact of these compounds appropriately, the rates and mechanisms of UXO corrosion in soil must be first understood.

Corrosion in soils occurs predominantly through pitting mechanisms or generalized corrosion (Jones, 1996). Pitting mechanisms on metal surfaces have recently been described in detail (Over and Seitsonen, 2002). In aerobic soils, the major oxidation/reduction reactions which drive corrosion of iron-based metals are:

$$2Fe \rightarrow 2\,Fe^{2+} + 4\,e^{-} \text{ (anodic reaction)} \quad (1)$$

$$O_2 + H_2O + 4\,e^{-} \rightarrow 4OH^{-} \text{ (cathodic reaction)} \quad (2)$$

Although it is understood that soil type influences corrosion (Romanoff, 1957), little knowledge exists on specific quantifiable relationships (Jarvis and Hedges, 1994).

This paper provides the results from a field survey of inactive Army ranges distributed throughout the mainland United States. Sampling occurred between June 1999 and August 2003. At each site, soil samples were collected close to the UXO and analyzed for various soil

properties, metal samples were collected from the UXO for corrosion analyses, and climate data was obtained from nearby weather stations. Alphabetic identifiers are used in place of specific site locations. A total of 161 UXO items were included in the survey.

Methods.

Field Methods. Data from fourteen different inactive Army training ranges were obtained in this study. Sites were selected if records indicated a known relatively short period of use so that found items could be dated. Field methods for this study included locating UXO items, sampling adjacent soil, and sampling the UXO metal. Soil samples were collected for chemical and physical analyses. Metal samples were collected for corrosion analyses. After a UXO was detected and uncovered, the item was given a unique ID (X-##, where X represents an alphabetic symbol referring to the specific site and ## represents a sequential numeric tag for each item found at a site). The item was photographed and samples were then collected.

A composite soil sample was collected from a depth equivalent to the depth of the item within six inches from the item and analyzed for soil physical and chemical properties. One discrete undisturbed soil core sample was collected for soil physical analyses using an AMS 6 inch core sampler and hammer assembly. For inert UXO items, undisturbed metal samples were obtained from the intact item with saw cuts. For UXO determined to have an explosive risk, the item was blown-in-place with a cover (usually plywood and sand bags) and the largest metal fragments were then collected.

Soil Analyses. A wide variety of soil analyses were performed. Cation concentrations (barium, calcium, iron, magnesium, manganese, sodium, aluminum, and potassium) were determined

using an inductively coupled argon plasma - atomic emission spectrometer (ICP). Cation exchange capacity (CEC) was then determined by the summation of calcium, magnesium, potassium, sodium, and aluminum concentrations. Ion selective electrodes were used to measure pH and oxidation-reduction potential (ORP). Titration methods were used to measure organic acids, bicarbonates, and chlorides. Organic content was determined using a dry combustion method. Sulfate concentration was measured using a turbidimetric method and sulfide concentration was measured using an ion selective electrode.

Several physical analyses were also performed. Volumetric moisture content and bulk density were measured by weighing undisturbed soil cores, drying the cores, re-weighing, and then by calculation. Porosity was determined by calculation using the bulk density and assuming a particle density of 2.65 g/cm^3. Soil samples were sieved using sieve sizes 30 and larger. The pore size distribution for particles passing through the #30 sieve was determined using a laser light scattering method. Soil classification was based on the Unified System of Soil Classification. At Sites A and B, soil cores were not collected because of explosive safety precautions and porosity was determined using a pycnometer.

Climate Data. Data on rainfall and air were obtained from the nearest weather station to each site in the National Oceanic and Atmospheric Administration (NOAA) network. The actual data were downloaded from the Columbia University International Research Institute for Climate Predictions web site (http://iri.Ideo.columbia.edu/climate).

Corrosion Analyses. Analyses to determine corrosion rate included an analysis of the surface scale as well as corrosion pitting. Initially soil was removed from the metal surface, and then

scales that were attached to the surface or in corrosion pits were collected for analysis. The scale was water washed to remove excess soil and dried at 120 ^{o}C for one hour. The scale was crushed into a fine powder. A sample of approximately 2 gram was subjected to a wet bench method to detect hydrocarbons, iron compounds, and carbonates (Case, 1977).

Corrosion pits were analyzed for total pit number, pit density, and properties of individual pits. The metal surface was cleaned to remove all soil. If the surface area was greater than 100 cm^2, the sample was examined to determine the area that had the deepest pits. An area of at least 100 cm^2 was cleaned to bare metal. If the sample was smaller than 100 cm^2, the entire sample was cleaned to bare metal.

A Dremel tool fixed with stainless steel drills was used to clean all residual material from the deepest pits. Material removed from the pits was collected and added to the wet bench scale analysis sample to determine if sulfides were present in the pits. A general description of the sample, the type of metallurgy, and a general description of the corrosion were recorded as well as any unusual observations. Cleaning of the metal surface was accomplished by sand blasting, if possible, or manually using sand paper for delicate samples.

The surface area and thickness of the sample was measured. Random pit depth measurements were made using a pit depth micrometer. At least 20 % of the pits in the 100 cm^2 sample area were measured. In the case of small samples, all of the pits were measured. The range of the pit depths was calculated. In cases where a few unusually deep pits were found, these pits were measured and recorded separately. After placing a 6.25 cm^2 (1 in^2) window on the metal surface, the number of pits in the window was then counted. Several random areas were analyzed and the average pit count was calculated and reported as pits/cm^2. Using the depth of the deepest pit and the estimated years of exposure, the corrosion rate was calculated.

The depth was expressed in μm. The average pitting corrosion rate was reported as μm per year (μm/yr).

Results and Discussion.

Site Characteristics. Fourteen sites were visited resulting in sampling of 161 items with analyses for soil characteristics and extent of corrosion. Most of the major ecosystem types of the continental U.S. were visited and sampled. Five sites were in temperate forests; two sites were in temperate grasslands; two sites were in steppes; two sites were in deserts; and the remaining four sites had areas of both temperate grasslands and temperate forests. Tables 1 and 2 present average selected properties for each ecosystem encountered. Several soil ions such as carbonates, calcium, and sodium had elevated concentrations in the desert and steppes ecosystems relative to the other ecosystems visited. In contrast, potassium concentrations were greater in the forest and grassland sites. The desert sites had alkaline soils with an average pH of 8.0 ± 0.2 while other sites had acidic soils. The steppes had near neutral pH with an average of 6.1 ± 0.5. The minimum pH was encountered at a site dominated by glacial soil pedalogic processes with an average pH of 3.9 ± 0.4 and a range of 3.0 to 4.8. This site was a mixture of temperate forests and temperate grasslands.

Table 1. Average site characteristics of selected soil chemical properties[1].

Ecosystem Type	No. of Samples	Carbonates	Calcium	Sodium	pH	Potassium
		(mg/kg soil)	(mg/kg soil)	(mg/kg soil)		(mg/kg soil)
Desert	23	1100 ± 420	2700 ± 560	250 ± 320	8.0 ± 0.2	120 ± 320
Steppes	16	490 ± 470	1700 ± 1000	80 ± 12	6.1 ± 0.5	20 ± 26
Temperate Forest	75	87 ± 230	410 ± 780	57 ± 35	5.1 ± 0.8	430 ± 690
Temperate Grassland	13	51 ± 120	300 ± 500	65 ± 61	5.5 ± 1.2	530 ± 1300
Temperate Forest/Grassland	59	13 ± 25	220 ± 430	64 ± 24	4.6 ± 1.1	990 ± 1300

[1] ± one standard deviation.

Of these various ecosystems, steppes and deserts both had rainfall rates less than 50 cm/yr (Table 2) while other ecosystems had significantly more rainfall. Oxidation reduction potential (ORP) was slightly lower in the desert and steppes environments than the temperate forests and grasslands. Mean air temperature did not vary significantly between the various ecosystems with a coefficient of variation for all sites of 22 %. It should be noted that each ecosystem type contained at least one site from the northern U.S. and one site from the southern U.S. including the desert ecosystem. Desert and steppes soils were a mix of loamy sands and sands. However, the steppes generally had a significant gravel percentage (average = 18 ± 16 %) while desert soils contained a small amount of gravels (average = 0.4 ± 0.7 %). Temperate forest sites had soils which included loams, sands, sandy loams, and silt loams. Gravels in the temperate forests averaged 7 ± 13 %. The temperate grassland sites had loams, sandy loams, loamy sands, and silty clay loams. Very little gravels were found at the temperate grassland sites (average = 1 ± 2 %). Sites which had areas of both temperate forests and temperate grasslands, the soils were loams, sands, sandy loams, loamy sands, and silt loams. The average gravel composition was 4 ± 9 %. Although the desert and steppes soils tended to have coarser textured soils than the forests and grasslands, the measured porosity was slightly greater in the forests and grasslands (Table 2). The average trend in soil moisture content for the ecosystems followed that of precipitation. Temperate forests had the highest average moisture content (23 ± 10 %) and annual precipitation (127 ± 5 cm/yr) Desert ecosystems had the lowest average moisture content (4 ± 4 %) and precipitation (25 ± 3 cm/yr). Organic content was similar for all the sites with the exception of temperate forests which had the largest amount of organic material (7 ± 4 %).

Table 2. Average site characteristics of selected physical properties (by ecosystem type)[1].

Ecosystem Type	Mean Air Temperature	Moisture Content	Organic Content	Porosity	Precipitation	ORP
	(°C)	(%)	(%)	(%)	(cm/yr)	(mV)
Desert	12 ± 9	4 ± 4	3 ± 1	43 ± 3	25 ± 3	180 ± 10
Steppes	8 ± 9	8 ± 6	3 ± 3	42 ± 5	33 ± 3	170 ± 50
Temperate Forest	11 ± 9	23 ± 10	7 ± 4	54 ± 16	127 ± 5	225 ± 120
Temperate Grassland	13 ± 8	13 ± 8	2 ± 1	50 ± 6	107 ± 5	220 ± 100
Temperate Forest/Grassland	10 ± 10	10 ± 8	3 ± 2	50 ± 13	104 ± 8	270 ± 60

[1] ± one standard deviation.

Extent of Corrosion. Sampled items collected had been buried over a large interval of time spanning from Civil War era through the 1990's. This range of exposure periods is illustrated in Figure 1. Metal samples were analyzed to determine the extent of corrosion. Corrosion was quantified in terms of pitting corrosion and generalized corrosion. However, because of variability in the initial metal thickness, only pitting corrosion will be discussed.

Figure 2 illustrates the range of pit depths measured. Although more than thirty different soil and climate parameters were measured for each item sampled, only rainfall and variables associated with rainfall and arid environments (such as temperature, volumetric water content, alkalinity, texture, etc.) showed any correlation to pit depth. The average maximum pit depth for samples found in areas with annual rainfall less than 50 cm/yr was 560 ± 120 μm (22 ± 5 mils with 95% confidence). Samples from sites with annual rainfall rates greater than 50 cm/yr had a higher average maximum pit depth of 970 ± 90 μm (38 ± 4 mils with 95% confidence). Ecosystems with annual precipitation greater than 50 cm/yr included deserts and steppes while those with less 50 cm/yr included temperate forests and grasslands. The distribution of maximum pit depths was much greater for samples collected from non-arid sites than from arid sites. These results indicate that areas with low rainfall (desert and steppes environments) generally produce less corrosive conditions.

Pit density was also measured and ranged from less than 1 to 21 pits per square cm of metal surface. The average pit density was 7 ± 4 pits/cm^2. Pit density was not found to correlate well with any soil characteristic.

The thickness of the UXO sampled ranged from 760 to 64,000 µm. No sample had a measured maximum pit depth greater than 0.25 cm. This suggests that within 150 years, corrosion processes will penetrate less than 0.25 cm for the types of ecosystems included in this survey. Although several rounds showed indications of perforations during analysis, all perforated rounds were less than 0.25 cm thick. However when UXO items were blown in place, the remaining fragments accounted for a small fraction of the original UXO. In these cases, perforated regions may have been completely destroyed due to their fragile condition.

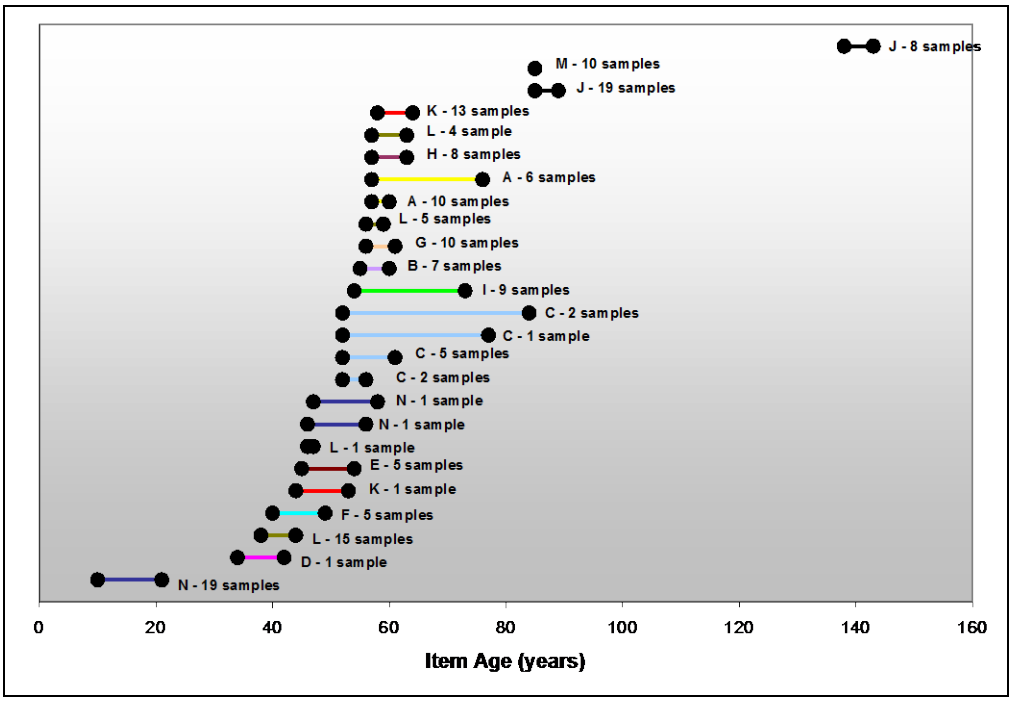

Figure 1. Exposure periods for sampled items (alphabetic designations refer to site ID).

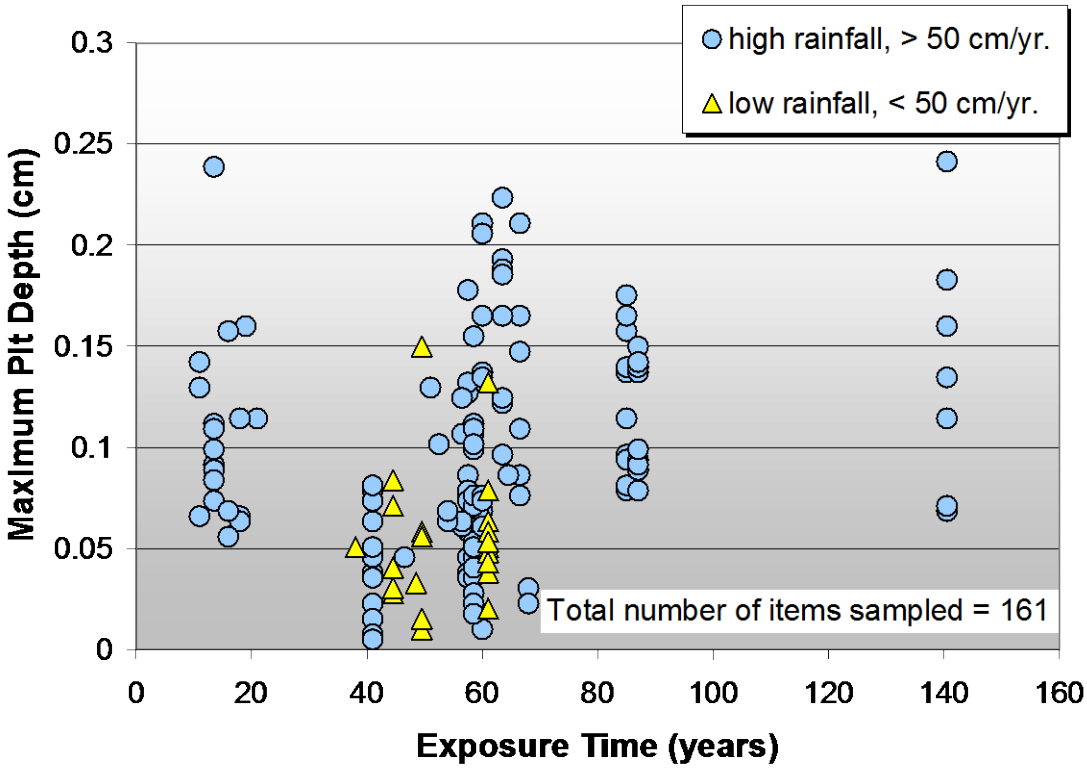

Figure 2. Maximum pit depths for entire data set.

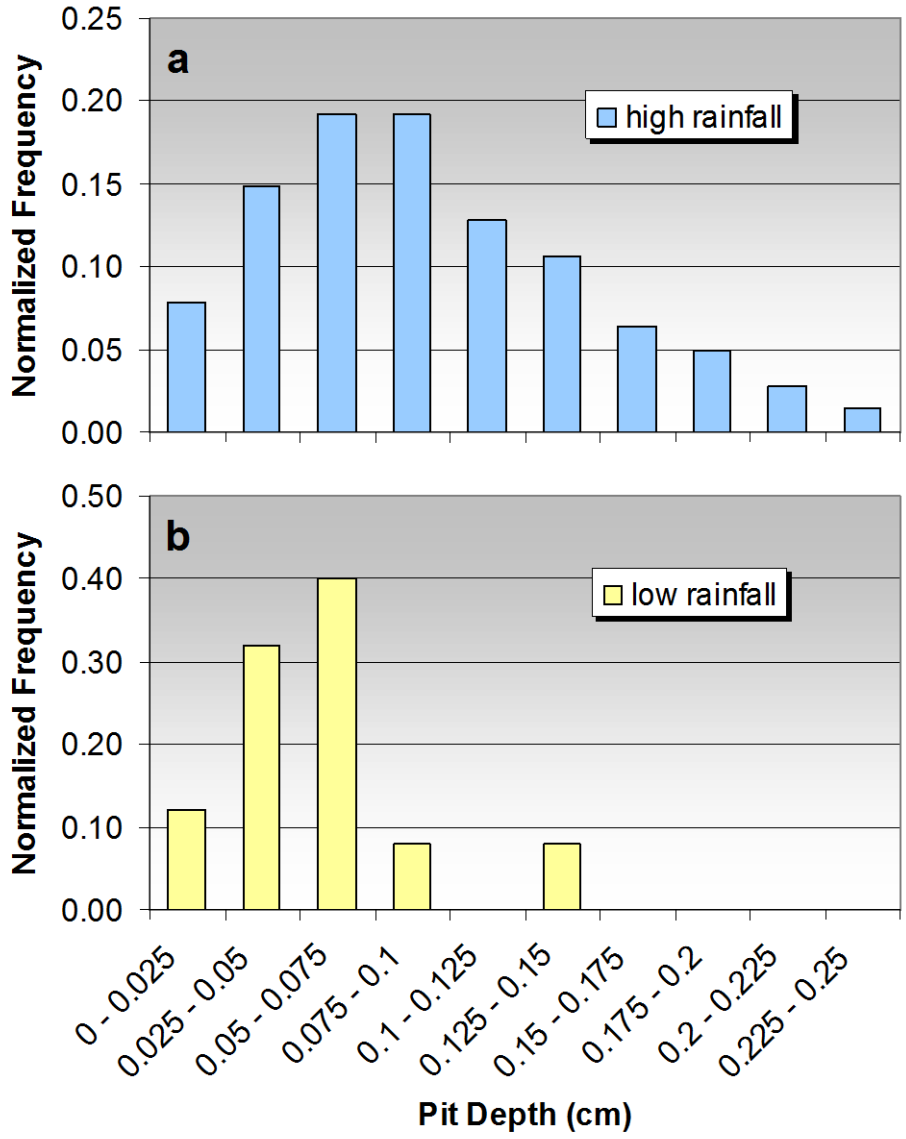

Figure 3. Frequency distributions of pit depths in (a) high rainfall (> 50 cm/yr), and (b) low rainfall (< 50 cm/yr) environments.

Visual Observations. Photographs were taken during field sampling of items as they were uncovered and sampled. Of the 161 items, three samples appeared to be cracked or partially detonated. The remaining 158 items were either intact unexploded ordnance or metal fragments from fully detonated rounds. During the field sampling expert explosive ordnance disposal

teams searched and excavated soil to make field identifications of on the types of rounds encountered and potential safety hazards. This activity allowed field technicians to differentiate qualitatively between UXO and low order detonations. Low order detonated rounds expose energetic material directly to the soil without the time lag associated with UXO corrosion. Consequently low order rounds present environmental risks much earlier than UXO because the metal containers must corrode before leaking explosives into the environment. Figure 4 presents two 60 mm rounds found in a temperate forest. Field notes indicated that item A-02 may have been a low order detonation. However, the photographs illustrate the difficulty in making this observation and the need to have experienced field personnel present.

Figure 4. Field photographs of ordnance (a) UXO (A-04) and (b) low order detonation ordnance (A-02).

Another important observation made during field activities is the extent of corrosion occurring on the upward facing portion of a UXO (topside) versus the downward facing portion of a UXO (bottom). Figure 5 presents pictures of two different rounds. Figures 5A and 5B present the top and bottom, respectively, for a 75 mm shrapnel round buried between 85 and 89

years in a temperate forest. Figures 5C and 5D present the top and bottom, respectively, for a 75 mm high explosive filled round buried between 45 and 54 years in a steppes. Figure 5 reveals that buried items corrode more rapidly on the bottom. This effect is likely the result of differences in matric forces between the soil and UXO combined with evapotranspiration. Since the capillary suction of water is less on the UXO surface than surrounding soil, water would not tend to accumulate on the upper side of the UXO surface. On the underside of the UXO, however, water would be expected to accumulate at the interface between the UXO and underlying soil due to the air entry potential of the soil. Evapotranspiration also contributes to less moisture on the top surface of an UXO items versus its bottom.

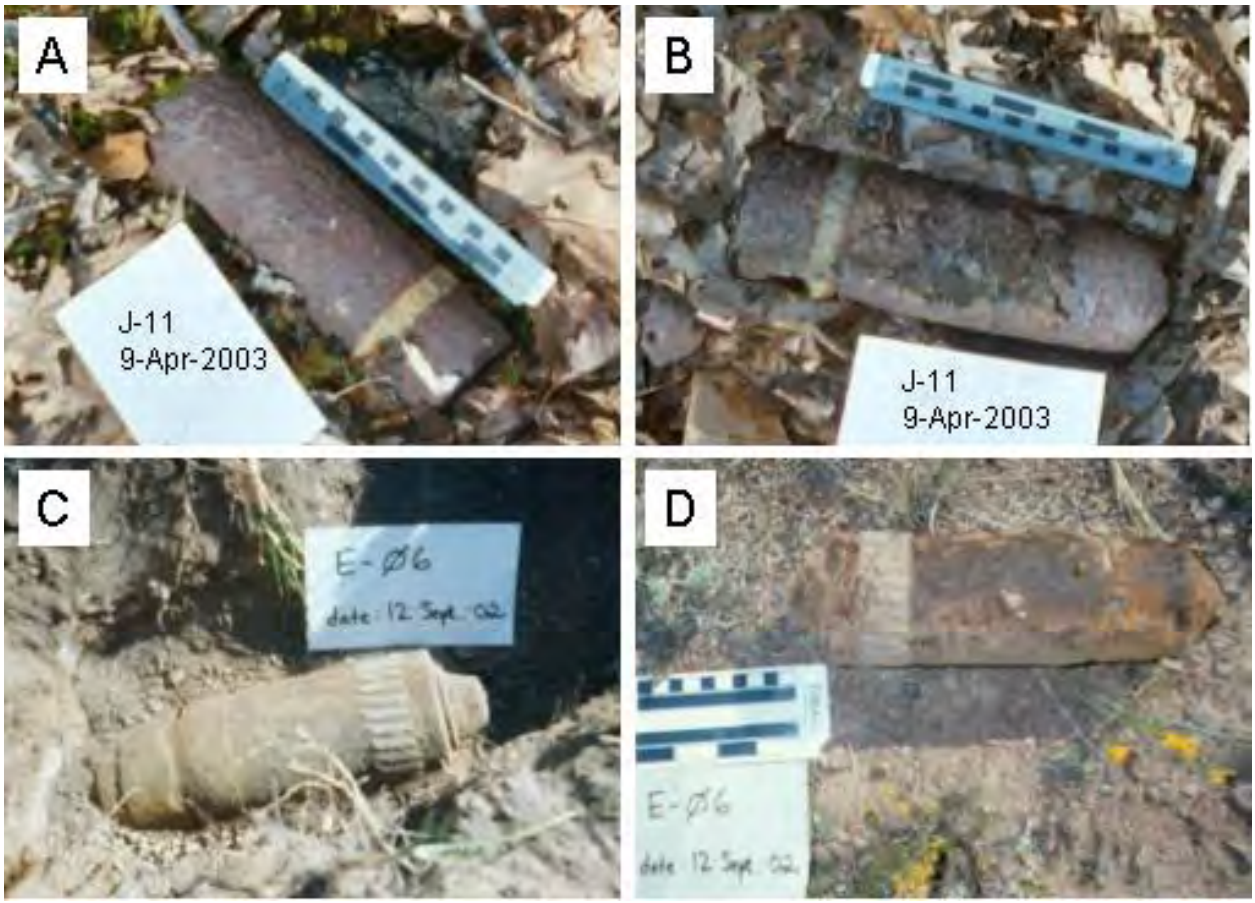

Figure 5. Effects of moisture on buried ordnance: (a) Top of item J-11 (75 mm shrapnel round), (b) Bottom of same round, (c) Top of item E-06 (76 mm high expolsive round), (d) Bottom of same item.

Acknowledgments. The authors wish to thank the U.S. Department of Defense Strategic Environmental Research and Development Program (SERDP) and the U.S. Army Environmental Center for their funding of this project. The authors also thank the U.S. Army Corps of Engineers, Huntsville for their assistance in providing support and access to many of the sites visited during this study. In addition, we thank Mr. William Veith, the US Army Corp of Engineers Environment Research and Development Center Environmental Laboratory and Cold Regions Research Engineering Laboratory for their field assistance and review of our work plan.

References.

Case, L.C., 1977. Guide to Identification of Scales and Probable Causes. PenWell Corp. Tulsa, OK.

Defense Science Board. 2003. Report of the Defense Science Board Task Force on Unexploded Ordnance. Office of the Under Secretary of Defense for Acquisition and Technology. Washington DC.

Jarvis, M.G. and M.R. Hedges. 1994. Use of Soil Maps to Predict the Incidence of Corrosion and the Need for Iron Mains Renewal. *JIWEM.* 8, Feb., 1994, 68-75.

Jones, D.A. 1996. Principles and Prevention of Corrosion. Prentice-Hall, Inc. Upper Saddle River, NJ.

Over, H. and A.P. Seitsonen. 2002. Oxidation of Metal Surfaces. *Science*. 297:2003-2005.

Romanoff, M. 1957. Underground Corrosion. Circular 579. National Institute of Standards and Technology, Houston, TX.

Appendix A2

UXO CORROSION MODEL PHASE III

TECHNICAL MANUAL

PRAXIS
ENVIRONMENTAL TECHNOLOGIES, INC.
1440 Rollins Road, Burlingame, California 94010
(650) 654-5488

UNIVERSITY OF LOUISIANA Lafayette

Table of Contents

List of Figures

List of Tables

Introduction

1.1 Background

This technical manual provides an overview and a detailed description of the third phase of the Unexploded Ordnance (UXO) Corrosion Model abbreviated as UXO Corr-Mod III. The model was developed at the University of Louisiana, Lafayette in conjunction with Praxis Environmental Technologies, Inc. Funding was provided by the US Department of Army, Army Environmental Center and the US Department of Defense, Strategic Environmental Research and Development Program. The basic functions of the model are to utilize soil and climatic data to (a) predict perforation times for UXO (based on metal thickness) and to (b) develop a corrosion rate profile as a function of time.

1.2 Initial Assumptions and Conceptual Description

UXO Corr-Mod III is based on a variety of initial assumptions. The dominant mechanisms of corrosion of buried UXO are pitting and generalized corrosion. The model estimates rates of corrosion based upon these two fundamental mechanisms. Other corrosion mechanisms are not considered. Pit corrosion is described as a one-dimensional, linear, quasi-steady state transport process. Pitting corrosion rates are determined by successively increasing the pit depth and estimating the time required to reach each depth. The estimation of generalized corrosion is based on pitting factors which are determined within the model.

The fundamental chemical reactions which drive UXO corrosion are assumed to be the oxidation of elemental iron (anodic reaction) and the reduction of gaseous oxygen (cathodic reaction). Thus, anaerobic soils are not currently considered in this model. The anodic reaction is written as:

$$2Fe \rightarrow 2Fe^{2+} + 4e^{-} \quad (1)$$

while the complimentary cathodic reaction is:

$$O_2 + H_2O + 4e^{-} \rightarrow 4OH^{-} \quad (2)$$

Initiation of pitting corrosion occurs when oxygen at the UXO surface creates an electrochemical demand for electrons to drive equation 2. The pit forms as elemental iron is oxidized locally creating an anode (equation 1). This process is illustrated in Figure 1.

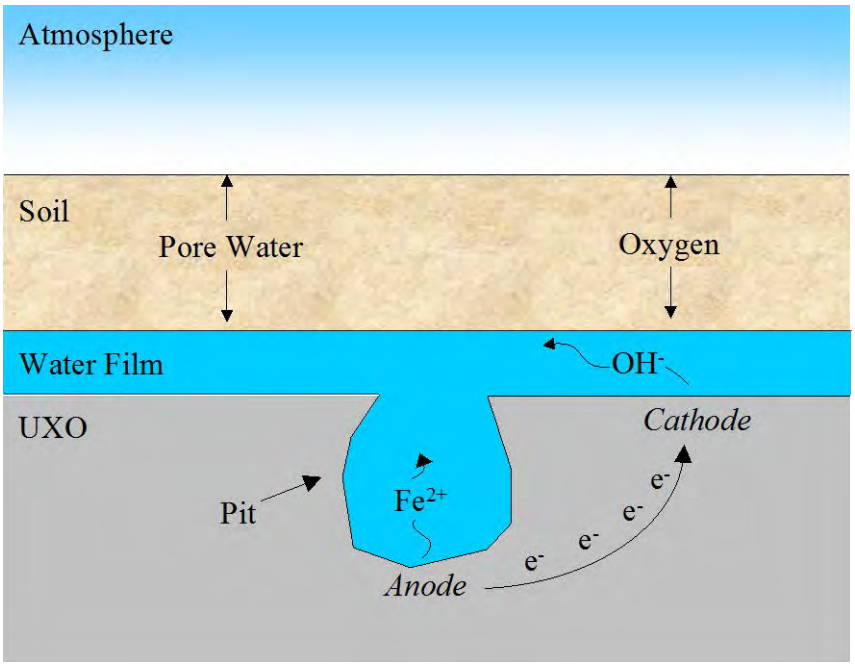

Figure 1. Schematic of newly formed electrochemical anode and cathode.

As the pits grow, hydroxides and ferrous iron accumulate within the pit creating the potential for iron hydroxide precipitates to form. Further, the presence of carbonates and calcium in the soil create the potential for the precipitation of iron carbonate and calcium carbonate. These precipitates eventually form scales at the mouth of the pit which drastically reduce the rates of diffusion of ions (such as ferrous iron and oxygen) in and out of the pit. Schematically this is shown in Figure 2.

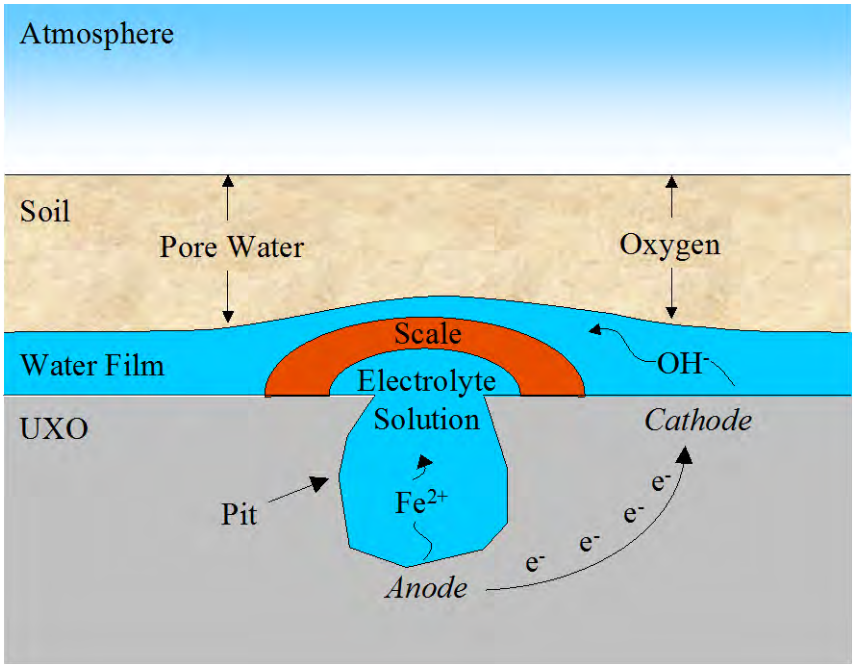

Figure 2. Scale formation over a pit.

Although pitting corrosion dominates the total corrosion rate at the beginning of the corrosion process, generalized corrosion occurs simultaneously. As scales form and reduce the pitting corrosion rate, generalized corrosion begins to impact the total corrosion rate more. Subsequently, at later times, the total corrosion rate is driven largely by generalized corrosion.

1.3 Model Components

The next sections will describe the assumptions and mathematics used to develop UXO-Corr-Mod III. The primary components (and their corresponding sections in this technical manual) are:

- Section 2: Estimation of characteristic pore water thickness around the UXO
- Section 3: Pitting Model (includes anode, cathode, and iron carbonate subroutines)
- Section 4: Scale formation and influence on pitting corrosion
- Section 5: Generalized Corrosion
- Section 6: Calculation of total corrosion rate and results (corrosion rate profile, time to perforation).

Figure 3 presents a flow chart illustrating these components.

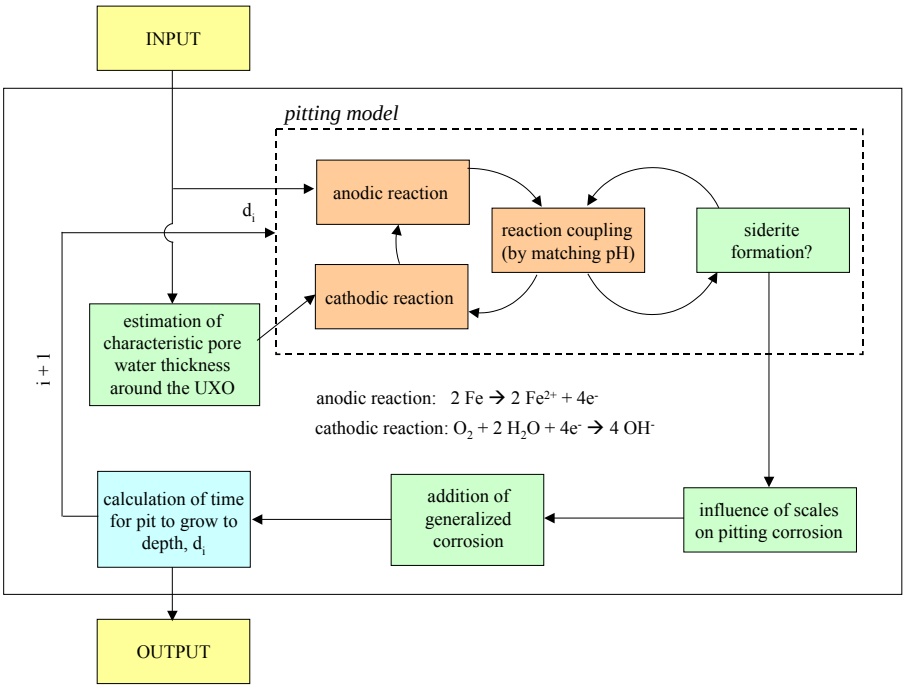

Figure 3. Flow chart of major components in UXO-Corr-Mod III.

2 Estimation of Characteristic Pore Water Thickness around the UXO

UXO-Corr-Mod III assumes that a water film exists which surrounds the UXO enabling the formation of electrochemical anodes and cathodes and the transfer of electrons to drive pitting corrosion. Subsequently, each set of soil and climatic parameters will produce a unique characteristic pore water thickness around a UXO item buried in soil. The estimation of water film thickness is developed from an attempt to characterize the rate at which oxygen can diffuse from the soil surface to the surface of a buried UXO (Figure 4).

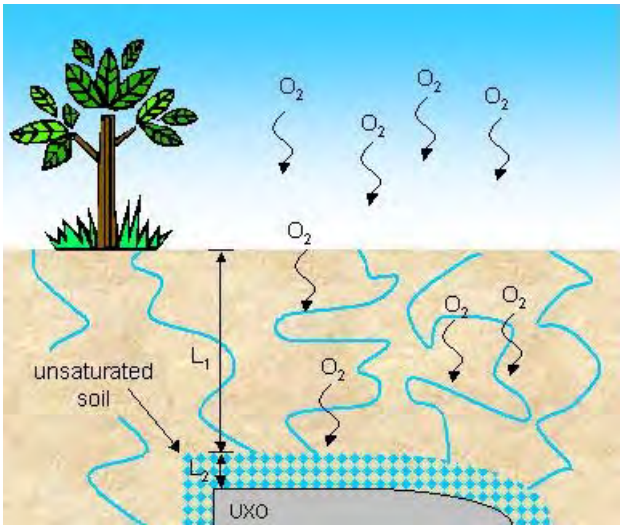

Figure 4. Oxygen movement into the soil via gaseous diffusion.

Oxygen transport is driven by a concentration gradient created by oxygen utilization within the soil. This gradient is created by oxygen utilization both at the UXO surface (due to corrosion) and from microbial activity throughout the soil. Within the soil pore network, gaseous oxygen partitions from the gaseous phase to the liquid phase where it is utilized (Figure 5). At some characteristic depth, L_1 (Figure 4), below the soil surface liquid oxygen concentrations are in equilibrium with the gas phase. Once in the liquid phase, oxygen is further transported through soil pore water to cathodic nodes on the UXO surface.

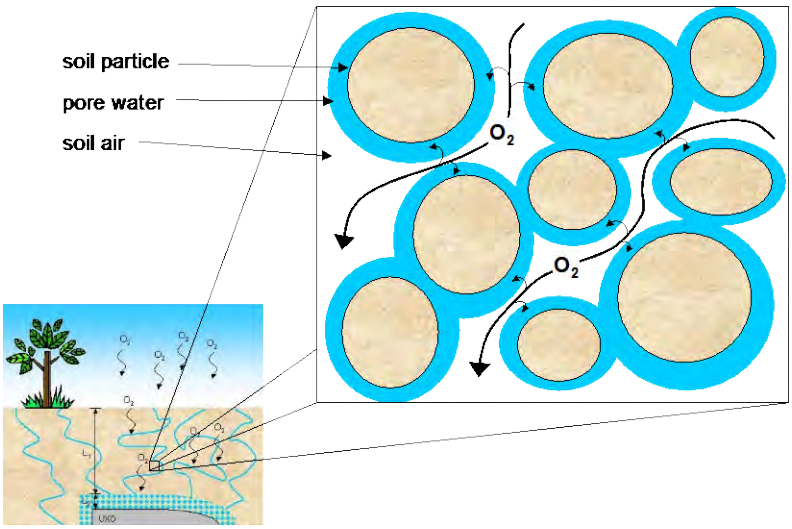

Figure 5. Oxygen partitioning from soil gas into pore water.

UXO-CorrMod III makes several assumptions in order to mathematically describe the transport of oxygen to the UXO surface. Conceptually, the model assumes that gaseous oxygen is transported through a soil-dependent characteristic length, L_1, where the oxygen is assumed to be in equilibrium between the gas and liquid phases. At this characteristic depth, the oxygen is further transported through pore water at the field moisture content over a second characteristic distance, L_2, to the UXO surface (Figure 6). For fine textured soils such as a clay, L_2, would generally be larger than for coarse textured soils such as a sand. The dependence of L_2 on soil texture is based on the water holding capacity which is greater for finer textured soils. Conversely, L_1 would be greater for coarse textured soils than fine textured soils. Since coarse textured soils generally have greater air filled porosity, gaseous oxygen is able to travel a longer distance before the effective equilibration depth is reached.

Gaseous oxygen transport through soil is dominated by diffusion and can be written, based on Fick's Law, as:

$$J^{a}_{O_2} = -D^{a}_{O_2} \cdot \tau_a \cdot \frac{dC_a}{dz} \tag{3}$$

Similarly, oxygen transport through soil pore water can be written as:

$$J^{w}_{O_2} = -D^{w}_{O_2} \cdot \tau_w \cdot \frac{dC_w}{dz} \tag{4}$$

where:

$J^{a}_{O_2}$ = flux rate of oxygen through air (mg/cm^2·sec),

$D^{a}_{O_2}$ = diffusivity of oxygen in air (0.178 cm^2/sec),

τ_a = tortuosity factor for gaseous diffusion (unitless),

C_a = concentration of oxygen in air (mg/L),
z = distance (cm),
$J_{O_2}^w$ = flux rate of oxygen through water (mg/cm^2·sec),
$D_{O_2}^w$ = diffusivity of oxygen in water (2.6 x 10^{-5} cm^2/sec),
τ_w = tortuosity factor for liquid diffusion (unitless), and
C_w = concentration of oxygen in water (mg/L).

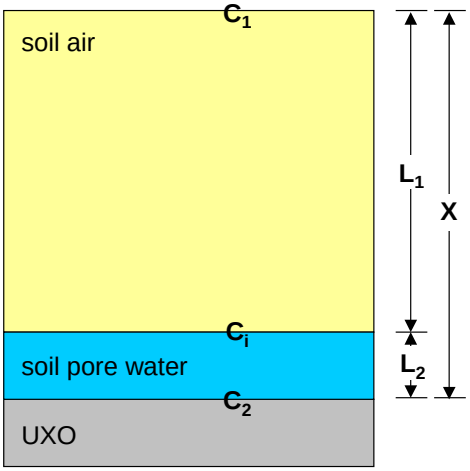

Figure 6. Conceptual regions for oxygen transport to UXO surface.

The tortuosity factors in equations 1 and 2 reflect the porous nature of soil. The tortuosity factor for gaseous diffusion is (Millington and Quirk, 1960):

$$\tau_a = \frac{a^{10/3}}{\phi^2} \tag{5}$$

Similarly, tortuosity for diffusion through liquid is:

$$\tau_w = \frac{\theta_v^{10/3}}{\phi^2} \tag{6}$$

where a is the air filled porosity, ϕ is the total porosity, and θ_v is the volumetric moisture content, all of which are dimensionless.

Under quasi-steady conditions, the flux rates of equations 1 and 2 are equal:

$$J_{O_2} = -D_{O_2}^a \cdot \tau_a \cdot \frac{C_1 - C_i}{L_1} = -D_{O_2}^w \cdot \tau_w \cdot \frac{C_i - C_2}{L_2} \tag{7}$$

where L_1 is the characteristic distance of oxygen diffusion through soil air, L_2 is the characteristic distance of oxygen diffusion through soil pore water to the UXO surface. C_i is oxygen concentration at the gas/liquid interface. In addition, the gas phase oxygen concentration is converted to liquid phase concentration using Henry's law. The dimensionless Henry's constant, H, is equal to C_a/C_l and at a pressure of 1 atm and temperature of 25°C is equal to 17.13. The oxygen concentration at the UXO surface, C_2, is assumed to be zero at the onset of corrosion. Equation 7 can be rearranged to yield:

$$L_2 = \tau_w \left(\frac{D_w C_1}{J_{O_2}} - \frac{D_w L_1}{D_a \tau_a} \right) \tag{8}$$

Where L_2 is the characteristic moisture length for aqueous oxygen diffusion. For moist soils where the UXO is shallow, L_1 and τ_a are both small which reduces equation 8 to:

$$L_2 \cong \tau_w \left(\frac{D_w C_1}{J_{O_2}} \right) \tag{9}$$

Now that L_2 is defined, a method must be developed which can calculate L_2 without prior estimation of J_{O2}. Romanoff, 1957 measured corrosion rates of steel buried in 47 different soils. Early in the corrosion process (less than five years), it is assumed that oxygen is in adequate supply and scale formation is at a minimum. Therefore pitting corrosion is dependent on the water film thickness surrounding the UXO. Corrosion rates from Romanoff, 1957 for samples buried in soil between 3 and 4 years were used to determine oxygen flux rates and their subsequent film thickness, L_2 based on equation 8. The method to calculate oxygen flux rate assumes equilibrium in equations 1 and 2, the corrosion reduction/oxidation equations, and assume 2 moles of Fe^{2+} generated for every mole of oxygen used. For Romanoff's soils, a simple empirical relationship was found between L_2 and θ_v with an r^2 of 0.88 (Figure 7):

$$L_2 = \frac{\theta_v^{2.3}}{1.9} \tag{10}$$

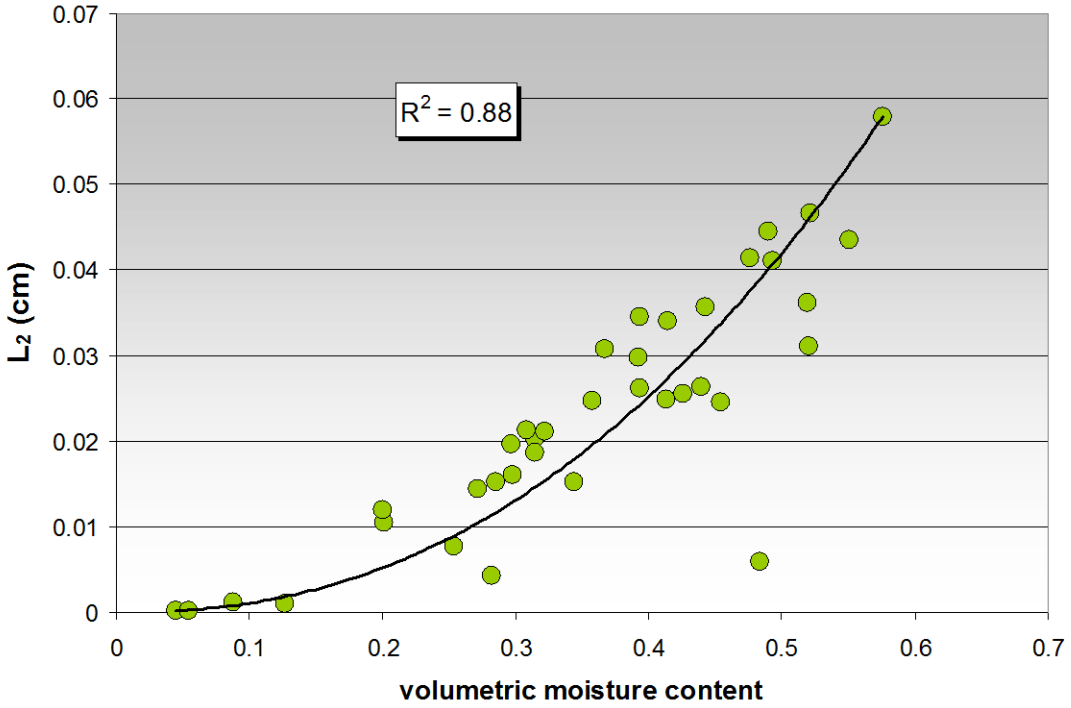

Figure 7. Correlation between L_2 and volumetric moisture content for Romanoff soils.

3 Pitting Model

The pitting model, which calculates the pitting corrosion rate for a specific pit depth, has three main components. The anodic reaction component calculates the rate of elemental iron oxidation. The cathodic reaction component calculates the rate of hydroxide generation. The third component equilibrates the two reaction rates by matching the pHs associated with each reaction. A fourth supplemental component to the pitting model determines whether iron carbonate (siderite) forms a scale on the pit surface. The presence of siderite scales effectively reduces the pitting corrosion rate to zero.

3.1 Anodic Reaction: Transport of Iron away from the UXO

The rate of iron oxidation determines the pitting corrosion rate. The flux rate of ferrous iron away from the metal surface of the pit determines the rate of oxidation of elemental iron (equation 1). The anodic reaction component calculates this ferrous iron flux rate which is dependent on the chemical equilibria of the ionic species present within the pit. The model determines, as a function of pit depth, sixteen equilibrium concentration values and a potential value inside the pit by solving simultaneously the diffusive flux equation written for each species. The sixteen chemical species involved in the anodic reaction routine are:

1. Fe^{2+}	5. H^+	9. HCO_3^-	13. CH_3COOH
2. H_2O	6. OH^-	10. Na^+	14. CH_3COO^-
3. $Fe(OH)^+$	7. CO_3^{2-}	11. Cl^-	15. $Fe(CH_3COO)^+$
4. $Fe(OH)_2$	8. H_2CO_3	12. $FeCl^+$	16. $Fe(CH3COO)_2$

The initial concentrations of these chemical species are based on measure soil solution concentrations of iron, carbonate and bicarbonate, organic acids, sodium, and chlorine, and pH. The electro–neutrality equation, sixteen flux equations, and equilibrium constant equations are solved simultaneously to yield the concentration of each parameter as a function of pit depth.

The reactions included in this system are:

$Fe \rightarrow Fe^{2+} + 2e^-$ (11)
$Fe^{2+} + H_2O \rightarrow Fe(OH)^+ + H^+$ (12)
$Fe(OH)^+ + H_2O \rightarrow Fe(OH)_2 + H^+$ (13)
$H_2O \rightarrow H^+ + OH^-$ (14)
$H^+ + HCO_3^- \rightarrow H_2CO_3$ (15)
$H^+ + CO_3^{2-} \rightarrow HCO_3^-$ (16)
$NaCl \rightarrow Na^+ + Cl^-$ (17)
$Fe^{2+} + Cl^- \rightarrow FeCl^+$ (18)
$CH_3COOH \rightarrow CH_3COO^- + H^+$ (19)
$Fe^{2+} + CH_3COO^- \rightarrow Fe(CH_3COO)^+$ (20)
$Fe(CH_3COO)^+ + CH_3COO^- \rightarrow Fe(CH_3COO)_2$ (21)
$Fe^{2+} + CO_3^{2-} \rightarrow FeCO_{3\,(S)}$ (22)

The flow of each species in a unidirectional system, under steady state conditions and in dilute solutions is given by:

$$J_i = -D_i\left[\frac{dC_i}{dx} + \frac{z_i F}{RT} C_i \frac{d\phi}{dx}\right] \tag{23}$$

Where, J_i is the flow of species 'i' in gm–mole / cm^2–sec;

D_i is the diffusion coefficient of 'i' in cm^2/sec;
C_i is the concentration of species 'i' in mol cm^{-3};
X is the depth of the pit in cm;
z_i is valence (unitless),
F is the Faraday constant;
R is the molar gas constant;
T is the absolute temperature in K;
$\frac{d\phi}{dx}$ is the electric field inside the pit, V cm^{-1}.

The following balanced flux equations can be written to describe the system. The only equation with a generation term is the iron balance which describes the release of iron ions at the bottom of the pit.

The flow of species containing 'Fe' atoms is given by

$$J_{Fe^{2+}} + J_{Fe(OH)^{+}} + J_{Fe(OH)2} + J_{FeCl^{+}} + J_{FeCH3COO^{+}} + J_{Fe(CH3COO)2} = -i/2F. \quad (24)$$

The flow of species containing ionizable 'H' atoms is given by

$$J_{H2O} + J_{H^{+}} + 2\,J_{H2CO3} + J_{HCO3^{-}} + J_{CH3COOH} = 0 \quad (25)$$

The flow of species containing hydroxide is given by

$$J_{H2O} + J_{Fe(OH)^{+}} + 2\,J_{Fe(OH)2} + J_{OH^{-}} = 0 \quad (26)$$

The flow of species containing carbonate is given by

$$J_{CO3^{2-}} + J_{H2CO3} + J_{HCO3^{-}} = 0 \quad (27)$$

The flow of species containing chloride is given by

$$J_{Cl^{-}} + J_{FeCl^{+}} = 0 \quad (28)$$

The flow of species containing sodium is given by

$$J_{Na+}=0 \quad (29)$$

The flow of species containing acetate is given by

$$J_{CH3COOH} + J_{CH3COO^{-}} + J_{FeCH3COO^{+}} + 2\,J_{Fe(CH3COO)2} = 0 \quad (30)$$

The condition for electro–neutrality is

$$\Sigma Z_i\, C_i = 0 \quad (31)$$

The equilibrium constants for the reactions (12) to (22) are:

$$K_1' = \frac{C_{Fe(OH)^{+}} C_{H^{+}}}{C_{Fe^{++}} C_{H_2O}} \quad (32)$$

$$K_2' = \frac{C_{Fe(OH)_2} C_{H^{+}}}{C_{Fe(OH)^{+}} C_{H_2O}} \quad (33)$$

$$K_3' = \frac{C_{H^{+}} C_{OH^{-}}}{C_{H_2O}} \quad (34)$$

$$K_4' = \frac{C_{H_2CO_3}}{C_{H^{+}} C_{HCO_3^{-}}} \quad (35)$$

$$K_5' = \frac{C_{HCO_3^{-}}}{C_{H^{+}} C_{CO_3^{-2}}} \quad (36)$$

$$K_6' = \frac{C_{FeCl^{+}}}{C_{Fe^{++}} C_{Cl^{-}}} \quad (37)$$

$$K_7' = \frac{C_{CH_3COO^{-}} C_{H^{+}}}{C_{CH_3COOH}} \quad (38)$$

$$K_8' = \frac{C_{(CH_3COO)_2 Fe}}{C_{CH_3COO^-} C_{Fe^{++}}} \tag{39}$$

The equations for the diffusion coefficients and the equilibrium constants were derived as a function of temperature. These mathematical relationships were coded as a stand-alone "pit" model and contains 3 separate subroutines (named tulane, linear, and linpac). These subroutines solve the coupled differential equations and linear equations by numerical methods. The tulane subroutine calculates the diffusion coefficients, equilibrium constants, bulk pH, saturated pH, amount of iron necessary for saturation, the concentrations of various species at the surface of the pit, and the pit potential. The linear equations (equations 24 through 31) are solved in the linpac subroutine. The solutions to the linear equations are used to solve the differential equations using the Runge–Kutta method. The Runge–Kutta subroutine calls the linear subroutine, which in turn calls the linpac subroutine, which solves the differential equations. Figure 11 shows an example plot of iron concentration values obtained as a function of fractional pit depth.

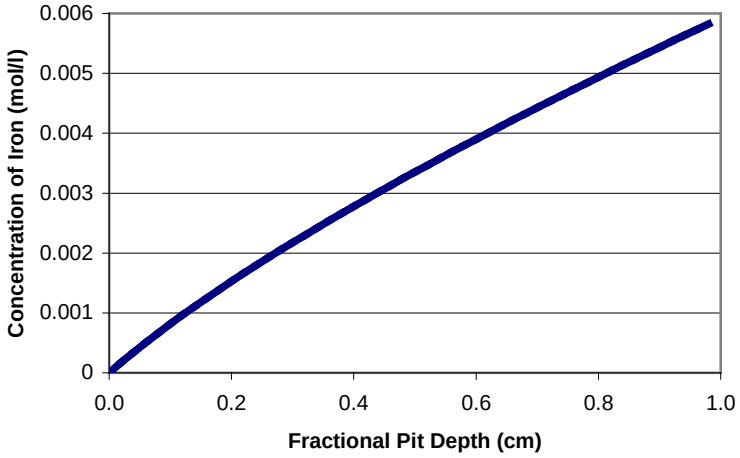

Figure 8. Iron concentration versus fractional pit depth.

Oxidation of elemental iron occurs over the entire length of the pit, not just at the pit bottom. Therefore for a specific pit depth, i, a distribution of corrosion rates occur over the length of the pit. The anodic reaction component of the pitting model calculates the corrosion rate at depth, i, by dividing the total depth into four increments and calculating the corrosion rate at each of these four increments. The final pitting corrosion rate for depth, i, is an average of the four increments. This means that the model is run at the total pit depth, 75% of the pit depth, half of the pit depth, and 25% of the pit depth. The average corrosion rate determined is the average of the four calculated corrosion rates.

3.2 Cathodic Reaction: Diffusion of Hydroxide at the UXO surface

As a result of the cathodic reduction of oxygen to hydroxide, a pH gradient is produced on the UXO surface. Equations 1 and 2 indicate that two hydroxide ions are generated for each atom of iron oxidized. This generation of OH^- ions occurs in the presence of a liquid film containing chlorides, organic acids, sodium, carbonate and bicarbonate, and complexes of iron. Similar to the iron pitting model described in section 3.1, 11 equilibrium reactions can be used to describe this system:

$Fe \rightarrow Fe^{2+}+2e^-$ (40)
$Fe^{2+}+H_2O \rightarrow Fe(OH)^+ + H^+$ (41)
$Fe(OH)^+ + H_2O \rightarrow Fe(OH)_2+H^+$ (42)
$H_2O \rightarrow H^+ + OH^-$ (43)
$H^+ + HCO_3^- \rightarrow H_2CO_3$ (44)
$H^+ + CO_3^{2-} \rightarrow HCO_3^-$ (45)
$Fe^{2+} + CO_3^{2-} \rightarrow FeCO_3$ (46)
$Fe^{2+} + Cl^- \rightarrow FeCl^+$ (47)
$CH_3COOH \rightarrow CH_3COO^- + H^+$ (48)
$Fe^{2+} + CH_3COO^- \rightarrow Fe(CH_3COO)^+$ (49)
$Fe(CH_3COO)^+ + CH_3COO^- \rightarrow Fe(CH_3COO)_2$ (50)

The flow of each species in a unidirectional system, under steady state conditions and in dilute solutions is given by:

$$J_i = -D_i\left[\frac{dC_i}{dx} + \frac{z_i F}{RT} C_i \frac{d\phi}{dx}\right] \quad (51)$$

Where, J_i is the flow of species 'i' in gm–mole / cm^2–sec;
D_i is the diffusion coefficient of 'i' in cm^2/sec;
C_i is the concentration of species 'i' in mol cm^{-3};
X is the depth of the water film on the UXO in cm;
z_i is the valence (unitless),
F is the Faraday constant;
R is the molar gas constant;
T is the absolute temperature in K; and
$\frac{d\phi}{dx}$ is the electric field inside water film on the UXO, V cm^{-1}.

From a mass balance, the following flux equations describe the full system with a generation term (-i/F) shown in the hydroxide equation.

The flow of species containing 'Fe' atoms is given by
$J_{Fe^{2+}} + J_{Fe(OH)^+} + J_{Fe(OH)2} + J_{FeCl^+} + J_{FeCH3COO^+} + J_{Fe(CH3COO)2} = 0$ (52)

The flow of species containing ionizable 'H' atoms is given by

$$J_{H2O} + J_{H}^{+} + 2\,J_{H2CO3} + J_{HCO3}^{-} + J_{CH3COOH} = 0 \quad (53)$$

The flow of species containing hydroxide is given by

$$J_{H2O} + J_{Fe(OH)}^{+} + 2\,J_{Fe(OH)2} + J_{OH}^{-} = -i/F \quad (54)$$

The flow of species containing carbonate is given by

$$J_{CO3}^{2-} + J_{H2CO3} + J_{HCO3}^{-} = 0 \quad (55)$$

The flow of species containing chloride is given by

$$J_{Cl}^{-} + J_{FeCl}^{+} = 0. \quad (56)$$

The flow of species containing sodium is given by

$$J_{Na}^{+} = 0. \quad (57)$$

The flow of species containing acetate is given by

$$J_{CH3COOH} + J_{CH3COO}^{-} + J_{FeCH3COO}^{+} + 2\,J_{Fe(CH3COO)2} = 0. \quad (58)$$

The condition for electro–neutrality is

$$\Sigma Z_i\, C_i = 0 \quad (59)$$

The method of solving these flux equations is identical to the iron–pitting model, and yields a hydroxide ion concentration distribution within the water film on the UXO surface. The pH value at the UXO surface is assumed to be in equilibrium with the pH within the pit.

3.3 Coupling of Anode and Cathode Reactions

The anodic reaction component described in section 3.1 estimates a pH value within the aqueous solution of the pit. The cathodic reaction component described in section 3.2 estimates a pH value at the UXO surface. At equilibrium these two pH values should be equivalent. The third component of the pitting model (shown in Figure 5) is an iterative process by which the corrosion rate in the anodic reaction component is varied until the pH at the wall converges with the pit.

Table 1 shows how the two models converge for the following conditions: a pit depth of 0.0.23 in, UXO water film thickness of 0.79 inches, bulk soil solution pH of 5.5, chlorides at 35 ppm, and a CO_2 partial pressure of 0.003 atm. The final pH at the wall after several iterations was 6.27, this was an increase of 0.77 pH units and produced a corrosion rate prediction from an initial value of 15 mpy to a final value of 7.7 mpy.

Table 1. Convergence of the Iron-Pitting and Hydroxide Diffusion Models

Iron Pitting Model (anodic reaction component)		**Hydroxide Diffusion Model (cathodic reaction component)**	
pH_{pit}	**CR (mpy)**	**pH_{wall}**	
5.5	29.741	6.0	
6.0	15.366	6.36	
6.36	5.896	6.24	
6.24	8.346	6.28	
6.28	7.419	6.27	
6.27	7.684	6.27	→ Convergence

3.4 Determination of Iron Carbonate Scale Formation

The formation of iron carbonate scales within a pit drastically reduces the corrosion rate and in many cases may halt the corrosion altogether. This is a result of the iron carbonate scale shutting down the anodic ability of the pit to further oxide the elemental iron. The formation of the scale is strongly dependent on the pH and the carbon dioxide partial pressure. In addition, the saturation pH at which iron carbonate scales form is dependent on the CO_2 partial pressure. The value of the saturation pH can be calculated using the equilibrium equation from Henry's Law (K_H), the first dissociation equation (K_1), and the second dissociation equation (K_2):

$$K_H = \frac{[H_2CO_3]}{P_{CO_2}} \tag{60}$$

$$K_1 = \frac{[H^+][HCO_3^-]}{[H_2CO_3]} \tag{61}$$

$$K_2 = \frac{[H^+][CO_3^{2-}]}{[HCO_3^-]} \tag{62}$$

$$pK_H = \begin{aligned} &2.238 + 6.348*10^{-3}*T - 9.972*10^{-6}*T^2 + 1.234*10^{-5}*P \\ &+ 0.0658*I^{0.5} - 0.033*I + 0.0479*I^{1.5} + 1.596*10^{-4}*T*I^{0.5} \end{aligned} \tag{63}$$

$$pK_1 = \begin{aligned} &6.331 - 8.278*10^{-4}*T + 7.142*10^{-6}*T^2 + 2.564*10^{-5}*P \\ &- 0.491*I^{0.5} + 0.379*I - 0.06506*I^{1.5} - 1.458*10^{-3}*T*I^{0.5} \end{aligned} \tag{64}$$

$$pK_2 = \begin{aligned} &10.511 - 4.123*10^{-3}*T + 9.297*10^{-6}*T^2 - 2.118*10^{-5}*P \\ &- 1.255*I^{0.5} + 0.867*I - 0.174*I^{1.5} - 1.588*10^{-3}*T*I^{0.5} \end{aligned} \tag{65}$$

Where, T is the temperature in °F, P is the pressure in pounds per square inch, absolute (psia), and I is the ionic strength of the solution. Based on equations 60 through 65 it was possible to determine the relationship between pCO_2 and pH_{sat}. Figure 9 shows a plot of this relationship.

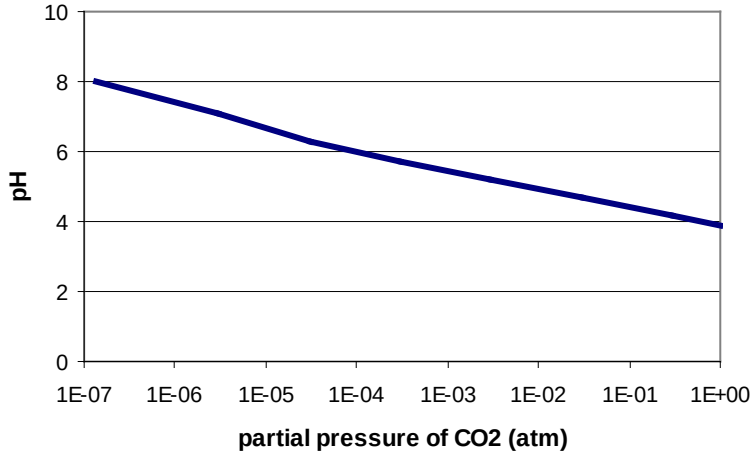

Figure 9. Calculated pH versus partial pressure of CO_2.

The following empirical relationship (based on 47 of the soils studied by Romanoff) has been developed, with an R^2 value of 0.994, to describe the relationship between pH_{sat} and pCO_2

$$pH_{sat} = (-0.56012 * \log_{10}(pCO_2)) + 3.843 \quad (66)$$

Equation 66 can be rearranged to allow the computer model to directly determine the partial pressure using pH_{bulk} .

$$\text{Partial Pressure of } CO_2 \text{ (atm)} = 10^{-\left[\frac{pH-3.843}{0.56012}\right]} \quad (67)$$

When the bulk pH value is lower than the corresponding pH_{sat}, then the input partial pressure is used in further calculations. When the bulk pH is greater than the corresponding pH_{sat}, then equation 67 is be used. The pCO_2/pH relationship is used at bulk pH values above pH_{sat} since iron carbonate scales have begun to form.

Once the iron pitting model is run, the iron and carbonate concentrations can be determined at the boundary of the pit. The equation used to determine the saturation point of iron carbonate is the solubility product.

$$K_{sp} = [a_{Fe^{2+}}] * [a_{CO_3^{2-}}] \quad (68)$$

where,
a_i – activity of species, i (where i is either ferrous iron or carbonate),
$pK_{sp} = 10.39 + (8.3961x10^{-3} \cdot T) + (3.1313x10^{-6} \cdot T^2) - (2.9939x10^{-9} \cdot T^3) + (2.553x10^{-11} \cdot T^4)$ (69)
T – Temperature in K.

The assumed corrosion rate used by the program is continually adjusted until equation 69 is satisfied.

4 Scale Formation and Ionic Diffusion through Scales

Pitting corrosion proceeds rapidly until iron hydroxide scales form and create a physical impediment to oxygen transport to the UXO surface and iron transport away from the pit. Scales form as a result of accumulation of products from the oxidation of elemental iron to ferrous iron and the reduction of oxygen to hydroxide ions (equations 1 and 2). The accumulation of ferrous iron and hydroxide ions in the pit solution enable the formation of scales within the pit (Figure 3).

Initially, pitting corrosion rates are high and lead to the accumulation of ferrous iron (Fe^{2+}) in solution. As the ferrous concentration in the pit increases, the following oxidation reaction occurs:

$$4Fe^{2+} \rightarrow 4Fe^{3+} + 4e^{-} \tag{70}$$

which can be coupled with equation 2:

$$O_2 + H_2O\ 4e^{-} \rightarrow 4OH^{-}$$

This results in a build up in ferric iron (Fe^{3+}) which is significantly less soluble than the ferrous form. For example, at pH 7 the concentration of Fe^{2+} can increase to at least 1000 ppm before precipitation of $Fe(OH)_2$ occurs, but the maximum concentration of Fe^{3+} that can exist without precipitation of $Fe(OH)_3$ is approximately 10^{-12} ppm. If some oxygen is available but the amount is not sufficient to oxidize all of the Fe^{2+} at the mouth of the pit, magnetite Fe_3O_4 may also precipitate:

$$6\ Fe^{2+} + 12\ OH^{-} + O_2 \rightarrow 2\ Fe_3O_4 + 6\ H_2O \tag{71}$$

As precipitation of scales occurs, the scales form a cap on the pit, which reduces the diffusion rates of ions and molecules (iron, oxygen, hydroxide, etc.) into and out of the pit. The thickness of the scale will grow with time as more iron hydroxides form. The chemical makeup and structure of the scale are controlled by the kinetics of precipitation, which initially favors the precipitation of $Fe(OH)_3$ (in the presence of excess oxygen). Other forms of Fe^{3+} precipitates are thermodynamically more stable such as Hematite (Fe_2O_3) and Goethite (FeOOH) will gradually form over an extended period of time. For example, the formation of hematite can be written as:

$$2\ Fe(OH)_3 \rightarrow Fe_2O_3 + 3\ H_2O \tag{72}$$

Although the reaction is thermodynamically favored, the formation of hematite proceeds slowly. The relative stability of various Fe^{3+} oxides and hydroxides can be seen in Figure 10, which shows the aqueous Fe^{3+} concentration in equilibrium with various precipitates at different pH values. Once scales have developed, and diffusion into and out of the pit have become a limiting factor in pitting corrosion, the gradual increase in scale thickness along with the gradual change in crystal structure will dramatically reduce the total corrosion rate. To account for the changes in total corrosion rate resulting from scale formation requires information on the scale growth

rate and permeability. Measurement techniques to quantify these parameters under various soil and climatic conditions are currently unavailable.

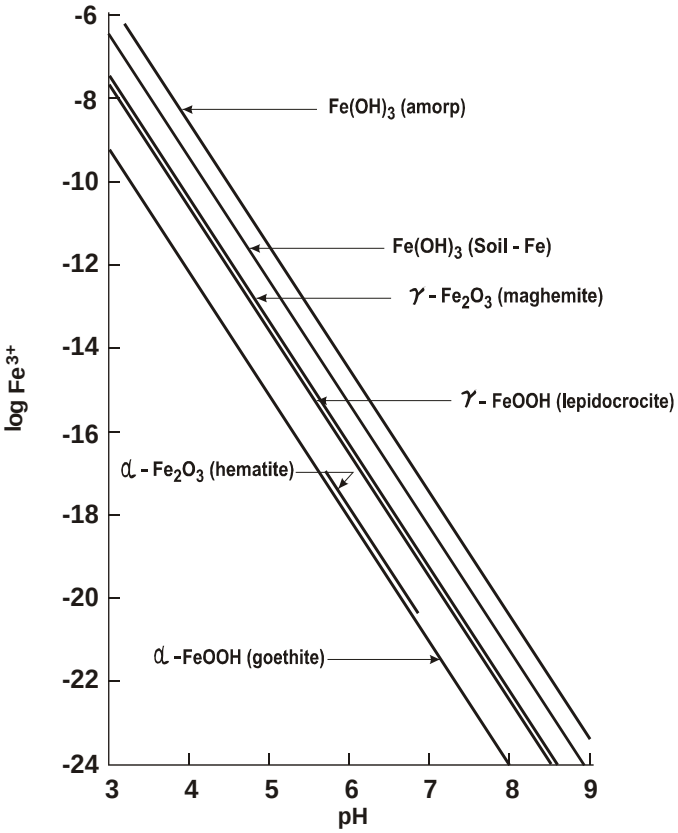

Figure 10. Ferric iron oxide phase diagram.

The dataset from Romanoff, 1957 was used with data from USAEC, 2003 to produce correction factors which can be applied to the pitting corrosion rate profile and account for the formation and growth of scales. Figure 11 presents the result of this analysis and illustrates how the diffusion factors are applied. Initially the Diffusion factors are nearly 1 indicating very little decrease in pitting corrosion rate. Past 50 years, the rate and growth of scales appear to fall into equilibrium with the growing pit such that scale diffusion factors become constant (Figure 12). At times greater than 70 years, many soils likely produce conditions where scale completely halt pitting corrosion. However data was not available to extend the prediction of scale factors to later times. Based on Figure 12, the scale diffusion factor is assumed to reach a constant value and thus applied to all later times. This assumption is conservative in that it allows for pitting corrosion to continue even if conditions halt the pitting process completely.

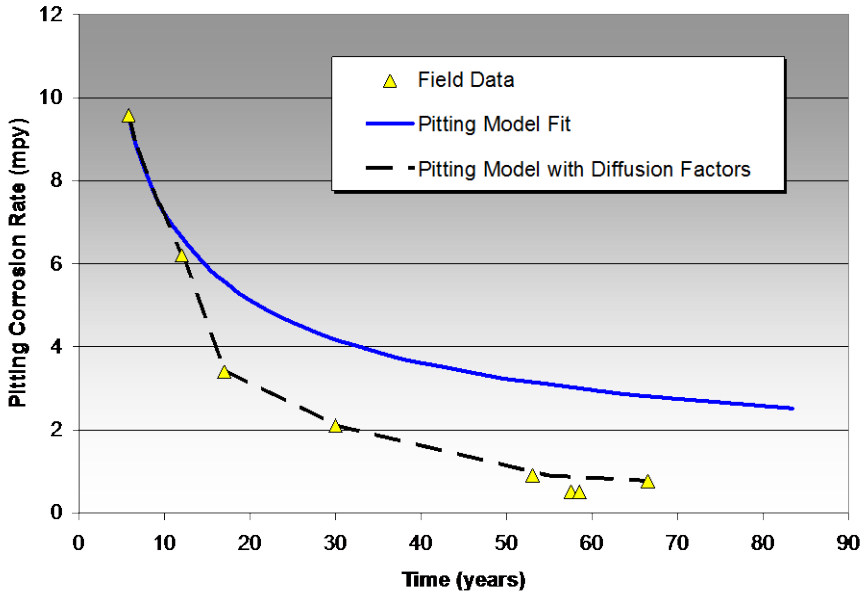

Figure 11. Addition of scale diffusion factors to pitting model results.

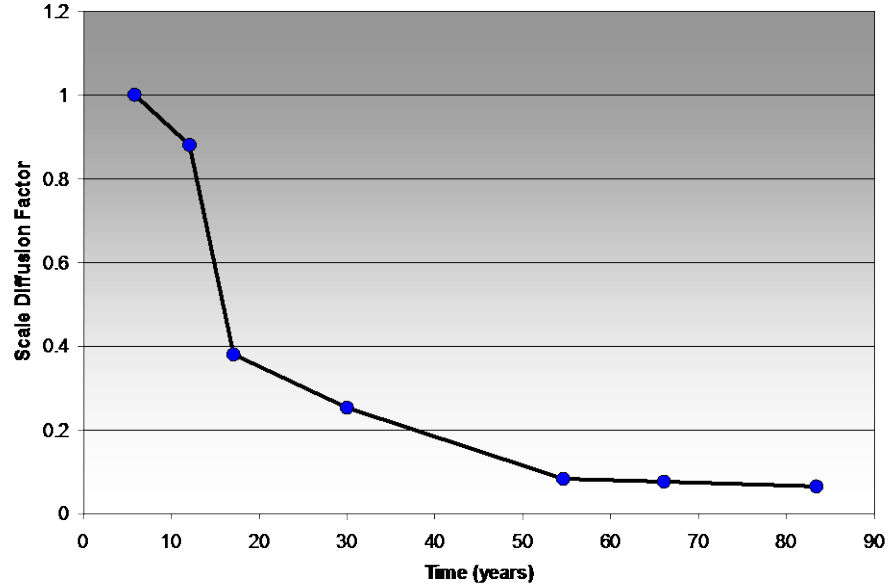

Figure 12. Scale diffusion factors versus time.

5 Pitting Factors and Generalized Corrosion

In addition to pitting corrosion, generalized corrosion also plays an important role on UXO corrosion in the soil. A pitting factor has been developed and correlated with soil physical properties to quantify the ratio generalized corrosion rate to pitting corrosion rate:

$$\text{Pitting Factor (unitless)} = \frac{\text{General Corrosion Rate}}{\text{Pitting Corrosion Rate}} \tag{73}$$

Pitting factors were determined using data from Sites A, C, and Y from the UXO Corrosion Study dataset (USAEC, 2003). These data represented a time period from 56 to 84 years. In addition, 18 year data from eleven different sites were obtained from Romanoff, 1957. Figure 13 shows a plot of the inverse pitting factor for these data. After approximately eight years, the inverse pitting factors decrease to between 3 and 10 years for the 18 year data. Inverse pitting factors from the UXO corrosion study also remained within the same range after 50 years. From this result, pitting factors are assumed to remain constant after 10 years and differences are assumed to be a result of soil and climatic properties.

A regression equation has been developed using pitting factors from the Romanoff, 1957 data and the UXO Corrosion Study data. The parameters considered in the correlation were resistance, moisture content, pH and porosity. The resultant is as follows:

$$PF = \left[-2.544\,E-04 * R + \left(\frac{43.03}{\theta_v}\right) - \left(\frac{1.478}{pH}\right) - (4.684E-02 * \phi) + 5.07372 \right]^{-1} \tag{74}$$

Where R = Resistivity in ohm–cm, θ_v = % Moisture Content, pH = pH of the soil, and ϕ = % Porosity. The R^2 value of the fit to the data was 0.86.

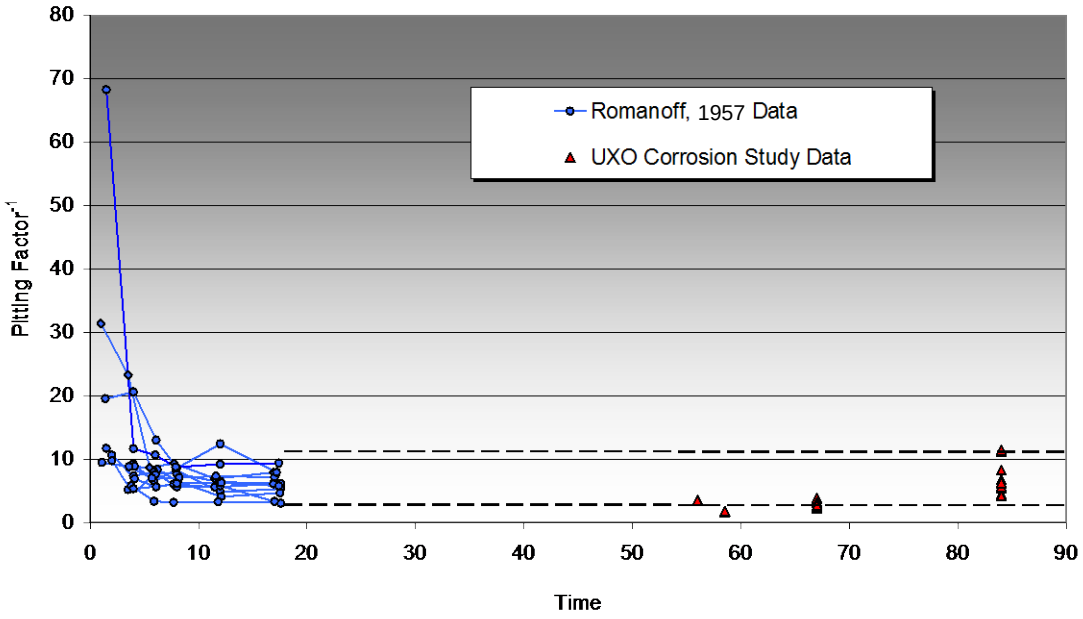

Figure 13. Pitting factors for Romanoff's soils and corrosion study sites A, C, and Y.

UXO-Corr-Mod III determines pitting corrosion rates at incremental pit depths. Once a pitting corrosion rate is calculated, the model applies the pitting factor to calculate the generalized corrosion rate. The total corrosion rate for a specific pit depth is then the sum of the pitting corrosion rate and the generalized corrosion rate.

6 Estimation of Corrosion Rates and Time to Perforation

UXO-Corr-Mod III produces results as either a corrosion rate profile or determines the time to failure for a given metal thickness. To create a corrosion rate profile (i.e. the change in corrosion rate over time), the model calculates corrosion rates at specific pit depths and the time required to reach each pit depth. To determine the time to perforation, the corrosion rate profile is first calculated up to the given metal thickness. The time to perforation is then estimated from the resulting corrosion rate profile.

7 References

Millington, R.J. and J.P. Quirk. 1959. Permeability of porous media. Nature 183:387-388.

Romanoff, M. 1957. Underground Corrosion. National Association of Corrosion Engineers, Houston, TX.

United States Army Environmental Center (USAEC). 2004. 2004 SERDP Final Technical Report - UXO Corrosion in Soil. USAEC. Aberdeen, MD.

Appendix A3

UXO CORROSION MODEL PHASE III USER'S MANUAL

PRAXIS
ENVIRONMENTAL TECHNOLOGIES, INC.
1440 Rollins Road, Burlingame, California 94010
(650) 654-5488

UNIVERSITY OF LOUISIANA Lafayette

Note: The installation disk containing the model includes a Read_me.txt file which provides a consolidated description on how to install this software.

Table of Contents

1.0 Introduction

This manual is designed to help the user to run the Phase III UXO Corrosion Model (UXO Corr-Mod III). This model has been developed by the University of Louisiana, Lafayette in conjunction with Praxis Environmental Technologies, Inc for the US Department of Army, Army Environmental Center (USAEC). Funding for this project was provided by both the USAEC and the Department of Defense, Strategic Environmental Research and Development Program (SERDP).

It is recommended that the user read this manual before attempting to run the model. This program runs on any Windows based PC and can be installed and accessed from a hard drive. To run this program, insert the CD–ROM into the CD–Drive and the following screen opens up automatically:

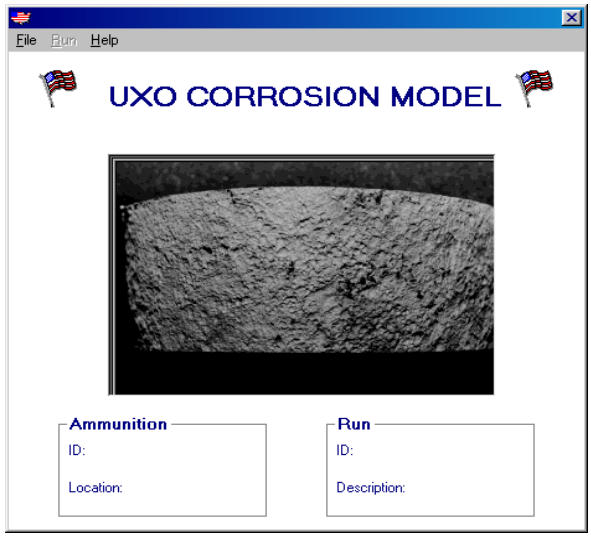

To install the model, run the Setup.exe file. After installation run the application "UXO Corrosion Model.exe".

2.0 Data Input

There are three ways to begin the program. One way is to create a new file and enter all the data and save it. The second method is to re–run the same data immediately and the third procedure is to open an existing file and change the previously saved data and then save it as a new run. One of the important features of this model is that multiple runs can be made for the same Ammunition ID and location with different parameters and the changes can be saved as a new run. This manual will help the user to operate the program in each of the cases described.

2.1 Case I: Creating a New File

2.1.1 System Selection

To open a new file select:
File>Ammunition ID>New:

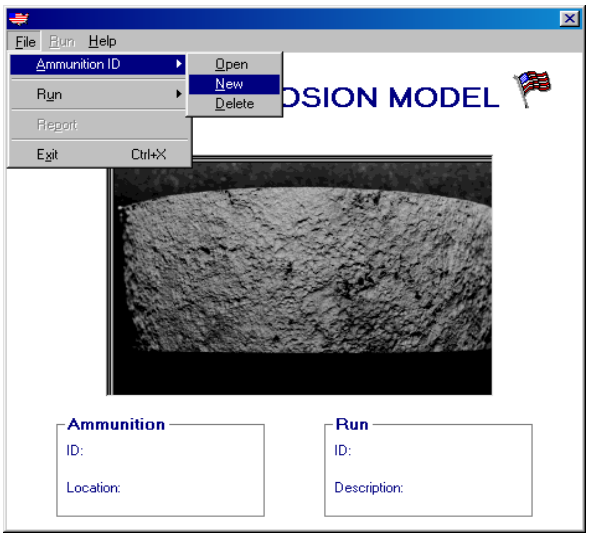

The following screen appears:

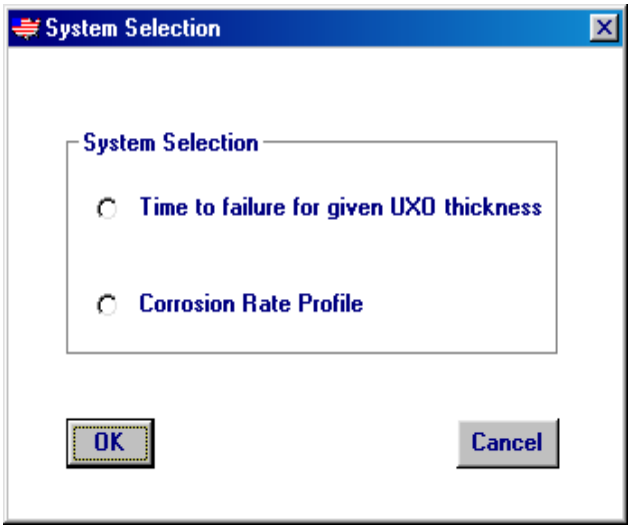

The system selection windows gives two choices, 'Time to failure for given UXO thickness' and 'Corrosion Rate Profile'. By choosing the first option, the program will calculate the time to failure of the UXO based on the total UXO's thickness. The second option will calculate the successive corrosion rate for an exposure period between 75 and 100 years at a pit

depth interval of 0.05 inches. The Corrosion Rate Profile is described further in Section 3.0. Choose the desired system and click **OK**.

The following window (below) is labeled 'Ammunition Info'. Type an Ammunition ID and the Location along with the Run ID and Run Description on the screen that follows. After inputting the information click **Add** and the information appears on the bottom of the first screen shown. After completion of the Ammunition Info window, the model proceeds to the input data windows. Click **Cancel** to return to the main menu.

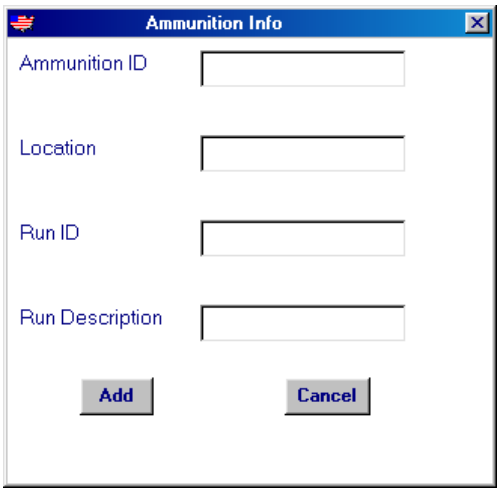

In case the user doesn't enter all the information that is required to save the data, one of the following four error screens appear (below). Click **OK** and enter the missing data.

2.1.2 Input Screen 1: Film Thickness Parameters

The 'Film Thickness Parameters' window has all the required input data to calculate the average water film thickness surrounding the UXO surface. Details about the film thickness calculation can be found in the Technical Manual. For the user's convenience, units are provided. Click **Next** to proceed to Input data Screen 2 or click **Back** to return to the previous screen. The **Cancel** button will take the user directly to the main screen.

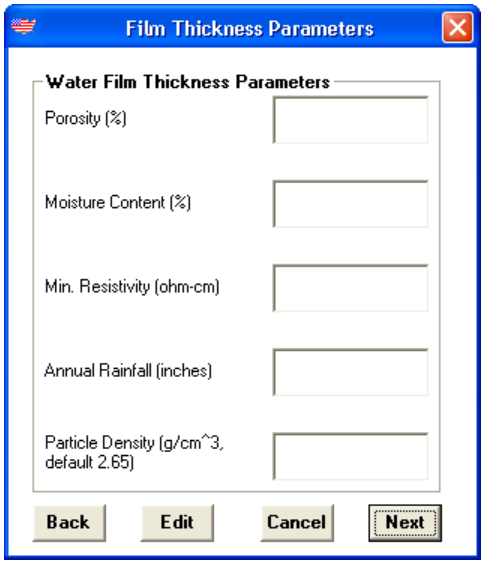

While entering data, only numerical values (including the decimal) are acceptable in the input text box. Other characters like $, @, #, etc., as well as the letters of the alphabet (including scientific notation) are not acceptable and will produce an input error.

If no value for particle density is entered, the model assumes a default value of 2.65. If the users fails to provide a value for porosity, moisture content resistivity, or annual rainfall, then one of the following four error screens will appear. Click **OK** and enter the missing data and click **Next** to proceed.

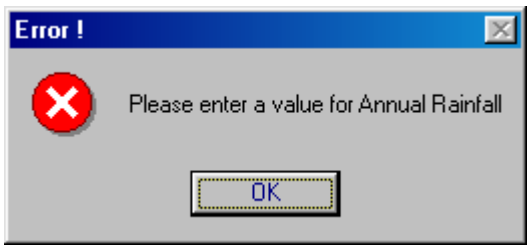

2.1.3 Input Screen 2: Physical Parameters

The 'Physical Parameters' window follows the 'Film Thickness Parameters' window and provides input data to the model. The input physical parameters describes the physical characteristics of and around the UXO.

A 'Metal Thickness' input is provided when running the 'Time to failure for given UXO thickness' system. The metal thickness is required to determine the time to perforation. Since the metal thickness is not needed to determine the corrosion rate profile, the 'Metal Thickness' input is not present in the Corrosion Rate Profile system. The user can either go back to Screen 1 (if there are any changes to be made in the previous data) or input the requested data and click **Next** to proceed further. The **Cancel** button will take the user directly to the main screen.

The following is Input Screen 2 for "Time to Failure" system and has four inputs. The Corrosion Rate Profile system has only four inputs.

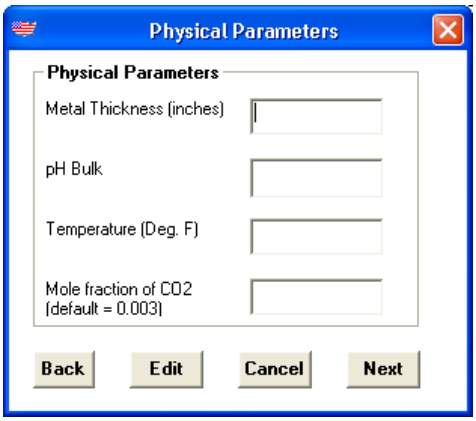

If left blank, the program takes default values for Temperature (75^{o}F) and carbon dioxide partial pressure (0.003 atm). If any of the other values are not entered one of the following screens will appear. Click **OK** and enter the missing data and continue onto the next screen.

2.1.4 Input Screen 3: Chemical Parameters

This window allows the user to input soil chemical analytical data into the model. The units for the various parameters should be mg/kg-soil. The user can also go back to the previous data screens, click 'Cancel' to return to the main menu, or click **Execute** to begin the program. The model assumes a default value of 0 mg/kg-soil for parameters that the user leaves blank. No error messages will appear for soil chemical parameters left empty.

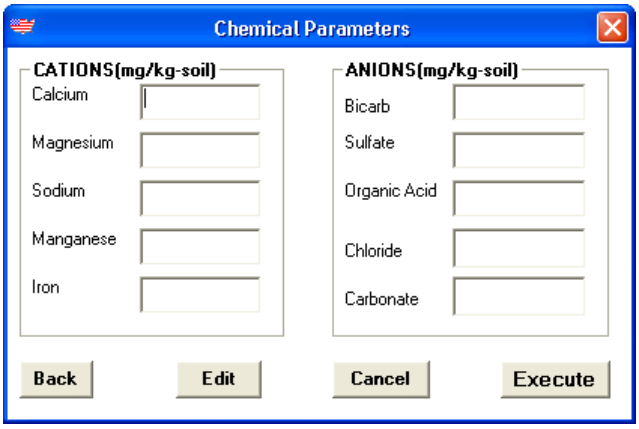

The following screen appears as the program is running. Allow a nominal time of 1–2 minutes for the complete calculation. This screen disappears after the calculations are completed.

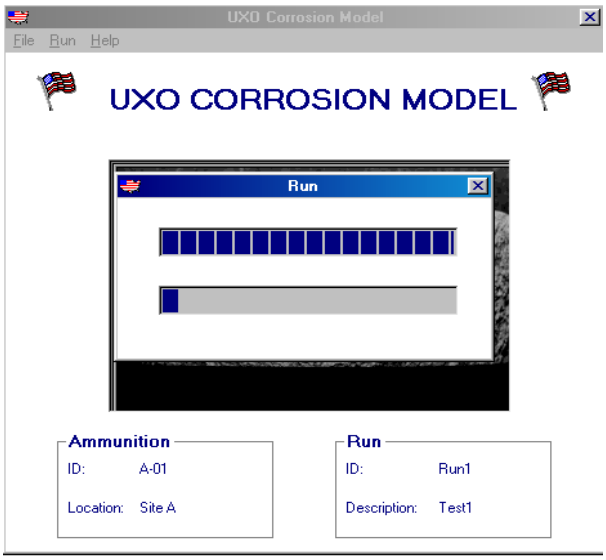

Once complete, the results can be examined by selecting the ***File>Report*** on the main menu. The user should note that higher pH conditions require longer running time.

UXO-Corr-Mod III has some limitations on acceptable soil properties. Anaerobic soils and calcareous soils are not valid for UXO-Corr-Mod III. When soils with calcareous conditions are inputted, the following error message appears,

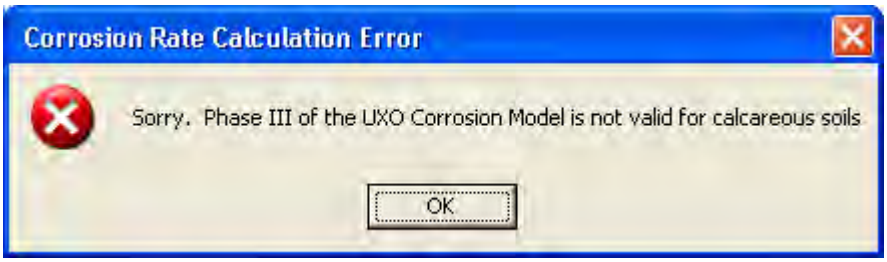

2.2 Case II: Re–run the Same File

To re–run the same Ammunition ID using different physical or chemical data the user can directly go to the main menu and click ***Run*** and the first input data screen will appear. The user can use the **Edit** button to change any of the input data and re–run the program.

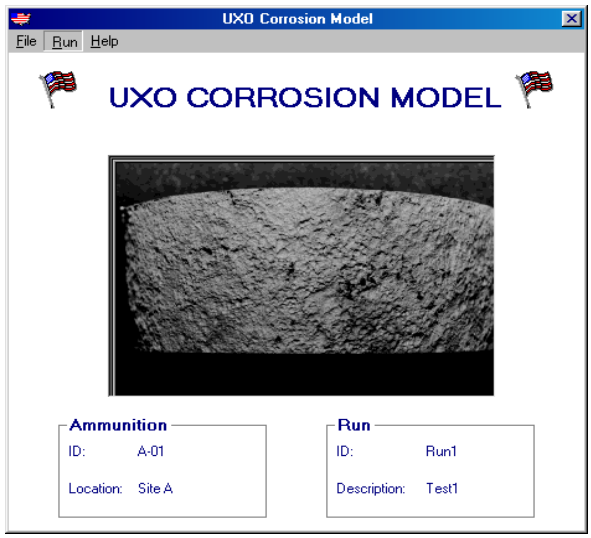

Note: *Run* is not active if the program has not been executed at least once.

Once the **Edit** button has been entered and changes made to the initial dataset, the following screens are displayed to save the changes. The program will ask the user if the data should be saved as a new run. Entering **Yes** will display the message box screen asking the user to provide the run description. The program runs even if the user clicks **No** but the altered data will not be saved.

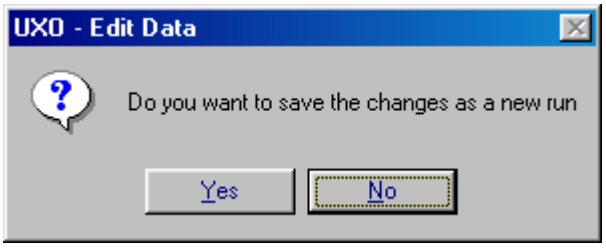

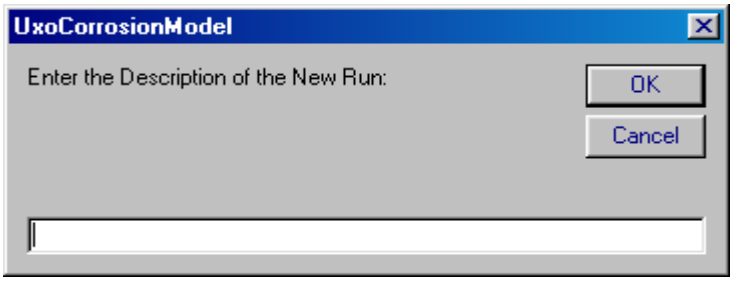

2.3 Case III: Run an Existing File

Select ***File>Open*** to open the window displaying the system selection (see Section 2.1.1). Separate input data files are stored for each system ('Time to Failure' or 'Corrosion Rate Profile'). Once the user chooses which run is to be run, then existing input data file may be selected.

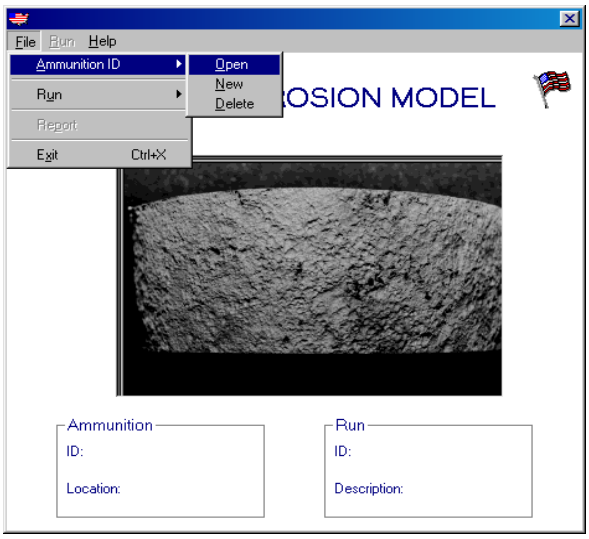

After the 'System Selection' window, the 'Ammunition Selection' window will appear. The user may then choose from existing data files from the 'Ammunition ID' scroll bar. Once the data file of interest is chosen, then the specific run should be chosen from the 'Run' scroll bar.

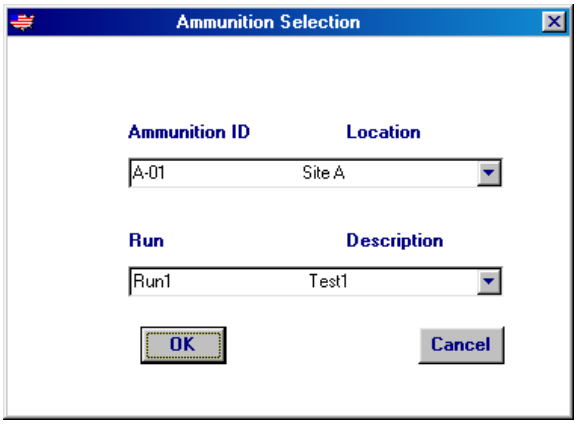

If Ammunition ID is not entered the following warning screen appears.

Once the appropriate file is selected, then the first input screen appears and the user can continue as described in section 2.1.2.

3.0 Results

UXO Corr-Mod III automatically generates a 'Results.txt' file for both the 'Time to failure' and 'Corrosion Rate Profile' systems. The Model additionally generates plots for the 'Corrosion Rate Profile' system. These results can be viewed by selecting ***File>Report>Results***. The sample screen for the result is as shown below. These results can be printed.

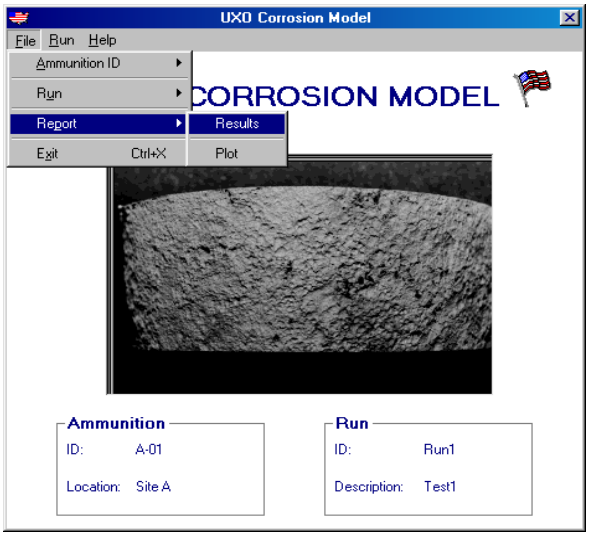

For the "Time to Failure" of the UXO of known thickness the output is a simple table. Table 1 shows the results for this system.

Table 1. Results for a Time To Failure System

**********RESULTS**********

Water Film Thickness	=1.20 inches
Pitting Factor	=3.41
pH at the wall	=5.65
Metal Thickness	=0.5 inches
Theoretical CR	=04.70 mpy

```
Adjusted CR                =00.32 mpy
Total CR                   =00.41 mpy
Time to failure            =1226.28 years
```

An example of the output information for the "Corrosion Rate Profile" system is shown in Table 2 below:

Table 2. Results for Corrosion Rate Profile System

```
**************************************************************************
                      Water Film Thickness      =1.20 inches
                      Pitting Factor            =3.41
                      pH at the wall            =5.46
************************ Corrosion Rate Profile ****************************
  Pit Depth    Time of Exposure    Theoretical CR     Adjusted CR     Total CR
    (in)           (yrs)              (mpy)             (mpy)          (mpy)

  0.050          01.07              46.62              46.62          60.28
  0.100          03.85              25.96              25.96          33.56
  0.150          07.86              19.07              18.52          23.95
  0.200          13.48              14.84              10.96          14.17
  0.250          20.51              12.19              03.86          04.99
  0.300          28.31              10.60              02.79          03.61
  0.350          38.29              09.14              01.79          02.31
  0.400          47.93              08.35              01.08          01.40
  0.450          60.66              07.42              00.59          00.76
  0.500          72.58              06.89              00.52          00.68
  0.550          86.48              06.36              00.46          00.59
```

The 'Corrosion Rate Profile' system plot can be viewed by selecting ***File>Report>Plot***. A typical plot is as shown below.

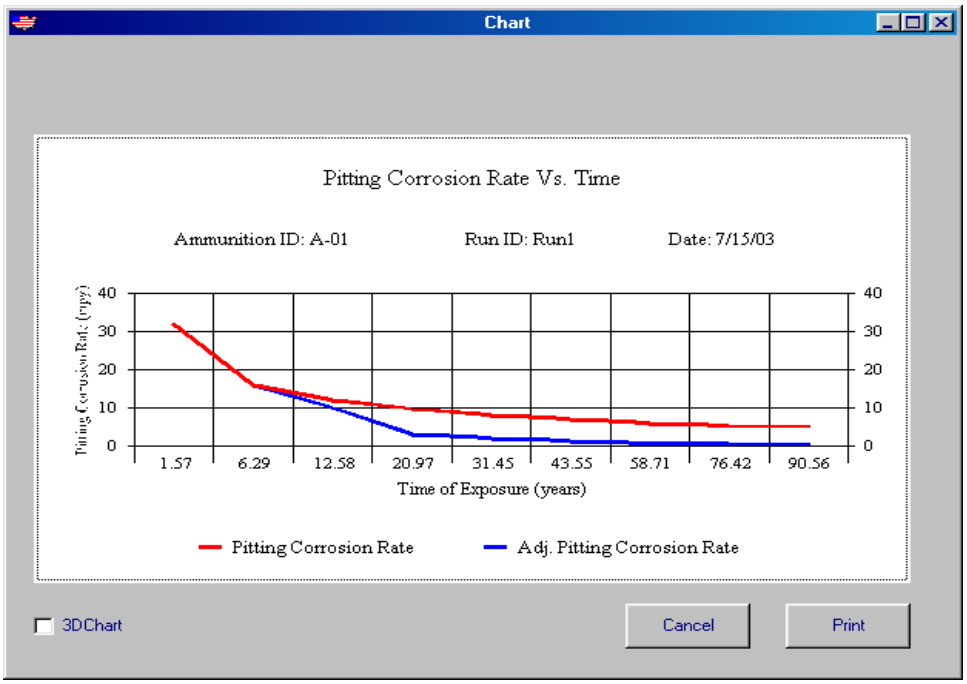

This plot can also be viewed 3–dimensionally by selecting '**3DChart'**. A typical 3-dimensional chart looks as shown below.

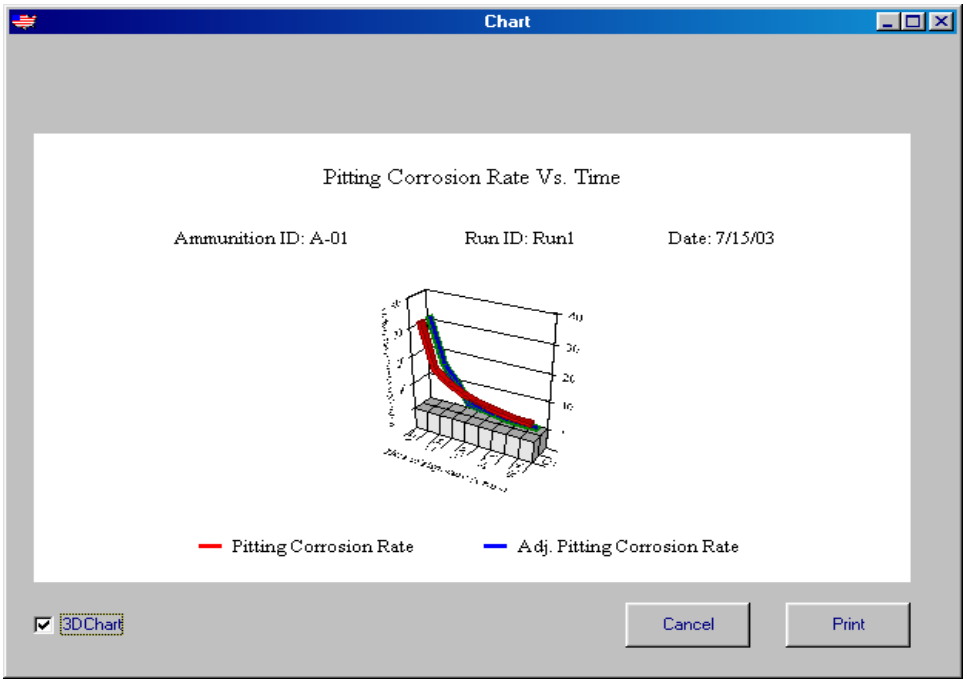

4.0 Deleting Files

4.1 Deleting an Entire Input Data File

In UXO Corr-Mod III, Input Data Files are called "Ammunition ID" Files. To delete an entire Ammunition ID file (and all of the associated runs) Select ***File>Ammunition>Delete***. This opens up a screen that contains a window with the saved Ammunition IDs.

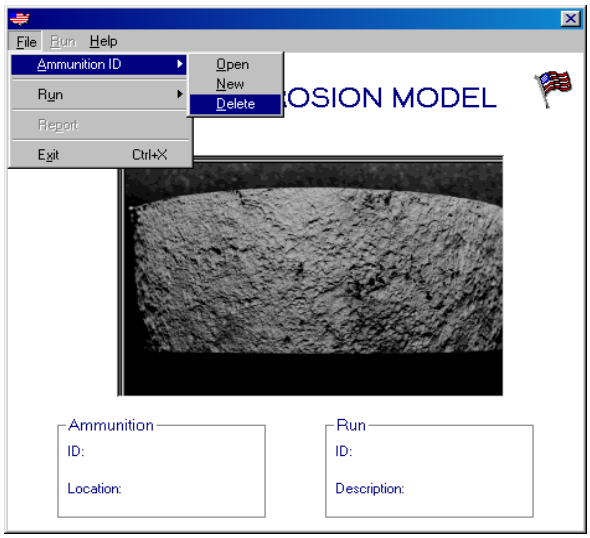

Select the Ammunition ID file, which contains the data that is to be deleted, by first choosing the correct system.

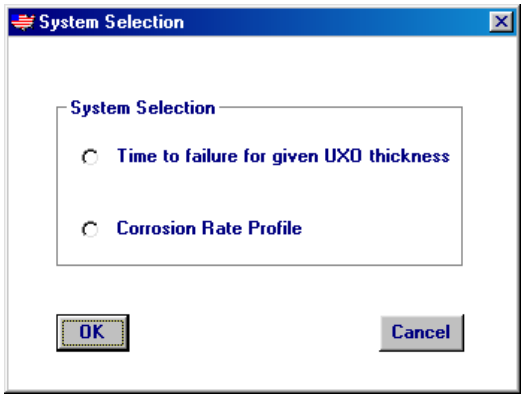

Next, select the unwanted Ammunition ID and press **Delete**. This will delete the Ammunition ID and all the runs associated with this ID. Click **Cancel** and the program returns to the main menu.

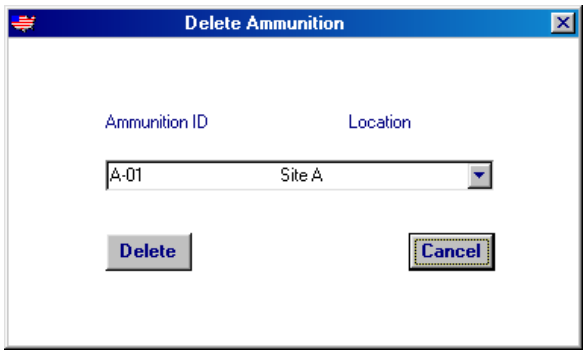

If Ammunition ID is not selected the following warning screen appears. Click **OK** and select the Ammunition ID to be deleted.

The following screen is displayed after the data is completely deleted from the memory.

4.2 Deleting a Single Run

To delete a single run of an Ammunition ID, select ***File>Run>Delete*** and click **Delete**. Choose the relevant system ('Time to failure' or 'Corrosion Rate Profile') and then select the Ammunition ID that the run is associated with. Finally choose the appropriate run to be deleted.

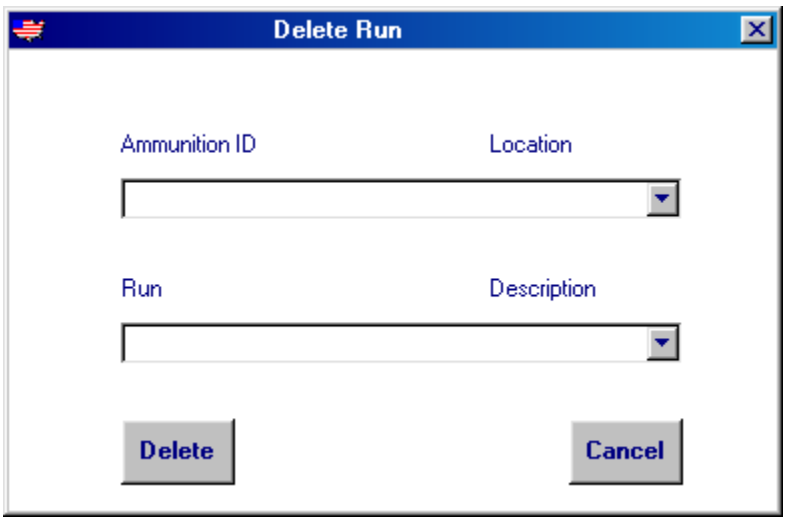

A message box appears which ensure that the users wants to delete the run and upon entering **Yes**, the file is deleted. Entering **No** returns to the main menu without any change to the run.

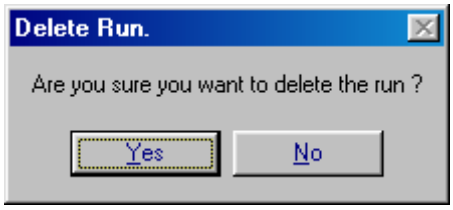

The following screen is displayed after the data is completely deleted.

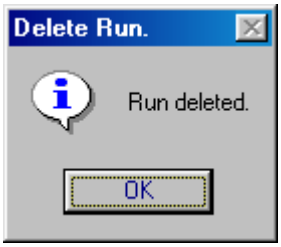

5.0 Accessing Manuals and the Input Data Sheet

The model includes a technical manual, user manual, and an input data sheet. These documents can be found in the Help tab. These three documents are in Microsoft Word format.

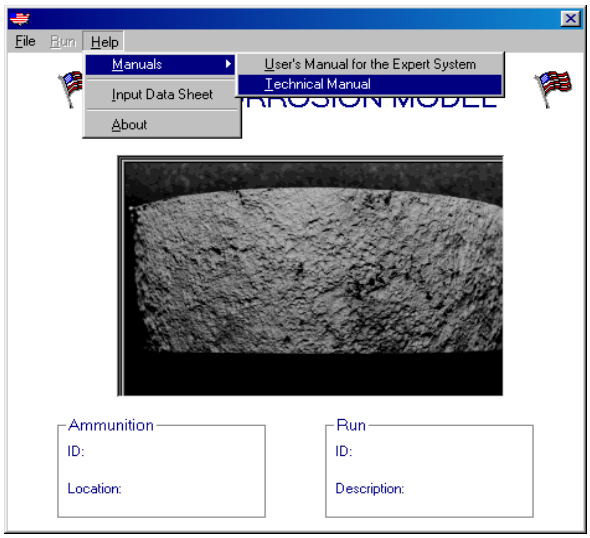

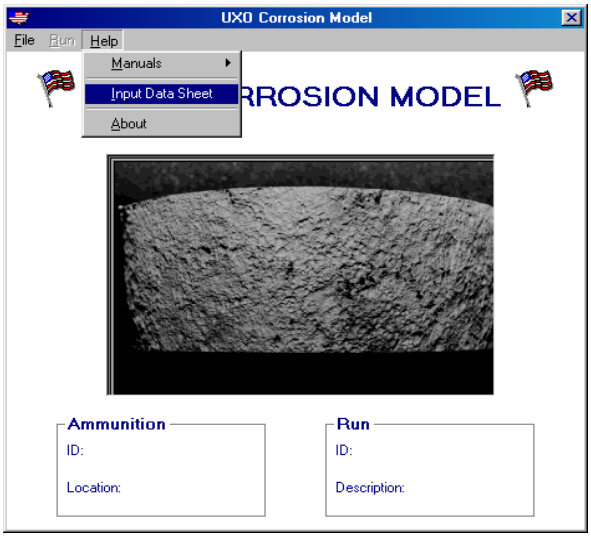

An input data sheet is provided in the model which lists all the input parameters. To view this Microsoft Word document Select ***Help>Input Data Sheet*** and the data sheet opens up. This can be filled out, printed, and saved.

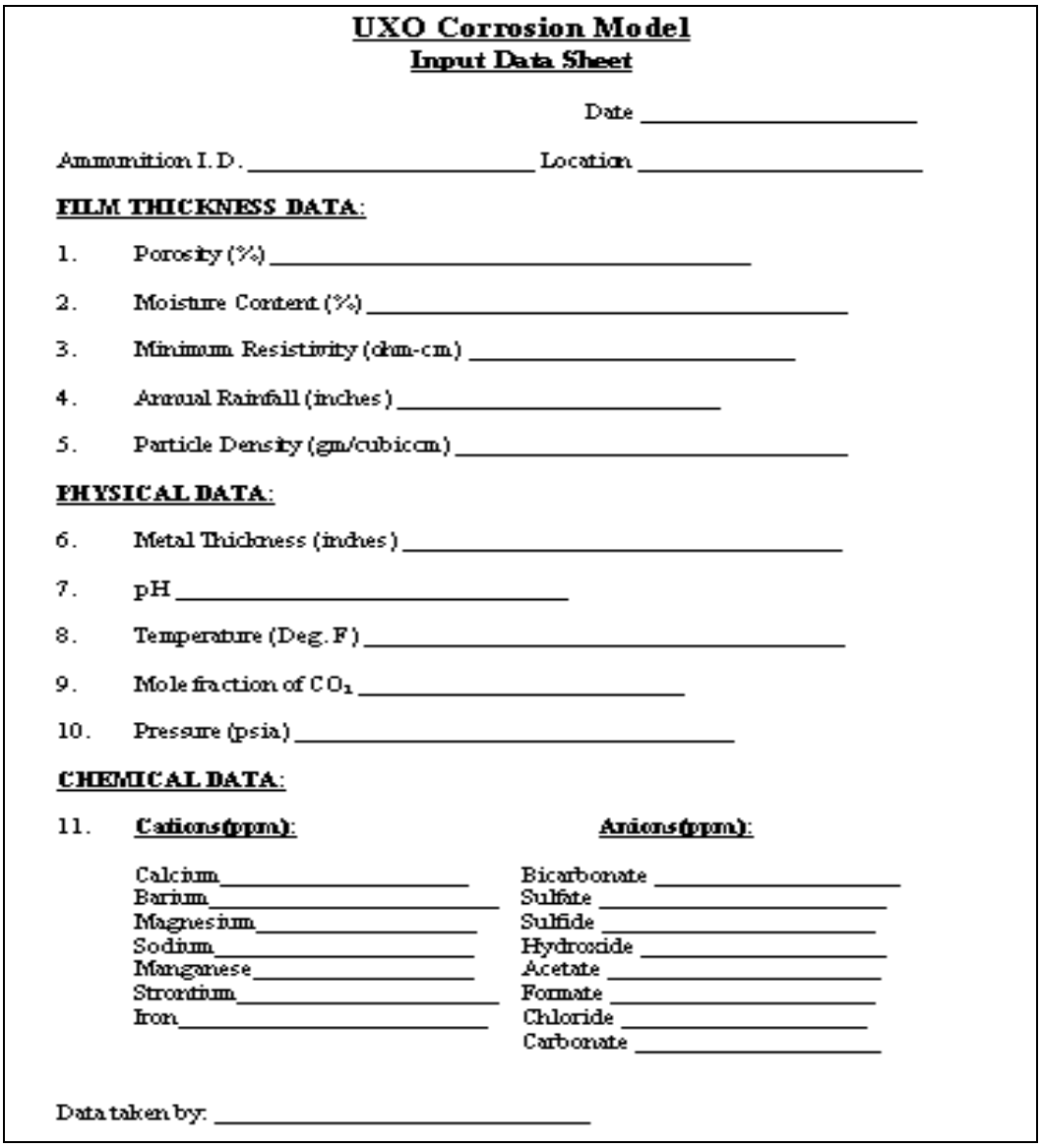

UXO Corrosion Model
Input Data Sheet

Date _____

Ammunition I.D. _____ Location _____

FILM THICKNESS DATA:

1. Porosity (%) _____
2. Moisture Content (%) _____
3. Minimum Resistivity (ohm-cm) _____
4. Annual Rainfall (inches) _____
5. Particle Density (gm/cubiccm) _____

PHYSICAL DATA:

6. Metal Thickness (inches) _____
7. pH _____
8. Temperature (Deg. F) _____
9. Mole fraction of CO_2 _____
10. Pressure (psia) _____

CHEMICAL DATA:

11. **Cations(ppm):** **Anions(ppm):**

Calcium_____	Bicarbonate _____
Barium_____	Sulfate _____
Magnesium_____	Sulfide _____
Sodium_____	Hydroxide _____
Manganese_____	Acetate _____
Strontium_____	Formate _____
Iron_____	Chloride _____
	Carbonate _____

Data taken by: _____

6.0 'About' and 'Disclaimer' Windows

Details about the disclaimer can be read by selecting ***Help>About***.

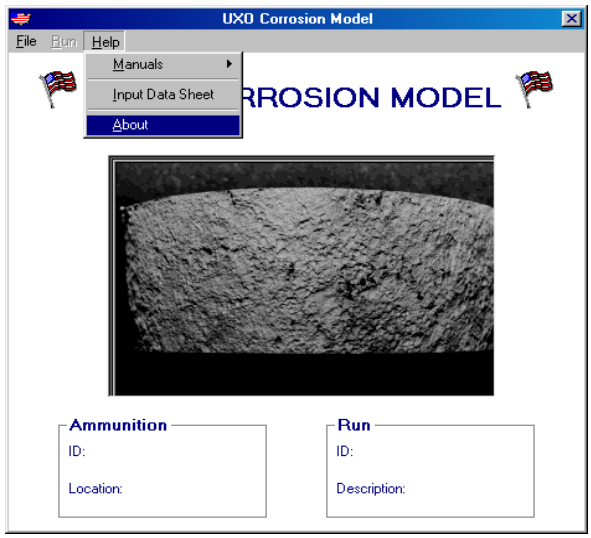
UXO Corrosion Model
File
Run
Help
Manuals
Input Data Sheet
About
RROSION MODEL
Ammunition
ID:
Location:
Run
ID:
Description:


About
This UXO Corrosion Model was developed at The University of Louisiana at Lafayette and sponsored by USAEC-SERDP Program (Project ID: 5TS5701C221)
Copyright 2003
Disclaimer
OK

If the user clicks on the **Disclaimer** button, the following message box about the disclaimer is displayed. Press **OK** to return to the main menu.

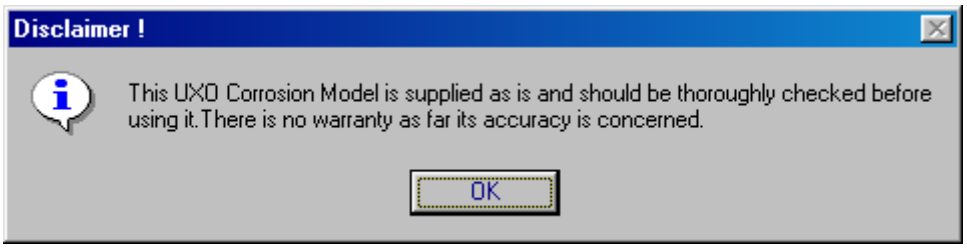

7.0 Closing the Program

There is only one way to close the UXO Corr-Mod III program. Select ***File>Exit*** on the main menu to exit the program.

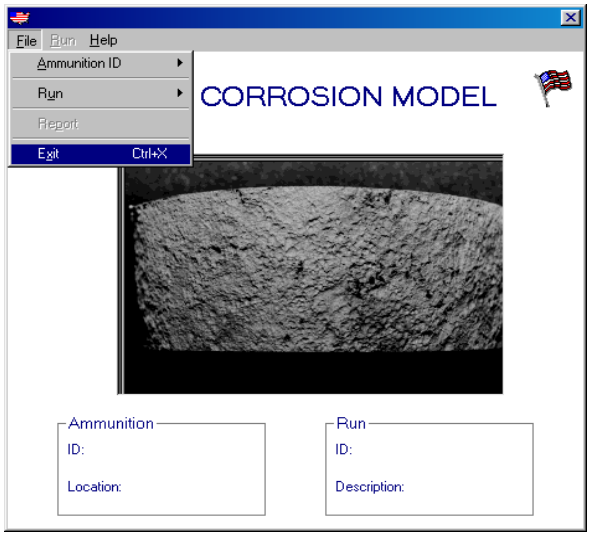

If the user tries to exit the program by closing the window the following screen appears:

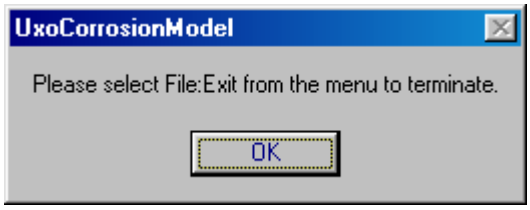

Appendix A4

ENERGETIC TRANSPORT MODEL

PRAXIS
ENVIRONMENTAL TECHNOLOGIES, INC.
1440 Rollins Road, Burlingame, California 94010
(650) 548-9288

Table of Contents

List of Figures

List of Tables

List of Variables

a	prolate spheroid x-axis radial distance
$a`$	V/2D
A_m	function defined by equation 47
A_{pit}	average cross-sectional area of a single pit
A_{uxo}	total outer surface area of the UXO
B	depth of vadose zone
b	prolate spheroid y-axis radial distance
C	soil pore water concentration
C_{sat}	energetic solubility in water
C_w	ground water concentration
$C_{w,max}$	maximum groundwater concentration
$\hat{C}_w$	integral transform of groundwater concentration
$\breve{C}(s)$	Laplace transform of $\hat{C}_w$
$C_{\infty,j}$	energetic concentration in water at the surface of the UXO shell
CN	National Resource Conservation Service (NRCS) curve number
d_1	upper depth of UXO in vadose zone
d_2	bottom depth of UXO in vadose zone
$d\%$	monthly percentage of daytime hours per year
D	effective diffusion coefficient, $\alpha_L I + D_m$
D_m	diffusion coefficient of energetic in water
$D_{m,j}$	diffusion coefficient of energetic, j, in water
$D_{w,x}$	effective diffusion and dispersion coefficient in the x-direction
$D_{w,y}$	effective diffusion and dispersion coefficient in the y-direction
$D_{w,\zeta}$	effective diffusion and dispersion coefficient in the ζ-direction
e	prolate spheroid eccentricity, $(1/a)\sqrt{a^2 - b^2}$
ET	cumulative evapotranspiration in inches per unit time
ET_m	monthly evapotranspiration
f_j	volumetric fraction of energetic, j, within the UXO fill
f_{oc}	fraction of carbon content in soil
G	spatially transform soil pore water concentration, $C/e^{a`z}$
$g(z,t)$	release of energetic from UXO (source term in vadose zone transport equation)
$g_0(t)$	
g_j	mass transfer coefficient for energetic, j, between the UXO and surrounding soil

g_{uxo}	mass transfer coefficient for energetic between the UXO and surrounding soil
$\widetilde{G}$	integral transform of G
H	aquifer thickness
I	cumulative infiltration rate in inches per unit time
J_0	mass flux of explosive contaminant entering groundwater from the vadose zone
K_d	distribution coefficient, 0.6 f_{oc} K_{ow}
K_{ow}	octanol-water coefficient for energetic
k_c	monthly empirical crop coefficient
k_i	monthly temperature coefficient
L	length of range in direction of groundwater flow
ℓ	pit depth (i.e. thickness of UXO shell)
M	total number of energetic lumps
$\dot{m}_{j,pits}$	mass release rate through perforated pits
$\dot{m}_{uxo}$	mass release rate from one UXO item
n_{pits}	density of through-pits (i.e. total number of pits/surface area of shell)
N_{uxo}	number of UXO items
n_{uxo}	density of UXO items in the range
$N(\beta_m)$	normalization integral for the vadose zone eigenvalue problem
$N(\beta_n)$	normalization integral for the groundwater eigenvalue problem
P	cumulative precipitation in inches per unit time
$\Re$	radius of the sphere (or characteristic dimension of the UXO such as the average of the length and width)
R	retardation coefficient in soil, ρ_b K_d + θ
R_w	retardation coefficient in groundwater, 1 + ρ_b K_d/ϕ
Re	Reynolds Number
RO	cumulative runoff in inches per unit time
s	Laplace transform variable
Sc	Schmidt Number
T	monthly mean temperature
$T_{1/2}$	energetic half-life in soil
t_{infil}	total infiltration period for transient infiltration events, t_k
U	pore velocity of groundwater
uf	monthly consumptive use factor
V	pore water velocity in the vadose zone
ν_w	kinematic viscosity of water (1.06 x 10^{-6} m^2/s, 49,400 in^2/yr)
W	width of the range
X	horizontal coordinate in the direction of groundwater flow
x	distance in direction of groundwater flow
Y	horizontal coordinate perpendicular to the direction of groundwater flow
Z	eigenfunction defined by equation 50
Z_w	eigenfunction for groundwater transport defined by equation 66
z	vertical coordinate where z = 0 at the ground surface
α_L	longitudinal dispersivity
α_m	transform variable defined by equation 48
α_s	$\cosh^{-1}(e^{-1})$

α_T	transverse dispersivity
β	geometric factor for approximating the explosive fill shape
β_m	eigenvalue defined by equation 52
β_n	eignevalue defined by equation 68
Γ	length of the cylinder
Δt_k	duration of a steady infiltration period with mass release rate, $\dot{m}_{uxo,k}$
ε	distance into pit of depth, ℓ
ζ	vertical coordinate in groundwater
$\Theta(\chi)$	Heaviside step function defined by equation 76
θ	volumetric soil moisture content
λ	first order degradation constant
λ_w	first-order degradation constant in groundwater
ρ_b	soil bulk density
τ	tortuosity in soil
ϕ	soil porosity

1. Introduction

A model has been developed which estimates energetic releases from buried and corroded UXO into groundwater. The overall purpose of the model is to provide an order-of-magnitude estimate for the maximum energetic groundwater concentration resulting from a UXO release. This report describes this model and is organized into eight sections. Section 2 describes equations used to describe site characteristics such as infiltration rates and presents site data and UXO data used to develop and test this model. Section 3 present a simplistic model which uses broad assumptions to provide a first screen of possible release risks. Use of this simplistic approach is helpful in understanding the overall processes and mechanisms governing energetic release and transport. Sections 4 through 6 present a detailed mathematical model for site conditions and energetics which the screening model in Section 3 indicates as a potential risk. Section 7 presents results of testing the model with data from the UXO corrosion study and Section 8 provides references. The detailed mathematical model (Section 4 through 6) has four components. The first component describes the mass transfer of energetics out of a single corroded UXO and into the surrounding soil. The second component extends the single item solution to multiple items over the area of a range. The third component is a model for the energetics transport through the vadose zone down to groundwater. The fourth and final component is a groundwater transport model describing the migration of energetics through an aquifer. Schematics of the system are shown in Figures 1 and 2.

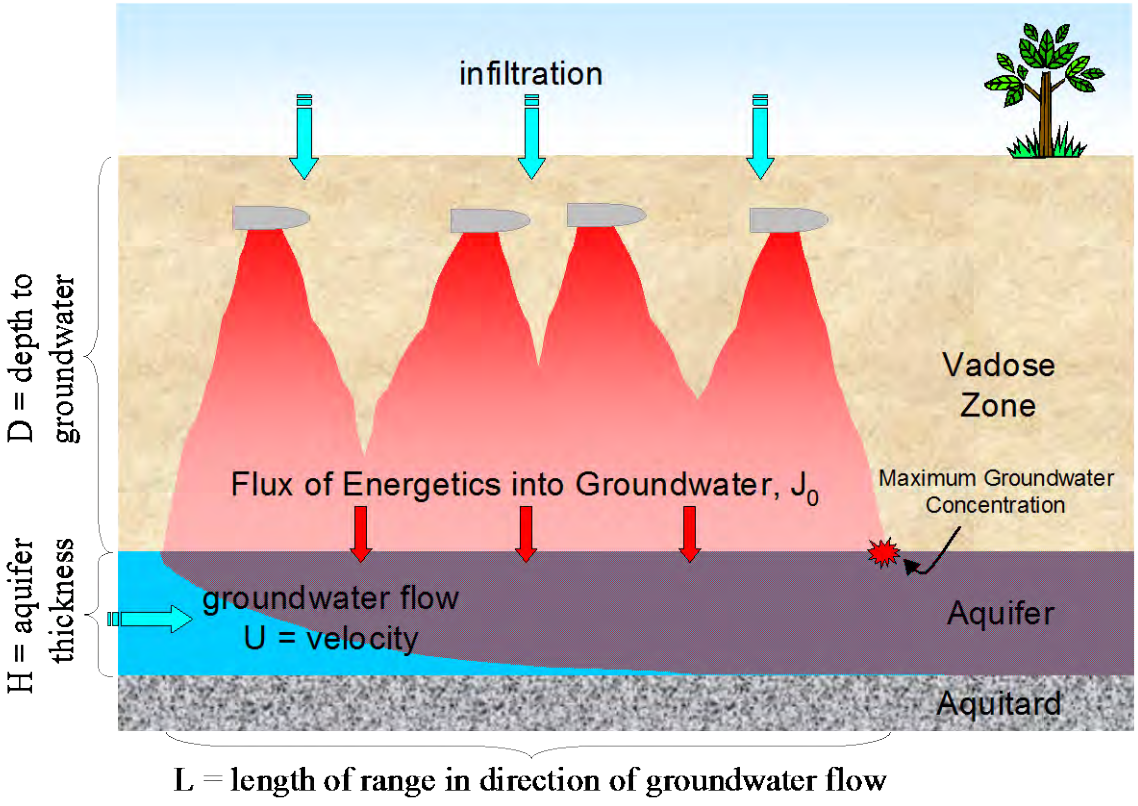

Figure 1. Description of Energetics Transport from UXO into Groundwater

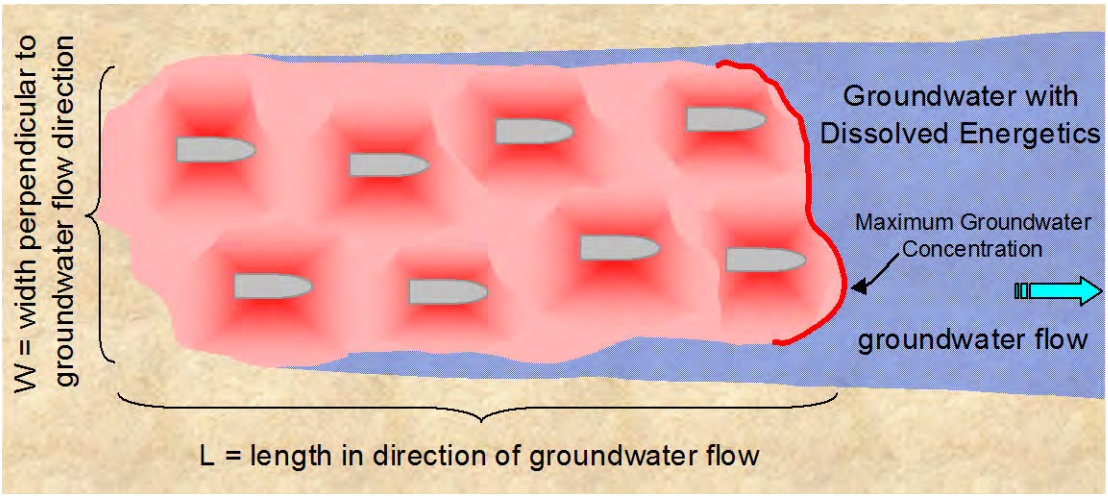

Figure 2. Plan View of Energetics Transport from UXO into Groundwater

2. Site Conditions and UXO Characteristics

Site parameters requiring specification to estimate the transport of energetics to groundwater begin with the UXO source characteristics (i.e., number and type of UXO and range dimensions) and also include soil physical properties and the site hydraulic properties (e.g., infiltration rate and groundwater velocity). Each of these parameter groups is discussed below.

2.1. UXO Source Characteristics

The compounds of widest concern with respect to corroding UXO are TNT and RDX. Historically, these explosive compounds make up the majority of fill in the mortars and bombs of non-inert UXO. The primary determinants for the release rate of energetics from corroded UXO are solubility in water (C_{sat}) and the diffusion coefficient in water (D_m). The potential groundwater concentration of an energetic is directly proportional to both its solubility and its diffusion coefficient. A previous study of energetic materials (Lynch et al., 2001) showed the solubilities of TNT and RDX in water are not significantly dependent on the pH of the water. Therefore, water solubility values cited in research literature are assumed to be indicative of the solubility in soil pore water. In a subsequent study (Lynch et al., 2002), the solubilities of TNT and RDX were effectively the pure component values during the co-dissolution of TNT and RDX in water. Hence, single component solubilities are also applicable to fill mixtures utilizing multiple energetics (e.g., Composition B). The solubility and other chemical and physical properties of TNT and RDX relevant to mass transport in soil are provided in Table 1. The diffusion coefficient for TNT is roughly three times the coefficient for RDX. In addition, the solubility of TNT is nearly triple over the RDX solubility such that the initial mass release rate of TNT, after corrosive failure of the casing, will be roughly nine times the rate of RDX.

Table 1. Energetic Physical and Chemical Properties

Property	Unit	TNT	RDX	Tetryl
Molecular Weight	g/mol	227.13	222.26	287.15
Density at 20 C	g/mL	1.654	1.82	1.57
Solubility at 20 C	mg/L	130	46	75
Diffusion Coefficient in Water	m^2/year	0.022	0.0067	
Log K_{ow}	-	1.60	0.87	2.4
Log K_{oc}	-	3.04	1.80	3.3
Drinking Water Guideline (Lifetime)	mg/L	0.002	0.002	

To estimate the total mass release rate of energetics from perforated UXO, the number and type of UXO (N_{uxo}) existing throughout the site must be estimated. In addition, the dimensions of the site where UXO are found must be defined. The area of a site and mathematical symbols are illustrated in Figure 2. The numbers of UXO at a given site are largely unknown but can be estimated from historical usage data or previous clearance data (e.g., Archives Search Report). The mass of energetic within each high explosive UXO must also be specified to determine the duration of a release after corrosive failure. Common high explosive UXO items are listed in Table 2 along with the most common explosive fill and the estimated mass of the fill.

Table 2. Properties of Common UXO

Type	High Explosive Fill	Fill Weight[1] (kg)	Shell Thickness (cm)
37-mm Mortar	Tetryl or TNT		0.64
60-mm Mortar	TNT or CompB	0.154	0.46
81-mm Mortar	TNT or CompB	0.553	0.47
105-mm Mortar	TNT or CompB	2.93	1.05
3-inch Stokes Mortar	Black Powder or TNT	1.23	0.46

[1]Values from "TM 9-1904, Ammunition Inspection Guide, March 1944"

As indicated in Table 2, Composition B (CompB) was often used as a more powerful replacement for TNT in the loading of some mortars. Composition B consists of 59% RDX, 40% TNT with 1% wax. Once a UXO shell is breached by corrosion, water may be imbibed through pits and then spread by capillary forces around the boundary between the explosive fill and the casing. The existence of "gaps" and small open volumes within the explosive fill material inside munitions is documented in the official army specifications for acceptance testing of newly produced artillery (Dept. of the Army, 1992). For example, gaps between the rear shell wall and the explosive fill as large as 0.038 cm are acceptable in new munitions. In addition, CompB is typically poured into shells at 85°C as a molten TNT slurry of RDX crystals.

2.2. Soil Physical Properties

As discussed below with the transport models, soil physical properties influencing the movement of energetic compounds through the soil include the soil porosity (ϕ), moisture content (θ), and organic carbon content (f_{oc}). The average values for these properties measured at a variety of sites for the UXO corrosion study are listed in Table 3. For effectively non-volatile compounds such as the energetics, transport is by advection with infiltrating pore water and, to a lesser extent, diffusion through pore water. Advection is governed by the infiltration rate and is discussed in the next section. The porosity and moisture content strongly influence the diffusion of compounds through the soil.

Table 3. Average Site Soil Properties

Site	Average Porosity, ϕ	Moisture Content, θ	Carbon Content, f_{oc}	Tortuosity τ	Gravel	Sand	Silt	Clay
	(%Vol)	(%Vol)	(%Mass)	(-)	(%Wt)	(%Wt)	(%Wt)	(%Wt)
A	63.5	19.3	4.5	0.010	13	39.6	38.4	9
B	48	7.5	1.1	0.0008	0	82.9	16.5	1.1
C	50	7.8	2.9	0.0008	0	64.4	28.3	7.3
D	45.5	21.8	5.0	0.030	0	88.4	9.4	2.1
E	39.8	11.8	3.1	0.005	25.6	54.3	16	4
F	44.5	2.4	1.3	0.00002	0	87.9	10.4	1.8
G	61.5	23.6	3.3	0.022	0	38.5	51.4	10.1
H	44.2	15.8	2.6	0.011	0.4	65.3	26.9	7.4
I	51.7	19	2.1	0.015	1	24.6	56	18.4
Z	34.3	22.5	4.4	0.059	0	49	48.8	1.9

A tortuosity factor (τ) is multiplied by the free-water diffusion coefficient (D_m) to account for the "torturous" path molecules must follow in diffusing through soil pore water. If the majority of pore space is occupied by air, then liquid diffusion is very slow because contaminants must diffuse primarily through very thin films of water presenting a relatively small cross-sectional area for diffusion compared to a fully saturated soil. Recent measurements suggest that saturation levels (i.e., θ/ϕ) greater than 0.16 to 0.20 yield high probabilities of connected pathways in porous media (Berkowitz and Hansen, 2001). Although the data in Table 3 represent only a single sample point in time, connected pathways for diffusion are likely at nearly all of the sites. However, the duration of residual water saturation exceeding 0.16 should be investigated by sampling throughout the year. The tortuosity factor is commonly calculated from (Millington and Quirk, 1961):

$$\tau = \frac{\theta^{10/3}}{\phi^2} \tag{1}$$

where

τ = unitless Millington/Quirk tortuosity factor for the water phase
ϕ = total soil porosity
θ = moisture content by total volume

Assuming the measured water content for each site is representative of the average soil saturation, values for the liquid diffusion tortuosity factor at the UXO corrosion study sites were calculated and are listed in Table 3. As shown in this table, the highest tortuosity was only 0.059 representing a 94% reduction in soil diffusion compared to free diffusion in water.

2.3. Site Hydraulic Conditions

The mass release rate of compounds from solid objects buried in soil can be predicted with correlations developed from a multitude of research efforts. These models for mass transfer and the subsequent migration of dissolved compounds toward groundwater are highly dependent on the water flow rate through the unsaturated soil. Hence, accurate estimates for the infiltration rate are essential for estimating realistic mass release rates. For now, a time-averaged infiltration rate is discussed; however, in a later section the impact of episodic precipitation versus an assumed steady infiltration on the mass release rate is explored. The time-averaged value is shown to be conservative (i.e., over-predicts the mass release rates).

Calculation of infiltration into a unit area of soil can be determined cumulatively for a given time interval (daily, monthly, annually). The calculation of cumulative infiltration is based on a simple water budget model:

$$I = P - RO - ET \quad (2)$$

where

I = cumulative infiltration in inches per unit time,
P = cumulative precipitation in inches per unit time,
RO = cumulative runoff in inches per unit time,
ET = cumulative evapotranspiration in inches per unit time.

I is a combination of both water storage in a unit volume of soil and deep percolation out of the unit volume. P is provided by (or calculated from) weather station data at the frequency of the unit time desired for calculations. Currently, the UXO corrosion database presents data compiled in the International Research Institute for Climate Prediction (IRI)/Lamont-Doherty Earth Observatory of Columbia University (LDEO) data library. The specific database used to compile precipitation data was the Global Climate Perspectives System (GCPS) from the National Oceanic Atmospheric Administration (NOAA) National Climate Data Center (NCDC). RO, runoff, may be determined using daily precipitation data and a runoff curve number developed by the National Resource Conservation Service (NRCS) where:

$$RO = P \cdot CN \quad (3)$$

and CN is the NRCS curve number. The CN value is based on soil type and vegetative cover and correlations were developed by the NRCS (USSCS, 1985) and may be found in that publication.

Evapotranspiration, ET, may be determined by a variety of methods. For the purposes of this study, the Blaney-Criddle method is used because it is derived solely from temperature data. Temperature data used in the UXO corrosion database were also compiled from the NOAA NCDC GCPS. The Blaney-Criddle method is:

$$ET_m = k_c \cdot k_i \cdot uf \quad (4)$$

$$k_i = 0.0173 \cdot T - 0.314 \quad (5)$$

$$uf = T \cdot d\%/100 \quad (6)$$

where:

ET_m = monthly evapotranspiration in inches
k_c = monthly empirical crop coefficient
k_i = monthly temperature coefficient
uf = monthly consumptive-use factor
T = monthly mean temperature in ^oF
d% = monthly percentage of daytime hours per year

Finally, an elevation correction is recommended that increases the evapotranspiration by 10 percent for each 1000 meter increase in elevation.

Calculated annualized infiltration rates for the UXO corrosion study sites are presented in Table 4. The calculations utilized the correlation presented above and are considered estimates of infiltration rates. One factor not included in the correlations is the relatively long-term presence of snow coverage in parts of the country. Snowfall creates a surface condition where melt rates may be consistently below the saturated hydraulic conductivity of the underlying soil yielding a relatively continuous infiltration rate. Snowfall may therefore make monthly-averaged mass transfer estimates more accurate, since the melting snow dampens the transient infiltration resulting from episodic rainfall.

The average groundwater concentration resulting from the release and transport of energetics to groundwater is inversely proportional to the groundwater velocity and the thickness of the aquifer (Section 3). If the velocity is high, a larger volume of water passes under the site for a given time interval effectively diluting the energetic mass entering the groundwater. In the same manner, a thick aquifer also passes a larger volume than a thin aquifer for the same groundwater velocity allowing more dilution to occur. Hence, the validity of forecasts for potential future groundwater concentrations of energetics from UXO perforated by corrosion is directly tied to the validity of the estimates for the groundwater velocity and aquifer thickness. These parameters are not readily available for most sites and usually require the installation of multiple groundwater monitoring wells and aquifer pumping tests to obtain accurate values. The pumping test with monitored drawdown at observation wells yields the aquifer permeability and then the difference

in water level among wells during ambient conditions allows a calculation of the groundwater velocity and direction. The aquifer thickness is usually obtained from geologic logs collected during the installation of monitoring wells. Without site-specific data, regional groundwater velocity and direction can be employed along with the regional aquifer thickness. The regional values are available from a number of local sources and the U.S. Geological Survey. The natural velocities of groundwater are generally small and may be as low as 1.5 meters per year although natural velocities as high as 730 meters per year have been observed (Kashef, 1986). Typical values range from 15 to 150 meters per year depending upon the aquifer material and recharge rate.

Table 4. Annualized Infiltration Rates

Site	Annual Infiltration	Site	Annual Infiltration
	(cm/yr)		(cm/yr)
A	15.7	F	1.0
B	3.3	G	15.5
C	13.0	H	21.8
D	1.8	I	2.5
E	1.0	Z	26.2

Detailed mathematical relationships for the transport of energetics from UXO into groundwater are developed in the following sections and include a discussion of the underlying assumptions.

3. Simplistic Model of Energetic Transport

A conservative estimate for the average concentration of an energetic in groundwater, beyond the range area, can be written immediately from a simple balance mass with reference to Figure 1:

$$C_{w,average}(x \geq L) = \frac{J_0 L}{UH} \tag{7}$$

where:

C_w = ground water concentration,
U = pore velocity of ground water,
J_0 = mass flux of explosive contaminant entering groundwater from the vadose zone,
x = distance in direction of groundwater flow,
L = length of range in direction of groundwater flow,
H = aquifer thickness.

The numerator in (7) represents the energetic mass entering the groundwater from the vadose zone per unit width of the range and the denominator represents the groundwater flowing under the range per unit width.

A simple estimate for the mass flux of energetics entering groundwater (J_0) can be determined if the mass release rate from one UXO item is available. The flux is simply the mass release rate of one item multiplied by the estimated number of items on the range (N_{uxo}) divided by the area of the range (see Figure 2):

$$J_0 = \frac{\dot{m}_{uxo} N_{uxo}}{LW} = \dot{m}_{uxo} n_{uxo} \tag{8}$$

where:

$\dot{m}_{uxo}$ = mass release rate from one UXO item,
N_{uxo} = number of uxo items,
W = width the range,
n_{uxo} = density of UXO items in the range.

A simple estimate for the mass release rate from each UXO can be taken from classical mass transfer for slow flow over a sphere buried in a porous medium (Bowman et al., 1961). As described in a later subsection, this rate is:

$$\dot{m}_{uxo} = 4\pi \Re \tau D_m C_{sat} \tag{9}$$

where $\Re$ is the radius of the sphere (or characteristic dimension of the UXO such as the average of the length and width), D_m is the diffusion coefficient of the energetic in water, τ is the tortuosity for diffusion in the soil, and C_{sat} is the solubility of the energetic in water. Substituting (8) and (9) into (7) yields a simple, order-of-magnitude estimate for the potential groundwater concentration of energetics <u>after</u> UXO have become thoroughly corroded and completely expose the explosive fill to the surrounding soil:

$$C_{w,average} = \frac{4\pi \Re \tau D_m C_{sat} n_{uxo} L}{UH} \quad \text{(after complete corrosion of the UXO shell)} \tag{10}$$

For example, using TNT (see Table 1 for properties) as the energetic in a UXO with a characteristic dimension of 1.6 inches (0.04 meter), soil with a tortuosity of 0.05, a high explosive filled UXO density of 100 per square kilometer, a range length of one kilometer, a groundwater velocity of 100 meters per year, and an aquifer thickness of 10 meters yields:

$$C_{w,average} = \frac{4\pi(0.04\,\text{m})(0.05)(0.022\,\text{m}^2/\text{yr})(130\,\text{g/m}^3)(100/\text{km}^2)(1000\,\text{km})}{(100\,\text{m/yr})(10\,\text{m})}$$

$$C_{w,average} = 0.007\,\text{g/m}^3 = 0.007\,\text{mg/L}$$

Under these conditions, the TNT has the potential to exceed the EPA Drinking Water Guideline for TNT of 0.002 mg/L and the more detailed analysis provided in this section would be warranted. Many assumptions, including no microbiological degradation of the energetic and limited dispersion are implicit in equation (10). Detailed analyses of the release and transport of energetics are provided in the remainder of this appendix. Higher mass release rates than predicted by (10) will occur if infiltration rates are high. Example calculations are provided for the UXO study sites to illustrate the application of the models. A flowchart summarizing the model calculations is provided in Figure 3. The following sections describe the detailed mathematical model of energetic release from a corroded UXO into groundwater.

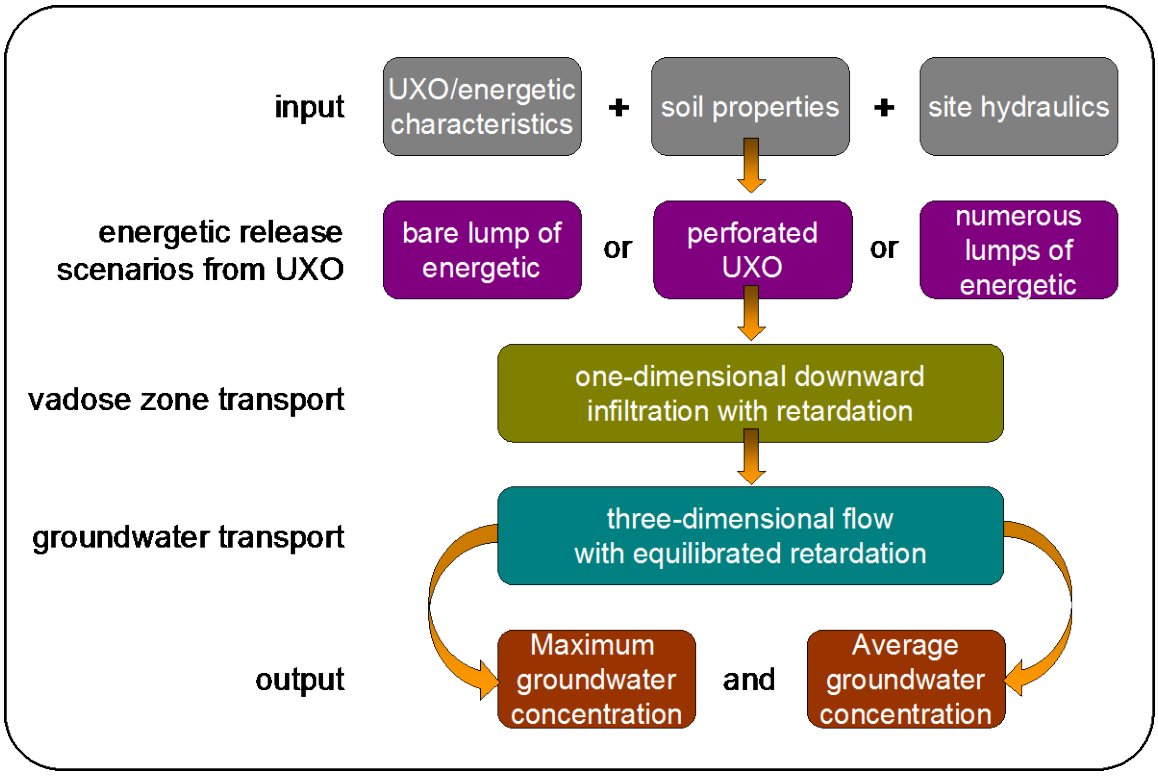

Figure 3. Flowchart for the UXO Energetics Transport Model Calculations

4. Release of Energetics from UXO into Surrounding Soil

This section presents UXO-specific models of energetic mass transfer from the explosive fill of a corroded UXO into surrounding soil. The models are based on existing correlations of mass transfer coefficients developed for advective and diffusive dissolution of solid objects buried in a porous medium. The general relationship for the mass release rate of an energetic compound from the fill in a corroded UXO into the surrounding soil is:

$$\dot{m}_{uxo} = g_{uxo} A_{uxo} C_{sat} \tag{11}$$

where:

$\dot{m}_{uxo}$ = mass release rate of energetic from the corroded UXO
g_{uxo} = mass transfer coefficient for energetic between the UXO and surrounding soil
A_{uxo} = total outer surface area of the UXO
C_{sat} = solubility of the energetic in the soil pore water

The mass transfer coefficient, g, must be determined experimentally and is a fluid mechanical property of the system. Mass transfer coefficients have been studied extensively for a vast array of flow configurations, shapes and areas. This work will make use of these studies to predict the mass transfer coefficient appearing in (11) for several scenarios of interest and for specified outer areas of the UXO.

Three scenarios are considered for mass transfer from a single UXO item:

- a single cylindrical lump of UXO fill with no casing (completely corroded),
- transport through corrosion pits perforating a UXO metal shell (partially corroded), and
- UXO fill broken into numerous chunks after complete corrosion of the shell.

The first case represents a conservative scenario for which no metal shell exists and the fill is completely exposed to the surrounding soil. The second scenario is more realistic and models the mass transfer of explosives from inside a steel UXO shell as purely diffusive through holes perforating the shell (i.e., through-going pits) followed by advection and diffusion into the surrounding soil. The third scenario represents an extreme case after total failure of the casing and considerable erosion of TNT in CompB.

These correlations all assume steady flow over an object with unchanging geometry and outer area. However, both the flow rate and the dimensions of the UXO fill will change with time. Because the UXO are located near the soil surface, the flow rate will vary almost in direction proportion with precipitation events. The fill volume and outer area will be reduced over time as the mass of the fill is dissolved away. As discussed in a later section, these temporal effects will reduce the mass release rate from the initial rate assuming a steady flow. The high, initial mass transfer rate assuming a steady flow will be used to calculate the highest potential groundwater concentration.

4.1. Cylindrical Lump of Bare Fill with No Metal Shell

A “neat” cylindrical lump of exposed fill provides a very conservative estimate for the leakage from a UXO by assuming corrosion completely exposes the fill to the surrounding soil environment. A typical high explosive UXO mortar is loaded with roughly 1.0 kg of CompB (59.5% TNT, 39.5% RDX and 1% paraffin binder) in the shape of a right cylinder. The impact of the paraffin is assumed to be negligible. The correlations provided below assume the outer surface of this cylindrical block of fill is always in direct contact with porous soil. A thin, stagnant boundary layer of soil pore water adjacent to the solid fill is assumed to be in constant chemical equilibrium with the fill (i.e., saturated with the fill constituents). Diffusion and advection of individual dissolved constituents through this concentration boundary layer are analyzed to predict the limiting dissolution rate of the low solubility energetics.

Advection-Dominated Mass Transfer

For sites with high infiltration rates (ie. 10-25 cm/yr), the following correlation from Powers et al. (1991) is applicable to the mass transfer coefficient of energetic j from a solid cylinder of mixed explosive fill:

$$g_j = f_j \frac{D_{m,j}}{2\Re} \frac{1.1068}{\theta} Re^{0.28} Sc^{0.33} \qquad \text{for} \quad Re < 10 \qquad (12)$$

$$Re = \frac{2\Re I}{\nu_w} = \text{Reynolds Number}$$

$$Sc = \frac{\nu_w}{D_{m,j}} = \text{Schmidt Number}$$

where:

g_j = mass transfer coefficient for energetic j between the UXO and surrounding soil
f_j = volume fraction of energetic j making up the UXO fill
$D_{m,j}$ = free diffusion coefficient for compound j in water
$\Re$ = radius of the cylinder
θ = soil moisture content
I = infiltration rate
ν_w = kinematic viscosity of water (1.01e-6 m^2/s = 49,400 in^2/yr)

This relationship was developed from dissolution experiments of solid cylinders in packed beds (Dwievedi and Updhyay, 1977). The relationship is valid for sites and UXO items with a Reynolds number less than 10. For a large cylinder with a radius of 15 cm, the infiltration rate yielding a Reynolds number of 10 is over 1,000 meters per year (12 cm per hour). Hence, this relationship is applicable to all sites since no site will exceed this infiltration rate on an annual basis and is unlikely to exceed this rate even during a storm event. Therefore, approximating the bare UXO fill as a buried right cylinder, the mass release rate of component j during steady infiltration is obtained from equation (12) substituted into (11):

$$\dot{m}_{uxo,j} = 1.1068\,\pi\, f_j\, C_{sat,j}\, (\Gamma + \Re) \frac{D_{m,j}}{\theta} \left(\frac{2\Re I}{\nu_w}\right)^{0.28} \left(\frac{\nu_w}{D_{m,j}}\right)^{0.33} \qquad (13)$$

where:

Γ = length of the cylinder

A typical, completely corroded scenario includes a bare cylindrical block of Composition B (60.5% RDX and 39.5% TNT) buried in the soil. The mass release rate of energetics as a function of infiltration rate for a single block of fill with a radius of 3.8 cm and a soil moisture content of 21.8% is provided in Figure 4.

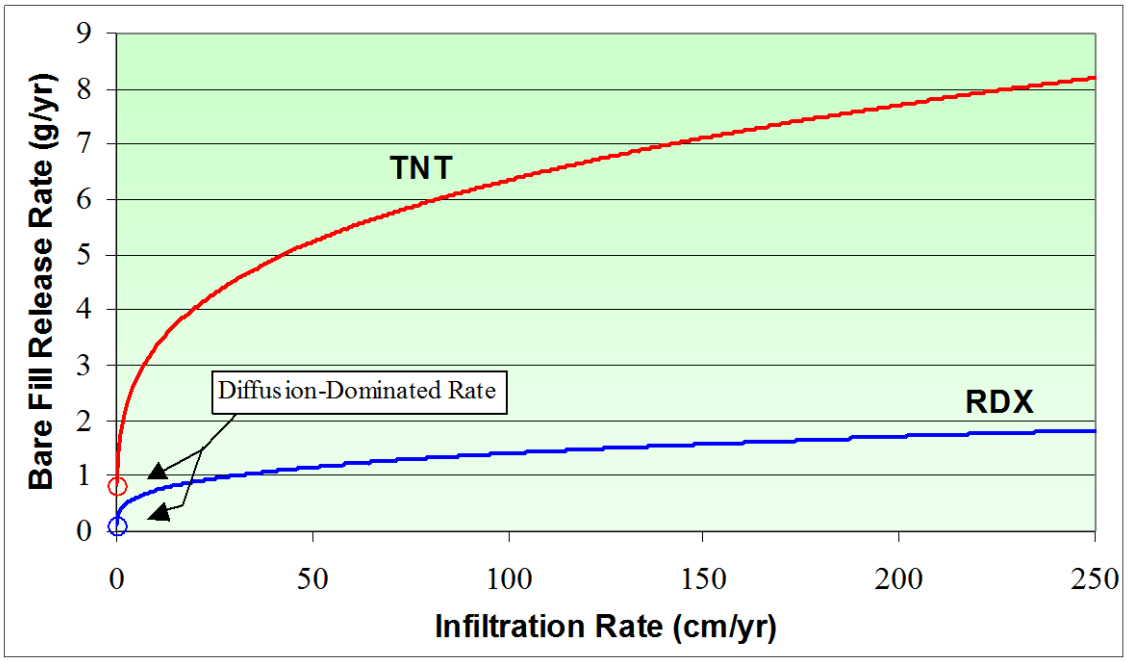

Figure 4. Mass Release Rate as a Function of Infiltration Rate for Bare Fill

Also from Dwievedi and Updhyay, 1977, the correlation for the initial mass release rate from a solid spherical object is:

$$\dot{m}_{uxo,j} = 1.1068\ f_j\ C_{sat}\ (2\pi\Re_{sphere})\frac{D_{m,j}}{\theta}\left(\frac{2\Re_{sphere} I}{\nu_w}\right)^{0.28}\left(\frac{\nu_w}{D_{m,j}}\right)^{0.33} \quad (14)$$

Diffusion-Dominated Mass Transfer

UXO items are located near the soil surface such that infiltration past an item is generally unsteady. During long periods the infiltration rate is close to zero and diffusion of energetics through the soil pore water is the dominant mechanism of transport away from the item. Under this condition, the following correlation from Chambre and Pigford (1982) is applicable to the mass transfer coefficient of energetic j from a solid cylinder of mixed explosive fill:

$$g_j = f_j \frac{\text{Volume}}{\text{Area}} \beta\tau D_{m,j} \quad (15)$$

where:

τ = tortuosity as defined by equation (1)

β = geometric factor for approximating the explosive fill shape

$\beta = 3/\Re^2$ for a sphere of radius $\Re$ (where a = b, Figure 5)

Sphere Outer Area $= 4\pi\Re^2$

Sphere Volume $= \frac{4}{3}\pi\Re^3$

$\beta = (3\ e)\ [\ b^2 \ln(\coth(\alpha_s))]^{-1}$ for a prolate spheroid (see Figure 5)

$e = \frac{1}{a}\sqrt{a^2 - b^2}$, the eccentricity

$\alpha_s = \cosh^{-1}(e^{-1})$

Prolate Spheroid Outer Area $= 2\pi b\left(b + \frac{a}{e}\sin^{-1} e\right)$

Prolate Spheroid Volume $= \frac{4}{3}\pi b^2 a$

The mass release rates for diffusion-dominated mass transfer from a sphere and a prolate spheroid are, substituting (15) into (11),

$$\dot{m}_{uxo.j} = 4\pi\Re f_j \tau D_{m,j} C_{sat,j} \quad \text{for a sphere} \tag{16}$$

$$\dot{m}_{uxo,j} = \frac{4}{3}\pi b^2 a \beta f_j \tau D_{m,j} C_{sat,j} \quad \text{for a prolate spheroid} \tag{17}$$

The calculated mass release rate for the completely corroded scenario of a bare cylindrical block of Composition B buried in the soil with a radius of 3.8 cm and a soil moisture content of 21.8% is indicated in Figure 4. For this example, the mass release rate of RDX when infiltration approaches zero is 0.15 grams per year and for TNT it is 0.83 grams per year.

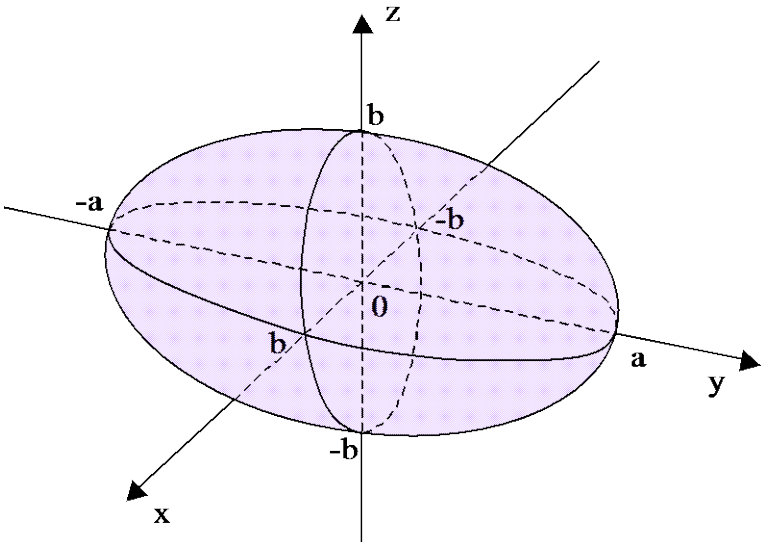

Figure 5. Prolate Spheroid Dimensions

4.2. Transport Through Corroded Pits

A more realistic scenario than a bare, buried object considers the release of energetics through pits breaching the metal shell surrounding the UXO explosive fill. This case can be envisioned as a large number of "holes" distributed uniformly over the surface of the shell. After the eventual failure via corrosion of the UXO shell, water is imbibed by capillary suction into the very thin gap between the explosive fill and the metal shell casing. Molecular diffusion of the energetic from the fill to the outer surface of the shell through the water adds a mass transfer constraint to the transport. The mass transfer correlations presented above for a bare object remain applicable. However, the surface solute concentration of energetic is only at the solubility limit where the shell is perforated, the rest of the fill surface covered by the UXO casing is not in contact with pore water. This is depicted in Figure 6. To determine the effective energetic concentration on the shell surface, equate the mass of energetic diffusing through pits to the mass transported into the surrounding soil under steady state conditions. The steady diffusion of energetic j through the pits yields the following mass release rate from the fill to the shell surface:

$$\dot{m}_{j,pits} = N_{pits} A_{pit} D_{m,j} \frac{dC}{d\varepsilon} = N_{pits} A_{pit} D_{m,j} \left(\frac{C_{sat,j} - C_{\infty,j}}{\ell} \right) \tag{18}$$

where:

$\dot{m}_{j,pits}$ = mass release rate through perforated pits
N_{pits} = total number of through-going pits on the UXO shell surface
A_{pit} = average cross-sectional area of single pits
$C_{\infty,j}$ = energetic concentration in water at the surface of the UXO shell
ℓ = depth of the pits (i.e., the thickness of the UXO shell)

Equating the total mass release rate from pits with the release rate into soil as described by equation (11) yields:

$$g_j A_{uxo} C_{\infty,j} = N_{pits} A_{pit} D_{m,j} \left(\frac{C_{sat,j} - C_{\infty,j}}{\ell} \right) \tag{19}$$

and, solving for the surface concentration yields:

$$C_{\infty,j} = C_{sat,j} \left(1 + \frac{g_j \ell}{n_{pits} A_{pit} D_{m,j}} \right)^{-1} \tag{20}$$

where:

n_{pits} = density of through-going pits (i.e., total number of pits/surface area of shell)

Substituting this relationship back into equation (11) yields the mass release rate of energetics from a UXO item covered with pits perforating its shell:

$$\dot{m}_{uxo,j} = g_j A_{uxo} C_{sat,j} \left(1 + \frac{g_j \ell}{n_{pits} A_{pit} D_{m,j}} \right)^{-1} \tag{21}$$

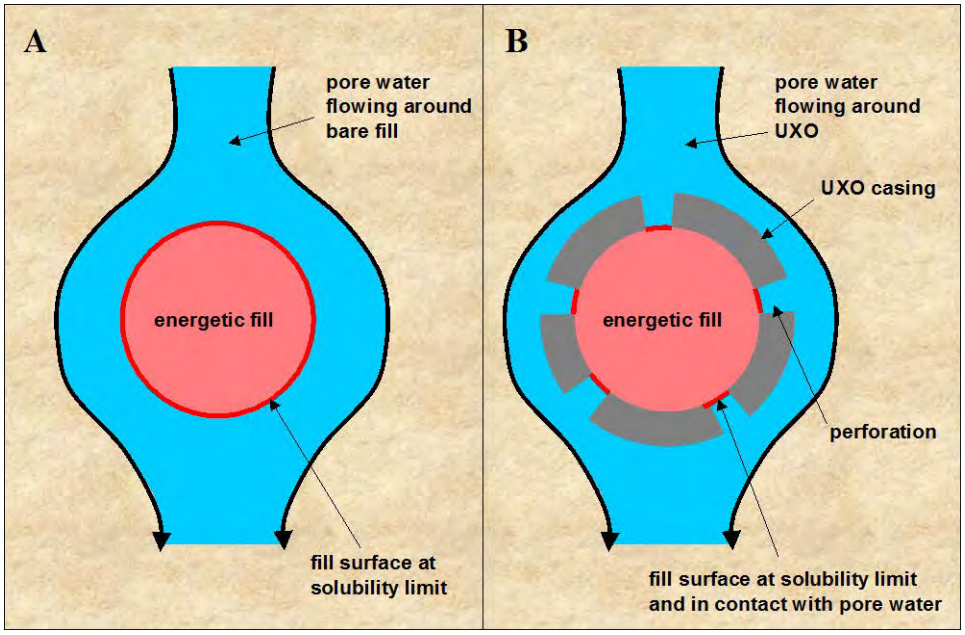

Figure 6. Schematic of pore water flow around A) a bare lump of energetic material and B) a perforated UXO

In this expression, the mass transfer coefficient g_j is given by equations (12) and (15) for advection-dominated and diffusion-dominated conditions, respectively. For very high infiltration rates, the mass transfer coefficient is relatively large and the concentration at the outside of the pit approaches zero. Under this condition, the mass release rate is determined solely by diffusion through the pits. Letting g approach infinity in (21) yields the right hand side of (18) with $C_{\infty,j}$=0.

From the UXO corrosion study, the average pit density (n_{pits}) for all the items measured was 7.3 pits per square centimeter of shell surface. A typical radius for the pit is about 0.05 cm (0.02 inches) yielding a cumulative area for the pits of about 6% of the total shell area. Mass release rates for diffusion through these pits as a function of infiltration rate are illustrated in Figure 7 assuming a shell thickness of 0.46 cm (e.g., 60-mm mortar) and applying the same conditions as for Figure 4 (i.e., 1-kg cylindrical block of Composition B with a radius of 3.8 cm inches and a soil moisture content of 21.8%).

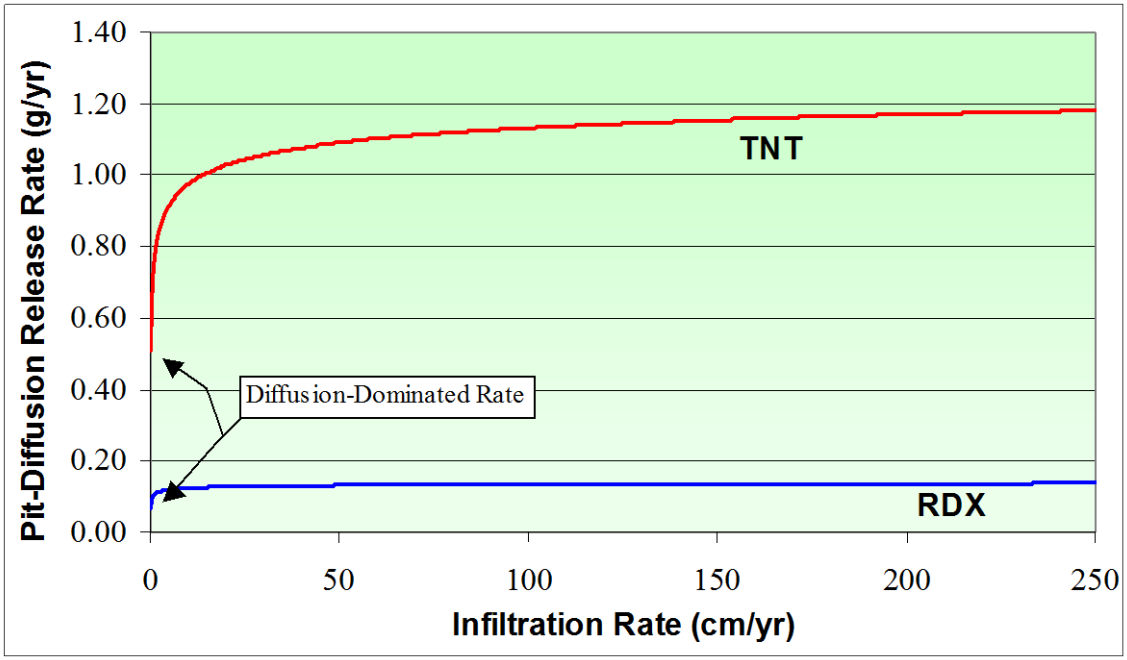

Figure 7. Mass Release Rate as a Function of Infiltration Rate for Corroded UXO Shell

Even at relatively low infiltration rates, the mass release rate is dominated by energetic diffusion through the perforating pits. For infiltration rates over 50 cm per year, the mass release rates of RDX and TNT approach 0.14 and 1.2 grams per year, respectively. The RDX value is significantly less than the TNT value because the RDX diffusion coefficient in water is about one third of the TNT diffusion coefficient (see Table 1). For infiltration rates approaching zero such that mass transfer from the shell to soil is dominated by diffusion, the mass release rates of RDX and TNT are about 0.07 and 0.5 grams per year, respectively. Under most scenarios, the mass release rate from corroded UXO with perforating pits will be dominated by diffusion through the pits and is strongly dependent on the number of perforating pits, the diameter of the pits, and the thickness of the shell.

4.3. Broken Fill of Numerous, Small Exposed Lumps

Section 4.1 describes a completely exposed cylinder of energetic which releases energetic material at a much higher rate than perforated UXO. This section considers, as a worst case, energetic release as mass transfer by advection and diffusion from a completely corroded UXO with the fill disarticulated into many small, spherical lumps. As indicated in Figure 1, the mass release rate of TNT is higher than RDX and can yield the disarticulation of the fill as the TNT holding the fill together is preferentially dissolved away. This action can leave many small lumps of RDX. In this worst case, the mass transfer from individual lumps is assumed independent of one another and the RDX mass release rate is the sum of the release from all lumps:

$$\dot{m}_{uxo} = \sum_{i=1}^{M} \dot{m}_{lump,i} \tag{22}$$

where M represents the total number of lumps. If all the RDX lumps are assumed to have the same spherical radius, then, utilizing equation (14), the total mass release rate of RDX is:

$$\dot{m}_{uxo,RDX} = M\left[1.1068\, C_{sat,RDX}\, (2\pi\Re_{lump})\, \frac{D_{m,RDX}}{\theta} \left(\frac{2\Re_{lump} I}{\nu_w}\right)^{0.28} \left(\frac{\nu_w}{D_{m,RDX}}\right)^{0.33}\right] \tag{23}$$

where:

$$\Re_{lump} = \left(\frac{3 f_{RDX} V_{uxo}}{4\pi M}\right)^{1/3} \tag{24}$$

and $f_{RDX} V_{uxo}$ represents the original volume of RDX for an intact UXO fill. Figure 8 illustrates the release rate from 600 grams of RDX in porous soil at various RDX particle sizes. The nominal construction of some CompB calls for mixing 0.04-cm (0.016-inch) RDX grains into molten TNT, so lump sizes at the far left of the figure may not be unrealistic after thorough corrosion of the shell and thorough erosion of TNT from the CompB. However, for a nominal initial mass of 600 grams, this grain size corresponds to over 500,000 tiny "lumps" and this number will not act independent of one another. The radius of 3.8 cm corresponds to roughly a single lump and the mass releases shown for various infiltration rates are consistent with the results presented in Figure 4 for bare fill.

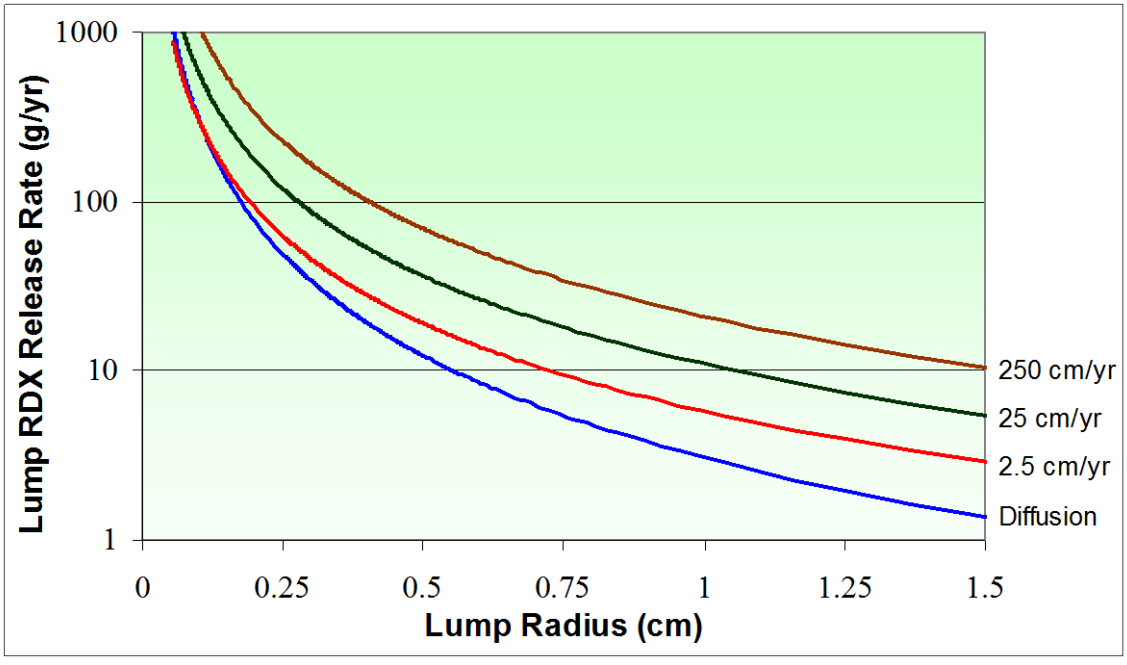

Figure 8. RDX Release Rate as a Function of Lump Size and Infiltration Rate for Bare Disarticulated Fill

4.4. Transient Infiltration

In most correlations for mass transfer, the flow rate over the buried object is assumed to be steady. However, rainfall is generally very episodic, i.e., it occurs infrequently for short durations. Below the soil surface the soil tends to smooth out the infiltration rate such that the infiltration rate can be relatively steady at depths greater than 3 meters. However, UXO are generally found from the soil surface down to a depth of about one foot and less frequently below three feet. Hence, the infiltration of water past most UXO items is highly transient. In addition, the correlation for the advectively-dominated mass transfer coefficient, equation (13), depends non-linearly on the water infiltration rate in the soil. In this section, a method is introduced to account for the transient nature of precipitation in calculating the mass release rate from exposed explosive fill and to illustrate the conservative nature of assuming a steady annual infiltration rate.

Assuming the near-surface infiltration for a site can be modeled as a series of steady infiltration periods, many of which are zero, the following relationship can be used to extend the steady mass release rates presented previously to transient conditions:

$$\dot{m}_{uxo} = \frac{1}{t_{inf\,il}} \sum_{k=1}^{K} \dot{m}_{uxo,k} \Delta t_k \quad \text{where} \quad t_{infil} = \sum_{k=1}^{K} \Delta t_k \tag{25}$$

where Δt_k is the duration of a steady infiltration period with mass release rate $\dot{m}_{uxo,k}$. The time period over which the infiltration is modeled should be one year to account for seasonal variations in precipitation. As an example, consider a site where the annual infiltration rate is 93 inches per year. Assuming a high precipitation rate where rainfall occurs on one day out of every three days uniformly throughout the year and that on each precipitation day 0.76 cm of water infiltrates the soil whereas no infiltration occurs on the other two days. Equation (25) applied to this scenario yields:

$$\begin{aligned} \dot{m}_{transient} &= \frac{121.7}{(365\ \text{days})}\left[(\dot{m}_{advective})(1\ \text{day}) + (\dot{m}_{diffusive})(2\ \text{days})\right] \\ &= (\dot{m}_{advective})\left(\tfrac{1}{3}\right) + (\dot{m}_{diffusive})\left(\tfrac{2}{3}\right) \end{aligned} \tag{26}$$

Under this scenario, the infiltration rate on the precipitation days is equivalent to 218 cm per year or triple the annual average and will yield higher mass release rates but for a shorter duration. Hence, this method is straightforward to apply to data from an actual site if the detailed precipitation and climate data are available.

To assess the relative impact of transient analysis versus steady analysis, divide equation (26) through by the mass release rate assuming a steady annual infiltration rate and substitute in equations (14) and (16) for the advective mass transfer and the diffusive mass transfer over a bare sphere of comp B, respectively:

$$\frac{\dot{m}_{transient}}{\dot{m}_{steady}} = \left(\frac{\dot{m}_{advective}}{\dot{m}_{steady}}\right) f_{advective} + \left(\frac{\dot{m}_{diffusive}}{\dot{m}_{steady}}\right) f_{diffusive}$$

$$= \left(\frac{1}{f_{transient}}\right)^{0.28} f_{transient} + \left[\frac{2\tau\theta}{1.1068}\left(\frac{2\Re I_{steady}}{\nu_w}\right)^{-0.28}\left(\frac{\nu_w}{D_{m,j}}\right)^{-0.33}\right]\left(1 - f_{transient}\right) \qquad (27)$$

where $f_{transient}$ represents the fraction of time in the precipitation (transient) state and $f_{diffusive}$ the fraction in the static (diffusive) state with the sum equal to one. For sites with significant infiltration, the diffusive term in (27) will be negligible and the first term is sufficient to estimate the impact of transient infiltration. For the example of infiltration one-third of the time (100 days), the transient mass release rate will be about 45% of the equivalent steady infiltration rate (see figure 9). In general, increasing infiltration rates with shorter durations will yield decreasing mass release rates. This is illustrated in Figure 9 where the conditions for Figure 4 are repeated except an annual infiltration rate of 93 inches per year is assumed. This plot shows the decreasing mass release rate with decreasing frequency of precipitation of increasing intensity yielding the same total annual precipitation (93 inches per year). The left hand side of the plot represents all precipitation occurring in a one-day-a-year event and the mass transfer is less than 20% of the total mass release rate if the infiltration was averaged over the entire year. If infiltration occurs only one-third of the days during the year, then averaging the infiltration over the entire year yields a mass release rate double the actual value. Hence, UXO energetic mass release rate calculations should use infiltration rates at the highest available precipitation sampling frequency.

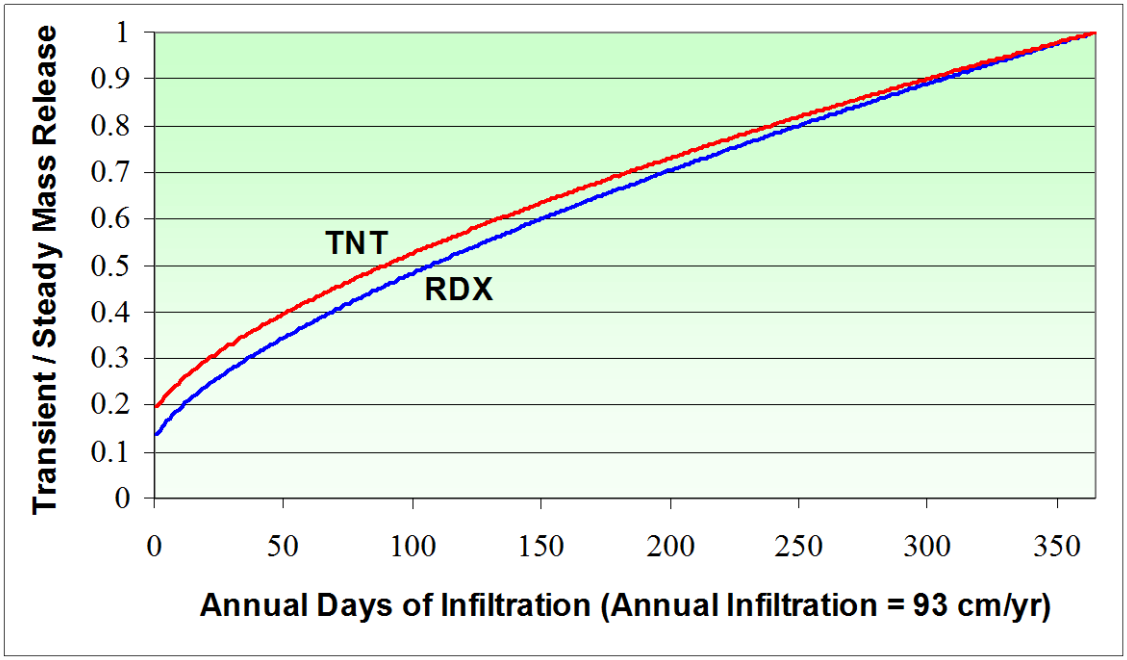

Figure 9. Comparison of Mass Release Rates Using an Annual Average Infiltration Rate (Steady) versus Transient Infiltration Data

5. Dissolved Energetic Transport through the Vadose Zone

The previous sections provided techniques for estimating the release rate of energetics from corroded UXO. In this section, the transport modeling of energetics is extended through the vadose zone to the interface with underlying groundwater. The mass release rates from the previous section are utilized as a source term for the vadose zone transport model. The model assumes infiltration rates are steady which is generally conservative for depths greater than 10 feet below the soil surface. In addition, the vadose zone is assumed to consist of soil with uniform physical and chemical properties.

The governing equation for one-dimensional transport of a single component by advection and diffusion through a vadose zone with uniform soil properties can be described by (Jury et al., 1983):

$$R\frac{\partial C}{\partial t} = D\frac{\partial^2 C}{\partial z^2} - I\frac{\partial C}{\partial z} - \lambda RC + g(z,t) \tag{28}$$

This one-dimensional formulation neglects the lateral diffusion and dispersion of the compound into surrounding vadose zone regions. The symbols in (28) are defined by:

C = soil pore water concentration
R = retardation coefficient (= $\rho_b K_d + \theta$)
ρ_b = soil bulk density
K_d = distribution coefficient (= $0.6\ f_{oc}\ K_{ow}$)
f_{oc} = fraction of organic carbon in soil (see Table 3)
K_{ow} = octanol-water coefficient for energetic (see Table 1)
D = effective diffusion and dispersion coefficient (= $\alpha_L\ I + D_m$)
α_L = longitudinal dispersivity
λ = first-order degradation constant
I = infiltration rate
$g(z,t)$ = release rate of energetic from UXO
z = vertical coordinate with zero equal to ground surface and increasing with depth

The retardation coefficient accounts for adsorption of the compounds to the solid soil particles. Boundary and initial conditions to solve (28) are:

$$C = 0 \qquad \text{at } z = 0,\ t > 0 \tag{29}$$

$$\frac{\partial C}{\partial z} = 0 \qquad \text{at } z = B,\ t > 0 \tag{30}$$

$$C = 0 \qquad \text{for } t = 0 \tag{31}$$

with the release rate of an explosive compound from the UXO defined by:

$$\left.\begin{array}{ll} g = g_0(t) & \text{for } 0 < t \le t_1 \\ g = 0 & \text{for } t > t_1 \end{array}\right\} \qquad \text{for } d_1 < z < d_2;\ 0 \text{ elsewhere} \quad (32)$$

The boundary condition at the top of the unsaturated zone is a specified concentration of zero. At the bottom of the vadose zone at depth B, compounds are assumed to enter groundwater by infiltration only. The source is assumed to be mass transfer of compounds from a UXO item. The release rate is modeled to occur uniformly within the volume occupied by the UXO item. This volume is assumed to be relatively small compared to the underlying vadoze zone. For now, only one item located from depth d_1 to d_2 is included in the model. The mass of the compound in the item is assumed to be depleted at time t_0.

5.1. Transport through the Vadose Zone

The solution to equation (28) subject to the conditions of equations (29) to (32) can be determined using a generalized integral transform technique (Mikhailov and Ozisik, 1984). The first step in solving the problem is the development of the appropriate integral transform and inversion formula for the space variable. This is achieved by considering the eigenvalue problem for the equivalent homogeneous problem. The second step is to apply this Fourier-type integral transform to equation (28). This transformation removes the partial derivatives with respect to the space variable yielding an ordinary differential equation (ODE) in time for the transformed pore water concentration. The next step is to solve the first-order ODE in time subject to the transformed initial condition. The final step is to apply the inversion formula for the space variable to obtain the desired solution for the concentration as a function of depth and time. Use of a Laplace transform for this problem leads to a very difficult numerical inversion while the inversion of the Fourier-type transform is explicit.

The first step in solving the problem is to recast the equations into a form suitable for an integral transform. Redefine the dependent variable as follows:

$$C = Ge^{a`z} \qquad \text{where } a` = \frac{V}{2D} \quad (33)$$

Substituting this variable transformation into (28) yields:

$$R\frac{\partial G}{\partial t} = D\frac{\partial^2 G}{\partial z^2} - \left(a`^2 D + \lambda R\right)G + g(z,t)e^{-a`z} \quad (34)$$

The variable-transformed boundary and initial conditions to solve (34) are:

$$G = 0 \qquad \text{at } z = 0,\ t > 0 \quad (35)$$

$$\frac{\partial G}{\partial z} + a`G = 0 \qquad \text{at } z = B,\ t > 0 \quad (36)$$

$$G = 0 \qquad \text{for } t = 0 \tag{37}$$

The appropriate eigenvalue problem for the integral transform in the space variable z to solve (34) is:

$$\frac{d^2Z}{dz^2} + \beta_m^2 Z = 0 \tag{38}$$

with boundary conditions:

$$Z = 0 \qquad \text{at } z = 0 \tag{39}$$

$$\frac{dZ}{dz} + a`Z = 0 \qquad \text{at } z = B \tag{40}$$

The solution to this eigenvalue problem allows the following integral transform and accompanying inversion formula to be defined:

$$\widetilde{G}(\beta_m, t) = \int_{z=0}^{B} Z(\beta_m, z')G(z', t)dz' \tag{41}$$

$$G(z,t) = \sum_{m=1}^{\infty} \frac{Z(\beta_m, z)}{N(\beta_m)} \widetilde{G}(\beta_m, t) \tag{42}$$

$N(\beta_m)$ is the normalization integral for the eigenvalue problem and is described in the next section. Applying the integral transform operator defined by (41) to the governing equation (34) yields:

$$R\frac{d\widetilde{G}}{dt} = D\int_{z=0}^{B} Z\frac{\partial^2 G}{\partial z^2}dz' - (a`^2 D + \lambda R)\widetilde{G} + g(t)\int_{z'=d_1}^{d_2} Z(\beta_m^2 z')e^{-a`z'}dz' \tag{43}$$

Applying integration by parts twice and substituting the eigenvalue governing equation yields:

$$\frac{d\widetilde{G}}{dt} + \frac{1}{R}(a`^2 D + \lambda R + D\beta_m^2)\widetilde{G} = \frac{g(t)}{R}\int_{z'=d_1}^{d_2} Z(\beta_m, z')e^{-a`z'}dz' \tag{44}$$

subject to a homogeneous initial condition:

$$\widetilde{G}(t=0) = 0 \tag{45}$$

The general solution to the first order ordinary differential equation (44) subject to (45) is readily obtained as:

$$\tilde{G}(t) = e^{-\alpha_m t} \int_{t'=0}^{t} e^{\alpha_m t'} A_m(t') dt' \tag{46}$$

where:

$$A_m(t) = \frac{g(t)}{R} \int_{z'=d_1}^{d_2} Z(\beta_m, z') e^{-a` z'} dz' \tag{47}$$

$$\alpha_m = \frac{1}{R}\left(a`^2 D + \lambda R + D\beta_m^2\right) \tag{48}$$

Using the inversion formulae (33) and (42), the solution to equation (28) may be written in terms of the eigenvalues and eigenfunctions as:

$$C(z,t) = e^{az} \sum_{m=1}^{\infty} \frac{Z(\beta_m, z)}{N(\beta_m)} e^{-\alpha_m t} \int_{t'=0}^{t} e^{\alpha_m t'} A_m(t') dt' \tag{49}$$

The solution to the eigenvalue problem posed by (38)-(40) is provided by Ozisik [1980] as:

$$Z(z, \beta_m) = \sin(\beta_m z) \tag{50}$$

$$N(\beta_m) = \frac{B\left(\beta_m^2 + a`^2\right) + a`}{2\left(\beta_m^2 + a`^2\right)} \tag{51}$$

$$\beta_m\text{'s are positive roots of,} \quad \beta_m \cot(\beta_m B) = -a` \tag{52}$$

The general solution for (28) as provided in (49) is now complete. To perform simulations of transport from a single UXO item located from depth d_1 to d_2, only the specification of the transient in the generation term remains. The simplest generation model assumes a steady generation rate from time 0 to time t_1 when the mass is completely depleted:

$$\left.\begin{array}{ll} g = g_0 & \text{for } 0 < t \le t_1 \\ g = 0 & \text{for } t > t_1 \end{array}\right\} \qquad \text{for } d_1 < z < d_2;\ 0 \text{ elsewhere} \tag{53}$$

Substituting this generation rate into (22) yields the solution:

$$C(z,t) = \frac{g_0}{R} \sum_{m=1}^{\infty} \frac{\sin(\beta_m z)}{N(\beta_m)} \left\{ \frac{e^{-\alpha_m t} - e^{-\alpha_m (t - t_1)}}{\alpha_m \left(a`^2 + \beta_m^2\right)} \right\} \left[ e^{-a`(d_2 - z)} \left\{ a` \sin(\beta_m d_2) + \beta_m \cos(\beta_m d_2) \right\} \right.$$
$$\left. - e^{-a`(d_1 - z)} \left\{ a` \sin(\beta_m d_1) + \beta_m \cos(\beta_m d_1) \right\} \right] \tag{54}$$

Another common model for the source term assumes an exponential decay in the generation rate:

$$g = g_0 e^{-\gamma t} \qquad \text{for } d_1 < z < d_2;\ 0 \text{ elsewhere} \tag{55}$$

Substituting this generation term into (49) yields the following solution:

$$C(z,t) = \frac{g_0}{R}\sum_{m=1}^{\infty}\frac{\sin(\beta_m z)\left(e^{-\gamma t} - e^{-\alpha_m t}\right)}{N(\beta_m)(\alpha_m - \gamma)\left(a`^2+\beta_m^2\right)}\left[e^{-a`(d_2-z)}\left\{a`\sin(\beta_m d_2)+\beta_m\cos(\beta_m d_2)\right\}\right.$$
$$\left. - e^{-a`(d_1-z)}\left\{a`\sin(\beta_m d_1)+\beta_m\cos(\beta_m d_1)\right\}\right] \tag{56}$$

If the source persists effectively to perpetuity, then the solution (54) reduces to:

$$C(z,t) = \frac{g_0}{R}\sum_{m=1}^{\infty}\frac{\sin(\beta_m z)}{N(\beta_m)}\left\{\frac{e^{-\alpha_m t} - e^{-\alpha_m (t-t_1)}}{\alpha_m\left(a^2+\beta_m^2\right)}\right\}\left[e^{-a(d_2-z)}\left\{a\sin(\beta_m d_2)+\beta_m\cos(\beta_m d_2)\right\}\right.$$
$$\left. - e^{-a(d_1-z)}\left\{a\sin(\beta_m d_1)+\beta_m\cos(\beta_m d_1)\right\}\right] \tag{57}$$

If the degradation is also zero, then (57) reduces to:

$$C(z,t) = \frac{g_0}{R}\sum_{m=1}^{\infty}\frac{\sin(\beta_m z)}{N(\beta_m)}\left\{\frac{e^{-\alpha_m t} - e^{-\alpha_m (t-t_1)}}{\alpha_m\left(a`^2+\beta_m^2\right)}\right\}\left[e^{-a(d_2-z)}\left\{a`\sin(\beta_m d_2)+\beta_m\cos(\beta_m d_2)\right\}\right.$$
$$\left. - e^{-a`(d_1-z)}\left\{a`\sin(\beta_m d_1)+\beta_m\cos(\beta_m d_1)\right\}\right] \tag{58}$$

5.2. Estimating the Time for Energetics to Reach Groundwater after Release

The time for energetics to reach groundwater after release can be estimated from scaling arguments applied to equation (28). If infiltration is the dominant mechanism for downward migration (i.e., diffusion and dispersion are negligible) then:

$$\text{Time to GW} \approx \frac{RB}{I} \tag{59}$$

where B is the depth to groundwater. For example, typical retardation coefficients for RDX and TNT are 1.3 and 4, respectively. For an infiltration rate of 20 inches per year and a depth to groundwater of 20 feet, the time to reach groundwater for RDX would be about 16 years. Under similar conditions, TNT would require almost 50 years.

TNT is known to degrade in soil. RDX degrades but more slowly than TNT. Hence, if the travel time to groundwater is long, then a significant proportion of the energetic may degrade in the vadose zone and the impact to groundwater will be minimal. This condition is expressed as:

$$\text{if } \left(\lambda >> \frac{I}{RB}\right) \text{ then energetic degrades before reaching GW} \quad (60)$$

The degradation constant is related to the half-life of a compound in soil via (van der Heijde et al., 1988):

$$\lambda = \frac{\ln(2)}{T_{1/2}}$$

where $T_{1/2}$ is the energetic half-life in soil. The estimated half-life of TNT in soils ranges from 1 to 6 months. This estimate was made on the basis of the estimated unacclimated aqueous aerobic biodegradation half-life (Howard et al. 1991). In laboratory tests by the EPA with sandy loam and sandy silt loam soils, the aerobic degradation half-life of TNT was determined to be only 5.7-7.7 days (USEPA 1989). Hence, values vary from site to site and range from 1 week to six months. Therefore, the degradation constants vary from 0.0038 day^{-1} to 0.1 day^{-1}. For a typical retardation coefficient of 4 and an infiltration rate of 50 cm per year, these degradation values suggest very little TNT will reach groundwater although degradation is highly site-specific. This is illustrated in Figure 10 which shows the amount of TNT remaining at an infiltration rate of 50 cm/yr as function of soil depth. Three half-lives are shown (1 week to 6 months).

In a recent study, half-lives for RDX were calculated from first-order rate constants for three soils measured in the laboratory and varied from 94 days to 154 days (Jenkins et al., 2003). The site-specific half-life of RDX was estimated in a lagoon 50 cm deep to range from over 2,000 days in winter to 456 days in summer (Army 1984). For a typical RDX retardation coefficient of 1.3 and an infiltration rate of 50 cm per year, the degradation constant [i.e., ln(2)/2,000 days = 0.00035 day^{-1}] suggests little RDX will reach groundwater if the depth to groundwater exceeds three meters even for this highly conservative half life estimate. This range of half-lives are depicted in Figure 11. As stated above, degradation is highly site-specific and laboratory measurements may not be directly applicable to field conditions.

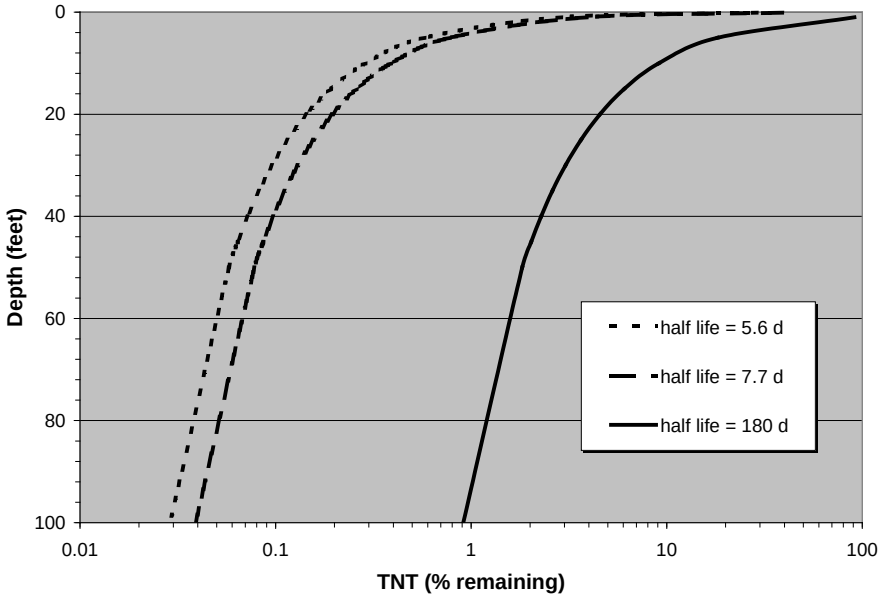

Figure 10. TNT Degradation for Three Different Half Lives at an Infiltration Rate of 50 cm/yr

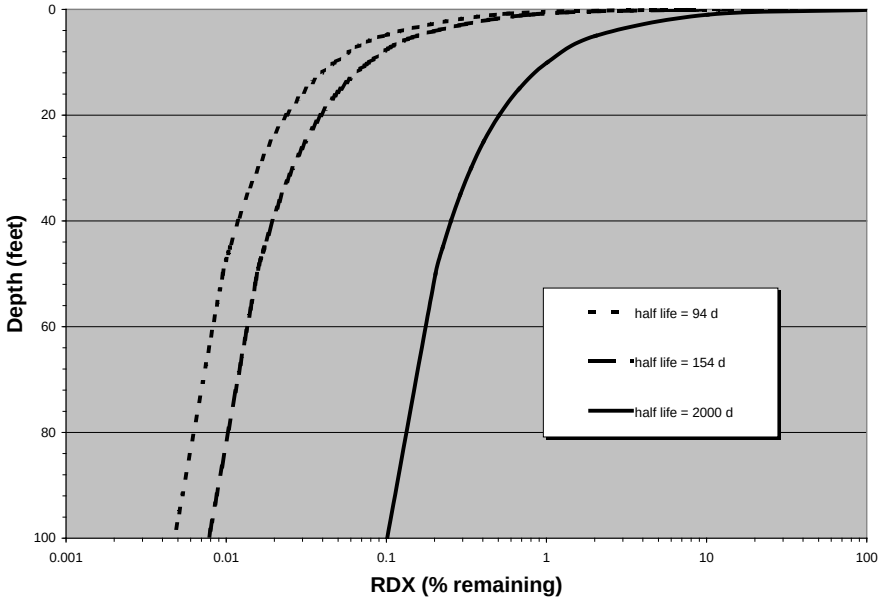

Figure 11. RDX Degradation for Three Different Half Lives at an Infiltration Rate of 50 cm/yr

6. Transport into Groundwater

The previous section described the transport of an energetic from its release at a corroded UXO through the vadose zone to the top of the water table. In this section, a model is described for calculating the potential impact of UXO energetic release on underlying groundwater. For convenience, a schematic describing the system is presented again (Figure 12). The three-

dimensional, transient transport of a dissolved energetic in unidirectional groundwater flow through a uniform, anisotropic aquifer is governed by (Bear, 1972):

$$R_w \frac{\partial C_w}{\partial t} = D_{w,x} \frac{\partial^2 C_w}{\partial x^2} + D_{y,x} \frac{\partial^2 C_w}{\partial y^2} + D_{w,\zeta} \frac{\partial^2 C_w}{\partial \zeta^2} - U \frac{\partial C_w}{\partial x} - \lambda_w R_w C_w \qquad (61)$$

with the definitions:

C_w = ground water concentration
R_w = retardation coefficient in groundwater (= $1+ \rho_b K_d/\phi$)
$D_{w,x}$ = effective diffusion and dispersion coefficient in the x-direction
$D_{w,y}$ = effective diffusion and dispersion coefficient in the y-direction
$D_{w,\zeta}$ = effective diffusion and dispersion coefficient in the ζ-direction
λ_w = first-order degradation constant in ground water
U = Darcy velocity of ground water
X = horizontal coordinate in the direction of groundwater flow
Y = horizontal coordinate perpendicular to the direction of groundwater flow
ζ = vertical coordinate

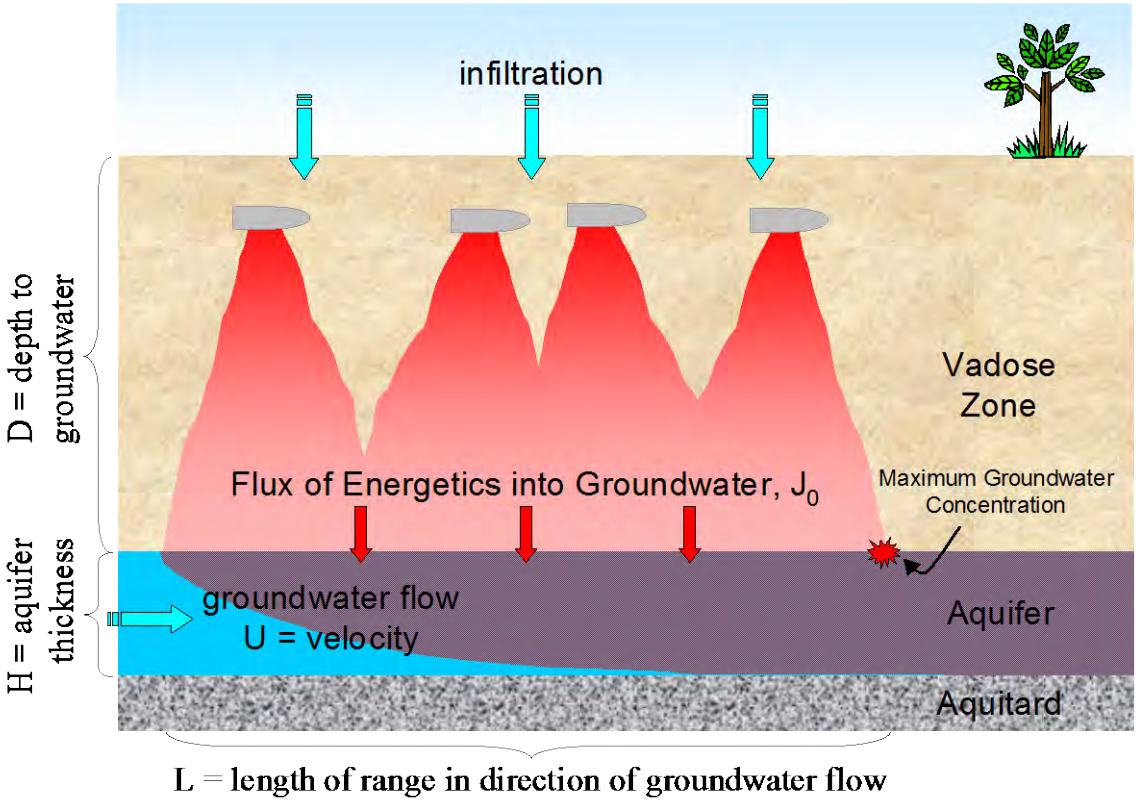

Figure 12. Description of Energetics Transport from UXO into Groundwater

The vertical coordinate equals zero at the bottom of the vadose zone and equals H (i.e. aquifer thickeness) at the bottom of the aquifer. If we assume the flux of contaminants from the vadose

zone is steady and endures to infinity (a very conservative assumption), the transient term can be dropped and steady-state concentration profiles will exist in groundwater. If we further neglect horizontal dispersion (x and y directions), then (61) reduces to:

$$D_{w,\zeta}\frac{\partial^2 C_w}{\partial \zeta^2} = U\frac{\partial C_w}{\partial x} + \lambda_w R_w C_w \tag{62}$$

subject to the boundary conditions:

$$-D_{w,z}\frac{\partial C_w}{\partial \zeta} = \begin{cases} J_0 & \text{at } \zeta = 0, \text{ and for } 0 < x \le L \\ 0 & \text{at } \zeta = 0, \text{ and for } x > L \end{cases} \tag{63a}$$

$$\frac{\partial C_w}{\partial \zeta} = 0 \qquad \text{at } \zeta = H,\ x > 0 \tag{63b}$$

$$C_w = 0 \qquad \text{at } x = 0,\ \text{all } \zeta \tag{63c}$$

where:

J_0 = mass flux of explosive contaminant entering groundwater from the vadose zone

The dispersion/diffusion coefficient in the ζ-direction is estimated by:

$$D_{w,\zeta} = \alpha_T\, U + D_m$$

where α_T is the transverse dispersivity and D_m is the effective molecular diffusion coefficient in the aquifer.

Equation (62) subject to boundary conditions (63) can be solved using Fourier and Laplace transformations. The appropriate eigenvalue problem for the integral transform in the space variable ζ is:

$$\frac{d^2 Z_w}{d\zeta^2} + \beta_n^2 Z_w = 0 \tag{64}$$

with boundary conditions:

$$\frac{dZ_w}{d\zeta} = 0 \qquad \text{at } \zeta = 0 \tag{65a}$$

$$\frac{dZ_w}{d\zeta} = 0 \qquad \text{at } \zeta = H \tag{65b}$$

The solution to this eigenvalue problem is provided by M. N. Ozisik ("Heat Conduction," 1980):

$$Z_w(\zeta,\beta_n) = \cos(\beta_n \zeta) \text{ for } n = 1,\infty \quad ; \quad Z(\zeta,\beta_0) = 1 \text{ for } n = 0 \tag{66}$$

$$N(\beta_n) = \frac{H}{2} \text{ for } n = 1,\infty \quad ; \quad N(\beta_0) = H \text{ for } n = 0 \tag{67}$$

$$\beta_n = \frac{n\pi}{H} \text{ for } n = 1,\infty \quad ; \quad \beta_0 = 0 \tag{68}$$

The solution to this eigenvalue problem allows the following integral transform and accompanying inversion formula to be defined (Ozisik, 1980):

$$\hat{C}_w(\beta_n, x) = \int_{\zeta=0}^{H} Z_w(\beta_n, \zeta') C_w(x, \zeta') d\zeta' \tag{69}$$

$$C_w(x,\zeta) = \sum_{n=0}^{\infty} \frac{Z_w(\beta_n,\zeta)}{N_w(\beta_n)} \hat{C}_w(\beta_n, x) \tag{70}$$

$N(\beta_n)$ is the normalization integral for the eigenvalue problem. Applying the integral transform operator defined by (69) to the governing equation (62) and initial condition at x = 0 yields:

$$D_{w,\zeta} \int_{\zeta=0}^{H} Z_w \frac{\partial^2 C_w}{\partial \zeta^2} d\zeta' = U \frac{d\hat{C}_w}{dx} + \lambda_w R_w \hat{C}_w \tag{71}$$

$$\hat{C}_w = 0 \qquad \text{at } x = 0 \tag{72}$$

Applying integration by parts twice and substituting in equation (64) yields:

$$\frac{d\hat{C}_w}{dx} + \frac{1}{U}\left(\lambda_w R_w + D_{w,\zeta}\beta_n^2\right)\hat{C}_w = -\frac{Z_w(\beta_n, \zeta = 0)}{U} D_{w,\zeta} \left.\frac{\partial C_w}{\partial \zeta}\right|_{\zeta=0} \tag{73}$$

subject to a homogeneous initial condition:

$$\hat{C}_w(x = 0) = 0 \tag{74}$$

As indicated by boundary condition (63a), the input flux from the vadose zone occurs uniformly over a finite length, L, and is zero elsewhere making the right hand side of equation (73) dependent on x. Substituting the boundary condition (63a) into (73) yields:

$$\frac{d\hat{C}_w}{dx} + \frac{1}{U}\left(\lambda_w R_w + D_{w,\zeta}\beta_n^2\right)\hat{C}_w = \frac{J_0}{U}\left[\Theta(x) - \Theta(x-L)\right] \tag{75}$$

where the Heaviside step function is defined by:

$$\Theta(\chi) = \begin{cases} 0 & \chi < 0 \\ 1/2 & \chi = 0 \\ 1 & \chi > 0 \end{cases} \tag{76}$$

This type of discontinuous forcing function is readily handled using the Laplace transform. Applying the Laplace transform to (75) subject to (74) and rearranging yields the transformed solution:

$$\breve{C}(s) = \frac{J_0\left(1 - e^{-Ls}\right)}{s\left(Us + \lambda_w R_w + D_{w,\zeta}\beta_n^2\right)} \tag{77}$$

The solution to (75) is found by applying the inverse Laplace transform to (77). The inverses are available from tabulations of the Laplace transform applied to functions and the accompanying inverses (e.g., "Handbook of Mathematical Functions with Formulas, Graphs, and Mathematical Tables," M. Abramowitz and I. A. Stegun, eds., 1964). The inverse function of (77) yields the solution for (75):

$$\hat{C}_w(x) = \frac{J_0}{\lambda_w R_w + D_{w,\zeta}\beta_n^2}\left\{1 - e^{-\frac{x}{U}\left(\lambda_w R_w + D_{w,\zeta}\beta_n^2\right)} - \Theta(x-L)\left[1 - e^{-\frac{(x-L)}{U}\left(\lambda_w R_w + D_{w,\zeta}\beta_n^2\right)}\right]\right\} \tag{78}$$

A special case occurs for the first eigenvalue, β_0, if λ equals zero. In this case, the solution to (75) is:

$$\hat{C}_w(x) = \frac{J_0}{U}\left[x - \Theta(x-L)(x-L)\right] \tag{79}$$

Using the inversion formula (70) applied to (78) and (79), the solution to equation (62) may be written in terms of the eigenvalues and eigenfunctions as:

$$C_w(x,\zeta) = J_0 \sum_{n=0}^{\infty} \frac{Z_w(\beta_n,\zeta)}{N_w(\beta_n)\left(\lambda_w R_w + D_{w,\zeta}\beta_n^2\right)} \times \left\{1 - e^{-\frac{x}{U}\left(\lambda_w R_w + D_{w,\zeta}\beta_n^2\right)} - \Theta(x-L)\left[1 - e^{-\frac{(x-L)}{U}\left(\lambda_w R_w + D_{w,\zeta}\beta_n^2\right)}\right]\right\} \quad \text{for } \lambda \neq 0 \tag{80}$$

$$C_w(x,\zeta) = \frac{J_0 Z_w(0,\zeta)}{U\, N_w(0)}\left[x - \Theta(x-L)(x-L)\right] + \frac{J_0}{D_{w,\zeta}} \sum_{n=1}^{\infty} \frac{Z_w(\beta_n,\zeta)}{\beta_n^2 N_w(\beta_n)} \left\{ 1 - e^{-x\left(\frac{D_{w,\zeta}\beta_n^2}{U}\right)} - \Theta(x-L)\left[1 - e^{-(x-L)\left(\frac{D_{w,\zeta}\beta_n^2}{U}\right)} \right] \right\} \quad \text{for } \lambda = 0 \quad (81)$$

Substituting the expressions from the eigenvalue problem given in (66) to (68) into (80) and (81) completes the solution of (62):

$$C_w(x,\zeta) = 2J_0 H \sum_{n=0}^{\infty} \frac{\cos\left(\frac{n\pi\zeta}{H}\right)}{\left(\lambda_w R_w H^2 + D_{w,\zeta} n^2\pi^2\right)} \times \left\{ 1 - e^{-\frac{x}{U}\left(\lambda_w R_w + D_{w,\zeta}\frac{n^2\pi^2}{H^2}\right)} - \Theta(x-L)\left[1 - e^{-\frac{(x-L)}{U}\left(\lambda_w R_w + D_{w,\zeta}\frac{n^2\pi^2}{H^2}\right)} \right] \right\} \quad \text{for } \lambda \neq 0 \quad (82)$$

$$C_w(x,\zeta) = \frac{J_0}{U\,H}\left[x - \Theta(x-L)(x-L)\right] + \frac{2J_0 H}{\pi^2 D_{w,\zeta}} \sum_{n=1}^{\infty} \frac{1}{n^2} \cos\left(\frac{n\pi\zeta}{H}\right) \left\{ 1 - e^{-x\left(\frac{D_{w,\zeta} n^2\pi^2}{UH^2}\right)} - \Theta(x-L)\left[1 - e^{-(x-L)\left(\frac{D_{w,\zeta} n^2\pi^2}{UH^2}\right)} \right] \right\} \quad \text{for } \lambda = 0 \quad (83)$$

These expressions are straightforward to evaluate. The summation is very well behaved and easily evaluated to a specified accuracy. Convergence of the series to a practical accuracy is generally achieved with a modest number of terms (e.g., 25).

For the problem specified by (62), the maximum concentration in groundwater will occur at the top of the aquifer (ζ=0) and at the trailing edge of the input from the vadose zone (x=L). To be conservative in forecasting this maximum, the degradation can also be neglected (λ=0) to yield:

$$C_{w,max} = \frac{J_0 L}{U\,H} + \frac{2J_0 H}{\pi^2 D_{w,\zeta}} \sum_{n=1}^{\infty} \frac{1}{n^2} \left\{ 1 - e^{-\left(\frac{L D_{w,\zeta} n^2\pi^2}{UH^2}\right)} \right\} \quad \text{for } \lambda = 0 \quad (84)$$

If the following condition is also satisfied:

$$\frac{LD_{w,\zeta}}{UH^2} > 0.5 \tag{85}$$

then the exponential term in (84) will always be much less than one and can be neglected. Equation (84) is then reduced to:

$$C_{w,max} = \frac{J_0 L}{U H} + \frac{2J_0 H}{\pi^2 D_{w,\zeta}} \sum_{n=1}^{\infty} \frac{1}{n^2} \tag{86}$$

The series in (86) converges to $\pi^2/6$ and therefore equation (86) reduces to:

$$C_{w,max} = J_0 \left(\frac{L}{UH} + \frac{H}{3D_{w,\zeta}} \right) \qquad \text{if} \quad \frac{LD_{w,\zeta}}{UH^2} > 0.5 \tag{87}$$

Beyond x=L, no additional mass is added to the groundwater. The contaminants become better mixed by vertical dispersion and ultimately reach a uniform, average concentration over the vertical extent of the aquifer. If no degradation occurs, the average concentration in the groundwater beyond x = L can be determined by integrating equation (83) over ζ from 0 to H, dividing the result by H, and setting x equal to L. The result is:

$$C_{w,average}(x \geq L) = \frac{J_0 L}{UH} \tag{88}$$

This expression is also obtainable from a simple mass balance. The numerator in (88) represents the mass entering the groundwater from the vadose zone per unit width of the range and the denominator represents the groundwater flowing under the range per unit width.

7. Application of UXO Energetics Transport Model to UXO Corrosion Study Sites

The steps for modeling the impact of energetics released from corroded UXO are summarized below:

1. Determine the characteristics of the range (number, type and distribution of high explosive filled UXO over the area of concern)
2. Specify the soil physical properties
3. Specify the infiltration rate, groundwater velocity and aquifer thickness
4. Select the appropriate mass transfer model for <u>individual</u> UXO
    - Advection-dominated bare fill [eqn (13) or (14) for a cylindrical or spherical shape]
    - Diffusion-dominated bare fill [eqn (16) or (17) for a sphere or prolate spheroid]
    - Pit Diffusion to Outer Mass Transfer [equation (21)]
    - Mass Release from Bare, Disarticulated Lumps [equation (23)]

5. Develop a model for transient infiltration from precipitation data and apply the appropriate mass transfer model for each steady infiltration rate
6. Sum the energetic mass release rates from individual UXO using the range characteristics
7. Apply the appropriate vadose zone transport model to estimate the mass flux entering groundwater
    - Constant mass release rate for a defined period [equation (54)]
    - Constant mass release rate for all time [equation (57)]
    - Exponentially decaying mass release rate [equation (56)]
    - Constant mass release rate for all time, no degradation [equation (58)]
8. Calculate groundwater concentrations resulting from the energetics release utilizing aquifer properties
    - Detailed concentration profiles [equation (82) or (83)]
    - Maximum groundwater concentration with no attenuation [equation (87)]
    - Average groundwater concentration leaving the range with no attenuation [equation (88)]

In this section the models are applied to the UXO Corrosion Study Sites. As indicated in Section 4, the degradation of energetics in the vadose zone can profoundly reduce the impact on underlying groundwater; however, for the present estimates the degradation is neglected entirely. Degradation rates are highly site-specific and difficult to measure and neglecting degradation yields conservative estimates for the impact on groundwater.

Recalling equations (1) and (2), the average groundwater concentration off–range can be estimated with the mass release rate from a single UXO item, assuming no attenuation or adsorption in the vadose zone:

$$C_{w,average}(x \geq L) = \frac{\dot{m}_{uxo} n_{uxo} L}{UH} \tag{89}$$

This expression illustrates that the resulting groundwater concentration varies linearly with the groundwater velocity, thickness of the aquifer, length of the range, and density of UXO items covering the range. These parameters were discussed in Section 2 and are often very difficult to estimate without a significant and varied field investigation.

Recalling Section 3, the mass release rate is a function of the infiltration rate, soil moisture content, energetic diffusion coefficient in water, energetic solubility in water, explosive fill geometry [e.g., see equation (13)], and degree of perforating corrosion pits [e.g., see equation (21)]. All of these parameters can be reasonably estimated such that reasonable estimates for the energetic release rate from a corroded UXO can be obtained.

Example results for the corrosion study sites are presented in Table 5 for 1-kg of CompB in the shape of a cylinder with a radius of 3.8 cm. For these results, the density of UXO items on the range is assumed to be 100 high explosive UXO items per square kilometer with a range length of one kilometer. The groundwater velocity and aquifer thickness are assumed to be 30 meters per year and 5 meters, respectively. These values are applied to all sites since no site-specific information was available. In this hypothetical UXO scenario, four of the ten sites had the potential to exceed groundwater standards for TNT (i.e., 0.002 mg/L) after thorough corrosion

leaves bare explosive fill and none of the sites exceeded the standards for RDX. None of the scenarios exceeded groundwater standards when diffusion through perforating pits was included. The release rate of RDX is generally an order-of-magnitude less than TNT because of its lower solubility and lower diffusivity in water than TNT It should be reiterated that degradation has been left out of this estimation and adsorption is assumed to be at equilibrium. Subsequently estimations for TNT are considered highly conservative since TNT readily degrades and would be attenuated non-equilibrium adsorption.

For TNT to exceed the groundwater standards under the pitting release scenario, the density of UXO items would generally have to approach 400 items per square kilometer and for RDX to approach the standards the density would need to be about 4,000 items per square kilometer. To illustrate this point, the results for Site B are plotted as a function of item density in Figures 13 and 14 for RDX and TNT, respectively. The plots include results assuming steady infiltration, periodic infiltration, and pit diffusion.

Table 5. Potential RDX Concentrations in Groundwater at Corrosion Study Sites.

Site	Annual Infiltration Rate, I	Moisture Content, θ	Annual Days of Precip.	Individual Mass Release Rate		Average Groundwater Concentration	
				Bare Fill	Pitted	Bare Fill	Pitted
	(in/yr)	(%Vol)	(Days)	(g/yr)	(g/yr)	(mg/L)	(mg/L)
A	15.7	19.3	149	0.60	0.081	0.0004	0.00005
B	3.3	7.5	133	0.87	0.075	0.00058	0.00005
C	13.0	7.8	157	1.50	0.094	0.0010	0.00006
D	1.8	21.8	196	0.37	0.091	0.00025	0.00006
E	1.0	11.8	175	0.51	0.088	0.00034	0.00006
F	1.0	2.4	151	1.97	0.080	0.0013	0.00005
G	15.5	23.6	160	0.52	0.084	0.00035	0.00006
H	21.8	15.8	155	0.78	0.082	0.00052	0.00006
I	2.5	19	149	0.40	0.083	0.00027	0.00006
Z	26.2	22.5	189	0.67	0.091	0.00044	0.00007

Table 6. Potential TNT Concentrations in Groundwater at Corrosion Study Sites.

Site	Annual Infiltration Rate, I	Moisture Content, θ	Annual Days of Precip.	Individual Mass Release Rate		Average Groundwater Concentration	
				Bare Fill	Pitted	Bare Fill	Pitted
	(in/yr)	(%Vol)	(Days)	(g/yr)	(g/yr)	(mg/L)	(mg/L)
A	15.7	19.3	149	2.9	0.71	0.0019	0.00047
B	3.3	7.5	133	4.2	0.68	**0.0028**	0.00045
C	13.0	7.8	157	6.9	0.84	**0.0046**	0.00056
D	1.8	21.8	196	1.8	0.74	0.0012	0.00049
E	1.0	11.8	175	2.5	0.75	0.0017	0.00050
F	1.0	2.4	151	9.1	0.73	**0.0061**	0.00048
G	15.5	23.6	160	2.6	0.73	0.0017	0.00048
H	21.8	15.8	155	3.7	0.73	**0.0025**	0.00048
I	2.5	19	149	2.0	0.70	0.0014	0.00047
Z	26.2	22.5	189	3.2	0.78	0.0021	0.00052

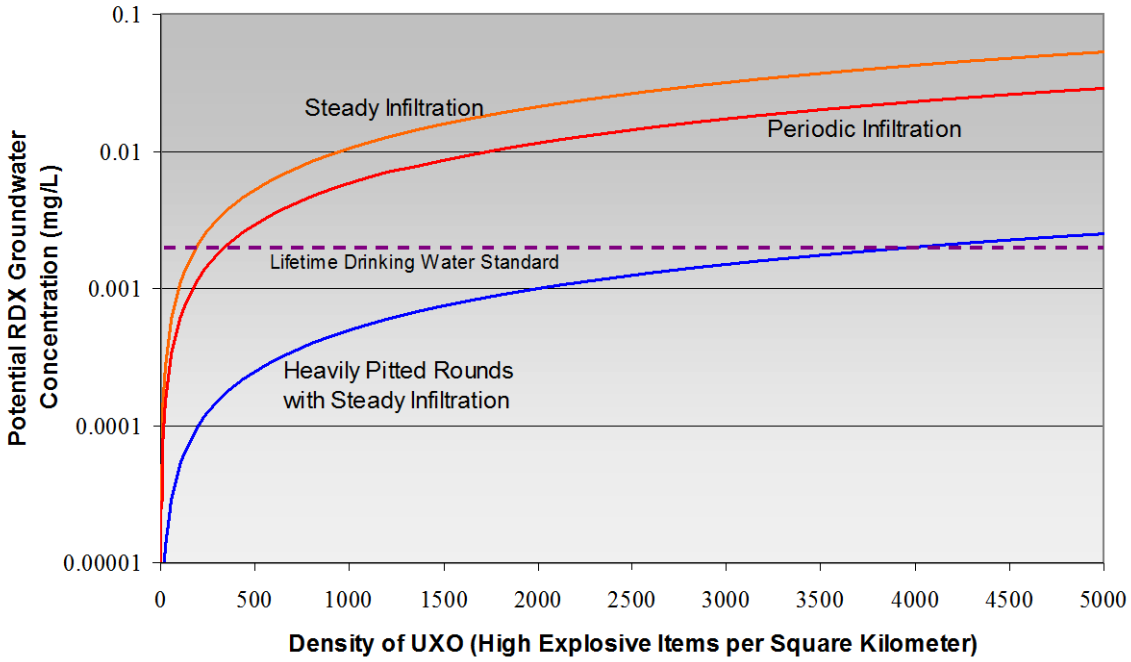

Figure 13. Potential RDX Groundwater Concentrations as a Function of UXO Density for Site B

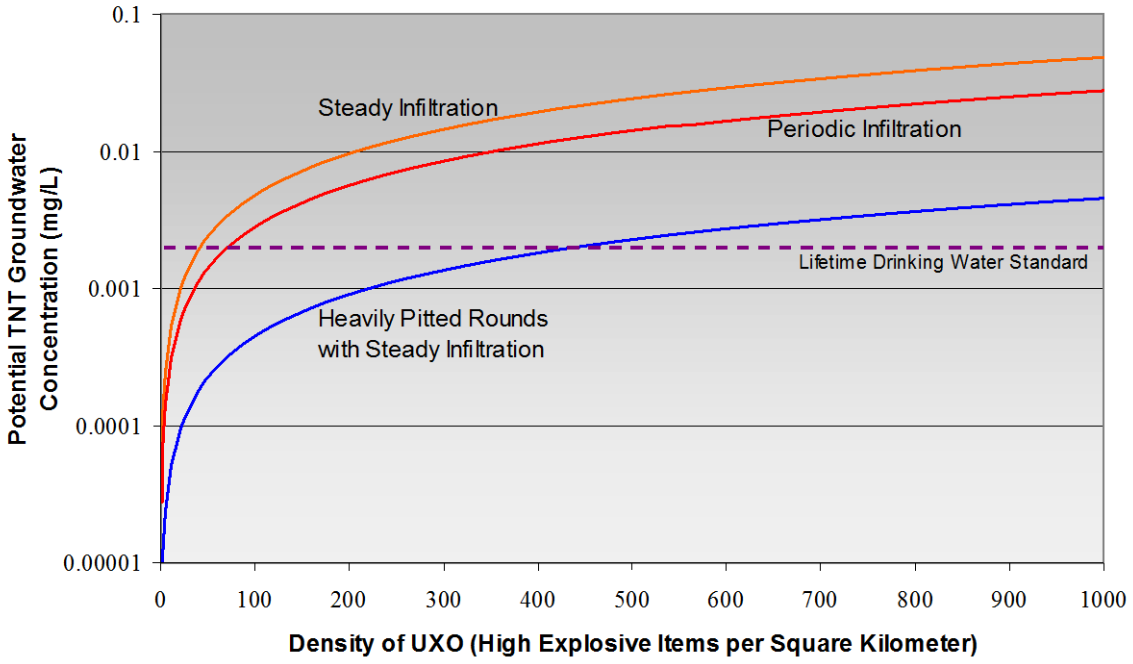

Figure 14. Potential TNT Groundwater Concentrations as a Function of UXO Density for Site B

8. References for the Energetics Transport Model

Bear, J., 1972, Dynamics of Fluids in Porous Media, Dover Books, pp. 764.

Berkowitz, B., and Hansen, D.P., 2001, A numerical study of the distribution of water in partially saturated porous rock, Transport in Porous Media, v 45, pp. 303-319

Chambre, P.L., Pigford, T.H., and Zavoshy, S., 1980, Solubility-limited fractional dissolution rate of vitrified waste in groundwater, Trans. Amer. Nucl. Soc., 33, p.185

Chambre, P.L., Pigford, T.H., Fujita, A., Kanki, T. ,Kobayashi, R.,Lung, H., Ting, D., Sato, Y., and Zavoshy, S., 1982, Analytical performance models for geologic repositories, LBL-14842

Chambre, P.L., and Pigford, T.H., 1984, Prediction of waste performance in a geologic repository, Mat. Res. Soc. Symp., Elsevier Science Pub. Co., vol. 26, pp. 985-1008

Howard PH, Boethling RS, Jarvis WF, et al. 1991. Handbook of environmental degradation rates. Chelsea, MI: Lewis Publishers, 454-455.

Jenkins, T.F., C. Bartolini,and T.A.Ranney, 2003, "Stability of CL-20, TNAZ, HMX, RDX, NG, and PETN in Moist,Unsaturated Soil," U.S. Army, ERDC/CRREL TR-03-7, April 2003.

Jia, C., Shing, K., and Yortsos, Y.C., November 1999, Advective mass transfer from stationary sources in porous media, WRR, v. 35, no. 11, pp. 3239-3251.

Kashef, A.I., 1986, Groundwater Engineering, McGraw-Hill, 512 p.

Kuechler, R., and Noack, K., 2002, Transport of reacting solutes through the unsaturated zone, Transport in Porous Media, v 49, pp. 361-375

Lynch, J.C., September 2002, Dissolution Kinetics of High Explosive Compounds (TNT, RDX, HMX), US Army Corps of Engineers, Engineer Research and Development Center, ERDC/EL TR-02-23.

Lynch, J.C., K.F. Meyers, J.M. Brannon, and J.J. Delfino, 2001, "Effects of pH and Temperature on the Aqueous Solubility and Dissolution Rate of 2,4,6-Trinitrotoluene (TNT), Hexahydro-1,3,5-trinitro-1,3,5-triazine (RDX), and Octahydro-1,3,5,7-tetranitro-1,3,5,7-tetrazocine (HMX)," *J.Chem. Eng. Data*, Vol. 46, pp. 1549-1555.

Lynch, J.C., J.M. Brannon, and J.J. Delfino, 2002, "Effects of Component Interactions on the Aqueous Solubilities and Dissolution Rates of the Explosive Formulations Octol, Composition B, and LX-14," *J.Chem. Eng. Data*, Vol. 47, pp. 542-549.

Millington and Quirk, 1961, Permeability of Porous Solids. *Trans. Faraday. Soc.* 57:1200-1207

Murphy, W.M., Oelkers, E.H., and Lichtner, P.C., 1989, Surface reaction versus diffusion control of mineral dissolution and growth rates in geochemical processes, Chemical Geology, v. 78, pp. 357-380.

Nitao, J.J., December 1989, Simulations of the near-field transport of radionuclides by liquid diffusion at Yucca Mountain – comparisons with and without backfill, LLNL report UCID 21466.

Pigford, T.H. (chairman), 1983, A study of the isolation system for geological disposal of radioactive wastes, National Academy Press

United States Army Environmental Center (USAEC), 2001 & 2000, Study of ammunition dud and low order detonation rates (Phases I and II), SFIM-AEC-PC-CR-200139. Aberdeen, MD.

United States Department of the Army (Army), 1984, Technical Manual TM 9-1300-214, Military Explosives. Washington, DC.

United States Department of the Army, 1992 (Army), Mil Spec for the 155mm HE Projectile, Loading, Assembly and Packing, Mil-P-60377B (AR).

United States Environmental Protection Agency (USEPA). 1989. Treatability potential for EPA listed hazardous wastes in soil. Report no. EPA/600/S2-89/011. Ada, OK: U.S. Environmental Protection Agency, Robert S. Kerr Environmental Research Laboratory. Document no. PB89-166581.

United States Soil Conservation Service (USSCS), 1985. National Engineering Handbook - Section 4 - Hydrology. Washington, DC: U.S. Department of Agriculture.

van der Heijde, P., A.I. El-Kadi, and S.A. Williams, 1988, Groundwater Modeling: An Overview and Status Report, U.S. EPA, EPA/600/2-89/028, December 1988.

Appendix A5

SUBMITTED ABSTRACTS

PRAXIS
ENVIRONMENTAL TECHNOLOGIES, INC.
1440 Rollins Road, Burlingame, California 94010
(650) 548-9288

December, 2002, Corrosion of Unexploded Ordnance, SERDP Annual Symposium, Washington, DC

March 2003, Corrosion Modeling of Unexploded Ordnance, Triservices Conference, Charlotte, NC.

December, 2003, Corrosion of Unexploded Ordnance, SERDP Annual Symposium, Washington, DC

December, 2002, SERDP Annual Symposium, Washington, DC

Corrosion of Unexploded Ordnance

Michael D. Chendorain, M.S.[1], LLoyd D. Stewart, PhD PE[1], Bonnie Packer, PhD[2]

[1]PRAXIS Environmental Technologies, Inc., 1440 Rollins Rd., Burlingame, CA 94010, 650-548-9288, praxis@praxis-enviro.com
[2]U.S. Army Environmental Center/Gamma Engineering, 5179 Hoadley Road, Aberdeen Proving Ground, MD 21010, 410-436-6846, bonnie.packer@USAEC.apgea.army.mil

Unexploded ordnance (UXO) lie buried at an estimated 1,500 sites encompassing 15 million acres. These items often contain explosive fill (e.g., RDX, TNT, etc.) posing an uncertain environmental risk. This talk presents results from an ongoing study to determine the corrosion rate and potential release of energetics from UXO into soil. The objective is to develop a model of predictive correlations for the corrosion rate of UXO metallic containers as a function of soil properties and climatic conditions. To date, the study includes soils and metal fragments from nearly 70 UXO at six inactive Army training facilities (WWI to WWII era).

For each item, soil samples were collected adjacent and short distances from the UXO. The soil samples were analyzed for chemical, physical and biological properties including UXO energetics. Metal fragments from the UXO were collected during disposal and analyzed for corrosion parameters (e.g., pit depths and scale chemistry) and metallurgy. Results of the soil analyses suggest the first six study sites exhibited characteristics of acidic, oxidizing inorganic soils. Using the maximum pit depth measured in each item and dating the exposure time, corrosion rates at the study sites range from 0.120 to 7.47 mils per year (mpy) equivalent to 65 to 4,000 years to perforate a one-half-inch-thick steel casing. Both the highest and lowest rates of corrosion were found in silt-dominated soils with significant coarse fractions. The average corrosion rate is 1.8 ± 1.5 mpy. For this initial small sample set, corrosion rate correlates inversely with sediment porosity (r^2 =0.58). Porosity may be a practical parameter to assess a soil's corrosive nature since porosity is temporally invariant, easy to measure, and related to important soil characteristics such as matric force and moisture regime. Of the nearly 70 different UXO sampled, only three had indications of energetic movement into soil. All three were 60 mm rounds (shell thickness of 0.183 inches) and one had the appearance of a low order detonation. Energetics from the other two items were detected below calculated calibration limits and the instrument detection limits.

Biological properties were measured including general aerobic and anaerobic microorganisms, acid producers, and sulfate-reducing bacteria. All were found in abundance both on and away from the UXO with the exception of sulfate reducing bacteria present at low concentrations. This suggests that any microbiological contribution to corrosion can be attributed to ubiquitous acid-producing microorganisms.

This study is ongoing and sampling activities are scheduled for approximately eight additional sites.

March 2003, Triservices Conference, Charlotte, NC.

Corrosion Modeling of Unexploded Ordnance

Lloyd D. Stewart, PhD, PE
PRAXIS Environmental Technologies, Inc.
1440 Rollins Road, Burlingame, CA 94010
650-548-9288, Bo@Praxis-Enviro.com

Co-Presenters: James Garber, PhD, University of Louisiana, Lafayette
Michael Chendorain, MS, PRAXIS Environmental Technologies, Inc.
Bonnie Packer, PhD, U.S. Army Environmental Center

Unexploded ordnance (UXO) lie buried at an estimated 1,500 sites encompassing 15 million acres. These items often contain explosive fill (e.g., RDX, TNT, etc.) posing an uncertain environmental risk. This talk presents the framework and example results from an ongoing effort to model the corrosion rate and ultimate perforation of UXO. The objective of the effort is to develop a predictive model for the corrosion rate of UXO metallic containers as a function of soil properties, climatic conditions, and UXO dimensions. To calibrate and validate the model, the overall study will include sampling and analyses of soil and metal fragments from UXO items (~100) located at more than ten former Army training facilities (WWI to WWII era).

The major mechanism driving the UXO corrosion model is pitting. The current version of the model assumes the container is made of steel. To initiate the modeling, conceptualization of the corrosion processes dominant for UXO led to two views. From an "outer" view, the processes included in the model are the movement of oxygen, moisture and salts in the soil surrounding the UXO. Potential limits on the rate of corrosion from this perspective include: (1) a depletion of oxygen at the UXO surface accompanied by slow transport of oxygen from the atmosphere, and (2) the generation of thick scales relatively impervious to iron and oxygen transport. From the "inner" view within a pit, the corrosion is described by a cathode (UXO/soil interface), anode (bottom of the pit), pit electrolyte, and iron migration within the pit. The model within the pit includes flux equations for multiple species including iron in a unidirectional system and in a dilute solution and must satisfy an electro-neutrality relationship. Chemical equilibrium must also be maintained. The rate of iron diffusion from the pit bottom to the surrounding soil determines the growth rate of the pit. To close the loop between the "inner" and "outer" corrosion models, the cathodic reaction occurring at the UXO/soil interface is modeled. The pH in a liquid film at this interface provides a matching point to iterate between the two models. The cathodic reaction raises the pH at the interface by generating hydroxides. The pH is a function of the liquid film on the UXO surface. To model the hydroxide transport, the thickness of the liquid film must be known. In our model of UXO corrosion, this film thickness is the first occurrence of an empirical relationship. This film thickness is being correlated with rainfall and other climate data and soil properties.

During the talk, the theoretical basis for the model will be explained along with a description of the required input parameters. Example calculations validating the model with field data will be presented.

December, 2003, SERDP Annual Symposium, Washington, DC

Corrosion of Unexploded Ordnance

Bonnie Packer, PhD
U.S. Army Environmental Center
5179 Hoadley Road
Aberdeen Proving Ground, MD 21010
410-436-6846
bonnie.packer@us.army.mil

Michael Chendorain, Lloyd D. Stewart, PhD, PE, Jim Garber, PhD, Kathy Kneirim, PhD

Unexploded ordnance (UXO) lie buried at an estimated 1,500 sites encompassing 15 million acres. These items often contain explosive fill (e.g., RDX, TNT, etc.) posing an uncertain environmental risk. Results from this study estimate the corrosion rate of buried UXO and potential release of energetics into soil. The primary objective is to develop a database of measured UXO corrosion rates for a range of environmental conditions. A secondary objective is to develop a model of predictive correlations for the UXO corrosion rate as a function of site-specific soil properties and climatic conditions. The study includes soils and metal fragments from more than 150 UXO at over ten sites with samples ranging from the Civil War through WWII.

Soil samples were collected near the UXO and analyzed for chemical and physical properties including UXO energetics. Metal fragments from the UXO were collected during disposal and analyzed for corrosion parameters (e.g., pit depths and scale chemistry) and metallurgy. Using the maximum pit depth measured in each item, the change in total thickness, and metal exposure time, corrosion rates range from 0.08 to 7.5 mils per year (mpy) with an average of 1.3 ± 1.3 mpy. Assuming a constant corrosion rate, the average perforation time for ¼-inch thick steel (similar to a 60-mm mortar) is 187 years. However, the corrosion rate is not constant and depends on the soil moisture condition, solution chemistry, and scale formation. Hence, single measurements of corrosion predict unrealistic times to perforation.

The corrosion model developed with this study estimates corrosion as a function of time by calculating the flux rates of oxygen, iron, moisture, and salts to and away from the UXO surface. Initially, corrosion rates are high as pits form and grow. After precipitation of iron oxides, corrosion rates decrease drastically. The model predicts scale formation and the impact on diffusive fluxes to and from the metal surface, thereby producing a more accurate perforation time than assuming a constant corrosion rate. The theoretical basis for the model will be explained. Model results will be compared with field data.

Of the more than 50 different UXO potentially containing high explosive material, only three had indications of energetic movement into soil. All three were 60 mm rounds (shell thickness of 0.18 inches) and one had the appearance of a low-order detonation. Energetics from the other two items were detected below calculated calibration limits and the instrument detection limits.

Appendix B

RESULTS
AND
SUPPLEMENTAL INFORMATION

PRAXIS
ENVIRONMENTAL TECHNOLOGIES, INC.
1440 Rollins Road, Burlingame, California 94010
(650) 654-5488

Contents

Sampling Protocol for Soil and Scrap Metal Sampling Procedures for UXO Corrosion Study

Background and Objectives

The US Army would like to know if UXO are significant sources of chemicals (i.e., TNT, RDX, HMX) found in the environment at current and former military training ranges. Do the explosives remain entombed or do the metal containers corrode and release the material? If the container survives impact intact, how long before it corrodes and releases material? How does the corrosion rate vary with soil type? With this information, prioritization for clearance and selection of future training sites can include an environmental component. To answer these questions, up to 200 total UXO items will be sampled along with the surrounding soil at five to six formerly used ranges. The sample collection procedure for each of the study ranges is provided below.

Field Practices for Corrosion Study Sampling at Each Study Range

This study is concerned with the corrosion of UXO buried below the land surface, not items lying on the surface or those in aquatic environments. Optimally, UXO selected for the study will be located 6 to 24 inches below the soil surface. After the identification of a buried item suspected to be UXO, the field procedures described below will be followed if worker safety is not compromised. The procedure includes sampling the soil to the side and underneath a UXO item prior to disposal and scrap metal after blowing the item in place. After sampling up to 40 items, sampling for the corrosion study will cease at the site.

Field Procedure

Sample ID	Step	Task
	1	Uncover item
	2	Fill out logsheet (note extent of corrosion)
	3	Note depth below ground surface of nose and base
	4	Fill out item date on index card and take 2 pictures of item (1 with flash, one without).
STEPS 5 AND 6 ARE TO BE PERFORMED IF ITEM IS BELIEVED TO BE HE.		
-SC1, -SC2, -SC3	5	Carefully dig out soil to fill a brass sleeve (use sleeves with 1 cap prefastened). The soil should be collected from directly underneath item. Preferably where a possible leak may have occurred. Place second cap on sleeve. Label sample and note time on logsheet.
		Note: **Collect soil only under safe conditions**
-SC4, -SC5, -SC6	6	Excavate beneath item up to a maximum depth of 1 foot. Collect soil into capped brass sleeves. Place second cap on sleeve, label sleeve, and note time on logsheet.
		Note: **Collect soil only under safe conditions**
-SC8	7	Add three brass sleeves to soil corer. Use sand trap if necessary. Core until sample corer is flush with ground. Pull device out of ground, carefully remove sleeves, and preserve middle sleeve by capping both ends. Label sample –SC8 and note time on logsheet. Cap a second of the remaining sleeves and label as –SC7. Note in logsheet if soil cores could not be collected by this method (safety reasons, too much rock, etc.)
		Note: Corer should be only lightly tightened.
-SP1	8	Fill **TWO** large 250 ml sample cups with soil. Label cups and note time.
	9	Soil sampling is complete.
	10	Collect frag samples (minimum of 6 pieces, maximum of 10) or send inert item. Collect frag samples in 250 ml cups in double bagged in ziploc freezer bags. Label and note time.
	11	Sampling is complete.
	12	Once up to five samples have been collected fill out chain of custody forms and ship samples and equipment back using provided FedEx forms.

Start Time: Item Number: Date: Completed:

Confirmed type of item: Generalized Corrosion: none slight moderate heavy

Sheet 1 of 1

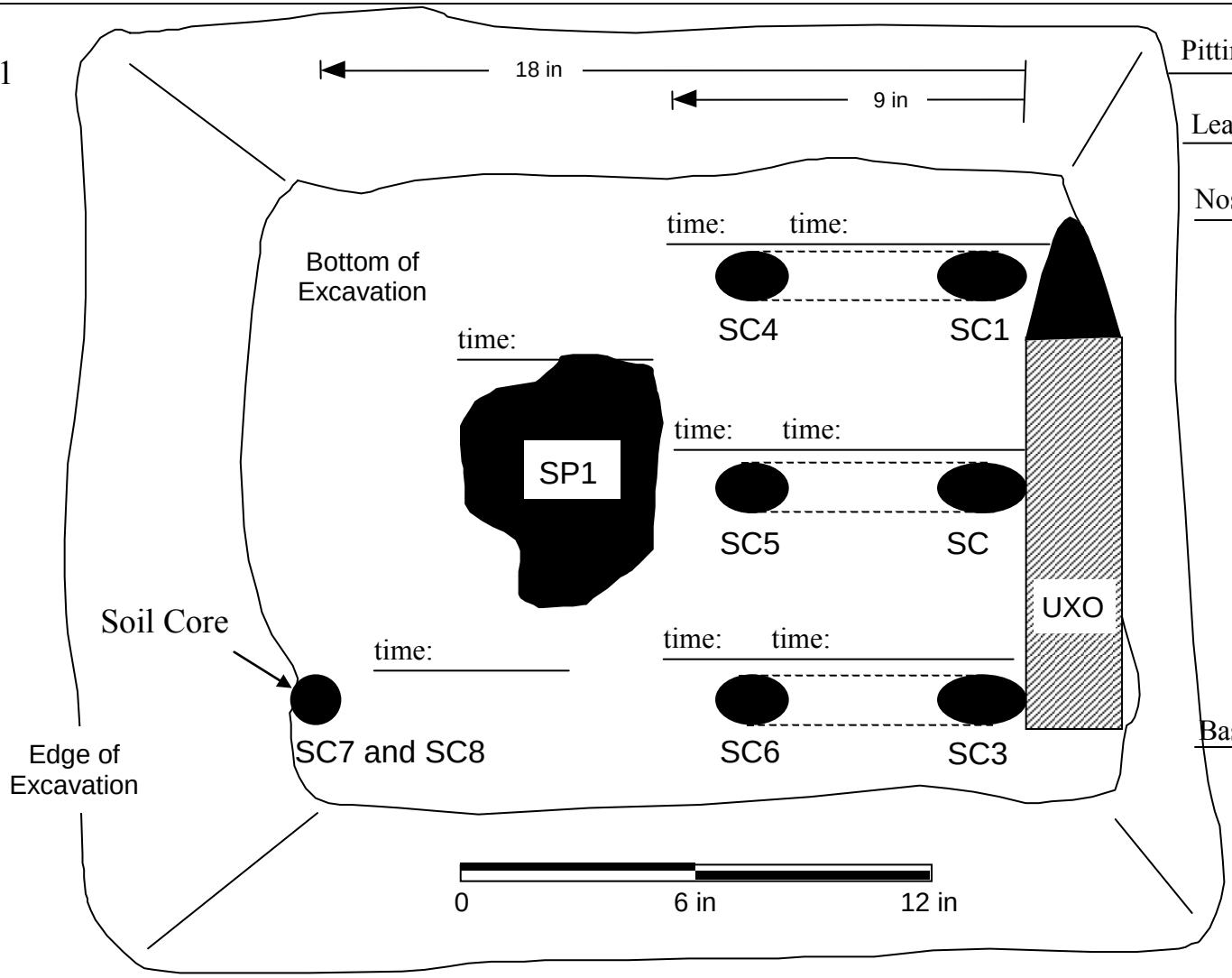

Pitting: n sl mod hvy

Leaks or cracks:

Nose depth:

-SC4, -SC5, and -SC6 to be collected 12 inches below -SC1, -SC2, -SC3

Base depth:

Additional Notes

Location of item:

Frag Collection Estimated Item Age:

Average Soil and Climate Properties

Site A

annual precipitation	42.8	± 25.3	in./year		
gravel	13.0	± 11.9	%		
sand	39.6	± 9.1	%		
silt	38.4	± 12.1	%		
clay	9.0	± 2.9	%		
initial resistivity	231941	± 150299	ohm-cm		
min. resistivity	8018	± 3734	ohm-cm		
carbonates	32.27	± 35.9	mg/kg		
organic acids	64	± 39	mg/kg		
chloride	81	± 34	mg/kg		
sulfate	70	± 58	mg/kg		
calcium	384	± 747	mg/kg		
mean	11.4	± 8.8	C		
moisture	19.3	± 6.8	%		
organic content	4.5	± 1.9	%		
bulk density		±	g/cm 3		
porosity	63.5	± 9.9	%		
particle density	2.66	± 0.10	%		
ORP	293	± 46	mV		
pH	5.30	± 1.02			
CEC	9.2	± 4.7	meq/100g		
iron	7	± 8	mg/kg		
magnesium	90	± 177	mg/kg		
manganese	3	± 2	mg/kg		
potassium	2697.	± 142	mg/kg		
sodium	37	± 11	mg/kg		
aluminum	174.9	± 121	mg/kg		

Notes:

Bulk density was not obtainable due to extremely shallow and gravelly soils.

Notes: Initial Resitivity data is skewed by data values greater than 1,000,000. Error reflects ± one standard deviation.

Site B

annual precipitation	31.9	± 28.4	in./year		
gravel	0.0	± 0.0	**%**		
sand	82.9	± 12.5	**%**		
silt	16.5	± 11.0	**%**		
clay	1.1	± 1.8	**%**		
initial resistivity	610571	± 488338	ohm-cm		
min. resistivity	22629	± 17741	ohm-cm		
carbonates	29.42	± 17.2	mg/kg		
organic acids	70	± 26	mg/kg		
chloride	134	± 82	mg/kg		
sulfate	67	± 104	mg/kg		
calcium	236	± 368	mg/kg		
mean	20.2	± 60.2	C		
moisture	7.5	± 7.2	**%**		
organic content	1.1	± 0.8	**%**		
bulk density	1.3	± 0.2	g/cm 3		
porosity	48.0	± 6.6	**%**		
particle density	2.58	± 0.06	**%**		
ORP	104	± 23	mV		
pH	6.08	± 0.48			
CEC	3.7	± 4.1	meq/100g		
iron	1	± 1	mg/kg		
magnesium	47	± 83	mg/kg		
manganese	7	± 12	mg/kg		
potassium	989.9	± 165	mg/kg		
sodium	74	± 74	mg/kg		
aluminum	13.99	± 14.7	mg/kg		

Notes: Initial Resitivity data is skewed by data values greater than 1,000,000. Error reflects ± one standard deviation.

Site C

annual precipitation	53.1	± 32.2	in./year		
gravel	0.0	± 0.0	**%**		
sand	64.4	± 10.0	**%**		
silt	28.3	± 8.7	**%**		
clay	7.3	± 2.6	**%**		
initial resistivity	851600	± 324406	ohm-cm		
min. resistivity	11420	± 5711	ohm-cm		
carbonates	20.58	± 16.8	mg/kg		
organic acids	113	± 125	mg/kg		
chloride	99	± 14	mg/kg		
sulfate	41	± 49	mg/kg		
calcium	208	± 320	mg/kg		
mean	16.8	± 68.2	C		
moisture	7.8	± 5.0	**%**		
organic content	2.9	± 1.4	**%**		
bulk density	1.3	± 0.3	g/cm 3		
porosity	50.0	± 12.7	**%**		
particle density	2.50	± 0.08	**%**		
ORP	192	± 48	mV		
pH	5.87	± 0.47			
CEC	1.3	± 0.9	meq/100g		
iron	2	± 2	mg/kg		
magnesium	28	± 40	mg/kg		
manganese	30	± 18	mg/kg		
potassium	38.04	± 19.1	mg/kg		
sodium	88	± 9	mg/kg		
aluminum	45.40	± 24.2	mg/kg		

Notes: Initial Resitivity data is skewed by data values greater than 1,000,000. Error reflects ± one standard deviation.

Site D

annual precipitation	16.2	± 16.5	in./year	**mean**	8.3	± 34.9	C
gravel	0.0	±	%	**moisture**	21.8	±	%
sand	88.4	±	%	**organic content**	5.0	±	%
silt	9.4	±	%	**bulk density**	1.4	±	g/cm 3
clay	2.1	±	%	**porosity**	45.5	±	%
				particle density	2.52	±	%
initial resistivity	45000	±	ohm-cm	**ORP**	177	±	mV
min. resistivity	970	±	ohm-cm	**pH**	7.80	±	
				CEC	17.0	±	meq/100g
carbonates	2353.	±	mg/kg	**iron**	2	±	mg/kg
organic acids	86	±	mg/kg	**magnesium**	72	±	mg/kg
chloride	94	±	mg/kg	**manganese**	0	±	mg/kg
sulfate	186	±	mg/kg	**potassium**	45.06	±	mg/kg
calcium	3650	±	mg/kg	**sodium**	1715	±	mg/kg
				aluminum	5.820	±	mg/kg

Notes: Initial Resitivity data is skewed by data values greater than 1,000,000. Error reflects ± one standard deviation.

Site E

annual precipitation	11.5	± 10.3	in./year		
gravel	25.6	± 13.0	**%**		
sand	54.3	± 11.7	**%**		
silt	16.0	± 6.9	**%**		
clay	4.0	± 2.5	**%**		
mean	6.4	± 21.8	C		
moisture	11.8	± 3.2	**%**		
organic content	3.1	± 2.8	**%**		
bulk density	1.6	± 0.1	g/cm 3		
porosity	39.8	± 5.1	**%**		
particle density		±	**%**		
initial resistivity	274545	± 195224	ohm-cm		
min. resistivity	2473	± 496	ohm-cm		
ORP	194	± 41	mV		
pH	5.92	± 0.43			
CEC	7.5	± 2.2	meq/100g		
carbonates	702.3	± 423.	mg/kg		
organic acids	116	± 26	mg/kg		
chloride	85	± 16	mg/kg		
sulfate	13	± 29	mg/kg		
calcium	2284	± 611	mg/kg		
iron	2	± 1	mg/kg		
magnesium	195	± 123	mg/kg		
manganese	2	± 1	mg/kg		
potassium	28.70	± 27.0	mg/kg		
sodium	82	± 12	mg/kg		
aluminum	6.201	± 1.42	mg/kg		

Notes: Initial Resitivity data is skewed by data values greater than 1,000,000. Error reflects ± one standard deviation.

Site F

annual precipitation	15.1 ± 13.3	in./year	**mean**	10.0 ± 9.0	C
gravel	0.0 ± 0.0	%	**moisture**	2.4 ± 1.3	%
sand	87.9 ± 4.0	%	**organic content**	1.3 ± 0.6	%
silt	10.4 ± 3.5	%	**bulk density**	1.4 ± 0.1	g/cm 3
clay	1.8 ± 0.5	%	**porosity**	44.5 ± 4.7	%
			particle density	2.57 ± 0.02	%
initial resistivity	605000 ± 360936	ohm-cm	**ORP**	136 ± 38	mV
min. resistivity	9530 ± 5434	ohm-cm	**pH**	6.38 ± 0.46	
			CEC	2.0 ± 0.7	meq/100g
carbonates	36.60 ± 20.4	mg/kg	**iron**	0 ± 0	mg/kg
organic acids	60 ± 21	mg/kg	**magnesium**	116 ± 90	mg/kg
chloride	108 ± 16	mg/kg	**manganese**	2 ± 1	mg/kg
sulfate	85 ± 32	mg/kg	**potassium**	0 ± 0	mg/kg
calcium	493 ± 185	mg/kg	**sodium**	69 ± 2	mg/kg
			aluminum	1.007 ± 0.21	mg/kg

Notes: Initial Resitivity data is skewed by data values greater than 1,000,000. Error reflects ± one standard deviation.

Site G

annual precipitation	55.8	± 31.6	in./year		
gravel	0.0	± 0.0	**%**		
sand	38.5	± 12.0	**%**		
silt	51.4	± 9.3	**%**		
clay	10.1	± 3.1	**%**		
initial resistivity	699300	± 405444	ohm-cm		
min. resistivity	13530	± 4112	ohm-cm		
carbonates	0	± 0	mg/kg		
organic acids	38	± 0	mg/kg		
chloride	90	± 23	mg/kg		
sulfate	67	± 63	mg/kg		
calcium	20	± 11	mg/kg		
mean	15.0	± 8.0	C		
moisture	23.6	± 10.8	**%**		
organic content	3.3	± 1.4	**%**		
bulk density	1.0	± 0.3	g/cm 3		
porosity	61.5	± 10.4	**%**		
particle density	2.58	± 0.04	**%**		
ORP	115	± 81	mV		
pH	4.72	± 0.40			
CEC	1.1	± 0.2	meq/100g		
iron	20	± 25	mg/kg		
magnesium	7	± 5	mg/kg		
manganese	2	± 4	mg/kg		
potassium	0.413	± 1.30	mg/kg		
sodium	65	± 6	mg/kg		
aluminum	192.0	± 47.0	mg/kg		

Notes: Initial Resitivity data is skewed by data values greater than 1,000,000. Error reflects ± one standard deviation.

Site H

annual precipitation	58.0	±	37.5	in./year	**mean**	19.0	± 7.0 C
gravel	0.3	±	0.7	**%**	**moisture**	15.2	± 4.5 **%**
sand	64.3	±	8.7	**%**	**organic content**	2.6	± 1.1 **%**
silt	27.9	±	7.2	**%**	**bulk density**	1.4	± 0.3 g/cm 3
clay	7.5	±	1.7	**%**	**porosity**	45.2	± 9.8 **%**
					particle density	2.61	± 0.05 **%**
initial resistivity	75000	±	30454	ohm-cm	**ORP**	308	± 46 mV
min. resistivity	8306	±	1352	ohm-cm	**pH**	5.24	± 0.36
					CEC	0.9	± 0.4 meq/100g
carbonates	17.16	±	26.6	mg/kg	**iron**	2	± 4 mg/kg
organic acids	47	±	17	mg/kg	**magnesium**	22	± 15 mg/kg
chloride	122	±	39	mg/kg	**manganese**	22	± 8 mg/kg
sulfate	80	±	67	mg/kg	**potassium**	37.77	± 80.8 mg/kg
calcium	170	±	68	mg/kg	**sodium**	20	± 20 mg/kg
					aluminum	36.60	± 40.3 mg/kg

Notes: Initial Resitivity data is skewed by data values greater than 1,000,000. Error reflects ± one standard deviation.

Site I

annual precipitation	42.8	± 25.8	in./year		
gravel	0.7	± 1.9	**%**		
sand	16.4	± 19.2	**%**		
silt	37.3	± 30.4	**%**		
clay	12.3	± 10.0	**%**		
initial resistivity	45667	± 47574	ohm-cm		
min. resistivity	13067	± 13076	ohm-cm		
carbonates	50.84	± 144.	mg/kg		
organic acids	58	± 63	mg/kg		
chloride	72	± 55	mg/kg		
sulfate	71	± 75	mg/kg		
calcium	256	± 556	mg/kg		
mean	14.4	± 8.9	C		
moisture	12.7	± 9.6	**%**		
organic content	2.1	± 1.6	**%**		
bulk density	0.8	± 0.6	g/cm 3		
porosity	34.5	± 26.0	**%**		
particle density	1.75	± 1.32	**%**		
ORP	195	± 150	mV		
pH	3.17	± 2.62			
CEC	1.3	± 1.5	meq/100g		
iron	1	± 2	mg/kg		
magnesium	18	± 16	mg/kg		
manganese	6	± 6	mg/kg		
potassium	0	± 0	mg/kg		
sodium	36	± 45	mg/kg		
aluminum	125.3	± 145.	mg/kg		

Notes: Initial Resitivity data is skewed by data values greater than 1,000,000. Error reflects ± one standard deviation.

Site J

annual precipitation	47.7	± 24.9	in./year		
gravel	15.9	± 17.0	**%**		
sand	40.2	± 12.6	**%**		
silt	33.2	± 11.6	**%**		
clay	13.2	± 6.0	**%**		
mean	10.7	± 9.5	C		
moisture	31.1	± 8.4	**%**		
organic content	11.3	± 3.3	**%**		
bulk density	0.8	± 0.2	g/cm 3		
porosity	67.7	± 6.9	**%**		
particle density	2.47	± 0.11	**%**		
initial resistivity	112038	± 141737	ohm-cm		
min. resistivity	17167	± 11994	ohm-cm		
ORP	281	± 30	mV		
pH	4.65	± 0.40			
CEC	1.5	± 1.3	meq/100g		
carbonates	22.88	± 57.5	mg/kg		
organic acids	36	± 5	mg/kg		
chloride	110	± 16	mg/kg		
sulfate	29	± 24	mg/kg		
calcium	286	± 427	mg/kg		
iron	5	± 12	mg/kg		
magnesium	16	± 15	mg/kg		
manganese	67	± 101	mg/kg		
potassium	1.793	± 4.28	mg/kg		
sodium	62	± 26	mg/kg		
aluminum	82.57	± 57.2	mg/kg		

Notes: Initial Resitivity data is skewed by data values greater than 1,000,000. Error reflects ± one standard deviation.

Site K

annual precipitation	8.2 ± 9.2	in./year	**mean**	12.3 ± 8.4	C
gravel	0.5 ± 0.7	**%**	**moisture**	3.1 ± 1.3	**%**
sand	83.3 ± 5.5	**%**	**organic content**	2.3 ± 0.6	**%**
silt	13.1 ± 4.8	**%**	**bulk density**	1.5 ± 0.1	g/cm 3
clay	3.1 ± 0.9	**%**	**porosity**	42.4 ± 3.3	**%**
			particle density	2.63 ± 0.03	**%**
initial resistivity	205732 ± 245904	ohm-cm	**ORP**	175 ± 10	mV
min. resistivity	5950 ± 1575	ohm-cm	**pH**	7.97 ± 0.15	
			CEC	8.3 ± 1.6	meq/100g
carbonates	1053. ± 332.	mg/kg	**iron**	0 ± 0	mg/kg
organic acids	80 ± 18	mg/kg	**magnesium**	111 ± 26	mg/kg
chloride	95 ± 13	mg/kg	**manganese**	0 ± 0	mg/kg
sulfate	5 ± 22	mg/kg	**potassium**	125.2 ± 58.5	mg/kg
calcium	2679 ± 536	mg/kg	**sodium**	186 ± 53	mg/kg
			aluminum	2.780 ± 0.42	mg/kg

Notes: Initial Resitivity data is skewed by data values greater than 1,000,000. Error reflects ± one standard deviation.

Site L

annual precipitation	32.4	± 23.5	in./year		
gravel	0.1	± 0.4	**%**	**mean**	6.6 ± 11.2 C
sand	90.7	± 5.4	**%**	**moisture**	5.2 ± 2.2 **%**
silt	6.1	± 4.4	**%**	**organic content**	2.1 ± 1.2 **%**
clay	3.0	± 1.2	**%**	**bulk density**	1.5 ± 0.2 g/cm 3
				porosity	42.9 ± 8.0 **%**
				particle density	2.60 ± 0.03 **%**
initial resistivity	547250	± 400951	ohm-cm	**ORP**	1502 ± 684 mV
min. resistivity	70831	± 15452	ohm-cm	**pH**	3.82 ± 0.53
				CEC	2.0 ± 0.6 meq/100g
carbonates	0	± 0	mg/kg	**iron**	0 ± 1 mg/kg
organic acids	57	± 45	mg/kg	**magnesium**	18 ± 11 mg/kg
chloride	107	± 12	mg/kg	**manganese**	16 ± 15 mg/kg
sulfate	39	± 23	mg/kg	**potassium**	373.3 ± 114. mg/kg
calcium	145	± 116	mg/kg	**sodium**	71 ± 19 mg/kg
				aluminum	52.41 ± 30.3 mg/kg

Notes: Initial Resitivity data is skewed by data values greater than 1,000,000. Error reflects ± one standard deviation.

Site Y

annual precipitation	34.8	± 22.8	in./year		
gravel	7.9	± 9.1	**%**		
sand	54.3	± 12.4	**%**		
silt	31.9	± 7.3	**%**		
clay	5.9	± 1.4	**%**		
initial resistivity	456740	± 471073	ohm-cm		
min. resistivity	880	± 425	ohm-cm		
carbonates	578.8	± 354.	mg/kg		
organic acids	124	± 40	mg/kg		
chloride	40	± 9	mg/kg		
sulfate	56	± 97	mg/kg		
calcium	2184	± 580	mg/kg		
mean	8.5	± 10.6	C		
moisture	8.5	± 3.1	**%**		
organic content	8.6	± 2.9	**%**		
bulk density	1.1	± 0.1	g/cm 3		
porosity	57.9	± 4.5	**%**		
particle density	2.56	± 0.06	**%**		
ORP	175	± 34	mV		
pH	6.69	± 0.19			
CEC	7.5	± 1.9	meq/100g		
iron	0	± 0	mg/kg		
magnesium	457	± 126	mg/kg		
manganese	19	± 16	mg/kg		
potassium	0	± 0	mg/kg		
sodium	40	± 76	mg/kg		
aluminum	2.651	± 0.54	mg/kg		

Notes: Initial Resitivity data is skewed by data values greater than 1,000,000. Error reflects ± one standard deviation.

Site Z

annual precipitation	45.4 ± 25.6	in./year	**mean**	10.3 ± 8.5	C
gravel	0.0 ± 0.0	%	**moisture**	22.5 ± 5.2	%
sand	49.0 ± 14.1	%	**organic content**	4.4 ± 2.2	%
silt	48.8 ± 13.5	%	**bulk density**	1.7 ± 0.3	g/cm 3
clay	1.9 ± 0.9	%	**porosity**	34.3 ± 6.4	%
			particle density	2.41 ± 0.29	%
initial resistivity	133810 ± 117590	ohm-cm	**ORP**	202 ± 172	mV
min. resistivity	8998 ± 4195	ohm-cm	**pH**	4.88 ± 0.32	
			CEC	7.4 ± 3.1	meq/100g
carbonates	1.917 ± 2.06	mg/kg	**iron**	103 ± 96	mg/kg
organic acids	89 ± 101	mg/kg	**magnesium**	7 ± 4	mg/kg
chloride	171 ± 46	mg/kg	**manganese**	1 ± 1	mg/kg
sulfate	10 ± 12	mg/kg	**potassium**	1527. ± 139.	mg/kg
calcium	6 ± 4	mg/kg	**sodium**	71 ± 4	mg/kg
			aluminum	121.6 ± 112.	mg/kg

Notes: Initial Resitivity data is skewed by data values greater than 1,000,000. Error reflects ± one standard deviation.

Corrosion Results

Site A — No. Sampled 17

maximum corrosion	1.771 mpy	141.2 years for 1/4 inch of metal
minimum corrosion	0.120 mpy	2083. years for 1/4 inch of metal
average corrosion rate	1.002 ± 0.453 mpy	249.4 years for 1/4 inch of metal
maximum pit depth	83 mils	**exposure period** 57 - 76 years
average pit depth	38 ± 21 mils	
Corrosion Model Minimum Perforation	5	years for 1/4 inch of metal
Corrosion Model Average Perforation	171 ± 193	years for 1/4 inch of metal

Site B — No. Sampled 7

maximum corrosion	1.603 mpy	156.0 years for 1/4 inch of metal
minimum corrosion	0.418 mpy	598.1 years for 1/4 inch of metal
average corrosion rate	0.990 ± 0.390 mpy	252.6 years for 1/4 inch of metal
maximum pit depth	52 mils	**exposure period** 55 - 60 years
average pit depth	30 ± 15 mils	
Corrosion Model Minimum Perforation	94	years for 1/4 inch of metal
Corrosion Model Average Perforation	539 ± 457	years for 1/4 inch of metal

Site C — No. Sampled 10

maximum corrosion	1.390 mpy	179.9 years for 1/4 inch of metal
minimum corrosion	0.140 mpy	1785. years for 1/4 inch of metal
average corrosion rate	0.714 ± 0.444 mpy	350.2 years for 1/4 inch of metal
maximum pit depth	49 mils	**exposure period** 52 - 84 years
average pit depth	27 ± 12 mils	
Corrosion Model Minimum Perforation	82	years for 1/4 inch of metal
Corrosion Model Average Perforation	553 ± 284	years for 1/4 inch of metal

Note: Appendix B2b represents output from the UXO Corrosion Study Database and includes standard deviations rather than confidence intervals.

Site D — No. Sampled 1

maximum corrosion	0.532 mpy	469.9 years for 1/4 inch of metal
minimum corrosion	0.532 mpy	469.9 years for 1/4 inch of metal
average corrosion rate	0.532 ± mpy	469.9 years for 1/4 inch of metal
maximum pit depth	20 mils	**exposure period** 34 - 42 years
average pit depth	20 ± mils	
Corrosion Model Minimum Perforation		years for 1/4 inch of metal
Corrosion Model Average Perforation		± years for 1/4 inch of metal

Site E — No. Sampled 5

maximum corrosion	1.202 mpy	208.0 years for 1/4 inch of metal
minimum corrosion	0.082 mpy	3048. years for 1/4 inch of metal
average corrosion rate	0.465 ± 0.449 mpy	538.1 years for 1/4 inch of metal
maximum pit depth	59 mils	**exposure period** 45 - 54 years
average pit depth	23 ± 22 mils	
Corrosion Model Minimum Perforation	142	years for 1/4 inch of metal
Corrosion Model Average Perforation	398 ± 221	years for 1/4 inch of metal

Site F — No. Sampled 5

maximum corrosion	0.837 mpy	298.7 years for 1/4 inch of metal
minimum corrosion	0.361 mpy	692.5 years for 1/4 inch of metal
average corrosion rate	0.582 ± 0.225 mpy	429.7 years for 1/4 inch of metal
maximum pit depth	33 mils	**exposure period** 40 - 49 years
average pit depth	20 ± 10 mils	
Corrosion Model Minimum Perforation	106	years for 1/4 inch of metal
Corrosion Model Average Perforation	760 ± 393	years for 1/4 inch of metal

Note: Appendix B2b represents output from the UXO Corrosion Study Database and includes standard deviations rather than confidence intervals.

Site G — No. Sampled 10

maximum corrosion	1.330 mpy	188.0 years for 1/4 inch of metal
minimum corrosion	0.190 mpy	1315. years for 1/4 inch of metal
average corrosion rate	0.586 ± 0.340 mpy	426.3 years for 1/4 inch of metal
maximum pit depth	43 mils	**exposure period** 56 - 61 years
average pit depth	23 ± 14 mils	
Corrosion Model Minimum Perforation	5	years for 1/4 inch of metal
Corrosion Model Average Perforation	84 ± 129	years for 1/4 inch of metal

Site H — No. Sampled 8

maximum corrosion	2.750 mpy	90.9 years for 1/4 inch of metal
minimum corrosion	0.470 mpy	531.9 years for 1/4 inch of metal
average corrosion rate	1.104 ± 0.751 mpy	226.5 years for 1/4 inch of metal
maximum pit depth	83 mils	**exposure period** 57 - 63 years
average pit depth	52 ± 23 mils	
Corrosion Model Minimum Perforation	49	years for 1/4 inch of metal
Corrosion Model Average Perforation	240 ± 140	years for 1/4 inch of metal

Site I — No. Sampled 9

maximum corrosion	1.660 mpy	150.6 years for 1/4 inch of metal
minimum corrosion	0.930 mpy	268.8 years for 1/4 inch of metal
average corrosion rate	1.358 ± 0.288 mpy	184.1 years for 1/4 inch of metal
maximum pit depth	88 mils	**exposure period** 54 - 73 years
average pit depth	65 ± 17 mils	
Corrosion Model Minimum Perforation	2	years for 1/4 inch of metal
Corrosion Model Average Perforation	8 ± 9	years for 1/4 inch of metal

Note: Appendix B2b represents output from the UXO Corrosion Study Database and includes standard deviations rather than confidence intervals.

Site J — No. Sampled 26

maximum corrosion	1.493 mpy	167.4 years for 1/4 inch of metal
minimum corrosion	0.192 mpy	1302. years for 1/4 inch of metal
average corrosion rate	0.848 ± 0.387 mpy	294.6 years for 1/4 inch of metal
maximum pit depth	95 mils	**exposure period** 85 - 143 years
average pit depth	48 ± 17 mils	
Corrosion Model Minimum Perforation	5	years for 1/4 inch of metal
Corrosion Model Average Perforation	31 ± 64	years for 1/4 inch of metal

Site K — No. Sampled 22

maximum corrosion	1.250 mpy	200.0 years for 1/4 inch of metal
minimum corrosion	0.372 mpy	672.0 years for 1/4 inch of metal
average corrosion rate	0.612 ± 0.215 mpy	408.3 years for 1/4 inch of metal
maximum pit depth	52 mils	**exposure period** 34 - 64 years
average pit depth	22 ± 10 mils	
Corrosion Model Minimum Perforation	0	years for 1/4 inch of metal
Corrosion Model Average Perforation	0 ± 0	years for 1/4 inch of metal

Site L — No. Sampled 32

maximum corrosion	1.308 mpy	191.1 years for 1/4 inch of metal
minimum corrosion	0.074 mpy	3378. years for 1/4 inch of metal
average corrosion rate	0.594 ± 0.355 mpy	420.7 years for 1/4 inch of metal
maximum pit depth	70 mils	**exposure period** 38 - 63 years
average pit depth	19 ± 13 mils	
Corrosion Model Minimum Perforation	0.05	years for 1/4 inch of metal
Corrosion Model Average Perforation	10 ± 15	years for 1/4 inch of metal

Note: Appendix B2b represents output from the UXO Corrosion Study Database and includes standard deviations rather than confidence intervals.

Site Y — No. Sampled 10

maximum corrosion	1.000 mpy	250.0 years for 1/4 inch of metal
minimum corrosion	0.360 mpy	694.4 years for 1/4 inch of metal
average corrosion rate	0.662 ± 0.209 mpy	377.9 years for 1/4 inch of metal
maximum pit depth	69 mils	**exposure period** 85 - 85 years
average pit depth	49 ± 14 mils	
Corrosion Model Minimum Perforation	76	years for 1/4 inch of metal
Corrosion Model Average Perforation	541 ± 320	years for 1/4 inch of metal

Site Z — No. Sampled 21

maximum corrosion	7.465 mpy	33.5 years for 1/4 inch of metal
minimum corrosion	0.771 mpy	324.3 years for 1/4 inch of metal
average corrosion rate	2.840 ± 1.551 mpy	88.0 years for 1/4 inch of metal
maximum pit depth	94 mils	**exposure period** 10 - 58 years
average pit depth	42 ± 17 mils	
Corrosion Model Minimum Perforation	3	years for 1/4 inch of metal
Corrosion Model Average Perforation	56 ± 46	years for 1/4 inch of metal

Total — No. Sampled 183

maximum corrosion	7.465 mpy	33.5 years for 1/4 inch of metal
minimum corrosion	0.074 mpy	3378. years for 1/4 inch of metal
average corrosion rate	1.054 ± 0.978 mpy	237.3 years for 1/4 inch of metal

Note: Appendix B2b represents output from the UXO Corrosion Study Database and includes standard deviations rather than confidence intervals.

Corrosion Results

Site A — No. Sampled 17

maximum corrosion	1.771 mpy	141.2 years for 1/4 inch of metal
minimum corrosion	0.120 mpy	2083. years for 1/4 inch of metal
average corrosion rate	1.002 ± 0.453 mpy	249.4 years for 1/4 inch of metal
maximum pit depth	83 mils	**exposure period** 57 - 76 years
average pit depth	38 ± 21 mils	
Corrosion Model Minimum Perforation	5	years for 1/4 inch of metal
Corrosion Model Average Perforation	171 ± 193	years for 1/4 inch of metal

Site B — No. Sampled 7

maximum corrosion	1.603 mpy	156.0 years for 1/4 inch of metal
minimum corrosion	0.418 mpy	598.1 years for 1/4 inch of metal
average corrosion rate	0.990 ± 0.390 mpy	252.6 years for 1/4 inch of metal
maximum pit depth	52 mils	**exposure period** 55 - 60 years
average pit depth	30 ± 15 mils	
Corrosion Model Minimum Perforation	94	years for 1/4 inch of metal
Corrosion Model Average Perforation	539 ± 457	years for 1/4 inch of metal

Site C — No. Sampled 10

maximum corrosion	1.390 mpy	179.9 years for 1/4 inch of metal
minimum corrosion	0.140 mpy	1785. years for 1/4 inch of metal
average corrosion rate	0.714 ± 0.444 mpy	350.2 years for 1/4 inch of metal
maximum pit depth	49 mils	**exposure period** 52 - 84 years
average pit depth	27 ± 12 mils	
Corrosion Model Minimum Perforation	82	years for 1/4 inch of metal
Corrosion Model Average Perforation	553 ± 284	years for 1/4 inch of metal

Note: Appendix B2b represents output from the UXO Corrosion Study Database and includes standard deviations rather than confidence intervals.

Site D — No. Sampled 1

maximum corrosion	0.532 mpy	469.9 years for 1/4 inch of metal
minimum corrosion	0.532 mpy	469.9 years for 1/4 inch of metal
average corrosion rate	0.532 ± mpy	469.9 years for 1/4 inch of metal
maximum pit depth	20 mils	**exposure period** 34 - 42 years
average pit depth	20 ± mils	
Corrosion Model Minimum Perforation		years for 1/4 inch of metal
Corrosion Model Average Perforation		± years for 1/4 inch of metal

Site E — No. Sampled 5

maximum corrosion	1.202 mpy	208.0 years for 1/4 inch of metal
minimum corrosion	0.082 mpy	3048. years for 1/4 inch of metal
average corrosion rate	0.465 ± 0.449 mpy	538.1 years for 1/4 inch of metal
maximum pit depth	59 mils	**exposure period** 45 - 54 years
average pit depth	23 ± 22 mils	
Corrosion Model Minimum Perforation	142	years for 1/4 inch of metal
Corrosion Model Average Perforation	398 ± 221	years for 1/4 inch of metal

Site F — No. Sampled 5

maximum corrosion	0.837 mpy	298.7 years for 1/4 inch of metal
minimum corrosion	0.361 mpy	692.5 years for 1/4 inch of metal
average corrosion rate	0.582 ± 0.225 mpy	429.7 years for 1/4 inch of metal
maximum pit depth	33 mils	**exposure period** 40 - 49 years
average pit depth	20 ± 10 mils	
Corrosion Model Minimum Perforation	106	years for 1/4 inch of metal
Corrosion Model Average Perforation	760 ± 393	years for 1/4 inch of metal

Note: Appendix B2b represents output from the UXO Corrosion Study Database and includes standard deviations rather than confidence intervals.

Site G — No. Sampled 10

maximum corrosion	1.330 mpy	188.0 years for 1/4 inch of metal
minimum corrosion	0.190 mpy	1315. years for 1/4 inch of metal
average corrosion rate	0.586 ± 0.340 mpy	426.3 years for 1/4 inch of metal
maximum pit depth	43 mils	**exposure period** 56 - 61 years
average pit depth	23 ± 14 mils	
Corrosion Model Minimum Perforation	5	years for 1/4 inch of metal
Corrosion Model Average Perforation	84 ± 129	years for 1/4 inch of metal

Site H — No. Sampled 8

maximum corrosion	2.750 mpy	90.9 years for 1/4 inch of metal
minimum corrosion	0.470 mpy	531.9 years for 1/4 inch of metal
average corrosion rate	1.104 ± 0.751 mpy	226.5 years for 1/4 inch of metal
maximum pit depth	83 mils	**exposure period** 57 - 63 years
average pit depth	52 ± 23 mils	
Corrosion Model Minimum Perforation	49	years for 1/4 inch of metal
Corrosion Model Average Perforation	240 ± 140	years for 1/4 inch of metal

Site I — No. Sampled 9

maximum corrosion	1.660 mpy	150.6 years for 1/4 inch of metal
minimum corrosion	0.930 mpy	268.8 years for 1/4 inch of metal
average corrosion rate	1.358 ± 0.288 mpy	184.1 years for 1/4 inch of metal
maximum pit depth	88 mils	**exposure period** 54 - 73 years
average pit depth	65 ± 17 mils	
Corrosion Model Minimum Perforation	2	years for 1/4 inch of metal
Corrosion Model Average Perforation	8 ± 9	years for 1/4 inch of metal

Note: Appendix B2b represents output from the UXO Corrosion Study Database and includes standard deviations rather than confidence intervals.

Site J — No. Sampled 26

maximum corrosion	1.493 mpy	167.4 years for 1/4 inch of metal
minimum corrosion	0.192 mpy	1302. years for 1/4 inch of metal
average corrosion rate	0.848 ± 0.387 mpy	294.6 years for 1/4 inch of metal
maximum pit depth	95 mils	**exposure period** 85 - 143 years
average pit depth	48 ± 17 mils	
Corrosion Model Minimum Perforation	5	years for 1/4 inch of metal
Corrosion Model Average Perforation	31 ± 64	years for 1/4 inch of metal

Site K — No. Sampled 22

maximum corrosion	1.250 mpy	200.0 years for 1/4 inch of metal
minimum corrosion	0.372 mpy	672.0 years for 1/4 inch of metal
average corrosion rate	0.612 ± 0.215 mpy	408.3 years for 1/4 inch of metal
maximum pit depth	52 mils	**exposure period** 34 - 64 years
average pit depth	22 ± 10 mils	
Corrosion Model Minimum Perforation	0	years for 1/4 inch of metal
Corrosion Model Average Perforation	0 ± 0	years for 1/4 inch of metal

Site L — No. Sampled 32

maximum corrosion	1.308 mpy	191.1 years for 1/4 inch of metal
minimum corrosion	0.074 mpy	3378. years for 1/4 inch of metal
average corrosion rate	0.594 ± 0.355 mpy	420.7 years for 1/4 inch of metal
maximum pit depth	70 mils	**exposure period** 38 - 63 years
average pit depth	19 ± 13 mils	
Corrosion Model Minimum Perforation	0.05	years for 1/4 inch of metal
Corrosion Model Average Perforation	10 ± 15	years for 1/4 inch of metal

Note: Appendix B2b represents output from the UXO Corrosion Study Database and includes standard deviations rather than confidence intervals.

Site Y — No. Sampled 10

maximum corrosion	1.000 mpy	250.0 years for 1/4 inch of metal
minimum corrosion	0.360 mpy	694.4 years for 1/4 inch of metal
average corrosion rate	0.662 ± 0.209 mpy	377.9 years for 1/4 inch of metal
maximum pit depth	69 mils	**exposure period** 85 - 85 years
average pit depth	49 ± 14 mils	
Corrosion Model Minimum Perforation	76	years for 1/4 inch of metal
Corrosion Model Average Perforation	541 ± 320	years for 1/4 inch of metal

Site Z — No. Sampled 21

maximum corrosion	7.465 mpy	33.5 years for 1/4 inch of metal
minimum corrosion	0.771 mpy	324.3 years for 1/4 inch of metal
average corrosion rate	2.840 ± 1.551 mpy	88.0 years for 1/4 inch of metal
maximum pit depth	94 mils	**exposure period** 10 - 58 years
average pit depth	42 ± 17 mils	
Corrosion Model Minimum Perforation	3	years for 1/4 inch of metal
Corrosion Model Average Perforation	56 ± 46	years for 1/4 inch of metal

Total — No. Sampled 183

maximum corrosion	7.465 mpy	33.5 years for 1/4 inch of metal
minimum corrosion	0.074 mpy	3378. years for 1/4 inch of metal
average corrosion rate	1.054 ± 0.978 mpy	237.3 years for 1/4 inch of metal

Note: Appendix B2b represents output from the UXO Corrosion Study Database and includes standard deviations rather than confidence intervals.

Appendix B3a: UXO Corrosion Study Results - Item Summaries

ID	UXO Item Information			Exposure Period	
	sample description	metallurgy	thickness (in)	min (yrs)	max (yrs)
A-01	60 mm - M49	Carbon Steel	0.183	57	60
A-02	60 mm - M49	Carbon Steel	0.183	57	60
A-03	60 mm - M49	Carbon Steel	0.183	57	60
A-04	60 mm - M49	Carbon Steel	0.183	57	60
A-05	37 mm - M54	Carbon Steel	0.25	57	60
A-06	60 mm - M49	Carbon Steel	0.183	57	60
A-07	3" stokes - MK1	Carbon Steel	0.18	57	76
A-08	60 mm - M49	Aluminum	0.183	57	60
A-11	3" stokes - MK1	Carbon Steel	0.18	57	76
A-12	3" stokes - MK1	Carbon Steel	0.18	57	76
A-14	81 mm - M43A1	Carbon Steel	0.185	57	60
A-15	3" stokes - MK1	Carbon Steel	0.18	57	76
A-16	60 mm - M49	Carbon Steel	0.183	57	60
A-17	3" stokes - MK1	Carbon Steel	0.18	57	76
A-18	3" stokes - MK1	Carbon Steel	0.18	57	76
A-19	81 mm - M43A1	Carbon Steel	0.185	57	60
A-20	81 mm - M43A1	Carbon Steel	0.185	57	60
B-01	anti-tank mine - M1	Carbon Steel	0.0625	55	60
B-02	105 mm - M51	Carbon Steel	0.414	55	60
B-03	4.2" mortar	Carbon Steel	0.214	55	60
B-04	105 mm - M51	Carbon Steel	0.414	55	60
B-05	4.2" mortar	Carbon Steel	0.214	55	60
B-06	anti-tank mine - M1B1	Carbon Steel	0.0625	55	60
B-07	105 mm - M51	Carbon Steel	0.414	55	60
C-01	60 mm - M49	Carbon Steel	0.183	52	61
C-02	anti-tank mine - M1	Carbon Steel	0.0625	52	61
C-03	landmine - M8	Carbon Steel	0.61	52	61
C-04	60 mm - M49	Carbon Steel	0.183	52	61
C-05	rifle grenade (smoke) - M22	Carbon Steel	0.043	52	77
C-06	anti-tank mine - M1B1	Carbon Steel	0.0625	52	61
C-07	2.36" rocket - M7	Carbon Steel	0.087	52	56
C-11	81 mm - M43A1	Carbon Steel	0.185	52	56
D-01	75 mm	Carbon Steel	0.142	34	42
E-01	155 mm	Carbon Steel	0.725	45	54
E-02	76 mm AP	Carbon Steel	0.555	45	54
E-05	105 mm - M51	Carbon Steel	0.414	45	54
E-09	point detonating fuze - M48A2	Carbon Steel, Brass, and Aluminum	n/a	45	54
E-11	76 mm	Carbon Steel	0.407	45	54
F-01	incendiary bomb - M69	carbon steel	0.05	40	49
F-02	incendiary bomb - M74	carbon steel	0.05	40	49
F-03	incendiary bomb - M69	carbon steel	0.05	40	49
F-04	incendiary bomb - M74	carbon steel	0.05	40	49
F-05	incendiary bomb - M74	carbon steel	0.05	40	49

ID	UXO Item Information			Exposure Period	
	sample description	metallurgy	thickness (in)	min (yrs)	max (yrs)
G-01	37 mm - M54	carbon steel	0.25	56	61
G-02	37 mm - M54	carbon steel	0.25	56	61
G-03	37 mm - M54	carbon steel	0.25	56	61
G-04	37 mm - M54	carbon steel	0.25	56	61
G-05	37 mm - M54	carbon steel	0.25	56	61
G-06	37 mm - M54	carbon steel	0.25	56	61
G-07	37 mm - M54	carbon steel	0.25	56	61
G-08	37 mm - M54	carbon steel	0.25	56	61
G-09	37 mm - M54	carbon steel	0.25	56	61
G-10	37 mm - M54	carbon steel	0.25	56	61
H-01	BDU-33	carbon steel	0.075	57	63
H-02	MK23 BDU	carbon steel	0.31	57	63
H-03	81 mm - M43A1	carbon steel	0.185	57	63
H-04	debris	carbon steel	0.03	57	63
H-05	37 mm - M54	carbon steel	0.25	57	63
H-06	2.36" rocket - M7	carbon steel	0.087	57	63
H-07	3" stokes mortar	carbon steel	0.18	57	63
H-08	anti-tank mine M1A1	carbon steel	0.0625	57	63
I-01	4.2" mortar	carbon steel	0.214	54	73
I-02	4.2" mortar	carbon steel	0.214	54	73
I-03	4.2" mortar	carbon steel	0.214	54	73
I-04	4.2" mortar	carbon steel	0.214	54	73
I-05	4.2" mortar	carbon steel	0.214	54	73
I-06	4.2" mortar	carbon steel	0.214	54	73
I-07	4.2" mortar	carbon steel	0.214	54	73
I-08	4.2" mortar	carbon steel	0.214	54	73
I-09	4.2" mortar	carbon steel	0.214	54	73
J-01	75 mm shrapnel round	carbon steel	0.381	85	89
J-02	75 mm shrapnel round	Carbon Steel	0.381	85	89
J-03	75 mm shrapnel round	Carbon Steel	0.381	85	89
J-04	75 mm shrapnel round		0.381	85	89
J-05	75 mm shrapnel round	Carbon Steel	0.381	85	89
J-06	75 mm shrapnel round		0.381	85	89
J-07	75 mm shrapnel round	Carbon Steel	0.381	85	89
J-08	75 mm shrapnel round	Carbon Steel	0.381	85	89
J-09	75 mm shrapnel round		0.381	85	89
J-10	75 mm shrapnel round		0.381	85	89
J-11	75 mm shrapnel round	Carbon Steel	0.381	85	89
J-12	75 mm shrapnel round	carbon steel	0.381	85	89
J-13	75 mm shrapnel round		0.381	85	89
J-14	75 mm shrapnel round		0.381	85	89
J-15	75 mm shrapnel round		0.381	85	89
J-20	civil war scrap	Carbon Steel	1.2	138	143
J-21	civil war scrap	Carbon Steel	2.3	138	143
J-23	civil war cannonball	Carbon Steel	2.5	138	143

ID	UXO Item Information			Exposure Period	
	sample description	metallurgy	thickness (in)	min (yrs)	max (yrs)
J-24	75 mm shrapnel round	Carbon Steel	0.381	85	89
J-25	4.7" shrapnel round	Carbon Steel	0.055	85	89
J-26	75 mm shrapnel round	Carbon Steel	0.381	85	89
K-01	MK76 BDU			34	43
K-02	OE scrap	Carbon Steel	0.06	44	53
K-03	M38	Carbon Steel	0.06	58	64
K-04	M38	Carbon Steel	0.06	58	64
K-05	M38	Carbon Steel	0.06	58	64
K-06	M38	Carbon Steel	0.06	58	64
K-07	M38	Carbon Steel	0.06	58	64
K-08	M38	Carbon Steel	0.06	58	64
K-09	M38	Carbon Steel	0.06	58	64
K-10	MK76 BDU	Carbon Steel		34	43
K-11	MK76 BDU	Carbon Steel		34	43
K-12	MK76 BDU	Carbon Steel		34	43
K-13	AN-M57 500 lb GP bomb	Carbon Steel		48	56
K-14	AN-M57 500 lb GP bomb	Carbon Steel		48	56
K-15	M38	Carbon Steel	0.06	58	64
K-16	M38	Carbon Steel	0.06	58	64
K-17	M38	Carbon Steel	0.06	58	64
K-18	M38	Carbon Steel	0.06	58	64
K-19	MK23 MOD1 BDU	Carbon Steel		46	51
K-20	M38	Carbon Steel	0.06	58	64
K-21	M38	Carbon Steel	0.06	58	64
K-22	M76 BDU			34	43
L-01	2.36" rocket	Carbon Steel	0.087	56	59
L-02	2.36" rocket	Carbon Steel	0.087	56	59
L-03	2.36" rocket	Carbon Steel	0.087	56	59
L-04	2.36" rocket	Carbon Steel	0.087	56	59
L-05	2.36" rocket	Carbon Steel	0.087	56	59
L-06	75 mm shrapnel round	Carbon Steel	0.381	38	44
L-07	37 mm	Carbon Steel	0.25	38	44
L-08	75 mm shrapnel round	Carbon Steel	0.381	38	44
L-09	37 mm	Carbon Steel	0.25	38	44
L-10	37 mm	Carbon Steel	0.25	38	44
L-11	75 mm shrapnel round	Carbon Steel	0.381	38	44
L-12	75 mm shrapnel round	Carbon Steel	0.381	38	44
L-13	75 mm shrapnel round	Carbon Steel	0.381	38	44
L-14	37 mm	Carbon Steel	0.25	38	44
L-15	37 mm	Carbon Steel	0.25	38	44
L-16	75 mm shrapnel round	Carbon Steel	0.381	38	44
L-17	75 mm shrapnel round	Carbon Steel	0.381	38	44
L-18	M9 rifle grenade (smoke)	Carbon Steel	0.067	38	44
L-19	M9 rifle grenade (smoke)	Carbon Steel	0.067	38	44
L-20	155 mm	Carbon Steel	0.725	38	44

ID	UXO Item Information			Exposure Period	
	sample description	metallurgy	thickness (in)	min (yrs)	max (yrs)
L-21	105 mm	Carbon Steel	0.414		
L-22	105 mm	Carbon Steel	0.414		
L-23	81 mm	Carbon Steel	0.185		
L-24	81 mm	Carbon Steel	0.185		
L-25	60 mm	Carbon Steel	0.183		
L-26	4.2" mortar	Carbon Steel	0.214		
L-27	75 mm shrapnel round	Carbon Steel	0.381	46	47
L-28	75 mm shrapnel round	Carbon Steel	0.381	57	63
L-31	37 mm	Carbon Steel	0.25	57	63
L-32	37 mm	Carbon Steel	0.25	57	63
Y-01	3" stokes mortar	carbon steel	0.18	85	85
Y-02	3" stokes mortar	carbon steel	0.18	85	85
Y-03	3" stokes mortar	carbon steel	0.18	85	85
Y-04	3" stokes mortar	carbon steel	0.18	85	85
Y-05	3" stokes mortar	carbon steel	0.18	85	85
Y-06	3" stokes mortar	carbon steel	0.18	85	85
Y-07	3" stokes mortar	carbon steel	0.18	85	85
Y-08	3" stokes mortar	carbon steel	0.18	85	85
Y-09	3" stokes mortar	carbon steel	0.18	85	85
Y-10	3" stokes mortar	carbon steel	0.18	85	85
Z-01	155 mm - nose cone	carbon steel		46	56
Z-02	155 mm - LIRT	carbon steel	0.725	47	58
Z-03	155 mm - LIRT	carbon steel	0.725	19	19
Z-04	155 mm - LIRT	carbon steel	0.725	10	17
Z-05	155 mm - LIRT	carbon steel	0.725	10	17
Z-06	155 mm - LIRT	carbon steel	0.725	11	11
Z-07	155 mm - LIRT	carbon steel	0.725	10	17
Z-08	155 mm - LIRT	carbon steel	0.725	10	17
Z-09	155 mm - LIRT	carbon steel	0.725	18	18
Z-10	155 mm - LIRT	carbon steel	0.725	10	17
Z-11	155 mm - LIRT	carbon steel	0.725	21	21
Z-12	155 mm - LIRT	carbon steel	0.725	16	16
Z-13	155 mm - LIRT	carbon steel	0.725	18	18
Z-14	155 mm - LIRT	carbon steel	0.725	11	11
Z-15	155 mm - LIRT	carbon steel	0.725	10	17
Z-16	155 mm - LIRT	carbon steel	0.725	10	17
Z-17	155 mm - LIRT	carbon steel	0.725	18	18
Z-18	155 mm - LIRT	carbon steel	0.725	11	11
Z-19	155 mm - LIRT	carbon steel	0.725	16	16
Z-20	155 mm - LIRT	carbon steel	0.725	10	17
Z-21	155 mm - LIRT	carbon steel	0.725	16	16

Appendix B3b: UXO Corrosion Study Results - Corrosion Results

ID	Corrosion Measurements						Corrosion Model Results	
	Pitting Corrosion Rate		General Corrosion Rate		Total Corrosion Rate		Time to Failure	Time to Failure for ¼ in. metal
	Min	Max	Min	Max	Min	Max		
	(mpy)	(mpy)	(mpy)	(mpy)	(mpy)	(mpy)	(years)	(years)
A-01	0.733	0.772	0.329	0.346	1.062	1.118	11	48
A-02	0.7	0.737	0.453	0.477	1.153	1.214	3	5
A-03	0.667	0.702	0.62	0.653	1.287	1.355	26	79
A-04	0.233	0.246	0.975	1.026	1.208	1.272	152	563
A-05	0.117	0.123	0	0	0.117	0.123	32	32
A-06	0.3	0.316	1.425	1.5	1.725	1.816	5	25
A-07	0.566	0.754	0	0	0.566	0.754	64	194
A-11	0.447	0.596	0	0	0.447	0.596	71	261
A-12	0.395	0.526	0	0	0.395	0.526	5	9
A-14	0.383	0.404	0.834	0.878	1.217	1.282	46	126
A-15	0.855	1.14	0.066	0.088	0.921	1.228	95	539
A-16	0.35	0.368	0.592	0.623	0.942	0.991	40	106
A-17	0.763	1.018	0	0	0.763	1.018	31	92
A-18	1.092	1.456	0.263	0.351	1.355	1.807	97	456
A-19	1.017	1.07	0.375	0.395	1.392	1.465	6	14
A-20	0.467	0.491	0	0	0.467	0.491	4	7
B-01	0.5	0.545	0.573	0.625	1.073	1.17	3	334
B-02	0.3	0.327	0.3	0.327	0.6	0.654	3348	1397
B-03	0.4	0.436	0	0	0.4	0.436	4	770
B-04	0.383	0.418	0.7	0.763	1.083	1.181	1734	692
B-05	0.833	0.909	0	0	0.833	0.909	71	140
B-06	0.25	0.273	0.854	0.932	1.104	1.205	2	94
B-07	0.867	0.945	0.667	0.728	1.534	1.673	1092	343
C-01	0.41	0.481	0.869	1.019	1.279	1.5	594	1008
C-02	0.689	0.808	0.238	0.279	0.927	1.087	6	653
C-03	0.803	0.942	0.098	0.115	0.901	1.057	2982	645
C-04	0.393	0.462	0.828	0.971	1.221	1.433	195	608
C-05	0.442	0.654	0.12	0.178	0.562	0.832	1	82
C-06	0.41	0.481	0	0	0.41	0.481	5	610
C-07	0.446	0.481	0	0	0.446	0.481	64	572
C-11	0.482	0.519	0	0	0.482	0.519	57	130
D-01	0.476	0.588	0	0	0.476	0.588	n/a[1]	n/a
E-01	1.093	1.311	0	0	1.093	1.311		
E-02	0.426	0.511	0	0	0.426	0.511		
E-05	0.074	0.089	0	0	0.074	0.089	1289	523
E-09	0.111	0.133	0	0	0.111	0.133		528
E-11	0.407	0.489	0	0	0.407	0.489	724	142
F-01	0.224	0.275	0.14	0.164	0.364	0.439	5	904
F-02	0.327	0.4	0.128	0.149	0.455	0.549	1	1127
F-03	0.571	0.7	0.158	0.185	0.729	0.885	6	940
F-04	0.245	0.3	0.081	0.095	0.326	0.395	2	106

ID	Corrosion Measurements						Corrosion Model Results	
	Pitting Corrosion Rate		General Corrosion Rate		Total Corrosion Rate		Time to Failure	Time to Failure for ¼ in. metal
	Min	Max	Min	Max	Min	Max		
	(mpy)	(mpy)	(mpy)	(mpy)	(mpy)	(mpy)	(years)	(years)
F-05	0.673	0.825	0.081	0.095	0.754	0.92	4	723
G-01	0.18	0.196	0.002	0.002	0.182	0.198	5	5
G-02	0.328	0.357	0.106	0.106	0.434	0.463	24	24
G-03	0.639	0.696	0.055	0.055	0.694	0.751	6	6
G-04	0.18	0.196	0.092	0.1	0.272	0.296	310	310
G-05	0.705	0.768	0.145	0.158	0.85	0.926	19	19
G-06	0.148	0.161	0.269	0.293	0.417	0.454	21	21
G-07	0.656	0.714	0.618	0.673	1.274	1.387	339	339
G-08	0.492	0.536	0.067	0.073	0.559	0.609	28	28
G-09	0.115	0.125	0.533	0.581	0.648	0.706	75	75
G-10	0.262	0.286	0.029	0.031	0.291	0.317	11	11
H-01	0.381	0.421	0.063	0.071	0.444	0.492	200	200
H-02	1.317	1.456	0	0	1.317	1.456	169	82
H-03	0.857	0.947	0.2095	0.232	1.067	1.179	69	223
H-04	0.476	0.526	0	0	0	0	1	132
H-05	1.286	1.421	1.333	1.474	2.619	2.895	49	49
H-06	1.032	1.14	0	0	1.032	1.14	7	466
H-07	0.841	0.9298	0.162	0.179	1.003	1.109	49	135
H-08	0.48	0.48	0	0	0.48	0.48	3	342
I-01	1.041	1.407	0.2	0.27	1.24	1.68	9	27
I-02	1.205	1.63	0.2	0.27	1.41	1.9	2	3
I-03	0.658	0.889	0.28	0.38	0.94	1.27	4	6
I-04	0.89	1.204	0.48	0.65	1.37	1.85	5	7
I-05	0.521	0.704	0.35	0.47	0.87	1.07	4	5
I-06	1	1.35	0.41	0.56	1.41	1.91	2	2
I-07	1.014	1.37	0.24	0.32	1.25	1.69		
I-08	0.671	0.907	0.12	0.16	0.79	1.07		
I-09	1	1.352	0.16	0.21	1.16	1.56		
J-01	0.44	0.46	0.557	0.583	0.995	1.042	52	8
J-02	0.66	0.69	0.616	0.645	1.279	1.339	32	5
J-03	0.61	0.64	0.508	0.532	1.115	1.168	32	5
J-05	0.39	0.41	0.557	0.583	0.95	0.995	51	9
J-07	0.44	0.46	0.44	0.461	0.878	0.919	59	10
J-08	0.42	0.44	0.655	0.686	1.071	1.121	73	13
J-11	0.62	0.65	0.655	0.686	1.273	1.333	47	7
J-12	0.4	0.42	0.665	0.696	1.069	1.12		
J-20	0.5	0.52	0.963	0.998	1.466	1.519		
J-21	0.31	0.33	0	0	0.315	0.326		
J-23	0.44	0.46	0	0	0.441	0.457		
J-24	0.35	0.36	0.518	0.542	0.866	0.907	314	45
J-25	0.63	0.66	0.078	0.082	0.707	0.741	0.49	12
J-26	0.44	0.46	0.381	0.399	0.819	0.858	83	18
K-02	0.25	0.3	0.24	0.28	1.37	1.64	n/a	n/a

ID	Corrosion Measurements						Corrosion Model Results	
	Pitting Corrosion Rate		General Corrosion Rate		Total Corrosion Rate		Time to Failure	Time to Failure for ¼ in. metal
	Min	Max	Min	Max	Min	Max		
	(mpy)	(mpy)	(mpy)	(mpy)	(mpy)	(mpy)	(years)	(years)
K-03	0.13	0.14	0.229	0.252	0.354	0.39	n/a	n/a
K-04	0.31	0.34	0.286	0.316	0.598	0.66	n/a	n/a
K-05	0.3	0.33	0.105	0.116	0.402	0.443	n/a	n/a
K-06	0.39	0.43	0.143	0.158	0.534	0.589	n/a	n/a
K-07	0.23	0.26	0.276	0.305	0.511	0.564	n/a	n/a
K-08	0.36	0.4	0.219	0.242	0.579	0.638	n/a	n/a
K-09	0.3	0.33	0.257	0.284	0.554	0.612	n/a	n/a
K-15	0.39	0.43	0.057	0.063	0.448	0.494	n/a	n/a
K-16	0.27	0.29	0.238	0.263	0.504	0.556	n/a	n/a
K-17	0.36	0.4	0.21	0.231	0.569	0.628	n/a	n/a
K-18	0.48	0.53	0.067	0.074	0.551	0.608	n/a	n/a
K-20	0.33	0.36	0.219	0.242	0.547	0.604	n/a	n/a
K-21	0.81	0.9	0	0	0.813	0.897	n/a	n/a
L-01	0.237	0.25	0.136	0.144	0.374	0.394	1	7
L-02	0.576	0.607	0.117	0.123	0.693	0.73	0.48	3
L-03	0.525	0.554	0.088	0.092	0.613	0.646	0.5	4
L-04	1.186	1.25	0.088	0.092	1.274	1.342	1	4
L-05	0.492	0.518	0.097	0.103	0.589	0.621	0.48	3
L-06	0.705	0.816	0.27	0.313	0.975	1.129	7	3
L-07	0.318	0.368	0.047	0.054	0.365	0.422	4	4
L-08	0.659	0.763	0.363	0.421	1.023	1.184	0.12	0.05
L-09	0.136	0.158	0	0	0.136	0.158	4	4
L-10	0.205	0.237	0	0	0.205	0.237	5	5
L-11	0.727	0.842	0.41	0.475	1.137	1.317	26	4
L-12	0.432	0.5	0.121	0.14	0.553	0.64	11	5
L-13	0.341	0.395	0.457	0.529	0.798	0.923	6	3
L-14	0.136	0.158	0	0	0.136	0.158	5	5
L-15	0.068	0.079	0	0	0.068	0.079	4	4
L-16	0.409	0.474	0.205	0.237	0.614	0.711	7	3
L-17	0.318	0.368	0.205	0.237	0.523	0.606	48	8
L-18	0.045	0.053	0.224	0.259	0.269	0.312		
L-19	0.568	0.658	0.168	0.194	0.736	0.852		
L-20	0.455	0.526	0.522	0.604	0.976	1.131	91	3
L-27	0.383	0.391	0.208	0.212	0.591	0.604	3	1
L-28	0.254	0.281	0.152	0.168	0.406	0.449	7	7
L-31	0.429	0.474	0.029	0.032	0.457	0.505	2	2
L-32	0.063	0.07	0.029	0.032	0.092	0.102	3	3
Y-01	0.64	0.64	0.06	0.06	0.7	0.7	205	681
Y-02	0.53	0.53	0.1	0.1	0.63	0.63	254	725
Y-03	0.73	0.73	0.06	0.06	0.79	0.79	53	142
Y-04	0.45	0.45	0.07	0.07	0.52	0.52	25	87
Y-05	0.76	0.76	0.17	0.17	0.93	0.93	101	509
Y-06	0.81	0.81	0.19	0.19	1	1	344	768

ID	Corrosion Measurements						Corrosion Model Results	
	Pitting Corrosion Rate		General Corrosion Rate		Total Corrosion Rate		Time to Failure	Time to Failure for ¼ in. metal
	Min	Max	Min	Max	Min	Max		
	(mpy)	(mpy)	(mpy)	(mpy)	(mpy)	(mpy)	(years)	(years)
Y-07	0.36	0.36	0	0	0.36	0.36	566	911
Y-08	0.435	0.435	0.08	0.08	0.515	0.515	346	808
Y-09	0.38	0.38	0.06	0.06	0.44	0.44	272	706
Y-10	0.65	0.65	0.08	0.08	0.73	0.73	0.29	76
Z-01	0.911	1.109			0.911	1.109		3
Z-02	0.69	0.851			0.69	0.851	1334	65
Z-03	3.316	3.316			3.316	3.316	1267	61
Z-04	5.529	9.4			5.529	9.4	721	14
Z-05	2.118	3.6			2.118	3.6	496	6
Z-06	2.364	2.364			2.364	2.364	636	11
Z-07	2.588	4.4			2.588	4.4	1184	56
Z-08	2.529	4.3			2.529	4.3	720	30
Z-09	1.444	1.444			1.444	1.444	1400	68
Z-10	1.706	2.9			1.706	2.9	2189	176
Z-11	2.143	2.143			2.143	2.143	1453	75
Z-12	3.875	3.875			3.875	3.875	1628	86
Z-13	2.5	2.5			2.5	2.5	1557	81
Z-14	5.091	5.091			5.091	5.091	1233	57
Z-15	2.059	3.5			2.059	3.5	600	13
Z-16	1.941	3.3			1.941	3.3	1094	54
Z-17	1.389	1.389			1.389	1.389	738	32
Z-18	4.636	4.636			4.636	4.636	2089	151
Z-19	1.375	1.375			1.375	1.375	1253	56
Z-20	2.294	3.9			2.294	3.9	145	7
Z-21	1.688	1.688			1.688	1.688	1694	87

[1] n/a - Model not valid for calcareous soils

Appendix B3c: UXO Corrosion Study Results - Climate Data

ID	Annual Precipitation Rate		Annual Mean Air Temperature	
	Average	Standard Deviation	Average	Standard Deviation
	(in./yr.)	(in./yr.)	(^{o}C)	(^{o}C)
A-01	42.8	25.3	11.4	8.8
A-02	42.8	25.3	11.4	8.8
A-03	42.8	25.3	11.4	8.8
A-04	42.8	25.3	11.4	8.8
A-05	42.8	25.3	11.4	8.8
A-06	42.8	25.3	11.4	8.8
A-07	42.8	25.3	11.4	8.8
A-08	42.8	25.3	11.4	8.8
A-11	42.8	25.3	11.4	8.8
A-12	42.8	25.3	11.4	8.8
A-14	42.8	25.3	11.4	8.8
A-15	42.8	25.3	11.4	8.8
A-16	42.8	25.3	11.4	8.8
A-17	42.8	25.3	11.4	8.8
A-18	42.8	25.3	11.4	8.8
A-19	42.8	25.3	11.4	8.8
A-20	42.8	25.3	11.4	8.8
B-01	31.9	28.4	20.2	60.2
B-02	31.9	28.4	20.2	60.2
B-03	31.9	28.4	20.2	60.2
B-04	31.9	28.4	20.2	60.2
B-05	31.9	28.4	20.2	60.2
B-06	31.9	28.4	20.2	60.2
B-07	31.9	28.4	20.2	60.2
C-01	53.1	32.2	16.8	68.2
C-02	53.1	32.2	16.8	68.2
C-03	53.1	32.2	16.8	68.2
C-04	53.1	32.2	16.8	68.2
C-05	53.1	32.2	16.8	68.2
C-06	53.1	32.2	16.8	68.2
C-07	53.1	32.2	16.8	68.2
C-11	53.1	32.2	16.8	68.2
D-01	16.2	16.5	8.3	34.9
E-01	11.5	10.3	6.4	21.8
E-02	11.5	10.3	6.4	21.8
E-05	11.5	10.3	6.4	21.8
E-09	11.5	10.3	6.4	21.8
E-11	11.5	10.3	6.4	21.8
F-01	15.1	13.3	10	9
F-02	15.1	13.3	10	9
F-03	15.1	13.3	10	9
F-04	15.1	13.3	10	9

ID	Annual Precipitation Rate		Annual Mean Air Temperature	
	Average	Standard Deviation	Average	Standard Deviation
	(in./yr.)	(in./yr.)	(^{o}C)	(^{o}C)
F-05	15.1	13.3	10	9
G-01	55.8	31.6	15	8
G-02	55.8	31.6	15	8
G-03	55.8	31.6	15	8
G-04	55.8	31.6	15	8
G-05	55.8	31.6	15	8
G-06	55.8	31.6	15	8
G-07	55.8	31.6	15	8
G-08	55.8	31.6	15	8
G-09	55.8	31.6	15	8
G-10	55.8	31.6	15	8
H-01	58	37.5	19	7
H-02	58	37.5	19	7
H-03	58	37.5	19	7
H-04	58	37.5	19	7
H-05	58	37.5	19	7
H-06	58	37.5	19	7
H-07	58	37.5	19	7
H-08	58	37.5	19	7
I-01	42.8	25.8	14.4	8.9
I-02	42.8	25.8	14.4	8.9
I-03	42.8	25.8	14.4	8.9
I-04	42.8	25.8	14.4	8.9
I-05	42.8	25.8	14.4	8.9
I-06	42.8	25.8	14.4	8.9
J-01	47.7	24.9	10.7	9.5
J-02	47.7	24.9	10.7	9.5
J-03	47.7	24.9	10.7	9.5
J-04	47.7	24.9	10.7	9.5
J-05	47.7	24.9	10.7	9.5
J-06	47.7	24.9	10.7	9.5
J-07	47.7	24.9	10.7	9.5
J-08	47.7	24.9	10.7	9.5
J-09	47.7	24.9	10.7	9.5
J-10	47.7	24.9	10.7	9.5
J-11	47.7	24.9	10.7	9.5
J-12	47.7	24.9	10.7	9.5
J-13	47.7	24.9	10.7	9.5
J-14	47.7	24.9	10.7	9.5
J-15	47.7	24.9	10.7	9.5
J-26	47.7	24.9	10.7	9.5
K-01	8.2	9.2	12.3	8.4
K-02	8.2	9.2	12.3	8.4

ID	Annual Precipitation Rate		Annual Mean Air Temperature	
	Average	Standard Deviation	Average	Standard Deviation
	(in./yr.)	(in./yr.)	(^{o}C)	(^{o}C)
K-03	8.2	9.2	12.3	8.4
K-04	8.2	9.2	12.3	8.4
K-05	8.2	9.2	12.3	8.4
K-06	8.2	9.2	12.3	8.4
K-07	8.2	9.2	12.3	8.4
K-08	8.2	9.2	12.3	8.4
K-09	8.2	9.2	12.3	8.4
K-10	8.2	9.2	12.3	8.4
K-11	8.2	9.2	12.3	8.4
K-12	8.2	9.2	12.3	8.4
K-13	8.2	9.2	12.3	8.4
K-14	8.2	9.2	12.3	8.4
K-15	8.2	9.2	12.3	8.4
K-16	8.2	9.2	12.3	8.4
K-17	8.2	9.2	12.3	8.4
K-18	8.2	9.2	12.3	8.4
K-19	8.2	9.2	12.3	8.4
K-20	8.2	9.2	12.3	8.4
K-21	8.2	9.2	12.3	8.4
K-22	8.2	9.2	12.3	8.4
L-01	32.4	23.5	6.6	11.2
L-02	32.4	23.5	6.6	11.2
L-03	32.4	23.5	6.6	11.2
L-04	32.4	23.5	6.6	11.2
L-05	32.4	23.5	6.6	11.2
L-06	32.4	23.5	6.6	11.2
L-07	32.4	23.5	6.6	11.2
L-08	32.4	23.5	6.6	11.2
L-09	32.4	23.5	6.6	11.2
L-10	32.4	23.5	6.6	11.2
L-11	32.4	23.5	6.6	11.2
L-12	32.4	23.5	6.6	11.2
L-13	32.4	23.5	6.6	11.2
L-14	32.4	23.5	6.6	11.2
L-15	32.4	23.5	6.6	11.2
L-16	32.4	23.5	6.6	11.2
L-17	32.4	23.5	6.6	11.2
L-18	32.4	23.5	6.6	11.2
L-19	32.4	23.5	6.6	11.2
L-20	32.4	23.5	6.6	11.2
L-21	32.4	23.5	6.6	11.2
L-22	32.4	23.5	6.6	11.2
L-23	32.4	23.5	6.6	11.2

ID	Annual Precipitation Rate		Annual Mean Air Temperature	
	Average	Standard Deviation	Average	Standard Deviation
	(in./yr.)	(in./yr.)	(^{o}C)	(^{o}C)
L-24	32.4	23.5	6.6	11.2
L-25	32.4	23.5	6.6	11.2
L-26	32.4	23.5	6.6	11.2
L-27	32.4	23.5	6.6	11.2
L-28	32.4	23.5	6.6	11.2
L-31	32.4	23.5	6.6	11.2
L-32	32.4	23.5	6.6	11.2
Y-01	34.8	22.8	8.49	10.58
Y-02	34.8	22.8	8.49	10.58
Y-03	34.8	22.8	8.49	10.58
Y-04	34.8	22.8	8.49	10.58
Y-05	34.8	22.8	8.49	10.58
Y-06	34.8	22.8	8.49	10.58
Y-07	34.8	22.8	8.49	10.58
Y-08	34.8	22.8	8.49	10.58
Y-09	34.8	22.8	8.49	10.58
Y-10	34.8	22.8	8.49	10.58
Z-01	45.4	25.6	10.3	8.5
Z-02	45.4	25.6	10.3	8.5
Z-03	45.4	25.6	10.3	8.5
Z-04	45.4	25.6	10.3	8.5
Z-05	45.4	25.6	10.3	8.5
Z-06	45.4	25.6	10.3	8.5
Z-07	45.4	25.6	10.3	8.5
Z-08	45.4	25.6	10.3	8.5
Z-09	45.4	25.6	10.3	8.5
Z-10	45.4	25.6	10.3	8.5
Z-11	45.4	25.6	10.3	8.5
Z-12	45.4	25.6	10.3	8.5
Z-13	45.4	25.6	10.3	8.5
Z-14	45.4	25.6	10.3	8.5
Z-15	45.4	25.6	10.3	8.5
Z-16	45.4	25.6	10.3	8.5
Z-17	45.4	25.6	10.3	8.5
Z-18	45.4	25.6	10.3	8.5
Z-19	45.4	25.6	10.3	8.5
Z-20	45.4	25.6	10.3	8.5
Z-21	45.4	25.6	10.3	8.5

Appendix B3d: UXO Corrosion Study Results - Soil Chemical Data

ID	CEC	HCO_3^-	CO_3^{2-}	Cl^-	Organic Acids	SO_4	Al^{3+}	Ca^{2+}	Fe^{2+}, Fe^{3+}	Mg^{2+}	Mn	K^+	Na^+
	(meq/100g)	(mg/kg soil)	(mg/kg soil)	(mg/kg soil)	(mg/kg soil)	(mg/kg soil)	(mg/kg soil)	(mg/kg soil)	(mg/kg soil)	(mg/kg soil)	(mg/kg soil)	(mg/kg soil)	(mg/kg soil)
A-01	1.91	0	0	103.5	75.06	120	264.72	12.96	5.16	5.52	2.88	313.2	16.8
A-02	3.27	0	0	90	37.53	0	381.36	24.84	31.9	9.78	1.26	642.6	25.2
A-03	5.05	22.88	0	103.5	37.53	60	213	9	3.12	4.26	4.02	1605	27
A-04	4.5	91.53	0	69	150.12	138	187.74	19.56	0.48	3.96	2.16	1408.2	31.8
A-05	7.44	45.765	0	60	75.06	12	216.06	13.02	3.06	4.38	5.16	2520.6	31.8
A-06	6.58	0	0	103.5	75.06	114	199.86	11.94	1.44	2.88	1.14	2217	28.2
A-07	16.35	114.4	0	17.25	12.51	16	1.62	150.55	0	78.12	0.66	5320.2	38.4
A-08	8.49	22.9	0	69	37.53	102	224.5	15.36	10	4.8	5.4	2911.2	36.6
A-11	7.2	22.9	0	69	37.53	102	224.5	15.36	10	4.8	5.4	2911.2	36.6
A-12	16.89	15.26	0	11.5	25.02	3	5.76	449.34	3	50.64	0.18	5999.4	45
A-14	5.66	0	0	91.8	75.06	24	142.2	10.86	13.2	3.96	0.6	1933.2	34.2
A-15	13.46	75.77	0	138	75.06	168	13.98	1793.9	0	541.7	4.2	2518.2	61.2
A-16	10.69	22.9	0	69	37.53	102	224.5	15.36	10	4.8	5.4	2911.2	36.6
A-17	15.56	68.65	0	90	37.53	102	4.62	2291.2	0	489.2	2.28	2974.2	48.6
A-18	14.26	45.77	0	138	150.12	132	35.82	1657.4	10.5	315.4	6.36	3312.6	51.6
A-19	9.27	0	0	69	75.06	0	338.88	20.82	9.66	5.1	0.6	3031.2	44.4
A-20	9.85	0	0	90	75.06	0	294.42	15.24	9.72	5.22	2.1	3330.6	40.8
B-01	9.29	22.89	0	90	37.53	0	31.08	41.1	1.2	6.42	1.26	3454.2	45
B-02	9.14	22.89	0	69	75.06	0	11.58	91.86	0	13.2	10.56	3367.2	47.4
B-03	0.13	45.77	0	90	37.53	6	7.5	27	0.06	5.4	0.6	0	1.8
B-04	0.19	45.77	0	90	75.06	12	2.76	47.64	0	2.64	0.36	0	12.6
B-05	0.5	22.89	0	120	112.59	12	6.06	61.98	2.46	4.38	0.84	21.78	56.4
B-06	2.09	0	0	300	75.06	222	0.66	352.02	0	69.12	2.88	38.88	189.6
B-07	4.46	45.77	0	180	75.06	216	38.32	1029.5	0.84	226.9	32.22	47.76	168
C-01	1.41	0	0	120	112.62	0	42.84	264.06	1.8	21.66	42	38.46	92.4
C-02	0.87	22.86	0	90	37.56	0	55.02	57.72	0.06	12.24	20.1	48.38	79.8
C-03	0.94	22.86	0	90	37.56	78	45.6	72.18	0	13.44	27.84	48.18	94.2
C-04	0.69	0	0	90	112.62	78	40.38	24.6	4.02	5.22	3.66	51.84	75.6
C-05	1.22	45.78	0	120	75.06	0	46.32	147.78	0	24.36	29.46	53.76	102.6
C-06	1.25	22.86	0	90	37.56	0	49.32	170.88	0	18.3	29.34	54.96	96.6
C-07	3.8	22.86	0	90	450.36	0	1.98	1093.5	0	141.4	65.1	48.72	82.8
C-11	0.81	0	0	120	150.12	54	80.4	41.64	1.74	10.86	8.7	14.76	74.4
D-01	17	2353	0	93.6	85.74	186	5.82	3649.7	1.56	71.58	0.3	45.06	1714.8
E-01	7.45	755.1	0	90	112.62	0	7.68	2624.5	2.16	87.96	1.08	21.06	104.4
E-02	13.04	709.38	0	90	112.62	0	6	2373.6	1.14	103.1	1.68	0	64.8
E-05	4.88	137.28	0	78.24	75.06	48	7.8	1262.8	2.7	291.4	2.34	56.04	82.2
E-09	7.25	540.74	0	90	150.12	0	5.94	2301.1	1.74	293.4	1.38	0	64.8
E-11	7.31	617.82	0	90	112.62	0	6.18	2545.5	1.5	111.4	0.9	49.68	79.8
F-01	2.76	22.88	0	90	37.53	132	1.38	753.6	0	139.6	3.36	0	69.6
F-02	1.06	22.85	0	120	37.56	42	0.84	238.86	0.3	37.56	1.62	0	70.5
F-03	1.64	45.77	0	90	75.06	84	0.9	435.66	0.42	64.5	1.32	0	66
F-04	2.67	68.65	0	120	75.06	78	1.02	514.98	0.12	262.1	1.26	0	69.6
F-05	1.92	22.88	0	120	75.06	90	0.9	523.32	0.06	76.62	3.6	0	67.8

ID	CEC	HCO_3^-	CO_3^{2-}	Cl^-	Organic Acids	SO_4	Al^{3+}	Ca^{2+}	Fe^{2+}, Fe^{3+}	Mg^{2+}	Mn	K^+	Na^+
	(meq/100g)	(mg/kg soil)	(mg/kg soil)	(mg/kg soil)	(mg/kg soil)	(mg/kg soil)	(mg/kg soil)	(mg/kg soil)	(mg/kg soil)	(mg/kg soil)	(mg/kg soil)	(mg/kg soil)	(mg/kg soil)
G-01	1.11	0	0	90	37.53	54	199.02	15.36	0.6	4.32	12.84	0	72
G-02	1.16	0	0	58.68	37.53	180	228.36	16.14	1.8	4.74	0.6	0	58.8
G-03	0.97	0	0	120	37.53	12	169.32	14.16	2.46	4.2	0.42	0	67.2
G-04	1.33	0	0	90	37.53	0	222.36	47.88	70.3	19.14	3.72	0	70.8
G-05	0.64	0	0	120	37.53	30	84.24	11.88	1.68	4.74	0.18	4.14	60.6
G-06	1.31	0	0	78.24	37.53	0	264.6	13.14	18.7	5.88	0.24	0	63
G-07	1.11	0	0	90	37.53	36	190.56	25.02	58.5	9.72	0.96	0	70.2
G-08	1.04	0	0	58.68	37.53	126	184.38	18	13.1	5.64	0.3	0	66
G-09	1.08	0	0	78.24	37.53	120	196.02	17.94	10.5	5.82	0.42	0	66
G-10	0.98	0	0	120	37.53	114	181.2	19.74	18.4	7.08	0.48	0	52.2
H-01	0.52	0	0	90	75.06	114	6	172.08	0	17.1	20.22	0	0
H-02	0.87	0	0	210	37.53	90	0.702	255.96	0.24	55.26	32.1	0	0
H-03	0.66	0	0	105	75.06	48	41.34	158.76	0	26.58	27.3	0	0
H-04	0.42	45.765	0	105	37.53	6	50.82	22.08	0.84	7.08	14.94	0	33.84
H-05	1.24	22.88	0	135	37.53	216	117.78	162.24	12.1	16.44	15.96	75.36	12.56
H-06	1.19	68.65	0	120	37.53	42	0.36	190.8	0	14.28	11.52	0	26.94
H-07	0.97	0	0	120	37.53	24	60.9	176.22	0.42	24.12	21.36	0	47.7
H-08	1.43	0	0	90	37.53	102	14.94	220.38	0.06	17.76	33.36	226.8	40.2
I-01	1.58	22.88	0	105	37.53	96	75.72	258.72	0.06	31.02	11.76	0	121.56
I-02	1.99	0	0	120	187.65	186	298.26	161.7	0.36	19.44	11.82	0	91.56
I-03	0.99	0	0	120	75.06	108	154.92	93.72	0.18	20.94	13.2	0	22.32
I-04	4.63	434.8	0	120	75.06	12	2.22	1720.1	0	47.46	0.06	0	30.3
I-05	1.04	0	0	90	37.53	66	215.64	52.62	0.6	25.74	9.3	0	0
I-06	1.78	0	0	90	112.59	174	381.18	14.4	5.04	16.74	4.8	0	59.34
J-01	1.91	0	0	90	37.53	66	78.36	145.8	0.24	10.26	96	0	52.74
J-02	5.61	22.88	0	120	37.53	42	34.62	900.78	0.9	48.36	358.9	0	76.5
J-03	1.15	0	0	150	37.53	54	89.58	188.4	0.48	8.4	78.36	0	72.54
J-04	1.9	91.53	0	120	37.53	6	2.82	557.52	0.96	33.9	368.9	0	81.78
J-05	1.89	22.88	0	120	37.53	0	34.62	512.52	0.96	35.88	234.1	0	77.82
J-06	0.87	0	0	120	37.53	0	22.56	175.38	0.3	12.18	86.76	0	68.52
J-07	0.83	0	0	120	37.53	54	126.18	37.38	2.64	5.16	23.28	0	56.7
J-08	0.77	0	0	90	37.53	48	176.88	38.16	9.78	5.46	13.8	0	0
J-09	0.74	0	0	90	37.53	0	105.66	38.04	3.12	4.68	42.3	0	54.06
J-10	1.08	0	0	90	37.53	24	211.44	35.16	30.2	8.7	67.98	0	39.54
J-11	0.8	0	0	120	37.53	54	112.5	57.12	7.68	6.6	18.78	0	48.78
J-12	1.49	45.765	0	90	37.53	0	124.98	245.46	58.3	22.56	87.84	3.36	71.52
J-13	0.84	22.88	0	90	19.53	0	62.1	73.32	0.6	7.44	65.16	8.34	86.04
J-14	2.88	91.53	0	105	37.53	0	4.62	856.2	0.18	53.94	86.04	17.7	106.68
J-15	5.38	274.59	0	105	37.53	0	2.94	1904.2	0.36	45.3	1.74	9.12	93.36
J-20	0.95	0	0	120	19.53	60	121.56	51.24	1.02	5.88	7.14	0	78.78
J-21	1.04	0	0	105	37.53	30	47.58	184.14	0.42	9.48	6.48	0	84.84
J-23	0.88	0	0	105	37.53	42	155.28	37.14	3.36	8.1	15.3	0	40.02
J-24	0.75	0	0	138	37.53	0	130.32	39	2.64	5.34	14.88	0	33.96

ID	CEC	HCO_3^-	CO_3^{2-}	Cl^-	Organic Acids	SO_4	Al^{3+}	Ca^{2+}	Fe^{2+}, Fe^{3+}	Mg^{2+}	Mn	K^+	Na^+
	(meq/100g)	(mg/kg soil)	(mg/kg soil)	(mg/kg soil)	(mg/kg soil)	(mg/kg soil)	(mg/kg soil)	(mg/kg soil)	(mg/kg soil)	(mg/kg soil)	(mg/kg soil)	(mg/kg soil)	(mg/kg soil)
J-25	0.48	0	0	105	37.53	48	72.78	28.86	1.32	2.94	14.04	0	29.1
J-26	0.57	0	0	115.2	37.53	36	115.44	35.7	4.92	5.4	10.56	0	7.26
K-01	5.95	457.65	495.48	75	75.06	0	2.34	2022.5	0	85.14	0	30.84	107.22
K-02	9.22	640.71	525.5	90	75.06	0	3.18	3047.6	0	190.6	0.06	58.38	155.34
K-03	8.26	640.71	525.50	90	75.06	0	2.52	2744.4	0	131.2	0	74.58	153.96
K-04	5.56	549.18	450.42	90	75.06	0	1.92	1785	0	85.98	0.06	57.54	137.28
K-05	6.45	846	694	90	112.59	0	2.22	2114	0	123.8	0	47.82	122.94
K-06	4.58	640.71	525.5	90	75.06	0	1.74	1461.1	0	50.04	0	62.46	128.46
K-07	8.85	320.4	262.7	90	75.06	0	3	2922.7	0	114.8	0.06	94.86	192.3
K-08	7.46	640.71	525.5	90	75.06	0	2.64	2372.8	0	107	0.06	140.28	168.3
K-09	8.25	457.65	375.36	75	75.06	0	2.64	2518.4	0	84.66	0.06	137.82	288.9
K-10	8.71	549.18	450.4	75	75.06	0	2.94	2844.5	0	98.22	0.06	124.86	202.08
K-11	8.81	389	319.0	90	112.59	0	2.76	2726.4	0	128.2	0.06	145.14	252.96
K-12	8.86	503.4	412.9	90	75.06	0	2.88	2739.4	0	125.6	0.12	113.52	276.9
K-13	8.83	778	638.1	120	75.06	0	2.88	2871.8	0	111.9	0.06	105.42	211.74
K-14	6.8	228.8	187.7	90	75.06	0	2.7	2365.4	0	86.64	0.06	50.028	93.96
K-15	8.72	686	563.04	105	75.06	0	2.88	2856.4	0	107	0.06	220.24	133.46
K-16	9.05	961	768	90	75.06	0	2.84	2904.7	0	104.6	0.06	183.61	206.2
K-17	9.36	80.9	656.9	105	75.06	0	3	2991.7	0	110.5	1.8	185.8	219.72
K-18	7.22	485.3	394.1	105	112.59	0	3.12	2146	0	108.1	0.06	184.54	214.8
K-19	10.41	800.9	656.9	120	112.59	0	3.3	3409	0	120.9	0.24	185.02	212.05
K-20	10.91	366.12	300	90	75.06	102	3.24	3608.8	0	125.8	0.78	183.9	208.64
K-21	9.87	778	638	105	75.06	0	3.24	3184	0	129.2	0.12	183.46	209
K-22	10.08	549	450	120	37.53	0	3.18	3309.1	0	107.6	0.06	185.29	206.2
L-01	2.36	0	0	90	37.53	36	7.44	378.84	0.12	41.76	31.14	377.4	57.6
L-02	1.71	0	0	105	37.53	36	32.28	193.98	0.06	28.8	13.14	317.4	41.4
L-03	1.42	0	0	120	37.53	48	24.42	144.18	0	28.74	7.8	261	43.2
L-04	0.86	0	0	120	37.53	12	9.9	68.1	0	11.88	3.6	159.6	45.6
L-05	1.2	0	0	105	75.06	30	29.34	125.1	0	23.82	8.52	194.4	42.6
L-06	1.01	0	0	105	75	42	47.34	75.6	0.3	12.42	12.24	151.2	46.8
L-07	1.36	0	0	90	187.65	18	83.16	93.42	0.3	18.3	22.74	205.2	51
L-08	4.08	0	0	90	75.06	42	40.02	212.4	0.3	22.8	15.54	202.8	52.8
L-09	1.49	0	0	105	37.53	18	44.82	165.66	0.06	27.06	9.78	222.6	52.8
L-10	2.71	0	0	90	37.53	6	28.08	458.52	0.36	55.74	73.14	386.4	57
L-11	1.64	0	0	105	37.53	48	40.62	162.12	0.24	17.4	9.48	297.6	57.6
L-12	2.04	0	0	120	37.53	36	83.04	231.3	0.48	16.08	20.88	328.2	57.6
L-13	1.38	0	0	105	37.53	48	82.92	48.66	0.24	10.62	8.1	252.6	60
L-14	2.84	0	0	105	37.53	30	27.42	519.42	0.12	36.42	44.34	403.8	59.4
L-15	2.04	0	0	120	37.53	18	73.92	195.3	0.24	29.64	24.42	340.8	64.8
L-16	1.84	0	0	120	37.53	42	107.34	39.78	0.78	7.32	15.9	382.2	76.8
L-17	1.86	0	0	120	150.12	48	74.82	76.8	0.78	14.64	18.84	390.6	75.6
L-18	2.37	0	0	90	37.53	12	63.66	172.92	0.42	12.48	23.4	511.8	79.8
L-19	2.51	0	0	120	37.53	0	95.82	148.38	3	21.24	50.52	516	86.4

ID	CEC	HCO_3^-	CO_3^{2-}	Cl^-	Organic Acids	SO_4	Al^{3+}	Ca^{2+}	Fe^{2+}, Fe^{3+}	Mg^{2+}	Mn	K^+	Na^+
	(meq/100g)	(mg/kg soil)	(mg/kg soil)	(mg/kg soil)	(mg/kg soil)	(mg/kg soil)	(mg/kg soil)	(mg/kg soil)	(mg/kg soil)	(mg/kg soil)	(mg/kg soil)	(mg/kg soil)	(mg/kg soil)
L-20	2.11	0	0	90	150.12	6	77.04	74.04	0.48	7.56	10.86	481.2	87.6
L-21	1.87	0	0	120	37.53	60	23.52	117.96	0.18	12.18	2.46	414.6	87
L-22	2.23	0	0	120	37.53	72	17.1	123.96	0.12	19.68	2.64	539.4	90.6
L-23	1.99	0	0	105	37.53	66	18.66	129.42	0.12	11.46	3.48	457.8	88.2
L-24	2.02	0	0	105	37.53	66	18.78	141.06	0.3	11.22	3.78	455.4	90
L-25	1.95	0	0	105	37.53	66	19.14	141.18	0.12	11.16	3.78	429.6	88.8
L-26	1.91	0	0	120	37.53	24	48.78	61.56	0.84	6.66	6.48	459.6	85.8
L-27	2	0	0	120	37.53	12	77.46	44.94	0.36	3.6	5.82	468.6	88.2
L-28	2	0	0	105	37.53	96	62.88	42.6	0.66	10.5	3.48	483.6	87
L-31	2.01	0	0	120	187.65	36	71.22	50.76	0.48	16.56	19.26	455.4	90
L-32	2.02	0	0	120	37.53	78	70.08	45.24	0.42	9.18	8.82	474.6	91.2
Y-01	4.94	274.59	0	42	150.12	0	1.98	1406.4	0	346.8	3.06	0	0
Y-02	5.09	228.8	0	30	150.12	0	2.1	1437.7	0.06	349.4	3.96	0	13.32
Y-03	7.48	297.5	0	42	112.59	60	2.7	2098.5	0	466.9	0.42	0	72.54
Y-04	6.74	228.8	0	42	75.06	6	2.58	2035.8	0	321.4	0.06	0	75.18
Y-05	10.72	366.1	0	60	150.12	252	3.66	3189.8	0.12	668.6	25.74	0	0
Y-06	10.08	617.8	0	42	187.65	222	3.42	2946.8	0.18	660.7	24.12	0	0
Y-07	7.08	709	0	30	75.06	6	2.46	2003.5	0	502.8	27.96	0	0
Y-08	6.77	823.8	0	30	75.06	0	2.34	1970.1	0	447.9	22.92	0	0
Y-09	8.37	1098	0	42	150.12	0	2.94	2591.2	0.36	459.4	41.4	0	0
Y-10	7.84	1144	0	42	112.59	18	2.34	2155.5	0.12	342.1	38.64	0	240
Z-01	14.4	0	0	204	480	27.6	51.4	18.9	257	11.1	0.18	1912	71.7
Z-02	3.25	2.44	0	240	60.1	36	29.9	6.84	17.8	3.84	0.6	1237	70.8
Z-03	11.2	3.66	0	240	48	30	152.8	5.04	112	6	0.3	1294	69
Z-04	10.5	2.44	0	180	6	18	214.4	6.3	178	8.76	0.42	1430	61.2
Z-05	3.01	4.88	0	270	12	0	1.92	3.72	1.56	2.04	0.3	1468	66.6
Z-06	8.02	4.88	0	180	132.1	0	0.96	6.06	0.48	2.64	0.54	1439	66
Z-07	4.56	0	0	150	48	0	230	7.02	149	10	0.66	1486	68.4
Z-08	6.66	4.88	0	210	48	12	30	3.72	19.1	2.7	0.12	1447	70.8
Z-09	8.22	0	0	180	216.1	0	274.8	3.9	212	12.1	0.42	1492	73.8
Z-10	7.59	0	0	120	84.1	0	301.1	4.62	246	13.8	0.78	1517	69.6
Z-11	10.3	0	0	150	36	0	303.1	4.92	264	11.9	0.48	1678	76.2
Z-12	6.92	4.88	0	150	60	12	104	7.08	72.5	6.24	0.42	1548	66
Z-13	7.35	0	0	180	12	0	42.6	10.3	31.3	6.3	0.42	1490	73.8
Z-14	10.5	3.66	0	120	72	0	24.6	10.4	19.1	4.2	0.36	1559	70.8
Z-15	9.66	0	0	180	96	30	66.9	8.16	46	5.1	3.84	1538	74.4
Z-16	6.73	1.22	0	210	72	18	295.4	6.72	216	12.1	2.22	1696	75.6
Z-17	6.47	1.22	0	150	72	6	72.7	3.06	44.6	4.08	0.96	1598	70.8
Z-18	6.72	0	0	120	72	18	228.1	4.98	174	8.88	0.6	1510	67.2
Z-19	6.62	0	0	120	48	0	127.2	4.44	97.5	6.06	0.48	1559	75
Z-20	4.3	1.22	0	150	96	6	0.66	4.92	0.54	1.98	0.12	1557	79.2
Z-21	1.55	4.88	0	90	96	0	1.8	2.88	1.08	1.5	0.12	1620	67.2

Appendix B3e: UXO Corrosion Study Results - Soil Physical Data

ID	Soil Classification		Gravel	Sand	Silt	Clay	Organic Content	Particle Density
	USDA	USCS						
			(%)	(%)	(%)	(%)	(%)	(g/cm^3)
A-01	silt loam	ML	0	32.94	56.46	10.61	7.6	2.56
A-02	gravelly loam	SM	23.73	36.74	34.04	6.49	8.03	2.72
A-03	silt loam with gravel	ML	3.74	32.92	49.66	13.69	3.42	2.7
A-04	sandy loam with gravel	SM	7.1	59.04	27.16	6.7	2.47	2.61
A-05	loam with gravel	SM-SP	3.56	43.72	44.09	8.62	4.79	2.43
A-06	gravelly loam	SM	18.02	36.91	36.34	8.73	3.12	2.79
A-07	gravelly sandy loam	SM	16.26	45.81	30.59	7.39	3.55	2.73
A-08	gravelly silt loam	SM	22.33	25.98	40.52	11.17	3.66	2.79
A-11	silt loam with gravel	ML	5.6	27.08	52.24	15.08	4.16	2.57
A-12	sandy loam with gravel	SM	3.92	55.18	34.51	6.39	2.58	2.59
A-14	loam with gravel	SM-SP	4.16	44.99	43.61	7.24	1.84	2.66
A-15	gravelly sandy loam	SM	35.12	37.3	20.97	6.61	6.83	2.71
A-16	loam with gravel	SM-SP	7.46	43.16	40.82	8.56	3.08	2.597
A-17	gravelly sandy loam	SM	34.87	42.34	17.85	4.94	5.83	2.79
A-18	gravelly sandy loam	SM	28.24	45.02	20.17	6.58	6.47	2.71
A-19	silt loam with gravel	ML	7.34	30.75	51.55	10.37	4.05	2.68
A-20	silt loam	ML	0	34.16	52.16	13.23	4.87	2.62
B-01	sand	SP	0	91.79	8.21	0	1.69	2.58
B-02	sand	SP	0	94.47	5.53	0	1.29	2.57
B-03	sand	SP	0	95.37	4.63	0	0.37	2.63
B-04	loamy sand	SM	0	84.7	17.2	1.09	0.31	2.66
B-05	loamy sand	SM	0	80.61	18.68	0.71	0.43	2.6
B-06	sandy loam	SM	0	63.48	31.55	4.97	1.48	2.52
B-07	sandy loam	SM	0	69.55	29.49	0.97	2.46	2.48
C-01	sandy loam	SM	0	67.1	22.99	9.91	4.02	2.64
C-02	sandy loam	SM	0	71.81	22.12	6.07	2.34	2.5
C-03	sandy loam	SM	0	69.24	27.63	3.13	2.48	2.59
C-04	sandy loam	SM	0	69.35	23.49	7.17	1.64	2.51
C-05	sandy loam	SM	0	75.1	22	2.89	2.51	2.46
C-06	sandy loam	SM	0	74.56	18.83	6.61	2.6	2.49
C-07	loam	ML	0	43.46	48.41	8.13	6.04	2.4
C-11	sandy loam	SM	0	61.06	29.89	9.06	1.25	2.54
D-01	sand	SP	0	88.36	9.39	2.11	4.96	2.52
E-01	gravelly loamy sand	SP	40.8	50.79	6.37	2.03	0.85	
E-02	gravelly sandy loam	SM	43.95	42.25	10.59	3.22	1.67	
E-05	gravelly sandy loam	SM	10.4	68.51	17.32	3.77	2.32	
E-09	gravelly loamy sand	SM	26.83	57.37	12.97	2.84	4.43	
E-11	gravelly loamy sand	SM	13.75	65.16	17.12	3.98	1.75	
F-01	loamy sand	SM	0	83.93	13.8	2.27	1.98	2.545
F-02	sand	SP	0	93.61	5.31	1.08	0.56	2.575
F-03	sand	SP	0	90.33	8.39	1.29	0.86	2.597
F-04	loamy sand	SP	0	85.84	12.14	2.02	1.49	2.562

ID	Soil Classification		Gravel	Sand	Silt	Clay	Organic Content	Particle Density
	USDA	USCS						
			(%)	(%)	(%)	(%)	(%)	(g/cm^3)
F-05	loamy sand	SP	0	85.63	12.18	2.18	1.63	2.568
G-01	silt loam	ML	0	24.03	59.7	16.26	4.05	2.59
G-02	loam	SM	0	51.43	41.72	6.85	2.66	2.61
G-03	silt loam	ML	0	37	50.82	12.18	2.01	2.62
G-04	silt loam	ML	0	15.48	71.36	13.15	6.92	2.504
G-05	loam	ML	0	43.36	47.61	9.06	2.03	2.62
G-06	sandy loam	SM-SP	0	56.15	37.74	6.11	2.93	2.6
G-07	silt loam	ML	0	36.26	53.79	9.95	2.62	2.58
G-08	silt loam	ML	0	37.24	52.88	9.87	2.57	2.59
G-09	silt loam	ML	0	39.43	50.64	9.93	3.48	2.52
G-10	loam	ML	0	44.8	47.7	7.5	3.47	2.58
H-01	sandy loam	SM	0	64.61	27.17	8.21	0.92	2.664
H-02	sandy loam	SM	1.81	54.74	32.81	10.65	2.63	2.615
H-03	sandy loam	SM	0.81	56.29	34.59	8.31	2.69	2.625
H-04	sandy loam	SM	0	68.41	25.26	6.33	2.89	2.639
H-05	sandy loam	SM	0	60.35	33.38	6.28	4.7	2.5
H-06	loamy sand	SM	0	76.1	18.32	5.59	1.44	2.631
H-07	sandy loam	SM	0	76.84	16.84	6.32	2.92	2.554
H-08	sandy loam	SM	0	57.28	34.78	7.94	2.75	2.623
I-01	silty clay loam	MH	0	8.91	69.42	21.68	3	2.612
I-02	silty clay loam	MH	0	12.38	69.23	18.39	2.65	2.668
I-03	silty clay loam	MH	0.16	16.8	60.12	22.92	3.37	2.61
I-04	loam with gravel	ML	5.72	33.74	46.33	14.21	3.3	2.603
I-05	sandy loam	SM	0	58.38	30.8	10.82	3.5	2.629
I-06	silty clay loam	MH	0	17.53	60.06	22.41	3.12	2.673
J-01	gravelly sandy loam	SM	18.96	43.18	29.38	8.48	14.5	2.56
J-02	gravelly sandy loam	SM	19.88	45.34	26.84	7.95	15.3	2.32
J-03	sandy loam with gravel	SM	4.26	57.77	32.85	5.12	11.6	2.441
J-04	gravelly loamy sand	SM	10.19	71.85	15.23	2.73	16.3	2.352
J-05	gravelly sandy loam	SM	16.8	58.06	19.42	5.72	14.8	2.314
J-06	gravelly sandy loam	SM	39.95	43.01	12.9	4.14	11.5	2.539
J-07	gravelly loam	GM	32.65	28.55	27.24	11.57	8.3	2.531
J-08	gravelly loam	GM	49.47	18.76	21.49	10.27	9.19	2.529
J-09	gravelly sandy loam	SM	18.85	52.1	20.87	8.18	15.5	2.514
J-10	loam	ML	0.97	43.61	38.42	17	6.29	2.661
J-11	silt loam	ML	0.91	27.25	55.53	16.3	9.55	2.412
J-12	loam with gravel	ML	4.64	44.38	35.2	15.78	18.5	2.113
J-13	gravelly silt loam	ML	10.1	24.82	45.68	19.41	12.3	2.361
J-14	gravelly sandy loam	SM	13.25	48.86	29.59	8.3	10.7	2.479
J-15	gravelly sandy loam	SM	35.73	48.72	11.23	4.32	14.6	2.64
J-20	gravelly loam	ML	12.98	22.63	43.56	20.83	8.8	2.501
J-21	gravelly loam	ML	15.58	24.45	42.33	17.64	9.34	2.505

ID	Soil Classification		Gravel	Sand	Silt	Clay	Organic Content	Particle Density
	USDA	USCS						
			(%)	(%)	(%)	(%)	(%)	(g/cm^3)
J-23	sandy loam with gravel	SM	2.78	51.42	33.17	12.63	10.9	2.479
J-24	loam	ML	0.73	36.32	39.92	23.02	9.05	2.567
J-25	loam with gravel	ML	4.4	36.76	41.03	17.8	10.4	2.461
J-26	loam with gravel	ML	3.29	35.3	40.04	21.37	6.72	2.552
K-01	sand	SP	0.92	92.29	5.22	1.56	2.46	2.687
K-02	sandy loam	SM	0	71.57	23.64	4.79	3.56	2.641
K-03	loamy sand	SM	1.8	79.43	15.45	3.32	3.28	2.604
K-04	sand	SP	0.25	91.99	5.77	1.99	2.15	2.519
K-05	loamy sand	SM	0	75.73	19.3	4.97	3.57	2.611
K-06	sand	SM	1.02	84.69	11.39	2.9	2.1	2.617
K-07	loamy sand	SM	0	82.9	14.49	2.61	1.77	2.621
K-08	loamy sand	SM	0	82.59	14.39	3.02	2.41	2.594
K-09	sand	SP	0.11	89.1	8.04	2.75	1.82	2.575
K-10	sand	SP	0.28	86.07	10.5	3.15	2.44	2.653
K-11	loamy sand	SM	0	84.79	11.94	3.27	2.29	2.636
K-12	loamy sand	SM	1.32	81.85	13.31	3.52	2.26	2.637
K-13	loamy sand	SP	0	85.27	11.33	3.4	1.62	2.661
K-14	sand	SP	0	90.48	7.49	2.03	1.28	2.645
K-15	loamy sand with gravel	SM	2.67	76.88	16.81	3.64	1.91	2.625
K-16	loamy sand	SM	0	78.19	17.66	4.15	1.52	2.65
K-17	sand	SP	1.27	91.02	6.08	1.64	2.09	2.643
K-18	loamy sand	SM	0	79.57	17.8	2.64	2.84	2.644
K-19	loamy sand	SM	0	81.19	15.11	3.7	2.41	2.628
K-20	loamy sand	SM	0	79.16	17.62	3.22	2.8	2.633
K-21	loamy sand	SM	0.41	84.2	12.47	2.91	2.46	2.622
K-22	loamy sand	SM	0	84.74	12.12	3.14	2.62	2.669
L-01	loamy sand	SM	0.29	80.16	14.7	4.85	2.21	2.617
L-02	loamy sand	SM	0.07	78.7	15.64	5.59	1.59	2.595
L-03	sandy loam	SM	0	74.2	20.39	5.41	1.72	2.622
L-04	sand	SP	2.38	91.11	4.16	2.35	0.78	2.638
L-05	loamy sand	SM	0	84.34	10.81	4.77	1.77	2.625
L-06	sand	SP	0	89.77	6.67	3.56	2	2.615
L-07	sand	SP	0	89.8	6.31	3.89	2.15	2.593
L-08	sand	SP	0	91.21	5.24	3.55	2.34	2.6
L-09	sand	SP	0	90.26	6.11	3.64	1.7	2.597
L-10	loamy sand	SP	0	86.08	9.76	4.16	3.07	2.578
L-11	sand	SP	0	90.92	5.57	3.5	2.04	2.603
L-12	sand	SP	0	90.25	6.72	3.03	2.26	2.62
L-13	sand	SP	0	92.37	5.22	2.42	1.88	2.616
L-14	loamy sand	SP	0	84.5	11.7	3.8	3.86	2.538
L-15	sand	SP	0	91.21	6.09	2.7	2.47	2.608
L-16	sand	SP	0.57	89.48	6.24	3.72	6.39	2.515

ID	Soil Classification		Gravel	Sand	Silt	Clay	Organic Content	Particle Density
	USDA	USCS						
			(%)	(%)	(%)	(%)	(%)	(g/cm^3)
L-17	sand	SP	0	91.48	5.12	3.4	2.53	2.604
L-18	sand	SP	0	88.06	8.05	3.9	4.73	2.535
L-19	sand	SP	0	93.12	4.15	2.73	2.05	2.577
L-20	sand	SP	0	94.18	3.83	2	2.14	2.615
L-21	sand	SP	0	94.83	3.09	2.08	2	2.573
L-22	sand	SP	0	94.77	3.48	1.74	1.18	2.607
L-23	sand	SP	0	96.97	1.67	1.37	0.86	2.611
L-24	sand	SP	0	95.94	2.52	1.54	0.86	2.599
L-25	sand	SP	0	97	1.73	1.27	0.86	2.636
L-26	sand	SP	0	95.56	1.87	1.58	1.05	2.63
L-27	sand	SP	0	95.17	2.56	2.27	1.46	2.611
L-28	sand	SP	0	93.36	4.14	2.51	1.17	2.621
L-31	sand	SP	0	93.69	3.65	2.66	1.63	2.629
L-32	sand	SP	0	95.37	2.66	1.97	1.21	2.613
Y-01	sandy loam	SM	0	70.1	25.52	4.38	5.13	2.673
Y-02	loamy sand	SM	0	78.69	18.26	3.05	4.86	2.63
Y-03	loam	ML	0	46.11	46.18	7.71	6.83	2.558
Y-04	sandy loam	SM	0	58.95	35.53	5.52	4.55	2.599
Y-05	gravelly sandy loam	SM	19.1	46.28	28.91	5.71	11.9	2.491
Y-06	gravelly sandy loam	SM	14.9	46.39	32.43	6.27	11.4	2.519
Y-07	sandy loam with gravel	SM	4.76	54.01	34.13	7.1	9.38	2.577
Y-08	sandy loam with gravel	SM	9.99	47.38	35.61	7.02	9.99	2.524
Y-09	gravelly sandy loam	SM	25.23	37.81	30.46	6.5	10.1	2.513
Y-10	sandy loam with gravel	SM	4.98	57.43	31.9	5.69	11.4	2.549
Z-01	sandy loam	SM	0	72	24.95	3.05	11.9	2.29
Z-02	sandy loam	SM	0	58.11	40.36	1.53	2.59	2.89
Z-03	silt loam	SM-SP	0	47.34	52.26	0.41	4.28	2.47
Z-04	silt loam	ML	0	40.32	58.94	0.74	5.41	2.54
Z-05	sandy loam	SM	0	63.1	36.21	0.69	1.6	2.8
Z-06	silt loam	SM-SP	0	43.8	53.93	2.27	4.19	2.82
Z-07	sandy loam	SM	0	63.15	35.68	1.17	2.61	2.68
Z-08	silt loam	ML	0	40.13	57.29	2.59	4.19	2.42
Z-09	silt loam	ML	0	39.52	50.6	1.91	3.88	2.23
Z-10	silt loam	ML	0	31.96	64.82	3.22	5.39	2.29
Z-11	silt loam	ML	0	41.73	56.68	1.59	5.26	1.58
Z-12	silt loam	ML	0	36.07	61.55	2.38	5.36	1.98
Z-13	silt loam	ML	0	40.78	56.8	2.42	4.92	2.55
Z-14	sandy loam	SM	0	60.71	37.59	1.7	5.63	2.35
Z-15	silt loam	ML	0	38.8	59.09	2.11	4.71	2.43
Z-16	sandy loam	SM	0	52.12	45.94	1.94	3.86	2.35
Z-17	silt loam	ML	0	37.81	58.9	3.29	4	2.5
Z-18	sandy loam	SM	0	52.92	46.19	0.89	4.32	2.44

ID	Soil Classification		Gravel	Sand	Silt	Clay	Organic Content	Particle Density
	USDA	USCS						
			(%)	(%)	(%)	(%)	(%)	(g/cm^3)
Z-19	silt loam	ML	0	45.63	52.38	1.98	4.77	2.31
Z-20	silt loam	ML	0	34.32	62.63	3.05	1.84	2.38
Z-21	sand	SP	0	87.75	11.86	0.39	0.72	2.38

Appendix B3f: UXO Corrosion Study - Soil Physical Properties (continued)

ID	Bulk Density	Volumetric Water Content	Porosity	Initial Resistivity	Minimum Resistivity	Red-Ox Potential	pH
	(g/cm^3)	(%)	(%)	(ohm-cm)	(ohm-cm)	(mV)	
A-01		32.12	78.65	165000	3900	289	4.8
A-02		36.95	85.03	395000	3200	322	4.1
A-03		20.46	64.8	615000	4600	300	4.9
A-04		12.27	51.65	275000	4800	328	5.2
A-05		22.47	72.33	185000	8600	341	4.5
A-06		19.16	67.17	170000	10500	350	4.6
A-07		13.51	68.9	70000	6200	263	6.9
A-08		19.16	67.17	305000	11000	359	5.2
A-11		23.52	59.9	175000	6500	334	5.1
A-12		14.46	49.93	165000	10800	271	7.6
A-14		13.55	53.7	375000	14500	336	5
A-15		14.39	61.18	75000	7200	251	6.2
A-16		12.26	50.96	250000	17000	297	4.9
A-17		14.97	56.84	48000	8000	255	6.9
A-18		18.13	57.62	45000	5400	209	5.8
A-19		18.57	62.79	250000	7100	251	4.3
A-20		21.93	71.3	380000	7000	227	4.3
B-01	1.28	21.05	50.27	62000	11000	120	6.1
B-02	1.38	1.2	46.34	1000000	33000		5.9
B-03	1.17	1.56	55.34	1000000	42000		6.6
B-04	1.15	2.1	56.93	1000000	42000		6.5
B-05	1.6	7.99	39.32	1000000	27000	70.7	6.4
B-06	1.47	12.09	41.74	22000	1500	119	5.2
B-07	1.33	6.6	46.33	190000	1900	107	5.9
C-01	1	2.62	61.92	1000000	11000	194.5	6
C-02	1.07	7.44	57.22	1000000	13000	209.7	5.6
C-03	1.23	6.93	52.4	1000000	12000	217	5.9
C-04	1.54	6.14	38.61	1000000	24000	201.2	5.9
C-05	1.74	9.8	29.03	440000	8650	248	6.5
C-06	1.14	8.15	54.13	1000000	8400	255	5.9
C-07	1.12	20.72	53.24	76000	2450	199.2	6.5
C-11	1.55	5.17	38.8	1000000	16000	165.3	5
D-01	1.37	21.84	45.53	45000	970	176.5	7.8
E-01				100000	2600		
E-02				65000	2900		
E-05	1.76	8.58	33.66	350000	3000	234	5.6
E-09	1.43	16.46	46.05	140000	2100	216	5.6
E-11	1.76	15.02	33.67	315000	1700	168	6.4
F-01	1.411	3.5	44.55	340000	4000	96.5	5.9
F-02	1.311	0.87	49.08	1000000	17500	99	6.4
F-03	1.332	1.3	48.7	365000	12500	175	6.5
F-04	1.475	2.5	42.42	1000000	7350	137.5	7.1

ID	Bulk Density	Volumetric Water Content	Porosity	Initial Resistivity	Minimum Resistivity	Red-Ox Potential	pH
	(g/cm^3)	(%)	(%)	(ohm-cm)	(ohm-cm)	(mV)	
F-05	1.595	3.76	37.88	320000	6300	172	6.1
G-01	1.111	25.6	57.12	520000	13500	-43	4.4
G-02	1.222	23.59	53.16	130000	9800	-5	4.6
G-03	1.232	23.08	52.99	280000	12500	101.5	4.5
G-04	0.646	44.33	74.89	63000	11500	148	5.6
G-05	0.522	24.44	80.09	1000000	22000	119.5	4.6
G-06	0.807	28.3	68.95	1000000	16000	190	4.6
G-07	1.123	15.35	56.48	1000000	15000	102.4	5.3
G-08	0.87	27.98	66.43	1000000	17000	160	4.7
G-09	1.253	1.19	50.29	1000000	8900	173	4.5
G-10	1.177	22	54.37	1000000	9100	200.5	4.5
H-01	1.657	10.99	37.79	110000	9900	291	5.1
H-02	1.671	13.31	36.02	67500	6300	327	5.1
H-03	1.382	17.3	47.35	61800	8400	319	5.2
H-04	1.888	14.22	28.46	135000	10500	329	5.2
H-05	1.17	24.87	53.21	54900	7400	371	4.9
H-06	1.23	14.13	53.25	62500	8200	277	6.1
H-07	1.193	15.7	53.28	52300	8200	329	5.1
H-08	1.25	11.06	52.35	56000	7550	218	5.2
I-01	1.285	20.62	50.82	38000	24000	259	4.9
I-02	1.248	17.67	53.21	43000	8000	357	3.8
I-03	1.186	19.46	54.56	130000	34000	320	4.4
I-04	1.42	16.7	45.43	21000	6100	243	7.5
I-05	1.264	18.92	51.9	100000	27000	273	4.3
I-06	1.22	20.54	54.37	79000	18500	307	3.7
J-01	0.755	36.89	70.49	29500	13500	279	4.4
J-02	0.604	37.9	73.94	28500	4400	294	4.3
J-03	0.604	41.51	75.37	30000	11500	332	4.4
J-04	0.796	28.49	66.17	13500	4800	310	4.5
J-05	0.667	35.56	71.19	28000	6250	251	4.5
J-06	1.198	20.46	52.81	52000	15000	260	4.8
J-07	1.016	23.44	59.86	112000	24000	270	4.5
J-08	1.087	17.52	57.04	120000	27500	276	4.5
J-09	0.827	17.79	67.12	180000	20000	210	4.4
J-10	0.913	25.78	65.69	310000	26000	303	4.4
J-11	0.596	39.86	75.3	49500	21000	325	4.5
J-12	0.392	49.53	81.45	85000	11500	289	4.3
J-13	0.58	42.97	75.45	140000	26000	272	4.7
J-14	0.834	26.09	66.38	28500	5100	301	4.9
J-15	1.095	20.96	58.54	48000	6600	239	6.2
J-20	0.846	33.44	64.96	57000	14000	316	4.4
J-21	0.952	33	61.98	23000	7100	260	4.9

ID	Bulk Density	Volumetric Water Content	Porosity	Initial Resistivity	Minimum Resistivity	Red-Ox Potential	pH
	(g/cm^3)	(%)	(%)	(ohm-cm)	(ohm-cm)	(mV)	
J-23	0.728	27.97	70.63	650000	42500	278	4.7
J-24	0.825	26.51	67.87	400000	47000	236	4.9
J-25	0.746	30.24	69.69	120000	19000	267	4.5
J-26	0.736	26.32	71.16	110000	28000	329	4.6
K-01	1.644	3.06	38.82	82000	9250	165	8.1
K-02	1.5	7.82	43.2	13100	3000	192	7.6
K-03	1.495	4.21	42.59	110000	4950	179	7.9
K-04	1.6	2.83	36.49	75000	4400	184	8
K-05	1.528	3	41.48	76500	4500	173	7.9
K-06	1.502	1.29	42.6	160000	9250	180	8.1
K-07	1.557	2.81	40.57	70000	6500	177	8.3
K-08	1.56	3.02	39.86	52000	6500	184	8.4
K-09	1.477	2.14	42.61	180000	8200	185	7.8
K-10	1.533	3.06	42.21	65000	6400	175	7.9
K-11	1.529	3.05	42.01	110000	6000	145	8
K-12	1.507	3.82	42.85	430000	5500	158	8
K-13	1.534	2.24	42.35	61000	5850	164	7.9
K-14	1.562	2.28	40.93	310000	7800	172	8
K-15	1.502	2.91	42.78	155000	5450	180	7.9
K-16	1.553	2.51	41.37	265000	5700	177	7.8
K-17	1.653	2.13	37.46	1000000	3800	171	7.8
K-18	1.545	3.5	41.57	50500	6100	178	7.9
K-19	1.368	2.05	47.94	300000	5200	186	8
K-20	1.452	5.12	44.84	770000	4950	179	7.9
K-21	1.368	2.62	47.81	150000	5700	168	8
K-22	1.309	3.15	50.96	41000	5900	179	7.9
L-01	1.657	6.82	36.7	110000	14500	244	4.1
L-02	1.759	7.06	32.24	190000	24500	250	3.8
L-03	1.83	6.6	30.21	225000	39000	297	4.1
L-04	1.81	4.05	31.39	200000	24000	294	3.8
L-05	1.607	7.99	38.76	77000	19000	329	3.7
L-06	1.592	3.51	39.14	1000000	62500	235	3.8
L-07	1.436	4.53	44.63	260000	8200	270	3.5
L-08	1.458	3.96	43.91	1.52	885000	39000	2.1
L-09	1.583	5.32	38.94	180000	15000	270	3.6
L-10	1.398	6.62	45.75	104500	9900	298	3.8
L-11	1.472	5.14	43.46	780000	52700	226	4
L-12	1.503	4.08	42.62	860000	23000	294	3.8
L-13	1.329	4.15	49.22	1000000	51500	203	3.7
L-14	1.229	8.76	51.56	325000	20000	301	4
L-15	1.516	6	41.88	250000	11000	286	3.8
L-16	0.796	10.98	68.33	1000000	31000	282	3.8

ID	Bulk Density	Volumetric Water Content	Porosity	Initial Resistivity	Minimum Resistivity	Red-Ox Potential	pH
	(g/cm^3)	(%)	(%)	(ohm-cm)	(ohm-cm)	(mV)	
L-17	1.315	4.41	49.51	990000	25000	233	4.1
L-18	0.7	8.53	65.67	1000000	13000	262	3.9
L-19	1.386	5.73	46.21	1000000	39000	297	3.9
L-20	1.456	4.66	44.32	300000	20000	343	3.6
L-21	1.629	2.45	36.7	1000000	130000	290	4.8
L-22	1.735	2.83	33.46	1000000	115000	301	4.8
L-23	1.553	2.71	40.52	1000000	140000	331	4.5
L-24	1.542	3.42	40.66	1000000	150000	339	4.6
L-25	1.565	2.01	40.63	1000000	140000	343	4.7
L-26	1.557	3.26	40.79	440000	33000	302	3.8
L-27	1.483	4.45	43.21	390000	22000	323	3
L-28	1.496	2.52	42.92	1000000	65500	244	3.6
L-31	1.477	6.28	43.82	79500	15000	345	3.3
L-32	1.497	3.21	42.71	600000	36800	297	3.5
Y-01	1.208	5.43	54.8	210000	1180	167	6.8
Y-02	1.225	5.13	53.05	170000	1200	182	6.9
Y-03	1.156	11.84	54.83	31500	830	204	6.7
Y-04	1.303	8.25	49.88	41000	1800	219	6.9
Y-05	0.935	12.73	62.48	34800	385	185	6.7
Y-06	0.961	13.8	61.85	80100	375	198	6.3
Y-07	1.066	6.47	58.62	1000000	890	172	6.6
Y-08	0.987	6.36	60.92	1000000	765	173	6.8
Y-09	0.987	6.98	60.73	1000000	685	159	6.6
Y-10	0.9663	8.29	62.1	1000000	690	93	6.6
Z-01	1.09	26.2	52.29	50000	3400	250	4.1
Z-02	1.95	17.33	32.75	35000	8000	254	5.1
Z-03	1.46	25.54	40.64	240000	7500	301	4.9
Z-04	1.53	22.48	39.88	240000	7000	321	4.7
Z-05	1.98	14.35	29.12	53000	13000	279	4.5
Z-06	1.84	21.86	34.96	200000	11000	300	4.7
Z-07	1.94	17.59	27.68	110000	15000	325	5
Z-08	1.51	26.25	37.7	140000	17000	307	5
Z-09	1.47	25.79	34.05	68000	4300	-158	5.1
Z-10	1.4	30.23	38.92	110000	4800	-108	5.2
Z-11	2.48	27.81	36.48	67000	5900	60	5.1
Z-12	1.51	25.64	23.71	160000	6150	296	5.2
Z-13	1.79	23.6	29.83	50000	5000	311	5.2
Z-14	1.48	25.01	36.97	110000	5500	318	4.9
Z-15	1.58	27.86	35.02	40000	13500	92.6	4.8
Z-16	1.71	21.71	27.16	54000	15000	39.2	5.1
Z-17	1.55	24.06	37.84	85000	15200	-195	4.9
Z-18	1.59	20.94	34.89	240000	7900	309	5.2

ID	Bulk Density	Volumetric Water Content	Porosity	Initial Resistivity	Minimum Resistivity	Red-Ox Potential	pH
	(g/cm^3)	(%)	(%)	(ohm-cm)	(ohm-cm)	(mV)	
Z-19	1.47	20.89	36.59	150000	5900	299	4.9
Z-20	1.73	19.66	27.54	58000	10000	323	4.2
Z-21	1.76	7.2	26.2	550000	7900	310	4.9